
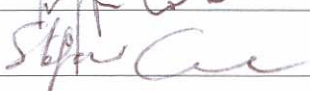
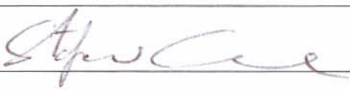
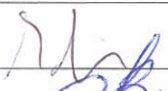





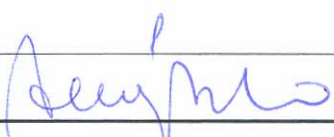




GRADIOMETER ON-ORBIT CALIBRATION PROCEDURE ANALYSIS

DCG No.:

Written by	Responsibility + handwritten signature if no informatic workflow tool
G. Catastini	Author 
S. Cesare	Author 
Verified by	
S. Cesare	Checker 
Approved by	
C. Gennaro	Gradiometer Manager 
 S. Silvestri	Product Assurance Manager  19.02.08
L. Candela	Configuration Management 
B. Vinai	System Manager 
A. Allasio	Program Manager 
N/A	Customer Approval
Documentation Manager	A. Berto 

The validations evidence are kept through the documentation management system.

DOCUMENT CHANGE RECORD

ISSUE	DATE	REASON FOR CHANGE	AFFECTED PARAGRAPHS
01	14 FEB. 2002	First issue	
02	18 DEC. 2003	Update of the K2 measurement procedure. Definition of a new procedure for the determination of the Inverse Calibration Matrices. Implementation of ESA and ONERA comments	All
03	9 MAY 2005	Update of the K2 and ICM measurement requirements. Refinement of the K2 measurement procedure and update of its performance analysis and test by numerical simulation. Completion of the ICM measurement procedure and update of its performance analysis and test by numerical simulation.	All
04	14 FEB. 2008	<p>New maximum values of common and differential K2 by construction.</p> <p>Update of the Gradiometer on-ground calibration purpose.</p> <p>Update of the K2 limits to be achieved by on-orbit calibration.</p> <p>New limits of the differential scale factors after calibration and scale factor drift (table 3.3.4 and 3.3.6).</p> <p>Update of the K2 in-flight measurement error analysis and duration of the proof mass shaking</p> <p>Update of the ICM in-flight measurement error analysis.</p> <p>Update of the numerical simulations of the K2 and ICM in-flight measurements</p>	<p>3.1.1</p> <p>3.2</p> <p>3.3-1</p> <p>3.3-2</p> <p>4.2</p> <p>5.2.2</p> <p>9.1, 9.2</p>

TABLE OF CONTENTS

1.	INTRODUCTION	4
1.1	PURPOSE	4
1.2	STRUCTURE OF THE DOCUMENT	4
2.	APPLICABLE AND REFERENCE DOCUMENTS	5
2.1	APPLICABLE DOCUMENTS	5
2.2	REFERENCE DOCUMENTS	5
3.	ON-ORBIT CALIBRATION OF THE GRADIOMETER: PURPOSE AND REQUIREMENTS	6
3.1	CALIBRATION MATRIX AND QUADRATIC FACTOR MATRIX	6
3.1.1	Limit Values of the Calibration Matrix Elements and of Quadratic Factors	10
3.2	PURPOSE OF THE GRADIOMETER ON-GROUND CALIBRATION	15
3.3	PURPOSE OF THE GRADIOMETER ON-ORBIT CALIBRATION	16
3.3.1	Quadratic Factors	16
3.3.2	Inverse Calibration Matrices	17
4.	DETERMINATION OF THE QUADRATIC FACTORS	22
4.1	METHOD DESCRIPTION	22
4.2	METHOD ANALYSIS	29
4.2.1	Systematic Errors	29
4.2.2	Random Errors	30
5.	DETERMINATION OF THE ELEMENTS OF THE INVERSE CALIBRATION MATRICES	34
5.1	METHOD DESCRIPTION	34
5.1.1	Fundamental Equations Set up and Process Outline	34
5.1.2	Step by Step Process	47
5.1.2.1	Iterative Process Inputs	47
5.1.2.2	Inputs Pre-processing	47
5.1.2.3	Iterative Loop Initialisation	50
5.1.2.4	Calibration Step 1	50
5.1.2.5	Calibration Step 2	58
5.1.2.6	Calibration Step 3	60
5.1.2.7	Step2 - Step 3 Loop Exit Condition	62
5.2	METHOD ANALYSIS	63
5.2.1	Systematic Errors	63
5.2.2	Random Errors	63
6.	REQUIREMENTS FOR DFACS AND GCD ARISING FROM IN-FLIGHT CALIBRATION	70
6.1	REQUIREMENTS ON THE DFACS	70
6.1.1	DFACS Performance Requirements for the Quadratic Factor Measurement	70
6.1.2	DFACS Performance Requirements for the Determination of the Inverse Calibration Matrices	71
6.2	REQUIREMENTS ON THE GRADIOMETER CALIBRATION DEVICE	71
7.	ACRONYMS AND ABBREVIATIONS	74
8.	APPENDIX A: VALUES OF THE GGT CONSIDERED FOR THE CALIBRATION ANALYSES	75
9.	APPENDIX B: NUMERICAL SIMULATIONS	76
9.1	NUMERICAL SIMULATIONS OF THE QUADRATIC FACTOR MEASUREMENT PROCEDURE	76
9.1.1	E2E Simulations of the Quadratic Factor Measurement Procedure	80
9.2	NUMERICAL SIMULATIONS OF THE ICM MEASUREMENT PROCEDURE	82
9.2.1	Calibration Set 1 Results: retrieved ICMs using nominal electrostatic gains	88
9.2.2	Calibration Set 2 Results: retrieved ICMs using measured electrostatic gains	89
9.2.3	Impact of ASH1 misalignment on Calibration and Science Performance	90
9.2.3.1	Performance with the Nominal ASH1 Misalignment	90
9.2.3.2	Performance with the Intermediate ASH1 Misalignment	91
9.2.3.3	Performance with the Worst Case ASH1 misalignment	92

1. INTRODUCTION

1.1 PURPOSE

The purpose of this technical note is to describe and analyse the methods defined for the on-orbit calibration of the GOCE Gradiometer, to identify their performances, limitations, and impacts on the system.

The results of this analysis represent the input for the definition of the Gradiometer on-orbit reference calibration plan.

1.2 STRUCTURE OF THE DOCUMENT

In section 3 the purpose of the on-orbit calibration of the Gradiometer is recalled and the applicable requirements are summarised.

In section 4 the method devised for the on-orbit measurement of the quadratic factors of the accelerometers are described and analysed, to identify under which conditions the specified calibration performance can be achieved.

In section 5 the methods devised for the on-orbit measurement of the elements of the inverse Calibration Matrices are described and analysed, to identify under which conditions the specified calibration performance can be achieved.

In section 6 the main requirements to be fulfilled by the DFACS and by the thrusters in order to make possible the achievement of the calibration objectives with the proposed approach are provided.

In section 9 the numerical simulations performed to verify the calibration methods performances are described and their results are provided.

2. APPLICABLE AND REFERENCE DOCUMENTS

All the documents in the following lists are applicable at their latest issue, unless differently and explicitly specified.

2.1 APPLICABLE DOCUMENTS

[AD 1] GOCE System Requirements Document for Phase B/C/D/E1 GO-RS-ESA-SY-0002

2.2 REFERENCE DOCUMENTS

[RD 1] Performance Requirements and Budgets for the Gradiometric Mission, GO-TN-AI-0027

[RD 2] Gradiometer Instrument Specification, GO-RQ-AI-0007

[RD 3] Gradiometer Performance Analysis and Budgets, GO-RP-ASC-0109

[RD 4] ONERA Support to Gradiometer system analysis – PM9, Minutes of Meeting GO-MI-AI-0166, November 14, 2002

[RD 5] Gradiometer Ground Calibration Plan, GO-PL-ONE-0009

[RD 6] J. Stoer, R. Bulirsch, Introduction to Numerical Analysis, Springer-Verlag 1980.

[RD 7] W. H. Press, B. P. Flannery, S. A. Teukolsky, W. T. Vetterling, Numerical Recipes – The art of scientific computing, Cambridge University Press 1986.

[RD 8] Review of GO-TN-AI-0069 Issue 2 and review of common scale factor retrieving process, ONERA fax GO-ONE-0236-2004, 17/06/2004

[RD 9] G. W. Stewart, Perturbation theory and least squares with errors in the variables.

[RD 10] Review of GO-TN-AI-0069, Fax GO-ONE-0488-2003, 19/11/2003

[RD 11] GO-RP-ASC-0919, Gradiometer FM Performances In Flight

3. ON-ORBIT CALIBRATION OF THE GRADIOMETER: PURPOSE AND REQUIREMENTS

3.1 CALIBRATION MATRIX AND QUADRATIC FACTOR MATRIX

Once the conditions for the gravimetric measurement have been established, i.e.:

- the drag-free condition has been established and the DFACS has brought the linear and angular accelerations, the angular rates and the attitude angles below the limits defined in [RD 1],
- the Gradiometer is set in its measurement mode,
- the satellite internal environment (thermal, electromagnetic, micro-vibration) has achieved the quietness necessary for all the internal disturbance sources contributions (self-gravity, coupling with magnetic field, structure microvibrations) to be under the limits defined in [RD 1],

the common-mode and differential-mode accelerations measured by the accelerometers in the One-Axis Gradiometer Reference Frames are still affected by errors due to:

1. Coupling of the residual common-mode and differential-mode accelerations with the differential and common scale factors of the accelerometer pairs;
2. Coupling of the residual common-mode and differential-mode accelerations with the differential and common misalignments of the Accelerometer Reference Frames (ARF) in the corresponding One-Axis Gradiometer Reference Frames (OAGRF);
3. Coupling of the residual common-mode and differential-mode accelerations with the differential and common coupling factors among the sensitive axes of the accelerometers (due to their non perfect orthogonality, etc.);
4. Coupling of the residual common-mode and differential-mode accelerations with the common and differential quadratic factors (or quadratic non linearity) of the accelerometer pairs.
5. Coupling of the residual common-mode accelerations with the phase difference of the accelerometers read-out channels and of the OAG structure vibration modes (this phase difference behaves like a frequency-dependent, differential scale factor).

With reference to Figure 3.1-1 for the nomenclature of the layout of the 6 accelerometers in the GOCE Gradiometer, the relationship between the common mode and the differential mode accelerations

$$\underline{a}'_{c,ij} = \frac{1}{2} (\underline{a}'_i + \underline{a}'_j), \underline{a}'_{d,ij} = \frac{1}{2} (\underline{a}'_i - \underline{a}'_j) \quad (ij = 14, 25, 36)$$

measured by the three accelerometer pairs (A_1, A_4) , (A_2, A_5) , (A_3, A_6) in their Accelerometer Reference Frames and the differential and common mode accelerations $(\underline{a}_{c,ij}, \underline{a}_{d,ij})$ experienced by the accelerometer proof masses in the corresponding One-Axis Gradiometer Reference Frames can be written as ([RD 1]):

$$\begin{pmatrix} \underline{a}'_{c,ij} \\ \underline{a}'_{d,ij} \end{pmatrix} = \mathbf{M}_{ij} \begin{pmatrix} \underline{a}_{c,ij} \\ \underline{a}_{d,ij} \end{pmatrix} + \frac{1}{2} \mathbf{K}2_{ij} \begin{pmatrix} (\underline{a}_{c,ij} + \underline{a}_{d,ij})^2 \\ (\underline{a}_{c,ij} - \underline{a}_{d,ij})^2 \end{pmatrix} + \begin{pmatrix} \underline{b}_{c,ij} \\ \underline{b}_{d,ij} \end{pmatrix} + \begin{pmatrix} \underline{n}_{c,ij} \\ \underline{n}_{d,ij} \end{pmatrix} \quad (3.1)$$

where \mathbf{M}_{ij} and $\mathbf{K}2_{ij}$ denote the "Calibration Matrix" and the "Quadratic Factor Matrix" and $\underline{b}_{c,ij}$ ($\underline{b}_{d,ij}$), $\underline{n}_{c,ij}$ ($\underline{n}_{d,ij}$) denote the common (differential) biases and noise of the accelerometer pair A_i, A_j :

$$\underline{b}_{c,ij} = \frac{1}{2} (\underline{b}_i + \underline{b}_j), \underline{b}_{d,ij} = \frac{1}{2} (\underline{b}_i - \underline{b}_j), \underline{n}_{c,ij} = \frac{1}{2} (\underline{n}_i + \underline{n}_j), \underline{n}_{d,ij} = \frac{1}{2} (\underline{n}_i - \underline{n}_j) \quad (ij = 14, 25, 36).$$

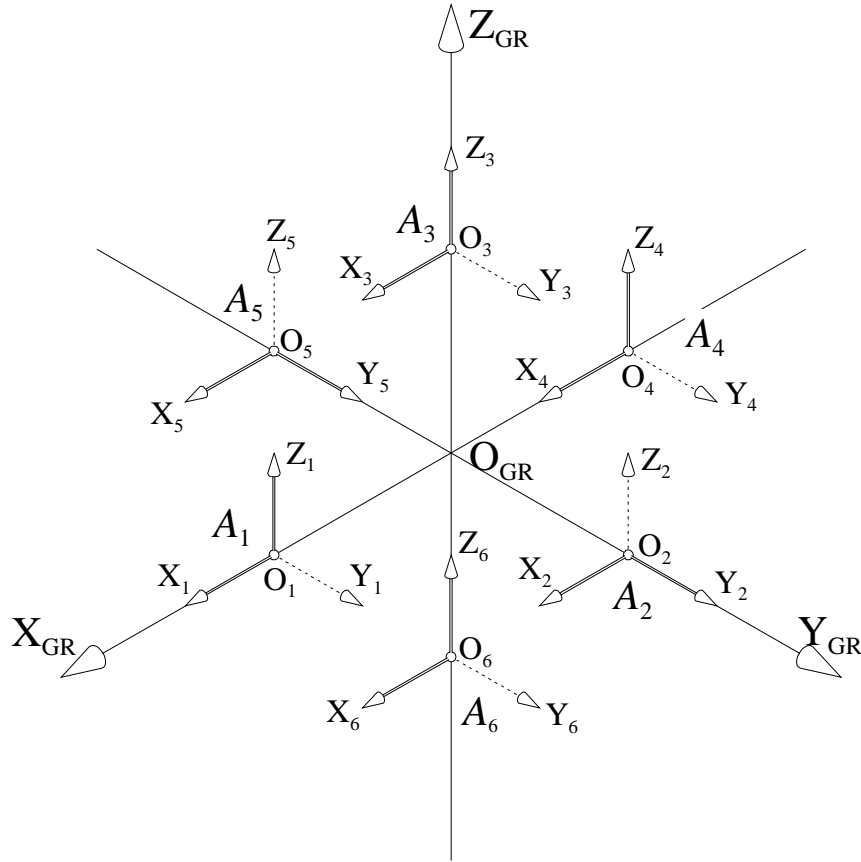


Figure 3.1-1: Accelerometer layout and sensitive axes orientation in the GOCE Gradiometer (the accelerometer ultra sensitive axes are indicated with thick arrows, while the less sensitive axes are indicated with dashed arrows)

The Calibration Matrix is built with the common and differential scale factors, misalignments and couplings of an accelerometer pair (a Calibration Matrix is defined for each One-Axis Gradiometer):

$$\mathbf{M}_{ij} = \begin{pmatrix} 1 + K_{c,ij,X} & \psi_{c,ij} + \varepsilon_{c,ij} & -\theta_{c,ij} + \eta_{c,ij} & K_{d,ij,X} & \psi_{d,ij} + \varepsilon_{d,ij} & -\theta_{d,ij} + \eta_{d,ij} \\ -\psi_{c,ij} + \varepsilon_{c,ij} & 1 + K_{c,ij,Y} & \phi_{c,ij} + \varsigma_{c,ij} & -\psi_{d,ij} + \varepsilon_{d,ij} & K_{d,ij,Y} & \phi_{d,ij} + \varsigma_{d,ij} \\ \theta_{c,ij} + \eta_{c,ij} & -\phi_{c,ij} + \varsigma_{c,ij} & 1 + K_{c,ij,Z} & \theta_{d,ij} + \eta_{d,ij} & -\phi_{d,ij} + \varsigma_{d,ij} & K_{d,ij,Z} \\ K_{d,ij,X} & \psi_{d,ij} + \varepsilon_{d,ij} & -\theta_{d,ij} + \eta_{d,ij} & 1 + K_{c,ij,X} & \psi_{c,ij} + \varepsilon_{c,ij} & -\theta_{c,ij} + \eta_{c,ij} \\ -\psi_{d,ij} + \varepsilon_{d,ij} & K_{d,ij,Y} & \phi_{d,ij} + \varsigma_{d,ij} & -\psi_{c,ij} + \varepsilon_{c,ij} & 1 + K_{c,ij,Y} & \phi_{c,ij} + \varsigma_{c,ij} \\ \theta_{d,ij} + \eta_{d,ij} & -\phi_{d,ij} + \varsigma_{d,ij} & K_{d,ij,Z} & \theta_{c,ij} + \eta_{c,ij} & -\phi_{c,ij} + \varsigma_{c,ij} & 1 + K_{c,ij,Z} \end{pmatrix} \equiv [1]_6 + d\mathbf{M}_{ij}$$

$$\equiv [1]_6 + \begin{pmatrix} [d\mathbf{M}]_{c,ij} & [d\mathbf{M}]_{d,ij} \\ [d\mathbf{M}]_{d,ij} & [d\mathbf{M}]_{c,ij} \end{pmatrix} \equiv \begin{pmatrix} [\mathbf{M}]_{c,ij} & [\mathbf{M}]_{d,ij} \\ [\mathbf{M}]_{d,ij} & [\mathbf{M}]_{c,ij} \end{pmatrix}, \quad [1]_6 = 6 \times 6 \text{ identity matrix}$$

$$[dM]_{c,ij} = \begin{pmatrix} dM_{c,ij,11} & dM_{c,ij,12} & dM_{c,ij,13} \\ dM_{c,ij,21} & dM_{c,ij,22} & dM_{c,ij,23} \\ dM_{c,ij,31} & dM_{c,ij,32} & dM_{c,ij,33} \end{pmatrix} = \begin{pmatrix} K_{c,ij,X} & \psi_{c,ij} + \varepsilon_{c,ij} & -\theta_{c,ij} + \eta_{c,ij} \\ -\psi_{c,ij} + \varepsilon_{c,ij} & K_{c,ij,Y} & \phi_{c,ij} + \varsigma_{c,ij} \\ \theta_{c,ij} + \eta_{c,ij} & -\phi_{c,ij} + \varsigma_{c,ij} & K_{c,ij,Z} \end{pmatrix}$$

$$[dM]_{d,ij} = \begin{pmatrix} dM_{d,ij,11} & dM_{d,ij,12} & dM_{d,ij,13} \\ dM_{d,ij,21} & dM_{d,ij,22} & dM_{d,ij,23} \\ dM_{d,ij,31} & dM_{d,ij,32} & dM_{d,ij,33} \end{pmatrix} = \begin{pmatrix} K_{d,ij,X} & \psi_{d,ij} + \varepsilon_{d,ij} & -\theta_{d,ij} + \eta_{d,ij} \\ -\psi_{d,ij} + \varepsilon_{d,ij} & K_{d,ij,Y} & \phi_{d,ij} + \varsigma_{d,ij} \\ \theta_{d,ij} + \eta_{d,ij} & -\phi_{d,ij} + \varsigma_{d,ij} & K_{d,ij,Z} \end{pmatrix}$$

with

$1 + K_{c,ij,X} (K_{d,ij,X})$: common (differential) scale factor of the accelerometer pair A_i, A_j along the X axis of the

$$\text{OAGRF: } 1 + K_{c,ij,X} = 1 + \frac{1}{2} (K_{i,X} + K_{j,X}), K_{d,ij,X} = \frac{1}{2} (K_{i,X} - K_{j,X}), \dots$$

$\phi_{c,ij} (\phi_{d,ij})$: common (differential) misalignment of the accelerometer pair A_i, A_j about the X axis of their OAGRF, ...

$\varsigma_{c,ij} (\varsigma_{d,ij})$: component along the X axis of the OAGRF of the common (differential) coupling among the axes of the accelerometer pair A_i, A_j , ...

For the adopted definition of the OAGRF (linked to the accelerometer centers), the common misalignment $\phi_{c,ij}$, $\theta_{c,ij}$, $\psi_{c,ij}$ include also the contribution of possible relative misalignments between two accelerometers of the same pair along the axes perpendicular to the OAG baseline (see [RD 1]).

The Quadratic Factor Matrix is built with the common and differential quadratic factors (also denoted as $K2$, for short) an accelerometer pair (a Quadratic Factor Matrix is defined for each One Axis Gradiometer):

$$K2_{ij} \equiv \begin{pmatrix} [K2]_{+,ij} & [K2]_{-,ij} \\ [K2]_{+,ij} & -[K2]_{-,ij} \end{pmatrix} = \begin{pmatrix} K2_{c,ij,X} + K2_{d,ij,X} & 0 & 0 & K2_{c,ij,X} - K2_{d,ij,X} & 0 & 0 \\ 0 & K2_{c,ij,Y} + K2_{d,ij,Y} & 0 & 0 & K2_{c,ij,Y} - K2_{d,ij,Y} & 0 \\ 0 & 0 & K2_{c,ij,Z} + K2_{d,ij,Z} & 0 & 0 & K2_{c,ij,Z} - K2_{d,ij,Z} \\ K2_{c,ij,X} + K2_{d,ij,X} & 0 & 0 & K2_{d,ij,X} - K2_{c,ij,X} & 0 & 0 \\ 0 & K2_{c,ij,Y} + K2_{d,ij,Y} & 0 & 0 & K2_{d,ij,Y} - K2_{c,ij,Y} & 0 \\ 0 & 0 & K2_{c,ij,Z} + K2_{d,ij,Z} & 0 & 0 & K2_{d,ij,Z} - K2_{c,ij,Z} \end{pmatrix}$$

with

$K2_{c,ij,X} (K2_{d,ij,X})$: common (differential) quadratic factor of the accelerometer pair A_i, A_j along the X axis of the OAGRF, ...

With this definition of $K2_{ij}$, the term $\frac{1}{2} K2_{ij} \begin{pmatrix} (\underline{a}_{c,ij} + \underline{a}_{d,ij})^2 \\ (\underline{a}_{c,ij} - \underline{a}_{d,ij})^2 \end{pmatrix}$ in the (3.1.1) expands as:

$$\frac{1}{2} K 2_{ij} \begin{pmatrix} (a_{c,ij} + a_{d,ij})^2 \\ (a_{c,ij} - a_{d,ij})^2 \end{pmatrix} = \frac{1}{2} K 2_{ij} \begin{pmatrix} (a_{c,ij,X} + a_{d,ij,X})^2 \\ (a_{c,ij,Y} + a_{d,ij,Y})^2 \\ (a_{c,ij,Z} + a_{d,ij,Z})^2 \\ (a_{c,ij,X} - a_{d,ij,X})^2 \\ (a_{c,ij,Y} - a_{d,ij,Y})^2 \\ (a_{c,ij,Z} - a_{d,ij,Z})^2 \end{pmatrix} = \begin{pmatrix} (a_{c,ij,X}^2 + a_{d,ij,X}^2) K 2_{c,ij,X} + 2 \cdot K 2_{d,ij,X} a_{c,ij,X} a_{d,ij,X} \\ (a_{c,ij,Y}^2 + a_{d,ij,Y}^2) K 2_{c,ij,Y} + 2 \cdot K 2_{d,ij,Y} a_{c,ij,Y} a_{d,ij,Y} \\ (a_{c,ij,Z}^2 + a_{d,ij,Z}^2) K 2_{c,ij,Z} + 2 \cdot K 2_{d,ij,Z} a_{c,ij,Z} a_{d,ij,Z} \\ (a_{c,ij,X}^2 + a_{d,ij,X}^2) K 2_{d,ij,X} + 2 \cdot K 2_{c,ij,X} a_{c,ij,X} a_{d,ij,X} \\ (a_{c,ij,Y}^2 + a_{d,ij,Y}^2) K 2_{d,ij,Y} + 2 \cdot K 2_{c,ij,Y} a_{c,ij,Y} a_{d,ij,Y} \\ (a_{c,ij,Z}^2 + a_{d,ij,Z}^2) K 2_{d,ij,Z} + 2 \cdot K 2_{c,ij,Z} a_{c,ij,Z} a_{d,ij,Z} \end{pmatrix}$$

The original differential mode acceleration experienced by the accelerometer proof masses in the OAGRFs, from which the GGT components are derived, are recovered from the measured common and differential mode accelerations by inverting the relationship (3.1), neglecting the contribution of the quadratic term and of the accelerometer bias and noise

$$\begin{pmatrix} a_{c,ij} \\ a_{d,ij} \end{pmatrix} = \mathbf{M}_{ij}^{-1} \begin{pmatrix} a'_{c,ij} \\ a'_{d,ij} \end{pmatrix} \equiv \mathbf{M}_{ij} \begin{pmatrix} a'_{c,ij} \\ a'_{d,ij} \end{pmatrix}, \quad (3.2)$$

where $\mathbf{M}_{ij} \equiv \mathbf{M}_{ij}^{-1}$ denotes the inverse Calibration Matrix:

$$\mathbf{M}_{ij} = \begin{pmatrix} \mathbf{M}_{ij,11} & \mathbf{M}_{ij,12} & \mathbf{M}_{ij,13} & \mathbf{M}_{ij,14} & \mathbf{M}_{ij,15} & \mathbf{M}_{ij,16} \\ \mathbf{M}_{ij,21} & \mathbf{M}_{ij,22} & \mathbf{M}_{ij,23} & \mathbf{M}_{ij,24} & \mathbf{M}_{ij,25} & \mathbf{M}_{ij,26} \\ \mathbf{M}_{ij,31} & \mathbf{M}_{ij,32} & \mathbf{M}_{ij,33} & \mathbf{M}_{ij,34} & \mathbf{M}_{ij,35} & \mathbf{M}_{ij,36} \\ \mathbf{M}_{ij,41} & \mathbf{M}_{ij,42} & \mathbf{M}_{ij,43} & \mathbf{M}_{ij,44} & \mathbf{M}_{ij,45} & \mathbf{M}_{ij,46} \\ \mathbf{M}_{ij,51} & \mathbf{M}_{ij,52} & \mathbf{M}_{ij,53} & \mathbf{M}_{ij,54} & \mathbf{M}_{ij,55} & \mathbf{M}_{ij,56} \\ \mathbf{M}_{ij,61} & \mathbf{M}_{ij,62} & \mathbf{M}_{ij,63} & \mathbf{M}_{ij,64} & \mathbf{M}_{ij,65} & \mathbf{M}_{ij,66} \end{pmatrix} = ([1]_6 + d\mathbf{M}_{ij})^{-1} \equiv [1]_6 - d\mathbf{M}_{ij}$$

By introducing for \mathbf{M}_{ij} the block form

$$\mathbf{M}_{ij} = \begin{pmatrix} [\mathbf{M}']_{c,ij} & [\mathbf{M}']_{d,ij} \\ [\mathbf{M}]_{d,ij} & [\mathbf{M}]_{c,ij} \end{pmatrix},$$

the (3.2) can be expanded as:

$$\underline{a}_{c,ij} = [\mathbf{M}']_{c,ij} \underline{a}'_{c,ij} + [\mathbf{M}']_{d,ij} \underline{a}'_{d,ij} \quad , \quad \underline{a}_{d,ij} = [\mathbf{M}]_{d,ij} \underline{a}'_{c,ij} + [\mathbf{M}]_{c,ij} \underline{a}'_{d,ij} .$$

Only the 3×3 sub-matrices $[\mathbf{M}]_{d,ij}$, $[\mathbf{M}]_{c,ij}$ including the elements of the last three rows of \mathbf{M}_{ij} need to be known in order to recover the original differential mode accelerations.

The quadratic factors of each accelerometer ($K2_{i,X}$, $K2_{i,Y}$, $K2_{i,Z}$) can be physically adjusted by operating on the numerical bias of the loop which controls the position of the accelerometer proof mass inside the electrode cage. So it is possible to change (reduce) the value of the common and differential quadratic factors of the three accelerometer pairs after the Gradiometer assembly.

On the other hand, it is not possible to modify the values of the accelerometer scale factors, couplings among the sensitive axes and orientations in the respective OAGs, after the accelerometer manufacturing and the Gradiometer assembly. The actual value of the elements of the calibration matrices along the in-orbit mission lifetime is thus determined by the result of the manufacturing/integration process and by the further modifications that they can suffer during the ground testing and handling, during the launch, and during the time spent on orbit.

3.1.1 Limit Values of the Calibration Matrix Elements and of Quadratic Factors

The limits specified in [RD 2] for the values of the common and differential scale factors, misalignment and coupling among the axes of the three accelerometer pair (and consequently for the values of the Calibration Matrices elements) not to be exceeded all along the GOCE on-orbit mission lifetime are in Table 3.1-1. The design and implementation of the accelerometers and of the Gradiometer shall guarantee that, as consequence of all the manufacturing/integration processes, ground activities, launch, on orbit lifetime effects, these limits are not exceeded. This is confirmed by the results of the current prediction of the in-flight performance of the Gradiometer [RD 11].

Sensor Pair	OAG Axis	Common, Differential Scale Factor	Common, Differential Misalignment + Coupling [rad]	
A ₁ , A ₄	X ↑ U	$K_{c,14,X}, K_{d,14,X} < 4.05 \cdot 10^{-3}$	$(\psi_{c,14} + \epsilon_{c,14}), (-\theta_{c,14} + \eta_{c,14}), (\psi_{d,14} + \epsilon_{d,14}), (-\theta_{d,14} + \eta_{d,14}) < 1.3 \cdot 10^{-4}$	
	Y → L	$K_{c,14,Y}, K_{d,14,Y} < 5.18 \cdot 10^{-2}$	$(-\psi_{c,14} + \epsilon_{c,14}), (-\psi_{d,14} + \epsilon_{d,14}), (\phi_{d,14} + \zeta_{d,14}) < 1.3 \cdot 10^{-4}$ $(\phi_{c,14} + \zeta_{c,14}) = \zeta_{c,14} < 1.0 \cdot 10^{-5}$ (for the OAGRF ₁ definition)	
	Z → U	$K_{c,14,Z}, K_{d,14,Z} < 4.05 \cdot 10^{-3}$	$(\theta_{c,14} + \eta_{c,14}), (\theta_{d,14} + \eta_{d,14}), (-\phi_{d,14} + \zeta_{d,14}) < 1.3 \cdot 10^{-4}$ $(-\phi_{c,14} + \zeta_{c,14}) = \zeta_{c,14} < 1.0 \cdot 10^{-5}$ (for the OAGRF ₁ definition)	
A ₂ , A ₅	X _i → U	$K_{c,25,X}, K_{d,25,X} < 4.05 \cdot 10^{-3}$	$(\psi_{c,25} + \epsilon_{c,25}), (\psi_{d,25} + \epsilon_{d,25}), (-\theta_{d,25} + \eta_{d,25}) < 1.3 \cdot 10^{-4}$ $(-\theta_{c,25} + \eta_{c,25}) = \eta_{c,25} < 1.0 \cdot 10^{-5}$ (for the OAGRF ₂ definition)	
	Y _i ↑ U	$K_{c,25,Y}, K_{d,25,Y} < 4.05 \cdot 10^{-3}$	$(-\psi_{c,25} + \epsilon_{c,25}), (\phi_{c,25} + \zeta_{c,25}), (-\psi_{d,25} + \epsilon_{d,25}), (\phi_{d,25} + \zeta_{d,25}) < 1.3 \cdot 10^{-4}$	
	Z _i → L	$K_{c,25,Z}, K_{d,25,Z} < 5.18 \cdot 10^{-2}$	$(-\phi_{c,25} + \zeta_{c,25}), (\theta_{d,25} + \eta_{d,25}), (-\phi_{d,25} + \zeta_{d,25}) < 1.3 \cdot 10^{-4}$ $(\theta_{c,25} + \eta_{c,25}) = \eta_{c,25} < 1.0 \cdot 10^{-5}$ (for the OAGRF ₂ definition)	
A ₃ , A ₆	X _i → U	$K_{c,36,X}, K_{d,36,X} < 4.05 \cdot 10^{-3}$	$(-\theta_{c,36} + \eta_{c,36}), (\psi_{d,36} + \epsilon_{d,36}), (-\theta_{d,36} + \eta_{d,36}) < 1.3 \cdot 10^{-4}$ $(\psi_{c,36} + \epsilon_{c,36}) = \epsilon_{c,36} < 1.0 \cdot 10^{-5}$ (for the OAGRF ₃ definition)	
	Y _i → L	$K_{c,36,Y}, K_{d,36,Y} < 5.18 \cdot 10^{-2}$	$(\phi_{c,36} + \zeta_{c,36}), (-\psi_{d,36} + \epsilon_{d,36}), (\phi_{d,36} + \zeta_{d,36}) < 1.3 \cdot 10^{-4}$ $(-\psi_{c,36} + \epsilon_{c,36}) = \epsilon_{c,36} < 1.0 \cdot 10^{-5}$ (for the OAGRF ₃ definition)	
	Z _i ↑ U	$K_{c,36,Z}, K_{d,36,Z} < 4.05 \cdot 10^{-3}$	$(\theta_{c,36} + \eta_{c,36}), (-\phi_{c,36} + \zeta_{c,36}), (\theta_{d,36} + \eta_{d,36}), (-\phi_{d,36} + \zeta_{d,36}) < 1.3 \cdot 10^{-4}$	

↑ : in-line axis, aligned to the baseline of the OAG to which the accelerometer belongs

→ : transversal axis, perpendicular to the baseline of the OAG to which the accelerometer belongs

U : accelerometer ultra sensitive axis, L : accelerometer less sensitive axis

[dM] _{c,14}			[dM] _{d,14}		
$dM_{c,14,11} < 4.05 \cdot 10^{-3}$	$dM_{c,14,12} < 1.3 \cdot 10^{-4}$	$dM_{c,14,13} < 1.3 \cdot 10^{-4}$	$dM_{d,14,11} < 4.05 \cdot 10^{-3}$	$dM_{d,14,12} < 1.3 \cdot 10^{-4}$	$dM_{d,14,13} < 1.3 \cdot 10^{-4}$
$dM_{c,14,21} < 1.3 \cdot 10^{-4}$	$dM_{c,14,22} < 5.18 \cdot 10^{-2}$	$dM_{c,14,23} < 1.0 \cdot 10^{-5}$	$dM_{d,14,21} < 1.3 \cdot 10^{-4}$	$dM_{d,14,22} < 5.18 \cdot 10^{-2}$	$dM_{d,14,23} < 1.3 \cdot 10^{-4}$
$dM_{c,14,31} < 1.3 \cdot 10^{-4}$	$dM_{c,14,32} < 1.0 \cdot 10^{-5}$	$dM_{c,14,33} < 4.05 \cdot 10^{-3}$	$dM_{d,14,31} < 1.3 \cdot 10^{-4}$	$dM_{d,14,32} < 1.3 \cdot 10^{-4}$	$dM_{d,14,33} < 4.05 \cdot 10^{-3}$

[dM] _{c,25}			[dM] _{d,25}		
$dM_{c,25,11} < 4.05 \cdot 10^{-3}$	$dM_{c,25,12} < 1.3 \cdot 10^{-4}$	$dM_{c,25,13} < 1.0 \cdot 10^{-5}$	$dM_{d,25,11} < 4.05 \cdot 10^{-3}$	$dM_{d,25,12} < 1.3 \cdot 10^{-4}$	$dM_{d,25,13} < 1.3 \cdot 10^{-4}$
$dM_{c,25,21} < 1.3 \cdot 10^{-4}$	$dM_{c,25,22} < 4.05 \cdot 10^{-3}$	$dM_{c,25,23} < 1.3 \cdot 10^{-4}$	$dM_{d,25,21} < 1.3 \cdot 10^{-4}$	$dM_{d,25,22} < 4.05 \cdot 10^{-3}$	$dM_{d,25,23} < 1.3 \cdot 10^{-4}$
$dM_{c,25,31} < 1.0 \cdot 10^{-5}$	$dM_{c,25,32} < 1.3 \cdot 10^{-4}$	$dM_{c,25,33} < 5.18 \cdot 10^{-2}$	$dM_{d,25,31} < 1.3 \cdot 10^{-4}$	$dM_{d,25,32} < 1.3 \cdot 10^{-4}$	$dM_{d,25,33} < 5.18 \cdot 10^{-2}$

[dM] _{c,36}			[dM] _{d,36}		
$dM_{c,36,11} < 4.05 \cdot 10^{-3}$	$dM_{c,36,12} < 1.0 \cdot 10^{-5}$	$dM_{c,36,13} < 1.3 \cdot 10^{-4}$	$dM_{d,36,11} < 4.05 \cdot 10^{-3}$	$dM_{d,36,12} < 1.3 \cdot 10^{-4}$	$dM_{d,36,13} < 1.3 \cdot 10^{-4}$
$dM_{c,36,21} < 1.0 \cdot 10^{-5}$	$dM_{c,36,22} < 5.18 \cdot 10^{-2}$	$dM_{c,36,23} < 1.3 \cdot 10^{-4}$	$dM_{d,36,21} < 1.3 \cdot 10^{-4}$	$dM_{d,36,22} < 5.18 \cdot 10^{-2}$	$dM_{d,36,23} < 1.3 \cdot 10^{-4}$
$dM_{c,36,31} < 1.3 \cdot 10^{-4}$	$dM_{c,36,32} < 1.3 \cdot 10^{-4}$	$dM_{c,36,33} < 4.05 \cdot 10^{-3}$	$dM_{d,36,31} < 1.3 \cdot 10^{-4}$	$dM_{d,36,32} < 1.3 \cdot 10^{-4}$	$dM_{d,36,33} < 4.05 \cdot 10^{-3}$

Table 3.1-1: Upper limits of the common and differential scale factors, misalignment and coupling of the three accelerometer pairs, and of the elements of dM_{ij} not to be exceeded all along the GOCE on-orbit mission lifetime

By introducing the upper limits of the elements of M_{ij} in the expansion of $([I]_6 + dM_{ij})^{-1}$, we can write the following relationships between dM_{ij} and M_{ij} :

$$\mathbf{MI}_{ij} = [1]_6 - d\mathbf{M}_{ij} + \Delta\mathbf{MI}_{ij}$$

$$\begin{pmatrix} MI_{ij,11} & MI_{ij,12} & MI_{ij,13} & MI_{ij,14} & MI_{ij,15} & MI_{ij,16} \\ MI_{ij,21} & MI_{ij,22} & MI_{ij,23} & MI_{ij,24} & MI_{ij,25} & MI_{ij,26} \\ MI_{ij,31} & MI_{ij,32} & MI_{ij,33} & MI_{ij,34} & MI_{ij,35} & MI_{ij,36} \\ MI_{ij,41} & MI_{ij,42} & MI_{ij,43} & MI_{ij,44} & MI_{ij,45} & MI_{ij,46} \\ MI_{ij,51} & MI_{ij,52} & MI_{ij,53} & MI_{ij,54} & MI_{ij,55} & MI_{ij,56} \\ MI_{ij,61} & MI_{ij,62} & MI_{ij,63} & MI_{ij,64} & MI_{ij,65} & MI_{ij,66} \end{pmatrix} = \begin{pmatrix} 1 - dM_{c,ij,11} & -dM_{c,ij,12} & -dM_{c,ij,13} & -dM_{d,ij,11} & -dM_{d,ij,12} & -dM_{d,ij,13} \\ -dM_{c,ij,21} & 1 - dM_{c,ij,22} & -dM_{c,ij,23} & -dM_{d,ij,21} & -dM_{d,ij,22} & -dM_{d,ij,23} \\ -dM_{c,ij,31} & -dM_{c,ij,32} & 1 - dM_{c,ij,33} & -dM_{d,ij,31} & -dM_{d,ij,32} & -dM_{d,ij,33} \\ -dM_{d,ij,11} & -dM_{d,ij,12} & -dM_{d,ij,13} & 1 - dM_{c,ij,11} & -dM_{c,ij,12} & -dM_{c,ij,13} \\ -dM_{d,ij,21} & -dM_{d,ij,22} & -dM_{d,ij,23} & -dM_{c,ij,21} & 1 - dM_{c,ij,22} & -dM_{c,ij,23} \\ -dM_{d,ij,31} & -dM_{d,ij,32} & -dM_{d,ij,33} & -dM_{c,ij,31} & -dM_{c,ij,32} & 1 - dM_{c,ij,33} \end{pmatrix} + \begin{pmatrix} \Delta MI_{ij,11} & \Delta MI_{ij,12} & \Delta MI_{ij,13} & \Delta MI_{ij,14} & \Delta MI_{ij,15} & \Delta MI_{ij,16} \\ \Delta MI_{ij,21} & \Delta MI_{ij,22} & \Delta MI_{ij,23} & \Delta MI_{ij,24} & \Delta MI_{ij,25} & \Delta MI_{ij,26} \\ \Delta MI_{ij,31} & \Delta MI_{ij,32} & \Delta MI_{ij,33} & \Delta MI_{ij,34} & \Delta MI_{ij,35} & \Delta MI_{ij,36} \\ \Delta MI_{ij,41} & \Delta MI_{ij,42} & \Delta MI_{ij,43} & \Delta MI_{ij,44} & \Delta MI_{ij,45} & \Delta MI_{ij,46} \\ \Delta MI_{ij,51} & \Delta MI_{ij,52} & \Delta MI_{ij,53} & \Delta MI_{ij,54} & \Delta MI_{ij,55} & \Delta MI_{ij,56} \\ \Delta MI_{ij,61} & \Delta MI_{ij,62} & \Delta MI_{ij,63} & \Delta MI_{ij,64} & \Delta MI_{ij,65} & \Delta MI_{ij,66} \end{pmatrix} \quad (3.3)$$

with

$\Delta MI_{14,11} < 3.3 \cdot 10^{-5}$	$\Delta MI_{14,12} < 1.6 \cdot 10^{-5}$	$\Delta MI_{14,13} < 2.2 \cdot 10^{-6}$	$\Delta MI_{14,14} < 3.3 \cdot 10^{-5}$	$\Delta MI_{14,15} < 1.6 \cdot 10^{-5}$	$\Delta MI_{14,16} < 2.2 \cdot 10^{-6}$
$\Delta MI_{14,21} < 1.6 \cdot 10^{-5}$	$\Delta MI_{14,22} < 5.9 \cdot 10^{-3}$	$\Delta MI_{14,23} < 8.7 \cdot 10^{-6}$	$\Delta MI_{14,24} < 1.6 \cdot 10^{-5}$	$\Delta MI_{14,25} < 5.9 \cdot 10^{-3}$	$\Delta MI_{14,26} < 8.7 \cdot 10^{-6}$
$\Delta MI_{14,31} < 2.2 \cdot 10^{-6}$	$\Delta MI_{14,32} < 8.7 \cdot 10^{-6}$	$\Delta MI_{14,33} < 3.3 \cdot 10^{-5}$	$\Delta MI_{14,34} < 2.2 \cdot 10^{-6}$	$\Delta MI_{14,35} < 8.7 \cdot 10^{-6}$	$\Delta MI_{14,36} < 3.3 \cdot 10^{-5}$
$\Delta MI_{14,41} < 3.3 \cdot 10^{-5}$	$\Delta MI_{14,42} < 1.6 \cdot 10^{-5}$	$\Delta MI_{14,43} < 2.2 \cdot 10^{-6}$	$\Delta MI_{14,44} < 3.3 \cdot 10^{-5}$	$\Delta MI_{14,45} < 1.6 \cdot 10^{-5}$	$\Delta MI_{14,46} < 2.2 \cdot 10^{-6}$
$\Delta MI_{14,51} < 1.6 \cdot 10^{-5}$	$\Delta MI_{14,52} < 5.9 \cdot 10^{-3}$	$\Delta MI_{14,53} < 8.7 \cdot 10^{-6}$	$\Delta MI_{14,54} < 1.6 \cdot 10^{-5}$	$\Delta MI_{14,55} < 5.9 \cdot 10^{-3}$	$\Delta MI_{14,56} < 8.7 \cdot 10^{-6}$
$\Delta MI_{14,61} < 2.2 \cdot 10^{-6}$	$\Delta MI_{14,62} < 8.7 \cdot 10^{-6}$	$\Delta MI_{14,63} < 3.3 \cdot 10^{-5}$	$\Delta MI_{14,64} < 2.2 \cdot 10^{-6}$	$\Delta MI_{14,65} < 8.7 \cdot 10^{-6}$	$\Delta MI_{14,66} < 3.3 \cdot 10^{-5}$

$\Delta MI_{25,11} < 3.3 \cdot 10^{-5}$	$\Delta MI_{25,12} < 2.2 \cdot 10^{-6}$	$\Delta MI_{25,13} < 8.7 \cdot 10^{-6}$	$\Delta MI_{25,14} < 3.3 \cdot 10^{-5}$	$\Delta MI_{25,15} < 2.2 \cdot 10^{-6}$	$\Delta MI_{25,16} < 8.7 \cdot 10^{-6}$
$\Delta MI_{25,21} < 2.2 \cdot 10^{-6}$	$\Delta MI_{25,22} < 3.3 \cdot 10^{-5}$	$\Delta MI_{25,23} < 1.6 \cdot 10^{-5}$	$\Delta MI_{25,24} < 2.2 \cdot 10^{-6}$	$\Delta MI_{25,25} < 3.3 \cdot 10^{-5}$	$\Delta MI_{25,26} < 1.6 \cdot 10^{-5}$
$\Delta MI_{25,31} < 8.7 \cdot 10^{-6}$	$\Delta MI_{25,32} < 1.6 \cdot 10^{-5}$	$\Delta MI_{25,33} < 5.9 \cdot 10^{-3}$	$\Delta MI_{25,34} < 8.7 \cdot 10^{-6}$	$\Delta MI_{25,35} < 1.6 \cdot 10^{-5}$	$\Delta MI_{25,36} < 5.9 \cdot 10^{-3}$
$\Delta MI_{25,41} < 3.3 \cdot 10^{-5}$	$\Delta MI_{25,42} < 2.2 \cdot 10^{-6}$	$\Delta MI_{25,43} < 8.7 \cdot 10^{-6}$	$\Delta MI_{25,44} < 3.3 \cdot 10^{-5}$	$\Delta MI_{25,45} < 2.2 \cdot 10^{-6}$	$\Delta MI_{25,46} < 8.7 \cdot 10^{-6}$
$\Delta MI_{25,51} < 2.2 \cdot 10^{-6}$	$\Delta MI_{25,52} < 3.3 \cdot 10^{-5}$	$\Delta MI_{25,53} < 1.6 \cdot 10^{-5}$	$\Delta MI_{25,54} < 2.2 \cdot 10^{-6}$	$\Delta MI_{25,55} < 3.3 \cdot 10^{-5}$	$\Delta MI_{25,56} < 1.6 \cdot 10^{-5}$
$\Delta MI_{25,61} < 8.7 \cdot 10^{-6}$	$\Delta MI_{25,62} < 1.6 \cdot 10^{-5}$	$\Delta MI_{25,63} < 5.9 \cdot 10^{-3}$	$\Delta MI_{25,64} < 8.7 \cdot 10^{-6}$	$\Delta MI_{25,65} < 1.6 \cdot 10^{-5}$	$\Delta MI_{25,66} < 5.9 \cdot 10^{-3}$

$\Delta MI_{36,11} < 3.3 \cdot 10^{-5}$	$\Delta MI_{36,12} < 8.7 \cdot 10^{-6}$	$\Delta MI_{36,13} < 2.2 \cdot 10^{-6}$	$\Delta MI_{36,14} < 3.3 \cdot 10^{-5}$	$\Delta MI_{36,15} < 8.7 \cdot 10^{-6}$	$\Delta MI_{36,16} < 2.2 \cdot 10^{-6}$
$\Delta MI_{36,21} < 8.7 \cdot 10^{-6}$	$\Delta MI_{36,22} < 5.9 \cdot 10^{-3}$	$\Delta MI_{36,23} < 1.6 \cdot 10^{-5}$	$\Delta MI_{36,24} < 8.7 \cdot 10^{-6}$	$\Delta MI_{36,25} < 5.9 \cdot 10^{-3}$	$\Delta MI_{36,26} < 1.6 \cdot 10^{-5}$
$\Delta MI_{36,31} < 2.2 \cdot 10^{-6}$	$\Delta MI_{36,32} < 1.6 \cdot 10^{-5}$	$\Delta MI_{36,33} < 3.3 \cdot 10^{-5}$	$\Delta MI_{36,34} < 2.2 \cdot 10^{-6}$	$\Delta MI_{36,35} < 1.6 \cdot 10^{-5}$	$\Delta MI_{36,36} < 3.3 \cdot 10^{-5}$
$\Delta MI_{36,41} < 3.3 \cdot 10^{-5}$	$\Delta MI_{36,42} < 8.7 \cdot 10^{-6}$	$\Delta MI_{36,43} < 2.2 \cdot 10^{-6}$	$\Delta MI_{36,44} < 3.3 \cdot 10^{-5}$	$\Delta MI_{36,45} < 8.7 \cdot 10^{-6}$	$\Delta MI_{36,46} < 2.2 \cdot 10^{-6}$
$\Delta MI_{36,51} < 8.7 \cdot 10^{-6}$	$\Delta MI_{36,52} < 5.9 \cdot 10^{-3}$	$\Delta MI_{36,53} < 1.6 \cdot 10^{-5}$	$\Delta MI_{36,54} < 8.7 \cdot 10^{-6}$	$\Delta MI_{36,55} < 5.9 \cdot 10^{-3}$	$\Delta MI_{36,56} < 1.6 \cdot 10^{-5}$
$\Delta MI_{36,61} < 2.2 \cdot 10^{-6}$	$\Delta MI_{36,62} < 1.6 \cdot 10^{-5}$	$\Delta MI_{36,63} < 3.3 \cdot 10^{-5}$	$\Delta MI_{36,64} < 2.2 \cdot 10^{-6}$	$\Delta MI_{36,65} < 1.6 \cdot 10^{-5}$	$\Delta MI_{36,66} < 3.3 \cdot 10^{-5}$

By combining the (3.3) with the limit values for the elements of \mathbf{M}_{ij} provided in Table 3.1-1, we can compute the upper limits for the elements of \mathbf{MI}_{ij} which are expected not to be exceeded all along the on-orbit mission lifetime. They are provided in Table 3.1-2.

$dMI_{14,11} < 4.1 \cdot 10^{-3}$	$MI_{14,12} < 1.5 \cdot 10^{-4}$	$MI_{14,13} < 1.3 \cdot 10^{-4}$	$MI_{14,14} < 4.1 \cdot 10^{-3}$	$MI_{14,15} < 1.5 \cdot 10^{-4}$	$MI_{14,16} < 1.3 \cdot 10^{-4}$
$MI_{14,21} < 1.5 \cdot 10^{-4}$	$dMI_{14,22} < 5.8 \cdot 10^{-2}$	$MI_{14,23} < 1.9 \cdot 10^{-5}$	$MI_{14,24} < 1.5 \cdot 10^{-4}$	$MI_{14,25} < 5.8 \cdot 10^{-2}$	$MI_{14,26} < 1.4 \cdot 10^{-4}$
$MI_{14,31} < 1.3 \cdot 10^{-4}$	$MI_{14,32} < 1.9 \cdot 10^{-5}$	$dMI_{14,33} < 4.1 \cdot 10^{-3}$	$MI_{14,34} < 1.3 \cdot 10^{-4}$	$MI_{14,35} < 1.4 \cdot 10^{-4}$	$MI_{14,36} < 4.1 \cdot 10^{-3}$

$MI_{14,41} < 4.1 \cdot 10^{-3}$	$MI_{14,42} < 1.5 \cdot 10^{-4}$	$MI_{14,43} < 1.3 \cdot 10^{-4}$	$dMI_{14,44} < 4.1 \cdot 10^{-3}$	$MI_{14,45} < 1.5 \cdot 10^{-4}$	$MI_{14,46} < 1.3 \cdot 10^{-4}$
$MI_{14,51} < 1.5 \cdot 10^{-4}$	$MI_{14,52} < 5.8 \cdot 10^{-2}$	$MI_{14,53} < 1.4 \cdot 10^{-4}$	$MI_{14,54} < 1.5 \cdot 10^{-4}$	$dMI_{14,55} < 5.8 \cdot 10^{-2}$	$MI_{14,56} < 1.9 \cdot 10^{-5}$
$MI_{14,61} < 1.3 \cdot 10^{-4}$	$MI_{14,62} < 1.4 \cdot 10^{-4}$	$MI_{14,63} < 4.1 \cdot 10^{-3}$	$MI_{14,64} < 1.3 \cdot 10^{-4}$	$MI_{14,65} < 1.9 \cdot 10^{-5}$	$dMI_{14,66} < 4.1 \cdot 10^{-3}$

$dMI_{25,11} < 4.1 \cdot 10^{-3}$	$MI_{25,12} < 1.3 \cdot 10^{-4}$	$MI_{25,13} < 1.9 \cdot 10^{-5}$	$MI_{25,14} < 4.1 \cdot 10^{-3}$	$MI_{25,15} < 1.3 \cdot 10^{-4}$	$MI_{25,16} < 1.4 \cdot 10^{-4}$
$MI_{25,21} < 1.3 \cdot 10^{-4}$	$dMI_{25,22} < 4.1 \cdot 10^{-3}$	$MI_{25,23} < 1.5 \cdot 10^{-4}$	$MI_{25,24} < 1.3 \cdot 10^{-4}$	$MI_{25,25} < 4.1 \cdot 10^{-3}$	$MI_{25,26} < 1.5 \cdot 10^{-4}$
$MI_{25,31} < 1.9 \cdot 10^{-5}$	$MI_{25,32} < 1.5 \cdot 10^{-4}$	$dMI_{25,33} < 5.8 \cdot 10^{-2}$	$MI_{25,34} < 1.4 \cdot 10^{-4}$	$MI_{25,35} < 1.5 \cdot 10^{-4}$	$MI_{25,36} < 5.8 \cdot 10^{-2}$
$MI_{25,41} < 4.1 \cdot 10^{-3}$	$MI_{25,42} < 1.3 \cdot 10^{-4}$	$MI_{25,43} < 1.4 \cdot 10^{-4}$	$dMI_{25,44} < 4.1 \cdot 10^{-3}$	$MI_{25,45} < 1.3 \cdot 10^{-4}$	$MI_{25,46} < 1.9 \cdot 10^{-5}$
$MI_{25,51} < 1.3 \cdot 10^{-4}$	$MI_{25,52} < 4.1 \cdot 10^{-3}$	$MI_{25,53} < 1.5 \cdot 10^{-4}$	$MI_{25,54} < 1.3 \cdot 10^{-4}$	$dMI_{25,55} < 4.1 \cdot 10^{-3}$	$MI_{25,56} < 1.5 \cdot 10^{-4}$
$MI_{25,61} < 1.4 \cdot 10^{-4}$	$MI_{25,62} < 1.5 \cdot 10^{-4}$	$MI_{25,63} < 5.8 \cdot 10^{-2}$	$MI_{25,64} < 1.9 \cdot 10^{-5}$	$MI_{25,65} < 1.5 \cdot 10^{-4}$	$dMI_{25,66} < 5.8 \cdot 10^{-2}$

$dMI_{36,11} < 4.1 \cdot 10^{-3}$	$MI_{36,12} < 1.9 \cdot 10^{-5}$	$MI_{36,13} < 1.3 \cdot 10^{-4}$	$MI_{36,14} < 4.1 \cdot 10^{-3}$	$MI_{36,15} < 1.4 \cdot 10^{-4}$	$MI_{36,16} < 1.3 \cdot 10^{-4}$
$MI_{36,21} < 1.9 \cdot 10^{-5}$	$dMI_{36,22} < 5.8 \cdot 10^{-2}$	$MI_{36,23} < 1.5 \cdot 10^{-4}$	$MI_{36,24} < 1.4 \cdot 10^{-4}$	$MI_{36,25} < 5.8 \cdot 10^{-2}$	$MI_{36,26} < 1.5 \cdot 10^{-4}$
$MI_{36,31} < 1.3 \cdot 10^{-4}$	$MI_{36,32} < 1.5 \cdot 10^{-4}$	$dMI_{36,33} < 4.1 \cdot 10^{-3}$	$MI_{36,34} < 1.3 \cdot 10^{-4}$	$MI_{36,35} < 1.5 \cdot 10^{-4}$	$MI_{36,36} < 4.1 \cdot 10^{-3}$
$MI_{36,41} < 4.1 \cdot 10^{-3}$	$MI_{36,42} < 1.4 \cdot 10^{-4}$	$MI_{36,43} < 1.3 \cdot 10^{-4}$	$dMI_{36,44} < 4.1 \cdot 10^{-3}$	$MI_{36,45} < 1.9 \cdot 10^{-5}$	$MI_{36,46} < 1.3 \cdot 10^{-4}$
$MI_{36,51} < 1.4 \cdot 10^{-4}$	$MI_{36,52} < 5.8 \cdot 10^{-2}$	$MI_{36,53} < 1.5 \cdot 10^{-4}$	$MI_{36,54} < 1.9 \cdot 10^{-5}$	$dMI_{36,55} < 5.8 \cdot 10^{-2}$	$MI_{36,56} < 1.5 \cdot 10^{-4}$
$MI_{36,61} < 1.3 \cdot 10^{-4}$	$MI_{36,62} < 1.5 \cdot 10^{-4}$	$MI_{36,63} < 4.1 \cdot 10^{-3}$	$MI_{36,64} < 1.3 \cdot 10^{-4}$	$MI_{36,65} < 1.5 \cdot 10^{-4}$	$dMI_{36,66} < 4.1 \cdot 10^{-3}$

$dMI_{ij,kk}$ = difference from unity of $MI_{ij,kk}$ ($MI_{ij,kk} = 1 + dMI_{ij,kk}$, $ij=14, 25, 36$, $k = 1, 2, 3, 4, 5, 6$)

Table 3.1-2: Expected upper limits for the values of the elements of MI_{ij} , all along the on-orbit mission lifetime

From the previous relationships between MI_{ij} and M_{ij} , following relationships are obtained between the sub-matrices of MI_{ij} :

$$[MI']_{c,ij} = [MI]_{c,ij} + [\Delta MI]_{c,ij}, \quad [MI']_{d,ij} = [MI]_{d,ij} + [\Delta MI]_{d,ij} \quad (3.4)$$

$$\begin{pmatrix} MI_{ij,11} & MI_{ij,12} & MI_{ij,13} \\ MI_{ij,21} & MI_{ij,22} & MI_{ij,23} \\ MI_{ij,31} & MI_{ij,32} & MI_{ij,33} \end{pmatrix} = \begin{pmatrix} MI_{ij,44} & MI_{ij,45} & MI_{ij,46} \\ MI_{ij,54} & MI_{ij,55} & MI_{ij,56} \\ MI_{ij,64} & MI_{ij,65} & MI_{ij,66} \end{pmatrix} + \begin{pmatrix} \Delta MI_{c,ij,11} & \Delta MI_{c,ij,12} & \Delta MI_{c,ij,13} \\ \Delta MI_{c,ij,21} & \Delta MI_{c,ij,22} & \Delta MI_{c,ij,23} \\ \Delta MI_{c,ij,31} & \Delta MI_{c,ij,32} & \Delta MI_{c,ij,33} \end{pmatrix},$$

$$\begin{pmatrix} MI_{ij,14} & MI_{ij,15} & MI_{ij,16} \\ MI_{ij,24} & MI_{ij,25} & MI_{ij,26} \\ MI_{ij,34} & MI_{ij,35} & MI_{ij,36} \end{pmatrix} = \begin{pmatrix} MI_{ij,41} & MI_{ij,42} & MI_{ij,43} \\ MI_{ij,51} & MI_{ij,52} & MI_{ij,53} \\ MI_{ij,61} & MI_{ij,62} & MI_{ij,63} \end{pmatrix} + \begin{pmatrix} \Delta MI_{d,ij,11} & \Delta MI_{d,ij,12} & \Delta MI_{d,ij,13} \\ \Delta MI_{d,ij,21} & \Delta MI_{d,ij,22} & \Delta MI_{d,ij,23} \\ \Delta MI_{d,ij,31} & \Delta MI_{d,ij,32} & \Delta MI_{d,ij,33} \end{pmatrix}$$

with

$\Delta MI_{c,14,11} = \Delta MI_{d,14,11} =$ $\Delta MI_{14,11} + \Delta MI_{14,44} < 6.6 \cdot 10^{-5}$	$\Delta MI_{c,14,12} = \Delta MI_{d,14,12} =$ $\Delta MI_{14,12} + \Delta MI_{14,45} < 3.2 \cdot 10^{-5}$	$\Delta MI_{c,14,13} = \Delta MI_{d,14,13} =$ $\Delta MI_{14,13} + \Delta MI_{14,46} < 4.4 \cdot 10^{-6}$
$\Delta MI_{c,14,21} = \Delta MI_{d,14,21} =$ $\Delta MI_{14,21} + \Delta MI_{14,54} < 3.2 \cdot 10^{-5}$	$\Delta MI_{c,14,22} = \Delta MI_{d,14,22} =$ $\Delta MI_{14,22} + \Delta MI_{14,55} < 1.2 \cdot 10^{-2}$	$MI_{c,14,23} = MI_{d,14,23} =$ $\Delta MI_{14,23} + \Delta MI_{14,56} < 1.7 \cdot 10^{-5}$
$\Delta MI_{c,14,31} = \Delta MI_{d,14,31} =$ $\Delta MI_{14,31} + \Delta MI_{14,64} < 4.4 \cdot 10^{-6}$	$\Delta MI_{c,14,32} = \Delta MI_{d,14,32} =$ $\Delta MI_{14,32} + \Delta MI_{14,65} < 1.7 \cdot 10^{-5}$	$\Delta MI_{c,14,33} = \Delta MI_{d,14,33} =$ $\Delta MI_{14,33} + \Delta MI_{14,66} < 6.6 \cdot 10^{-5}$

$\Delta MI_{c,25,11} = \Delta MI_{d,25,11} =$ $\Delta MI_{25,11} + \Delta MI_{25,44} < 6.6 \cdot 10^{-5}$	$\Delta MI_{c,25,12} = \Delta MI_{d,25,12} =$ $\Delta MI_{25,12} + \Delta MI_{25,45} < 4.4 \cdot 10^{-6}$	$\Delta MI_{c,25,13} = \Delta MI_{d,25,13} =$ $\Delta MI_{25,13} + \Delta MI_{25,46} < 1.7 \cdot 10^{-5}$
$\Delta MI_{c,25,21} = \Delta MI_{d,25,21} =$ $\Delta MI_{25,21} + \Delta MI_{25,54} < 4.4 \cdot 10^{-6}$	$\Delta MI_{c,25,22} = \Delta MI_{d,25,22} =$ $\Delta MI_{25,22} + \Delta MI_{25,55} < 6.6 \cdot 10^{-5}$	$MI_{c,25,23} = MI_{d,25,23} =$ $\Delta MI_{25,23} + \Delta MI_{25,56} < 3.2 \cdot 10^{-5}$
$\Delta MI_{c,25,31} = \Delta MI_{d,25,31} =$ $\Delta MI_{25,31} + \Delta MI_{25,64} < 1.7 \cdot 10^{-5}$	$\Delta MI_{c,25,32} = \Delta MI_{d,25,32} =$ $\Delta MI_{25,32} + \Delta MI_{25,65} < 3.2 \cdot 10^{-5}$	$\Delta MI_{c,25,33} = \Delta MI_{d,25,33} =$ $\Delta MI_{25,33} + \Delta MI_{25,66} < 1.2 \cdot 10^{-2}$

$\Delta MI_{c,36,11} = \Delta MI_{d,36,11} =$ $\Delta MI_{36,11} + \Delta MI_{36,44} < 6.6 \cdot 10^{-5}$	$\Delta MI_{c,36,12} = \Delta MI_{d,36,12} =$ $\Delta MI_{36,12} + \Delta MI_{36,45} < 1.7 \cdot 10^{-5}$	$\Delta MI_{c,36,13} = \Delta MI_{d,36,13} =$ $\Delta MI_{36,13} + \Delta MI_{36,46} < 4.4 \cdot 10^{-6}$
$\Delta MI_{c,36,21} = \Delta MI_{d,36,21} =$ $\Delta MI_{36,21} + \Delta MI_{36,54} < 1.7 \cdot 10^{-5}$	$\Delta MI_{c,36,22} = \Delta MI_{d,36,22} =$ $\Delta MI_{36,22} + \Delta MI_{36,55} < 1.2 \cdot 10^{-2}$	$MI_{c,36,23} = MI_{d,36,23} =$ $\Delta MI_{36,23} + \Delta MI_{36,56} < 3.2 \cdot 10^{-5}$
$\Delta MI_{c,36,31} = \Delta MI_{d,36,31} =$ $\Delta MI_{36,31} + \Delta MI_{36,64} < 4.4 \cdot 10^{-6}$	$\Delta MI_{c,36,32} = \Delta MI_{d,36,32} =$ $\Delta MI_{36,32} + \Delta MI_{36,65} < 3.2 \cdot 10^{-5}$	$\Delta MI_{c,36,33} = \Delta MI_{d,36,33} =$ $\Delta MI_{36,33} + \Delta MI_{36,66} < 6.6 \cdot 10^{-5}$

Finally, by taking also into account that the coupling among the accelerometer axes are $\epsilon_{c,ij}$, $\epsilon_{d,ij}$, $\eta_{c,ij}$, $\eta_{d,ij}$, $\zeta_{c,ij}$, $\zeta_{d,ij} < 10^{-5}$ (specification), the following relationships can be established among the elements of the MI_{ij} sub-matrices:

- $MI_{14,12} = -MI_{14,21} + \Delta MI_{14,12-21}$, $\Delta MI_{14,12-21} = -2\epsilon_{c,14} + \Delta MI_{14,12} + \Delta MI_{14,21} < 5.2 \cdot 10^{-5}$ (3.5)
- $MI_{14,13} = -MI_{14,31} + \Delta MI_{14,13-31}$, $\Delta MI_{14,13-31} = -2\eta_{c,14} + \Delta MI_{14,13} + \Delta MI_{14,31} < 2.4 \cdot 10^{-5}$
- $MI_{14,23} = -MI_{14,32} + \Delta MI_{14,23-32}$, $\Delta MI_{14,23-32} = -2\zeta_{c,14} + \Delta MI_{14,23} + \Delta MI_{14,32} < 3.7 \cdot 10^{-5}$
- $MI_{14,15} = -MI_{14,24} + \Delta MI_{14,15-24}$, $\Delta MI_{14,15-24} = -2\epsilon_{d,14} + \Delta MI_{14,15} + \Delta MI_{14,24} < 5.2 \cdot 10^{-5}$
- $MI_{14,16} = -MI_{14,34} + \Delta MI_{14,16-34}$, $\Delta MI_{14,16-34} = -2\eta_{d,14} + \Delta MI_{14,16} + \Delta MI_{14,34} < 2.4 \cdot 10^{-5}$
- $MI_{14,26} = -MI_{14,35} + \Delta MI_{14,26-35}$, $\Delta MI_{14,26-35} = -2\zeta_{d,14} + \Delta MI_{14,26} + \Delta MI_{14,35} < 3.7 \cdot 10^{-5}$
- $MI_{14,42} = -MI_{14,51} + \Delta MI_{14,42-51}$, $\Delta MI_{14,42-51} = -2\epsilon_{d,14} + \Delta MI_{14,42} + \Delta MI_{14,51} < 5.2 \cdot 10^{-5}$
- $MI_{14,43} = -MI_{14,61} + \Delta MI_{14,43-61}$, $\Delta MI_{14,43-61} = -2\eta_{d,14} + \Delta MI_{14,43} + \Delta MI_{14,61} < 2.4 \cdot 10^{-5}$
- $MI_{14,53} = -MI_{14,62} + \Delta MI_{14,53-62}$, $\Delta MI_{14,53-62} = -2\zeta_{d,14} + \Delta MI_{14,53} + \Delta MI_{14,62} < 3.7 \cdot 10^{-5}$
- $MI_{14,45} = -MI_{14,54} + \Delta MI_{14,45-54}$, $\Delta MI_{14,45-54} = -2\epsilon_{c,14} + \Delta MI_{14,45} + \Delta MI_{14,54} < 5.2 \cdot 10^{-5}$
- $MI_{14,46} = -MI_{14,64} + \Delta MI_{14,46-64}$, $\Delta MI_{14,46-64} = -2\eta_{c,14} + \Delta MI_{14,46} + \Delta MI_{14,64} < 2.4 \cdot 10^{-5}$
- $MI_{14,56} = -MI_{14,65} + \Delta MI_{14,56-65}$, $\Delta MI_{14,56-65} = -2\zeta_{c,14} + \Delta MI_{14,56} + \Delta MI_{14,65} < 3.7 \cdot 10^{-5}$
- $MI_{25,12} = -MI_{25,21} + \Delta MI_{25,12-21}$, $\Delta MI_{25,12-21} = -2\epsilon_{c,25} + \Delta MI_{25,12} + \Delta MI_{25,21} < 2.4 \cdot 10^{-5}$
- $MI_{25,13} = -MI_{25,31} + \Delta MI_{25,13-31}$, $\Delta MI_{25,13-31} = -2\eta_{c,25} + \Delta MI_{25,13} + \Delta MI_{25,31} < 3.7 \cdot 10^{-5}$
- $MI_{25,23} = -MI_{25,32} + \Delta MI_{25,23-32}$, $\Delta MI_{25,23-32} = -2\zeta_{c,25} + \Delta MI_{25,23} + \Delta MI_{25,32} < 5.2 \cdot 10^{-5}$
- $MI_{25,15} = -MI_{25,24} + \Delta MI_{25,15-24}$, $\Delta MI_{25,15-24} = -2\epsilon_{d,25} + \Delta MI_{25,15} + \Delta MI_{25,24} < 2.4 \cdot 10^{-5}$
- $MI_{25,16} = -MI_{25,34} + \Delta MI_{25,16-34}$, $\Delta MI_{25,16-34} = -2\eta_{d,25} + \Delta MI_{25,16} + \Delta MI_{25,34} < 3.7 \cdot 10^{-5}$
- $MI_{25,26} = -MI_{25,35} + \Delta MI_{25,26-35}$, $\Delta MI_{25,26-35} = -2\zeta_{d,25} + \Delta MI_{25,26} + \Delta MI_{25,35} < 5.2 \cdot 10^{-5}$
- $MI_{25,42} = -MI_{25,51} + \Delta MI_{25,42-51}$, $\Delta MI_{25,42-51} = -2\epsilon_{d,25} + \Delta MI_{25,42} + \Delta MI_{25,51} < 2.4 \cdot 10^{-5}$
- $MI_{25,43} = -MI_{25,61} + \Delta MI_{25,43-61}$, $\Delta MI_{25,43-61} = -2\eta_{d,25} + \Delta MI_{25,43} + \Delta MI_{25,61} < 3.7 \cdot 10^{-5}$
- $MI_{25,53} = -MI_{25,62} + \Delta MI_{25,53-62}$, $\Delta MI_{25,53-62} = -2\zeta_{d,25} + \Delta MI_{25,53} + \Delta MI_{25,62} < 5.2 \cdot 10^{-5}$
- $MI_{25,45} = -MI_{25,54} + \Delta MI_{25,45-54}$, $\Delta MI_{25,45-54} = -2\epsilon_{c,25} + \Delta MI_{25,45} + \Delta MI_{25,54} < 2.4 \cdot 10^{-5}$
- $MI_{25,46} = -MI_{25,64} + \Delta MI_{25,46-64}$, $\Delta MI_{25,46-64} = -2\eta_{c,25} + \Delta MI_{25,46} + \Delta MI_{25,64} < 3.7 \cdot 10^{-5}$
- $MI_{25,56} = -MI_{25,65} + \Delta MI_{25,56-65}$, $\Delta MI_{25,56-65} = -2\zeta_{c,25} + \Delta MI_{25,56} + \Delta MI_{25,65} < 5.2 \cdot 10^{-5}$
- $MI_{36,12} = -MI_{36,21} + \Delta MI_{36,12-21}$, $\Delta MI_{36,12-21} = -2\epsilon_{c,36} + \Delta MI_{36,12} + \Delta MI_{36,21} < 3.7 \cdot 10^{-5}$

• $MI_{36,13} = -MI_{36,31} + \Delta MI_{36,13-31},$	$\Delta MI_{36,13-31} = -2\eta_{c,36} + \Delta MI_{36,13} + \Delta MI_{36,31} < 2.4 \cdot 10^{-5}$
• $MI_{36,23} = -MI_{36,32} + \Delta MI_{36,23-32},$	$\Delta MI_{36,23-32} = -2\zeta_{c,36} + \Delta MI_{36,23} + \Delta MI_{36,32} < 5.2 \cdot 10^{-5}$
• $MI_{36,15} = -MI_{36,24} + \Delta MI_{36,15-24},$	$\Delta MI_{36,15-24} = -2\varepsilon_{d,36} + \Delta MI_{36,15} + \Delta MI_{36,24} < 3.7 \cdot 10^{-5}$
• $MI_{36,16} = -MI_{36,34} + \Delta MI_{36,16-34},$	$\Delta MI_{36,16-34} = -2\eta_{d,36} + \Delta MI_{36,16} + \Delta MI_{36,34} < 2.4 \cdot 10^{-5}$
• $MI_{36,26} = -MI_{36,35} + \Delta MI_{36,26-35},$	$\Delta MI_{36,26-35} = -2\zeta_{d,36} + \Delta MI_{36,26} + \Delta MI_{36,35} < 5.2 \cdot 10^{-5}$
• $MI_{36,42} = -MI_{36,51} + \Delta MI_{36,42-51},$	$\Delta MI_{36,42-51} = -2\varepsilon_{d,36} + \Delta MI_{36,42} + \Delta MI_{36,51} < 3.7 \cdot 10^{-5}$
• $MI_{36,43} = -MI_{36,61} + \Delta MI_{36,43-61},$	$\Delta MI_{36,43-61} = -2\eta_{d,36} + \Delta MI_{36,43} + \Delta MI_{36,61} < 2.4 \cdot 10^{-5}$
• $MI_{36,53} = -MI_{36,62} + \Delta MI_{36,53-62},$	$\Delta MI_{36,53-62} = -2\zeta_{d,36} + \Delta MI_{36,53} + \Delta MI_{36,62} < 5.2 \cdot 10^{-5}$
• $MI_{36,45} = -MI_{36,54} + \Delta MI_{36,45-54},$	$\Delta MI_{36,45-54} = -2\varepsilon_{c,36} + \Delta MI_{36,45} + \Delta MI_{36,54} < 3.7 \cdot 10^{-5}$
• $MI_{36,46} = -MI_{36,64} + \Delta MI_{36,46-64},$	$\Delta MI_{36,46-64} = -2\eta_{c,36} + \Delta MI_{36,46} + \Delta MI_{36,64} < 2.4 \cdot 10^{-5}$
• $MI_{36,56} = -MI_{36,65} + \Delta MI_{36,56-65},$	$\Delta MI_{36,56-65} = -2\zeta_{c,36} + \Delta MI_{36,56} + \Delta MI_{36,65} < 5.2 \cdot 10^{-5}$

In case no adjustment operation is performed, the maximum values that the common and differential quadratic factors can achieve all along the mission lifetime are determined by the manufacturing/integration of the accelerometers and their electronics and by the further modifications that they can suffer during the ground testing and handling, during launch, and during all the time spent on orbit.

Table 3.1-3 provides the worst case values of the common and differential K2 of the three accelerometer pairs obtained by on-ground construction (ref. [RD 11]), and that should be maintained also in flight¹ before the first calibration.

Differently from the scale factors, misalignments and couplings among axes, the accelerometer quadratic factors can be physically adjusted (reduced) once their value is known. The limit values achieved by the quadratic factors during the measurement phases are therefore the result of their adjustment during the in-flight calibration and of their successive drifts².

Sensor Pair	OAGRF axis			Common Quadratic Factors	Differential Quadratic Factors
A ₁ , A ₄	X	↑	U	$K2_{c,14,X} < 1206 \text{ s}^2/\text{m}$	$K2_{d,14,X} < 1206 \text{ s}^2/\text{m}$
	Y	→	L	$K2_{c,14,Y} < 1 \text{ s}^2/\text{m}$	$K2_{d,14,Y} < 1 \text{ s}^2/\text{m}$
	Z	→	U	$K2_{c,14,Z} < 1206 \text{ s}^2/\text{m}$	$K2_{d,14,Z} < 1206 \text{ s}^2/\text{m}$
A ₂ , A ₅	X	→	U	$K2_{c,25,X} < 1206 \text{ s}^2/\text{m}$	$K2_{d,25,X} < 1206 \text{ s}^2/\text{m}$
	Y	↑	U	$K2_{c,25,Y} < 1206 \text{ s}^2/\text{m}$	$K2_{d,25,Y} < 1206 \text{ s}^2/\text{m}$
	Z	→	L	$K2_{c,25,Z} < 1 \text{ s}^2/\text{m}$	$K2_{d,25,Z} < 1 \text{ s}^2/\text{m}$
A ₃ , A ₆	X	→	U	$K2_{c,36,X} < 1206 \text{ s}^2/\text{m}$	$K2_{d,36,X} < 1206 \text{ s}^2/\text{m}$
	Y	→	L	$K2_{c,36,Y} < 1 \text{ s}^2/\text{m}$	$K2_{d,36,Y} < 1 \text{ s}^2/\text{m}$
	Z	↑	U	$K2_{c,36,Z} < 1206 \text{ s}^2/\text{m}$	$K2_{d,36,Z} < 1206 \text{ s}^2/\text{m}$

↑ : in-line axis, aligned to the baseline of the OAG to which the accelerometer belongs
 → : transversal axis, perpendicular to the baseline of the OAG to which the accelerometer belongs
 U : accelerometer ultra sensitive axis, L : accelerometer less sensitive axis

Table 3.1-3: Worst case values of the common and differential quadratic factors obtained by on-ground construction).

¹ The K2 values set during the on-ground calibration are not maintained in the ground-to-orbit transition. This is due to the large control voltage (800 V, less sensitive axis) which must be applied on ground to suspend the proof mass, and that is reduced to nearly 0 V in flight, during the measurement phases. On the other hand, the values of K2 by construction are expected to be maintained on orbit before the first calibration.

² In principle it is possible to adjust the K2 values already during the on-ground calibration. But these values are not maintained in the ground-to-orbit transition because of the large control voltage (800 V, less sensitive axis) which must be applied on ground to suspend the proof mass, and that is reduced to nearly 0 V in flight, during the measurement phases. On the other hand, the values of K2 by construction are expected to be maintained on orbit (ref. [RD 4]).

3.2 PURPOSE OF THE GRADIOMETER ON-GROUND CALIBRATION

The purpose of the Gradiometer calibration performed on ground is:

- To measure the value of a sub-set of elements of the Calibration Matrices (common and differential scale factors, misalignments and inter-axis couplings), so to verify that, after the manufacturing, integration and alignment of the One Axis Gradiometers, the specified limits of Table 3.1.1 have not been exceeded.
- To verify the thermal sensitivity of the in-line differential scale factor.
- To measure the by-construction value of the accelerometer quadratic factors along the two ultra sensitive axes and to verify the feasibility of the K2 adjustment by proof mass displacement.

The acceleration measurement limitations imposed by the on-ground environment and the need of using some of the accelerometer readouts to actively control the pendulum bench (on which the Gradiometer ground calibration is performed) during the shaking, do not allow to measure the other quadratic factors and the other elements of the Calibration Matrices (see [AD 1]). The elements of the Calibration Matrices which can be measured on ground for each accelerometer pairs are listed in Table 3.2-1. These measurements have been performed only on one accelerometer pair (ASH FM01 and ASH FM03).

The quadratic factor measurements have been performed on the ASH FM05 and ASH FM06, among those installed on the Gradiometer flight model.

Sensor Pair	OAG Axis	Common, Differential Scale Factor	Common, Differential Misalignment + Coupling	
A ₁ , A ₄	X ↑ U	$K_{d,14,X} \equiv dM_{d,14,11}$	$(-\theta_{c,14} + \eta_{c,14}) \equiv dM_{c,14,13}$	$(\psi_{d,14} + \epsilon_{d,14}) \equiv dM_{d,14,12}$
	Y → L		$(-\psi_{d,14} + \epsilon_{d,14}) \equiv dM_{d,14,21}$	$(\phi_{d,14} + \zeta_{d,14}) \equiv dM_{d,14,23}$
	Z → U		$(\theta_{c,14} + \eta_{c,14}) \equiv dM_{c,14,31}$	$(\theta_{d,14} + \eta_{d,14}) \equiv dM_{d,14,31}$
A ₂ , A ₅	X _i → U		$(\psi_{c,25} + \epsilon_{c,25}) \equiv dM_{c,25,12}$	$(\psi_{d,25} + \epsilon_{d,25}) \equiv dM_{d,25,12}$
	Y _i ↑ U	$K_{d,25,Y} \equiv dM_{d,25,22}$	$(-\psi_{c,25} + \epsilon_{c,25}) \equiv dM_{c,25,21}$	$(-\psi_{d,25} + \epsilon_{d,25}) \equiv dM_{d,25,21}$
	Z _i → L		$(\theta_{d,25} + \eta_{d,25}) \equiv dM_{d,25,31}$	$(-\phi_{d,25} + \zeta_{d,25}) \equiv dM_{d,25,32}$
A ₃ , A ₆	X _i → U		$(-\theta_{c,36} + \eta_{c,36}) \equiv dM_{c,36,13}$	$(\psi_{d,36} + \epsilon_{d,36}) \equiv dM_{d,36,12}$
	Y _i → L		$(-\psi_{d,36} + \epsilon_{d,36}) \equiv dM_{d,36,21}$	$(\phi_{d,36} + \zeta_{d,36}) \equiv dM_{d,36,23}$
	Z _i ↑ U	$K_{d,36,Z} \equiv dM_{d,36,33}$	$(\theta_{c,36} + \eta_{c,36}) \equiv dM_{c,36,31}$	$(\theta_{d,36} + \eta_{d,36}) \equiv dM_{d,36,31}$

$[dM]_{c,14}$			$[dM]_{d,14}$		
		$dM_{c,14,13}$	$dM_{d,14,11}$	$dM_{d,14,12}$	$dM_{d,14,13}$
			$dM_{d,14,21}$		$dM_{d,14,23}$
$dM_{c,14,31}$			$dM_{d,14,31}$	$dM_{d,14,32}$	

$[dM]_{c,25}$			$[dM]_{d,25}$		
	$dM_{c,25,12}$			$dM_{d,25,12}$	$dM_{d,25,13}$
$dM_{c,25,21}$			$dM_{d,25,21}$	$dM_{d,25,22}$	$dM_{d,25,23}$
			$dM_{d,25,31}$	$dM_{d,25,32}$	

$[dM]_{c,36}$			$[dM]_{d,36}$		
		$dM_{c,36,13}$		$dM_{d,36,12}$	$dM_{d,36,13}$
			$dM_{d,36,21}$		$dM_{d,36,23}$
$dM_{c,36,31}$			$dM_{d,36,31}$	$dM_{d,36,32}$	$dM_{d,36,33}$

Table 3.2-1: Elements of M_{ij} measurable during the on-ground calibration

3.3 PURPOSE OF THE GRADIOMETER ON-ORBIT CALIBRATION

3.3.1 Quadratic Factors

To get a substantial reduction of the resulting gradiometric error related to the quadratic factors, their common-mode and differential-mode value must remain below the limits specified in Table 3.3-1 during the measurement phases. For the K2 along the accelerometer less sensitive axis ($K2_{c,14,Y}$, $K2_{d,14,Y}$, $K2_{c,25,Z}$, $K2_{d,25,Z}$, $K2_{c,36,Y}$, $K2_{d,36,Y}$) this limit should be fulfilled all along the mission lifetime “by construction” (no in-flight intervention is nominally required for LS-axes). For the other quadratic factors an in-flight measurement and adjustment is required. The maximum value that can be achieved by the quadratic factors is the result of the limits under which these elements have been reduced during the on-orbit calibration and of the successive variations of these quantities (by components drifts, ageing, ...). From the current estimations, it is expected a K2 drift of not more than $1 \text{ s}^2/\text{m}$ [RD 3] in one month (specified minimum time between two successive calibrations during the measurement phase [AD 3]). Therefore, the result of each in-flight calibration process of the K2 shall be a physical reduction of their values at least below the limits provided in Table 3.3-2. The accuracy by which the quadratic factors of the ultra sensitive axes can be adjusted, assuming their perfect knowledge, is $< 4.5\%$ of their initial value (ref. [RD 2])³. Therefore, the in-flight calibration process of the quadratic factors shall provide a measurement of their values with a maximum error not exceeding the limits provided in Table 3.3-4⁴.

Sensor Pair	OAG Axis	Common, Differential Quadratic Factors
A ₁ , A ₄	X ↑ U	$K2_{c,14,X} \leq 10 \text{ s}^2/\text{m}$, $K2_{d,14,X} \leq 4 \text{ s}^2/\text{m}$
	Y → L	$K2_{c,14,Y}$, $K2_{d,14,Y} \leq 10 \text{ s}^2/\text{m}$
	Z → U	$K2_{c,14,Z}$, $K2_{d,14,Z} \leq 10 \text{ s}^2/\text{m}$
A ₂ , A ₅	X _i → U	$K2_{c,25,X}$, $K2_{d,25,X} \leq 10 \text{ s}^2/\text{m}$
	Y _i ↑ U	$K2_{c,25,Y} \leq 7 \text{ s}^2/\text{m}$, $K2_{d,25,Y} \leq 4 \text{ s}^2/\text{m}$
	Z _i → L	$K2_{c,25,Z}$, $K2_{d,25,Z} \leq 10 \text{ s}^2/\text{m}$
A ₃ , A ₆	X _i → U	$K2_{c,36,X}$, $K2_{d,36,X} \leq 10 \text{ s}^2/\text{m}$
	Y _i → L	$K2_{c,36,Y}$, $K2_{d,36,Y} \leq 10 \text{ s}^2/\text{m}$
	Z _i ↑ U	$K2_{c,36,Z} \leq 7 \text{ s}^2/\text{m}$, $K2_{d,36,Z} \leq 4 \text{ s}^2/\text{m}$

Table 3.3-1: Limits under which the quadratic factors must remain during the measurement phases

Sensor Pair	OAG Axis	Common, Differential Quadratic Factors
A ₁ , A ₄	X ↑ U	$K2_{c,14,X} \leq 9 \text{ s}^2/\text{m}$, $K2_{d,14,X} \leq 3 \text{ s}^2/\text{m}$
	Y → L	In-flight calibration not needed for $K2_{c,14,Y}$, $K2_{d,14,Y}$
	Z → U	$K2_{c,14,Z}$, $K2_{d,14,Z} \leq 9 \text{ s}^2/\text{m}$
A ₂ , A ₅	X _i → U	$K2_{c,25,X}$, $K2_{d,25,X} \leq 9 \text{ s}^2/\text{m}$
	Y _i ↑ U	$K2_{c,25,Y} \leq 6 \text{ s}^2/\text{m}$, $K2_{d,25,Y} \leq 3 \text{ s}^2/\text{m}$
	Z _i → L	In-flight calibration not needed for $K2_{c,25,Z}$, $K2_{d,25,Z}$
A ₃ , A ₆	X _i → U	$K2_{c,36,X}$, $K2_{d,36,X} \leq 9 \text{ s}^2/\text{m}$
	Y _i → L	In-flight calibration not needed for $K2_{c,36,Y}$, $K2_{d,36,Y}$
	Z _i ↑ U	$K2_{c,36,Z} \leq 6 \text{ s}^2/\text{m}$, $K2_{d,36,Z} \leq 3 \text{ s}^2/\text{m}$

Table 3.3-2: Limits under which the quadratic factors have to be reduced during the in-flight calibration process

³ This means that, assuming a perfect knowledge of the K2 value, the error committed in the computation and in-flight implementation of the corresponding correction shall lead to a resulting residual value of K2 below 4.5% of the initial value.

⁴ The reduction of the K2 within their final limits will require some measurement-correction iterations. The maximum measurement error has been computed assuming that at the iteration N-1, the K2 is twice the final limit. For instance: $K2_{d,14,X}(N-1) = 6 \text{ s}^2/\text{m} \rightarrow K2_{d,14,X}(N-1) = 2.7$ (measurement error) + $6 \cdot 0.045$ (correction accuracy) $\cong 3 \text{ s}^2/\text{m}$.

Sensor Pair	OAG Axis	Common, Differential Quadratic Factors
A_1, A_4	X \uparrow U	$K2_{c,14,X} < 8.2 \text{ s}^2/\text{m}, K2_{d,14,X} < 2.7 \text{ s}^2/\text{m}$
	Y \rightarrow L	In-flight calibration not needed for $K2_{c,14,Y}, K2_{d,14,Y}$
	Z \rightarrow U	$K2_{c,14,Z}, K2_{d,14,Z} < 8.2 \text{ s}^2/\text{m}$
A_2, A_5	$X_i \rightarrow$ U	$K2_{c,25,X}, K2_{d,25,X} < 8.2 \text{ s}^2/\text{m}$
	$Y_i \uparrow$ U	$K2_{c,25,Y} < 5.5 \text{ s}^2/\text{m}, K2_{d,25,Y} < 2.7 \text{ s}^2/\text{m}$
	$Z_i \rightarrow$ L	In-flight calibration not needed for $K2_{c,25,Z}, K2_{d,25,Z}$
A_3, A_6	$X_i \rightarrow$ U	$K2_{c,36,X}, K2_{d,36,X} < 8.2 \text{ s}^2/\text{m}$
	$Y_i \rightarrow$ L	In-flight calibration not needed for $K2_{c,36,Y}, K2_{d,36,Y}$
	$Z_i \uparrow$ U	$K2_{c,36,Z} < 5.5 \text{ s}^2/\text{m}, K2_{d,36,Z} < 2.7 \text{ s}^2/\text{m}$

Table 3.3-3: Measurement accuracy of the quadratic factors to be provided by the in-flight calibration process

In summary, taking into account that no significant variations of the quadratic factors by construction are expected from ground to orbit, the in-flight calibration can be restricted to the 12 terms (LS axes should not require calibration):

$$K2_{c,14,X}, K2_{d,14,X}, K2_{c,14,Z}, K2_{d,14,Z}, K2_{c,25,X}, K2_{d,25,X}, K2_{c,25,Y}, K2_{d,25,Y}, K2_{c,36,X}, K2_{d,36,X}, K2_{c,36,Z}, K2_{d,36,Z}.$$

After the first in-orbit measurement and adjustment of the quadratic factors within the limits specified in Table 3.3-2, a further calibration process is necessary in case the variations of the in line differential $K2$ elements exceed $1 \text{ s}^2/\text{m}$, or in case exceptional events occur (accelerometer failures, etc..) resulting in loss of control of the proof masses with collisions against the stops, or in a re-configuration of the detectors (failure of one detector).

3.3.2 Inverse Calibration Matrices

To get a substantial reduction of the resulting gradiometric error related to the accelerometer scale factors, axes misalignments and couplings, the elements of the inverse Calibration Matrices MI_{ij} involved in the recovery of the original differential accelerations $\underline{a}_{d,ij}$ (i.e. the elements contained in the sub-matrices $[MI]_{d,ij}, [MI]_{c,ij}$) must be known with the accuracy specified in Table 3.3-4 during the measurement phases. From the upper limits, provided in Table 3.1-2, expected not to be exceeded along the mission lifetime by the elements of MI_{ij} (condition ensured by the Gradiometer design and construction), it turns out that the knowledge accuracy requirements of Table 3.3-4 are already fulfilled for the elements:

- $MI_{14,51}, MI_{14,53}, MI_{14,54}, MI_{14,56}, MI_{14,64}, MI_{14,65}$
- $MI_{25,42}, MI_{25,43}, MI_{25,45}, MI_{25,46}, MI_{25,61}, MI_{25,62}, MI_{25,64}, MI_{25,65}$
- $MI_{36,45}, MI_{36,46}, MI_{36,51}, MI_{36,53}, MI_{36,54}, MI_{36,56}$

This means that, to comply with the knowledge accuracy requirements, it is sufficient to assume a null value for these elements. Consequently they do not need to be necessarily measured during the on-orbit calibration, unless for verifying that their expected maximum value has not been actually exceeded.

Moreover, by considering the relationships (3.5) between the off-diagonal elements of $[MI]_{c,ij}, [MI]_{d,ij}$, it turns out that, if the elements

$$MI_{14,42}, MI_{14,43}, MI_{14,45}, MI_{14,46}, MI_{14,62}, MI_{14,65}, \\ MI_{25,43}, MI_{25,46}, MI_{25,51}, MI_{25,53}, MI_{25,54}, MI_{25,56}, \\ MI_{36,42}, MI_{36,45}, MI_{36,61}, MI_{36,62}, MI_{36,64}, MI_{36,65},$$

are known with the accuracy specified in Table 3.3-4, then the symmetric elements

$$MI_{14,51}, MI_{14,61}, MI_{14,54}, MI_{14,64}, MI_{14,53}, MI_{14,56},$$

$$MI_{25,61}, MI_{25,64}, MI_{25,42}, MI_{25,62}, MI_{25,45}, MI_{25,65},$$

$$MI_{36,51}, MI_{36,54}, MI_{36,43}, MI_{36,53}, MI_{36,46}, MI_{36,56},$$

can be simply obtained as follows, with the maximum measurement error indicated in parentheses:

$$\begin{aligned}
 MI_{14,51} &= -MI_{14,42} \quad (\delta MI_{14,51} = \delta MI_{14,42} + \Delta MI_{14,42-51} < 5 \cdot 10^{-6} + 5.2 \cdot 10^{-5} = 5.7 \cdot 10^{-5}) \\
 MI_{14,61} &= -MI_{14,43} \quad (\delta MI_{14,61} = \delta MI_{14,43} + \Delta MI_{14,43-61} < 5 \cdot 10^{-6} + 2.4 \cdot 10^{-5} = 2.9 \cdot 10^{-5}) \\
 MI_{14,54} &= -MI_{14,45} \quad (\delta MI_{14,54} = \delta MI_{14,45} + \Delta MI_{14,45-54} < 5.1 \cdot 10^{-5} + 5.2 \cdot 10^{-5} = 1.03 \cdot 10^{-4}) \\
 MI_{14,64} &= -MI_{14,46} \quad (\delta MI_{14,64} = \delta MI_{14,46} + \Delta MI_{14,46-64} < 5.1 \cdot 10^{-5} + 2.4 \cdot 10^{-5} = 7.5 \cdot 10^{-5}) \\
 MI_{14,53} &= -MI_{14,62} \quad (\delta MI_{14,53} = \delta MI_{14,62} + \Delta MI_{14,53-62} < 5 \cdot 10^{-5} + 3.7 \cdot 10^{-5} = 8.7 \cdot 10^{-5}) \\
 MI_{14,56} &= -MI_{14,65} \quad (\delta MI_{14,56} = \delta MI_{14,65} + \Delta MI_{14,56-65} < 1.5 \cdot 10^{-4} + 3.7 \cdot 10^{-5} = 1.87 \cdot 10^{-4}) \\
 \\
 MI_{25,61} &= -MI_{25,43} \quad (\delta MI_{25,61} = \delta MI_{25,43} + \Delta MI_{25,43-61} < 1.5 \cdot 10^{-4} + 3.7 \cdot 10^{-5} = 1.87 \cdot 10^{-4}) \\
 MI_{25,64} &= -MI_{25,46} \quad (\delta MI_{25,64} = \delta MI_{25,46} + \Delta MI_{25,46-64} < 1.5 \cdot 10^{-4} + 3.7 \cdot 10^{-5} = 1.87 \cdot 10^{-4}) \\
 MI_{25,42} &= -MI_{25,51} \quad (\delta MI_{25,42} = \delta MI_{25,51} + \Delta MI_{25,42-51} < 5 \cdot 10^{-6} + 2.4 \cdot 10^{-5} = 2.9 \cdot 10^{-5}) \\
 MI_{25,62} &= -MI_{25,53} \quad (\delta MI_{25,62} = \delta MI_{25,53} + \Delta MI_{25,53-62} < 5 \cdot 10^{-6} + 5.2 \cdot 10^{-5} = 5.7 \cdot 10^{-5}) \\
 MI_{25,45} &= -MI_{25,54} \quad (\delta MI_{25,45} = \delta MI_{25,54} + \Delta MI_{25,45-54} < 5.1 \cdot 10^{-5} + 2.4 \cdot 10^{-5} = 7.5 \cdot 10^{-5}) \\
 MI_{25,65} &= -MI_{25,56} \quad (\delta MI_{25,65} = \delta MI_{25,56} + \Delta MI_{25,56-65} < 5.1 \cdot 10^{-5} + 5.2 \cdot 10^{-5} = 1.03 \cdot 10^{-4}) \\
 \\
 MI_{36,51} &= -MI_{36,42} \quad (\delta MI_{36,51} = \delta MI_{36,42} + \Delta MI_{36,42-51} < 5 \cdot 10^{-5} + 3.7 \cdot 10^{-5} = 8.7 \cdot 10^{-5}) \\
 MI_{36,54} &= -MI_{36,45} \quad (\delta MI_{36,54} = \delta MI_{36,45} + \Delta MI_{36,45-54} < 1.5 \cdot 10^{-4} + 3.7 \cdot 10^{-5} = 1.87 \cdot 10^{-4}) \\
 MI_{36,43} &= -MI_{36,61} \quad (\delta MI_{36,43} = \delta MI_{36,61} + \Delta MI_{36,43-61} < 5 \cdot 10^{-6} + 2.4 \cdot 10^{-5} = 2.9 \cdot 10^{-5}) \\
 MI_{36,53} &= -MI_{36,62} \quad (\delta MI_{36,53} = \delta MI_{36,62} + \Delta MI_{36,53-62} < 5 \cdot 10^{-6} + 5.2 \cdot 10^{-5} = 5.7 \cdot 10^{-5}) \\
 MI_{36,46} &= -MI_{36,64} \quad (\delta MI_{36,46} = \delta MI_{36,64} + \Delta MI_{36,46-64} < 5.1 \cdot 10^{-5} + 2.4 \cdot 10^{-5} = 7.5 \cdot 10^{-5}) \\
 MI_{36,56} &= -MI_{36,65} \quad (\delta MI_{36,56} = \delta MI_{36,65} + \Delta MI_{36,56-65} < 5.1 \cdot 10^{-5} + 5.2 \cdot 10^{-5} = 1.03 \cdot 10^{-4})
 \end{aligned} \tag{3.6}$$

For the elements $MI_{14,51}, MI_{14,61}, MI_{14,54}, MI_{14,64}, MI_{14,53}, MI_{25,42}, MI_{25,62}, MI_{25,45}, MI_{25,65}, MI_{36,51}, MI_{36,43}, MI_{36,53}, MI_{36,46}, MI_{36,56}$, the accuracy so obtained is smaller than the specification, even if for all these elements but $MI_{14,61}, MI_{36,43}$ the knowledge “by construction” is already sufficient. For the elements $MI_{14,56}, MI_{25,61}, MI_{25,64}, MI_{36,54}$, the accuracy so obtained is slightly larger than the specification, but also for these elements the knowledge “by construction” is already sufficient (they don’t need to be necessarily measured in flight).

In summary, only for 32 elements of the IMCs the in-flight measurement is strictly necessary (see Table 3.3-5).

Row	Required knowledge accuracy of the elements of MI_{14} involved in the computation of $a_{d,14}$					
4 th	$\delta MI_{14,41} \leq 1.4 \cdot 10^{-5}$	$\delta MI_{14,42} \leq 5.0 \cdot 10^{-6}$	$\delta MI_{14,43} \leq 5.0 \cdot 10^{-6}$	$\delta MI_{14,44} \leq 2.02 \cdot 10^{-3}$	$\delta MI_{14,45} \leq 5.1 \cdot 10^{-5}$	$\delta MI_{14,46} \leq 5.1 \cdot 10^{-5}$
5 th	$\delta MI_{14,51} \leq 1.5 \cdot 10^{-4}$	$\delta MI_{14,52} \leq 5.5 \cdot 10^{-4}$	$\delta MI_{14,53} \leq 1.5 \cdot 10^{-4}$	$\delta MI_{14,54} \leq 1.5 \cdot 10^{-4}$	$\delta MI_{14,55} \leq 1.01 \cdot 10^{-2}$	$\delta MI_{14,56} \leq 1.5 \cdot 10^{-4}$
6 th	$\delta MI_{14,61} \leq 5.0 \cdot 10^{-5}$	$\delta MI_{14,62} \leq 5.0 \cdot 10^{-5}$	$\delta MI_{14,63} \leq 5.8 \cdot 10^{-5}$	$\delta MI_{14,64} \leq 1.5 \cdot 10^{-4}$	$\delta MI_{14,65} \leq 1.5 \cdot 10^{-4}$	$\delta MI_{14,66} \leq 2.02 \cdot 10^{-3}$
Row	Required knowledge accuracy of the elements of MI_{25} involved in the computation of $a_{d,25}$					
4 th	$\delta MI_{25,41} \leq 1.5 \cdot 10^{-4}$	$\delta MI_{25,42} \leq 1.5 \cdot 10^{-4}$	$\delta MI_{25,43} \leq 1.5 \cdot 10^{-4}$	$\delta MI_{25,44} \leq 2.1 \cdot 10^{-3}$	$\delta MI_{25,45} \leq 1.5 \cdot 10^{-4}$	$\delta MI_{25,46} \leq 1.5 \cdot 10^{-4}$
5 th	$\delta MI_{25,51} \leq 5.0 \cdot 10^{-6}$	$\delta MI_{25,52} \leq 1.4 \cdot 10^{-5}$	$\delta MI_{25,53} \leq 5.0 \cdot 10^{-6}$	$\delta MI_{25,54} \leq 5.1 \cdot 10^{-5}$	$\delta MI_{25,55} \leq 2.02 \cdot 10^{-3}$	$\delta MI_{25,56} \leq 5.1 \cdot 10^{-5}$
6 th	$\delta MI_{25,61} \leq 1.5 \cdot 10^{-4}$	$\delta MI_{25,62} \leq 1.5 \cdot 10^{-4}$	$\delta MI_{25,63} \leq 5.5 \cdot 10^{-4}$	$\delta MI_{25,64} \leq 1.5 \cdot 10^{-4}$	$\delta MI_{25,65} \leq 1.5 \cdot 10^{-4}$	$\delta MI_{25,66} \leq 1.01 \cdot 10^{-2}$
Row	Required knowledge accuracy of the elements of MI_{36} involved in the computation of $a_{d,36}$					
4 th	$\delta MI_{36,41} \leq 5.8 \cdot 10^{-5}$	$\delta MI_{36,42} \leq 5.0 \cdot 10^{-5}$	$\delta MI_{36,43} \leq 5.0 \cdot 10^{-5}$	$\delta MI_{36,44} \leq 2.02 \cdot 10^{-3}$	$\delta MI_{36,45} \leq 1.5 \cdot 10^{-4}$	$\delta MI_{36,46} \leq 1.5 \cdot 10^{-4}$
5 th	$\delta MI_{36,51} \leq 1.5 \cdot 10^{-4}$	$\delta MI_{36,52} \leq 5.5 \cdot 10^{-4}$	$\delta MI_{36,53} \leq 1.5 \cdot 10^{-4}$	$\delta MI_{36,54} \leq 1.5 \cdot 10^{-4}$	$\delta MI_{36,55} \leq 1.01 \cdot 10^{-2}$	$\delta MI_{36,56} \leq 1.5 \cdot 10^{-4}$
6 th	$\delta MI_{36,61} \leq 5.0 \cdot 10^{-6}$	$\delta MI_{36,62} \leq 5.0 \cdot 10^{-6}$	$\delta MI_{36,63} \leq 1.4 \cdot 10^{-5}$	$\delta MI_{36,64} \leq 5.1 \cdot 10^{-5}$	$\delta MI_{36,65} \leq 5.1 \cdot 10^{-5}$	$\delta MI_{36,66} \leq 2.02 \cdot 10^{-3}$

Table 3.3-4: Knowledge accuracy of $[MI]_{d,ij}, [MI]_{c,ij}$ ($ij=14, 25, 36$) required during the measurement phases

Row	Elements of MI_{14} involved in the computation of $a_{d,14}$					
4 th	$MI_{14,41}$	$MI_{14,42}$	$MI_{14,43}$	$MI_{14,44}$	$MI_{14,45}$	$MI_{14,46}$
5 th	$MI_{14,51} (= 0)$	$MI_{14,52}$	$MI_{14,53} (= 0)$	$MI_{14,54} (= 0)$	$MI_{14,55}$	$MI_{14,56} (= 0)$
6 th	$MI_{14,61} (= -MI_{14,43})$	$MI_{14,62}$	$MI_{14,63}$	$MI_{14,64} (= 0)$	$MI_{14,65} (= 0)$	$MI_{14,66}$
Row	Elements of MI_{25} involved in the computation of $a_{d,25}$					
4 th	$MI_{25,41}$	$MI_{25,42} (= 0)$	$MI_{25,43} (= 0)$	$MI_{25,44}$	$MI_{25,45} (= 0)$	$MI_{25,46} (= 0)$
5 th	$MI_{25,51}$	$MI_{25,52}$	$MI_{25,53}$	$MI_{25,54}$	$MI_{25,55}$	$MI_{25,56}$
6 th	$MI_{25,61} (= 0)$	$MI_{25,62} (= 0)$	$MI_{25,63}$	$MI_{25,64} (= 0)$	$MI_{25,65} (= 0)$	$MI_{25,66}$
Row	Elements of MI_{36} involved in the computation of $a_{d,36}$					
4 th	$MI_{36,41}$	$MI_{36,42}$	$MI_{36,43} (= -MI_{36,61})$	$MI_{36,44}$	$MI_{36,45} (= 0)$	$MI_{36,46} (= 0)$
5 th	$MI_{36,51} (= 0)$	$MI_{36,52}$	$MI_{36,53} (= 0)$	$MI_{36,54} (= 0)$	$MI_{36,55}$	$MI_{36,56} (= 0)$
6 th	$MI_{36,61}$	$MI_{36,62}$	$MI_{36,63}$	$MI_{36,64}$	$MI_{36,65}$	$MI_{36,66}$

Elements whose knowledge accuracy requirement is fulfilled “by construction” (use the value in brackets).

Elements whose knowledge accuracy requirement is fulfilled by exploiting the equality in brackets.

Elements whose value needs to be measured during the on-orbit calibration.

Table 3.3-5: In flight calibration needs for the elements of the inverse Calibration Matrices

The knowledge accuracy of the ICM elements during the measurement phase depend on the accuracy by which they are measured during the calibration phase and on the successive variations of these quantities (by components drifts, ageing, thermo-elastic deformations, ...). In Table 3.3-6 the tolerable limits to the maximum variation of the ICM elements in the minimum period between two successive calibrations (1 month as per [AD 1]) are provided. These limits are fulfilled by the expected in-flight behaviour of the Gradiometer [RD 11].

Therefore, the result of each in-flight measurement of the ICM elements shall provide their values with the accuracy not exceeding the limits provided in Table 3.3-7 (requested accuracy – maximum monthly drift of the elements). These limits define the objective of the in-flight calibration of the gradiometer. They are specified here for all the elements, even those for which the in-flight measurement is not strictly needed because their knowledge accuracy requirement is already fulfilled “by construction”.

Therefore, the result of each in-flight measurement of the ICM elements shall provide their values with the accuracy not exceeding the limits provided in Table 3.3-7 (requested accuracy – maximum monthly drift of the elements). Again, the measurement of $MI_{14,43}$, $MI_{36,61}$ with the specified accuracy also provides the values of $MI_{14,61}$, $MI_{36,43}$ with the needed accuracy through the relationships (3.6). By comparing the required measurement accuracy of the ICM elements (Table 3.3-7) with their limit values (Table 3.1-2), we get the limit for the relative error by which these elements must be measured in flight. These relative errors are also provided in Table 3.3-7.

The other elements of MI_{ij} (i.e. those contained in $[MI']_{c,ij}$, $[MI']_{d,ij}$) are not planned to be measured on orbit. However, thanks to the relationships (3.4), as a consequence of the knowledge of $[MI]_{d,ij}$, $[MI]_{c,ij}$, they will be also known with the accuracy provided in Table 3.3-8 (computed under the assumption that $[MI]_{d,ij}$, $[MI]_{c,ij}$ are known with the required accuracy).

After the first in-orbit measurement of the elements of the ICM, a further calibration process is necessary in case the variations of these elements exceed the limits of Table 3.3-6, or in case exceptional events occur (accelerometer failures, etc..) resulting in a loss of control of any of the proof masses with collisions against the stops, or in a re-combination of the science outputs (failure of one science branch).

Row	Upper limits for the monthly variations of the MI_{14} elements to be measured in flight					
4 th	$\delta MI_{14,41} \leq 9.05 \cdot 10^{-6}$	$\delta MI_{14,42} \leq 5.0 \cdot 10^{-7}$	$\delta MI_{14,43} \leq 5.0 \cdot 10^{-7}$	$\delta MI_{14,44} \leq 2.0 \cdot 10^{-5}$	$\delta MI_{14,45} \leq 1.0 \cdot 10^{-6}$	$\delta MI_{14,46} \leq 1.0 \cdot 10^{-6}$
5 th	$\delta MI_{14,51} \leq 5.0 \cdot 10^{-5}$	$\delta MI_{14,52} \leq 5.0 \cdot 10^{-5}$	$\delta MI_{14,53} \leq 5.0 \cdot 10^{-5}$	$\delta MI_{14,54} \leq 1.0 \cdot 10^{-4}$	$\delta MI_{14,55} \leq 1.0 \cdot 10^{-4}$	$\delta MI_{14,56} \leq 1.0 \cdot 10^{-4}$
6 th	$\delta MI_{14,61} \leq 5.0 \cdot 10^{-6}$	$\delta MI_{14,62} \leq 5.0 \cdot 10^{-6}$	$\delta MI_{14,63} \leq 9.05 \cdot 10^{-6}$	$\delta MI_{14,64} \leq 1.0 \cdot 10^{-4}$	$\delta MI_{14,65} \leq 1.0 \cdot 10^{-4}$	$\delta MI_{14,66} \leq 2.0 \cdot 10^{-5}$
Row	Upper limits for the monthly variations of the MI_{25} elements to be measured in flight					
4 th	$\delta MI_{25,41} \leq 5.0 \cdot 10^{-5}$	$\delta MI_{25,42} \leq 5.0 \cdot 10^{-5}$	$\delta MI_{25,43} \leq 5.0 \cdot 10^{-5}$	$\delta MI_{25,44} \leq 1.0 \cdot 10^{-4}$	$\delta MI_{25,45} \leq 1.0 \cdot 10^{-4}$	$\delta MI_{25,46} \leq 1.0 \cdot 10^{-4}$
5 th	$\delta MI_{25,51} \leq 5.0 \cdot 10^{-7}$	$\delta MI_{25,52} \leq 9.05 \cdot 10^{-6}$	$\delta MI_{25,53} \leq 5.0 \cdot 10^{-7}$	$\delta MI_{25,54} \leq 1.0 \cdot 10^{-6}$	$\delta MI_{25,55} \leq 2.0 \cdot 10^{-5}$	$\delta MI_{25,56} \leq 1.0 \cdot 10^{-6}$
6 th	$\delta MI_{25,61} \leq 5.0 \cdot 10^{-5}$	$\delta MI_{25,62} \leq 5.0 \cdot 10^{-5}$	$\delta MI_{25,63} \leq 5.0 \cdot 10^{-5}$	$\delta MI_{25,64} \leq 1.0 \cdot 10^{-4}$	$\delta MI_{25,65} \leq 1.0 \cdot 10^{-4}$	$\delta MI_{25,66} \leq 1.0 \cdot 10^{-4}$
Row	Upper limits for the monthly variations of the MI_{36} elements to be measured in flight					
4 th	$\delta MI_{36,41} \leq 9.05 \cdot 10^{-6}$	$\delta MI_{36,42} \leq 5.0 \cdot 10^{-6}$	$\delta MI_{36,43} \leq 5.0 \cdot 10^{-6}$	$\delta MI_{36,44} \leq 2.0 \cdot 10^{-5}$	$\delta MI_{36,45} \leq 1.0 \cdot 10^{-4}$	$\delta MI_{36,46} \leq 1.0 \cdot 10^{-4}$
5 th	$\delta MI_{36,51} \leq 5.0 \cdot 10^{-5}$	$\delta MI_{36,52} \leq 5.0 \cdot 10^{-5}$	$\delta MI_{36,53} \leq 5.0 \cdot 10^{-5}$	$\delta MI_{36,54} \leq 1.0 \cdot 10^{-4}$	$\delta MI_{36,55} \leq 1.0 \cdot 10^{-4}$	$\delta MI_{36,56} \leq 1.0 \cdot 10^{-4}$
6 th	$\delta MI_{36,61} \leq 5.0 \cdot 10^{-7}$	$\delta MI_{36,62} \leq 5.0 \cdot 10^{-7}$	$\delta MI_{36,63} \leq 9.05 \cdot 10^{-6}$	$\delta MI_{36,64} \leq 1.0 \cdot 10^{-6}$	$\delta MI_{36,65} \leq 1.0 \cdot 10^{-6}$	$\delta MI_{36,66} \leq 2.0 \cdot 10^{-5}$

Table 3.3-6: Tolerable upper limits for the variation of the elements of $[MI]_{d,ij}$, $[MI]_{c,ij}$ ($ij=14, 25, 36$) to be measured in flight, in the minimum period between two successive on-orbit calibrations (1 month)

Row	Upper limit for the absolute measurement error of the elements of MI_{14} involved in the computation of $\underline{a}_{d,14}$					
4 th	$\delta MI_{14,41} \leq 4.7 \cdot 10^{-6}$	$\delta MI_{14,42} \leq 4.5 \cdot 10^{-6}$	$\delta MI_{14,43} \leq 4.5 \cdot 10^{-6}$	$\delta MI_{14,44} \leq 2.0 \cdot 10^{-3}$	$\delta MI_{14,45} \leq 5.0 \cdot 10^{-5}$	$\delta MI_{14,46} \leq 5.0 \cdot 10^{-5}$
5 th	$\delta MI_{14,51} \leq 1.0 \cdot 10^{-4}$	$\delta MI_{14,52} \leq 5.0 \cdot 10^{-4}$	$\delta MI_{14,53} \leq 1.0 \cdot 10^{-4}$	$\delta MI_{14,54} \leq 5.0 \cdot 10^{-5}$	$\delta MI_{14,55} \leq 1.0 \cdot 10^{-2}$	$\delta MI_{14,56} \leq 5.0 \cdot 10^{-5}$
6 th	$\delta MI_{14,61} \leq 4.5 \cdot 10^{-5}$	$\delta MI_{14,62} \leq 4.5 \cdot 10^{-5}$	$\delta MI_{14,63} \leq 4.87 \cdot 10^{-5}$	$\delta MI_{14,64} \leq 5.0 \cdot 10^{-5}$	$\delta MI_{14,65} \leq 5.0 \cdot 10^{-5}$	$\delta MI_{14,66} \leq 2.0 \cdot 10^{-3}$
Row	Upper limit for the absolute measurement error of the elements of MI_{25} involved in the computation of $\underline{a}_{d,25}$					
4 th	$\delta MI_{25,41} \leq 1.0 \cdot 10^{-4}$	$\delta MI_{25,42} \leq 1.0 \cdot 10^{-4}$	$\delta MI_{25,43} \leq 1.0 \cdot 10^{-4}$	$\delta MI_{25,44} \leq 2.0 \cdot 10^{-3}$	$\delta MI_{25,45} \leq 5.0 \cdot 10^{-5}$	$\delta MI_{25,46} \leq 5.0 \cdot 10^{-5}$
5 th	$\delta MI_{25,51} \leq 4.5 \cdot 10^{-6}$	$\delta MI_{25,52} \leq 4.7 \cdot 10^{-6}$	$\delta MI_{25,53} \leq 4.5 \cdot 10^{-6}$	$\delta MI_{25,54} \leq 5.0 \cdot 10^{-5}$	$\delta MI_{25,55} \leq 2.0 \cdot 10^{-3}$	$\delta MI_{25,56} \leq 5.0 \cdot 10^{-5}$
6 th	$\delta MI_{25,61} \leq 1.0 \cdot 10^{-4}$	$\delta MI_{25,62} \leq 1.0 \cdot 10^{-4}$	$\delta MI_{25,63} \leq 5.0 \cdot 10^{-4}$	$\delta MI_{25,64} \leq 5.0 \cdot 10^{-5}$	$\delta MI_{25,65} \leq 5.0 \cdot 10^{-5}$	$\delta MI_{25,66} \leq 1.0 \cdot 10^{-2}$
Row	Upper limit for the absolute measurement error of the elements of MI_{36} involved in the computation of $\underline{a}_{d,36}$					
4 th	$\delta MI_{36,41} \leq 4.87 \cdot 10^{-5}$	$\delta MI_{36,42} \leq 4.5 \cdot 10^{-5}$	$\delta MI_{36,43} \leq 4.5 \cdot 10^{-5}$	$\delta MI_{36,44} \leq 2.0 \cdot 10^{-3}$	$\delta MI_{36,45} \leq 5.0 \cdot 10^{-5}$	$\delta MI_{36,46} \leq 5.0 \cdot 10^{-5}$
5 th	$\delta MI_{36,51} \leq 1.0 \cdot 10^{-4}$	$\delta MI_{36,52} \leq 5.0 \cdot 10^{-4}$	$\delta MI_{36,53} \leq 1.0 \cdot 10^{-4}$	$\delta MI_{36,54} \leq 5.0 \cdot 10^{-5}$	$\delta MI_{36,55} \leq 1.0 \cdot 10^{-2}$	$\delta MI_{36,56} \leq 5.0 \cdot 10^{-5}$
6 th	$\delta MI_{36,61} \leq 4.5 \cdot 10^{-6}$	$\delta MI_{36,62} \leq 4.5 \cdot 10^{-6}$	$\delta MI_{36,63} \leq 4.7 \cdot 10^{-6}$	$\delta MI_{36,64} \leq 5.0 \cdot 10^{-5}$	$\delta MI_{36,65} \leq 5.0 \cdot 10^{-5}$	$\delta MI_{36,66} \leq 2.0 \cdot 10^{-3}$

Row	Upper limit for the relative measurement error of the elements of MI_{14} involved in the computation of $\underline{a}_{d,14}$					
4 th	$\delta r MI_{14,41} \leq 0.1\%$	$\delta r MI_{14,42} \leq 3.1\%$	$\delta r MI_{14,43} \leq 3.4\%$	$\delta r MI_{14,44} \leq 49\%$	$\delta r MI_{14,45} \leq 34.2\%$	$\delta r MI_{14,46} \leq 37.8\%$
5 th	$\delta r MI_{14,51} \leq 68.4\%$	$\delta r MI_{14,52} \leq 0.9\%$	$\delta r MI_{14,53} \leq 72.1\%$	$\delta r MI_{14,54} \leq 34.2\%$	$\delta r MI_{14,55} \leq 17.3\%$	$\delta r MI_{14,56} \leq 267\%$
6 th	$\delta r MI_{14,61} \leq 34.1\%$	$\delta r MI_{14,62} \leq 32.4\%$	$\delta r MI_{14,63} \leq 1.2\%$	$\delta r MI_{14,64} \leq 37.8\%$	$\delta r MI_{14,65} \leq 267\%$	$\delta r MI_{14,66} \leq 49\%$
Row	Upper limit for the relative measurement error of the elements of MI_{25} involved in the computation of $\underline{a}_{d,25}$					
4 th	$\delta r MI_{25,41} \leq 2.4\%$	$\delta r MI_{25,42} \leq 75.7\%$	$\delta r MI_{25,43} \leq 72.1\%$	$\delta r MI_{25,44} \leq 49\%$	$\delta r MI_{25,45} \leq 37.8\%$	$\delta r MI_{25,46} \leq 267\%$
5 th	$\delta r MI_{25,51} \leq 3.4\%$	$\delta r MI_{25,52} \leq 0.1\%$	$\delta r MI_{25,53} \leq 3.1\%$	$\delta r MI_{25,54} \leq 37.8\%$	$\delta r MI_{25,55} \leq 49\%$	$\delta r MI_{25,56} \leq 34.2\%$
6 th	$\delta r MI_{25,61} \leq 72.1\%$	$\delta r MI_{25,62} \leq 68.4\%$	$\delta r MI_{25,63} \leq 0.9\%$	$\delta r MI_{25,64} \leq 267\%$	$\delta r MI_{25,65} \leq 34.2\%$	$\delta r MI_{25,66} \leq 17.3\%$
Row	Upper limit for the relative measurement error of the elements of MI_{36} involved in the computation of $\underline{a}_{d,36}$					
4 th	$\delta r MI_{36,41} \leq 1.2\%$	$\delta r MI_{36,42} \leq 32.4\%$	$\delta r MI_{36,43} \leq 34.1\%$	$\delta r MI_{36,44} \leq 49\%$	$\delta r MI_{36,45} \leq 267\%$	$\delta r MI_{36,46} \leq 37.8\%$
5 th	$\delta r MI_{36,51} \leq 72.1\%$	$\delta r MI_{36,52} \leq 0.9\%$	$\delta r MI_{36,53} \leq 68.4\%$	$\delta r MI_{36,54} \leq 267\%$	$\delta r MI_{36,55} \leq 17.3\%$	$\delta r MI_{36,56} \leq 34.2\%$
6 th	$\delta r MI_{36,61} \leq 3.4\%$	$\delta r MI_{36,62} \leq 3.1\%$	$\delta r MI_{36,63} \leq 0.1\%$	$\delta r MI_{36,64} \leq 37.8\%$	$\delta r MI_{36,65} \leq 34.2\%$	$\delta r MI_{36,66} \leq 49\%$

These elements are “by construction” significantly smaller than the required knowledge accuracy

Table 3.3-7: Measurement accuracy (above) and relative error (below) of the elements of $[MI]_{d,ij}$, $[MI]_{c,ij}$ ($ij=14, 25, 36$) to be provided by the Gradiometer on-orbit calibration

Row	$[MI']_{c,14}$			$[MI']_{d,14}$		
1 st	$\delta MI_{14,11} \leq 2.1 \cdot 10^{-3}$	$\delta MI_{14,12} \leq 8.3 \cdot 10^{-5}$	$\delta MI_{14,13} \leq 5.5 \cdot 10^{-5}$	$\delta MI_{14,14} \leq 7.7 \cdot 10^{-5}$	$\delta MI_{14,15} \leq 3.7 \cdot 10^{-5}$	$\delta MI_{14,16} \leq 9.4 \cdot 10^{-6}$
2 nd	$\delta MI_{14,21} \leq 1.8 \cdot 10^{-4}$	$\delta MI_{14,22} \leq 2.2 \cdot 10^{-2}$	$\delta MI_{14,23} \leq 1.7 \cdot 10^{-4}$	$\delta MI_{14,24} \leq 1.8 \cdot 10^{-4}$	$\delta MI_{14,25} \leq 1.3 \cdot 10^{-2}$	$\delta MI_{14,26} \leq 1.7 \cdot 10^{-4}$
3 rd	$\delta MI_{14,31} \leq 1.5 \cdot 10^{-4}$	$\delta MI_{14,32} \leq 2.0 \cdot 10^{-4}$	$\delta MI_{14,33} \leq 2.1 \cdot 10^{-3}$	$\delta MI_{14,34} \leq 5.4 \cdot 10^{-5}$	$\delta MI_{14,35} \leq 6.7 \cdot 10^{-5}$	$\delta MI_{14,36} \leq 1.2 \cdot 10^{-4}$
Row	$[MI']_{c,25}$			$[MI']_{d,25}$		
1 st	$\delta MI_{25,11} \leq 2.2 \cdot 10^{-3}$	$\delta MI_{25,12} \leq 1.5 \cdot 10^{-4}$	$\delta MI_{25,13} \leq 1.7 \cdot 10^{-4}$	$\delta MI_{25,14} \leq 2.2 \cdot 10^{-4}$	$\delta MI_{25,15} \leq 1.5 \cdot 10^{-4}$	$\delta MI_{25,16} \leq 1.7 \cdot 10^{-4}$
2 nd	$\delta MI_{25,21} \leq 5.5 \cdot 10^{-5}$	$\delta MI_{25,22} \leq 2.1 \cdot 10^{-3}$	$\delta MI_{25,23} \leq 8.3 \cdot 10^{-5}$	$\delta MI_{25,24} \leq 9.4 \cdot 10^{-6}$	$\delta MI_{25,25} \leq 7.7 \cdot 10^{-5}$	$\delta MI_{25,26} \leq 3.7 \cdot 10^{-5}$
3 rd	$\delta MI_{25,31} \leq 1.7 \cdot 10^{-4}$	$\delta MI_{25,32} \leq 1.8 \cdot 10^{-4}$	$\delta MI_{25,33} \leq 2.2 \cdot 10^{-2}$	$\delta MI_{25,34} \leq 1.7 \cdot 10^{-4}$	$\delta MI_{25,35} \leq 1.8 \cdot 10^{-4}$	$\delta MI_{25,36} \leq 1.3 \cdot 10^{-2}$
Row	$[MI']_{c,36}$			$[MI']_{d,36}$		
1 st	$\delta MI_{36,11} \leq 2.1 \cdot 10^{-3}$	$\delta MI_{36,12} \leq 1.7 \cdot 10^{-4}$	$\delta MI_{36,13} \leq 1.5 \cdot 10^{-4}$	$\delta MI_{36,14} \leq 1.2 \cdot 10^{-4}$	$\delta MI_{36,15} \leq 6.7 \cdot 10^{-5}$	$\delta MI_{36,16} \leq 5.4 \cdot 10^{-5}$
2 nd	$\delta MI_{36,21} \leq 1.7 \cdot 10^{-4}$	$\delta MI_{36,22} \leq 2.2 \cdot 10^{-2}$	$\delta MI_{36,23} \leq 1.8 \cdot 10^{-4}$	$\delta MI_{36,24} \leq 1.7 \cdot 10^{-4}$	$\delta MI_{36,25} \leq 1.3 \cdot 10^{-2}$	$\delta MI_{36,26} \leq 1.8 \cdot 10^{-4}$
3 rd	$\delta MI_{36,31} \leq 5.5 \cdot 10^{-5}$	$\delta MI_{36,32} \leq 8.3 \cdot 10^{-5}$	$\delta MI_{36,33} \leq 2.1 \cdot 10^{-3}$	$\delta MI_{36,34} \leq 9.4 \cdot 10^{-6}$	$\delta MI_{36,35} \leq 3.7 \cdot 10^{-5}$	$\delta MI_{36,36} \leq 7.7 \cdot 10^{-5}$

Table 3.3-8: Knowledge accuracy of the elements of $[MI']_{c,ij}$, $[MI']_{d,ij}$ ($ij=14, 25, 36$) obtained from the knowledge of the elements of $[MI]_{c,ij}$, $[MI]_{d,ij}$ with the accuracy specified in Table 3.3-4

4. DETERMINATION OF THE QUADRATIC FACTORS

The accelerometer quadratic non linearity can be physically adjusted on-orbit, so to reduce its contribution to the gradiometric error below the specification. This operation must be performed before measuring the Calibration Matrix. In fact, the determination of this matrix assumes that the remaining errors that still affect the measurement of the common-mode and differential-mode accelerations in the OAGRF are only those due to the coupling of these accelerations with the differential and common scale factors, misalignments and coupling between axes of the accelerometer pairs.

The reduction of the quadratic factors below the limits provided in Table 3.3.2 requires their determination with the accuracy limits of Table 3.3.3 at least.

The measurement of $K2$ is based on a method devised by D. Lamarre, which does not require any shaking of the whole satellite by means of thrusters, but only the shaking of the individual accelerometer proof masses achieved by means of the proof-mass detection/control electrodes. This method is described in details in the following section.

4.1 METHOD DESCRIPTION

This method exploits the basic characteristic of a non-linear accelerometer that under an input acceleration a provides an output acceleration proportional to both a and a^2 :

$$a' = K \cdot a + K2 \cdot a^2$$

Thus, by introducing a sinusoidal component at frequency ν_e in the input acceleration

$$a = A_e \cdot \sin(2\pi\nu_e \cdot t)$$

we get in the output a DC component and a component at $2 \cdot \nu_e$.

$$\begin{aligned} a' &= K \cdot A_e \cdot \sin(2\pi\nu_e \cdot t) + K2 \cdot A_e^2 \cdot \sin^2(2\pi\nu_e \cdot t) = K \cdot A_e \cdot \sin(2\pi\nu_e \cdot t) + K2 \cdot A_e^2 \cdot \frac{1 - \cos(4\pi\nu_e \cdot t)}{2} \\ &= \frac{1}{2} K2 \cdot A_e^2 + K \cdot A_e \cdot \sin(2\pi\nu_e \cdot t) - \frac{1}{2} K2 \cdot A_e^2 \cdot \cos(4\pi\nu_e \cdot t) \end{aligned}$$

Rather than obtaining the quadratic factor $K2$ from the component at $2 \cdot \nu_e$, $\frac{1}{2} K2 \cdot A_e^2 \cdot \cos(4\pi\nu_e \cdot t)$, "Lamarre's method" works on

the DC term $\frac{1}{2} K2 \cdot A_e^2$. A train of sinusoidal accelerations (or of another kind of regular signal) is periodically applied to the proof mass. The frequency of the sinusoid is chosen to be well above the cut-off frequency of the transfer function filtering the

output acceleration ($\nu_e = 1/T_e \gg \nu_{cutoff}$), so that the components $K \cdot A_e \cdot \sin(2\pi\nu_e \cdot t)$ and $\frac{1}{2} K2 \cdot A_e^2 \cdot \cos(4\pi\nu_e \cdot t)$ are not "visible" in

the accelerometer output. The period T_s of the sinusoid application is instead chosen as $\nu_s = 1/T_s < \nu_{cutoff}$ so that the periodic sequence of DC components produced by the accelerometer non linearity is detectable. The relationship between the sinusoidal input and the output acceleration is graphically depicted in the following Figure 4.1-1.

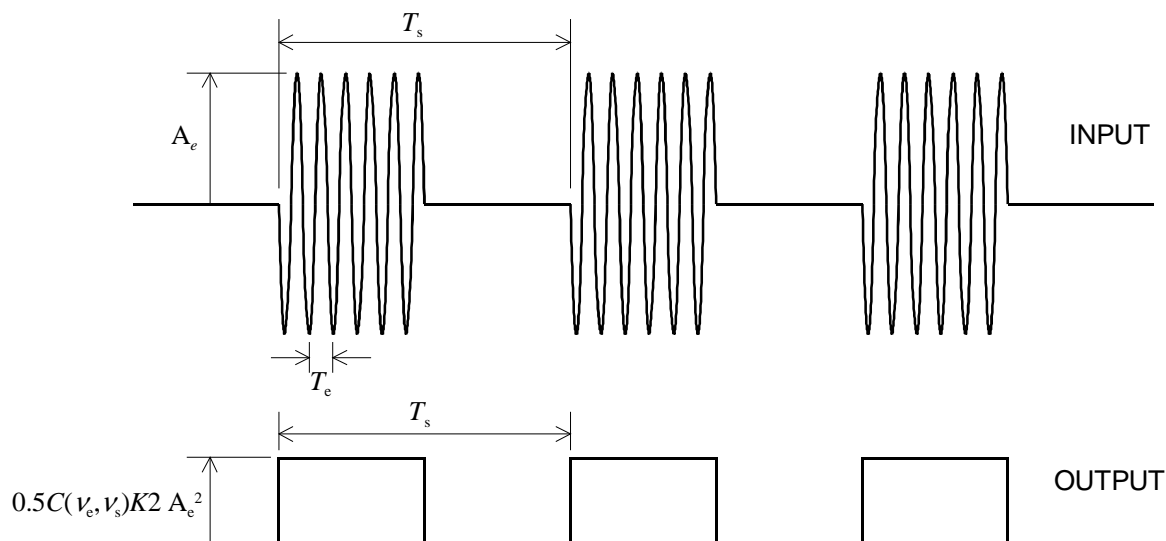
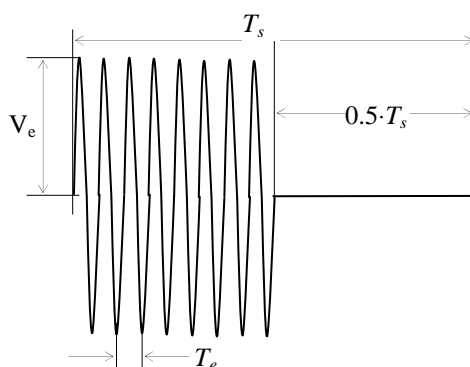


Figure 4.1-1: Relationship between the proof mass shaking acceleration and the accelerometer output acceleration

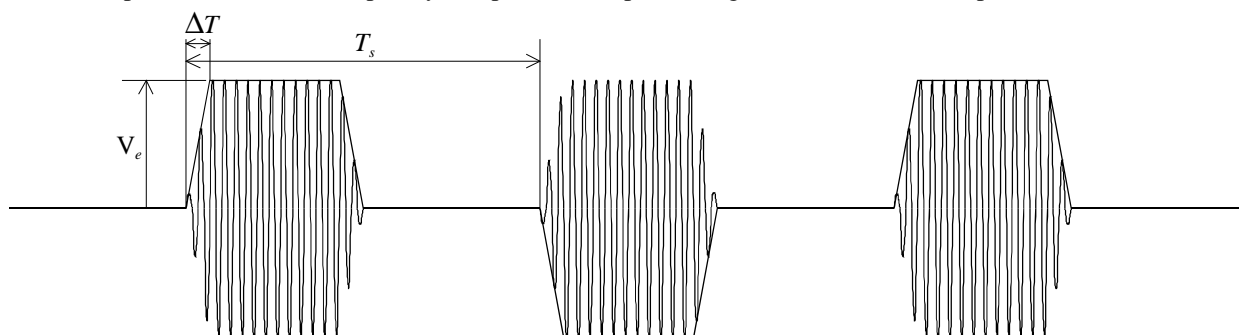
To measure the quadratic factor $K2_{i,k}$ of the accelerometer A_i ($i = 1, \dots, 6$) along its axis k ($k = X, Y$ or Z axis of the Accelerometer Reference Frame), the GA&E S/W adds to the value of the voltage ($V_{c,k}$), computed by the PID law for the control of the proof-mass of linear degree of freedom k , a quantity (V_s) which over a time period T_s has the following profile:

$$V_s(t) = V_e \cdot \sin(2\pi v_e \cdot t), \text{ for } T_{\text{start}} \leq t \leq 0.5 \cdot T_s$$

$$V_s(t) = 0, \text{ for } 0.5 \cdot T_s < t \leq T_s.$$



In the actual implementation the profile is slightly different. In fact numerical simulations of this method (Appendix B, section 9.1) shows that to avoid overshoots of the proof mass controller and generation of spurious signals at the frequency v_s , the sinusoidal pattern must be enveloped by a trapezoidal shape with sign inversion at each T_s period.



The quantity V_s is added to $V_{c,k}$ just after the PID control law, before the control voltages are re-combined for their distribution among the 8 electrode pairs, and converted in analogue signal by the DAC, and after the DFAC output branch as indicated in the scheme of Figure 4.1-2.

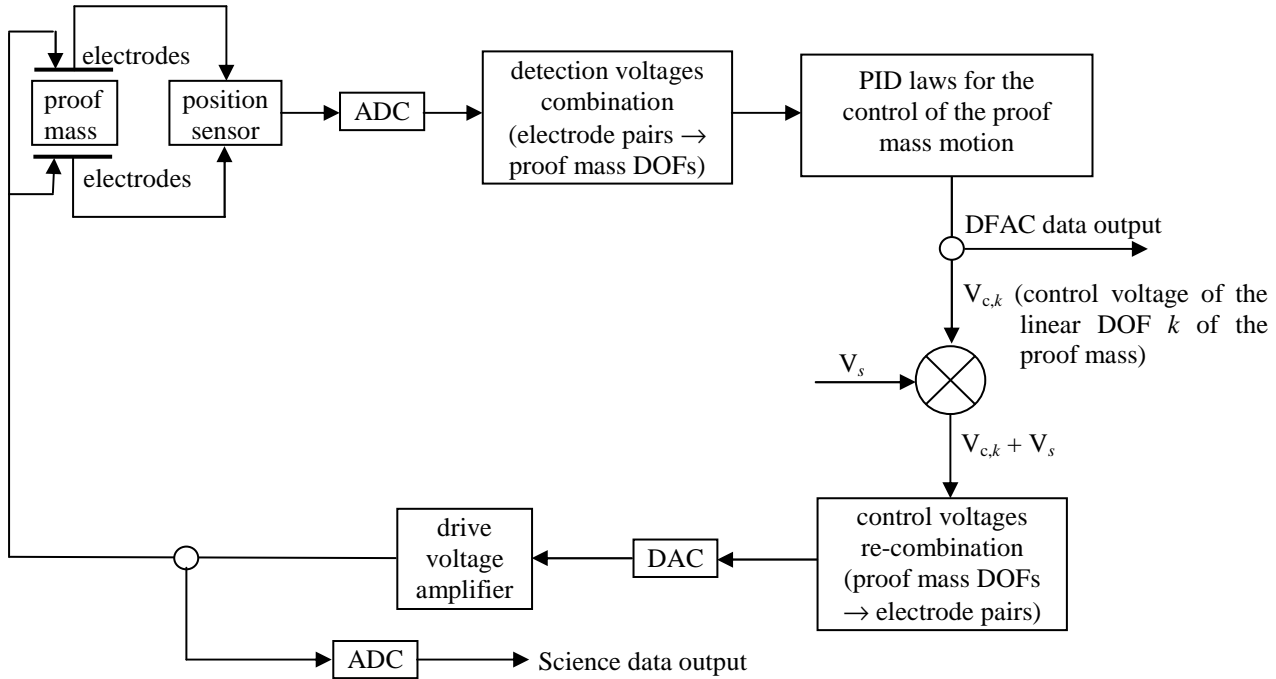


Figure 4.1-2: Scheme of the proof mass control loop with the insertion point of the shaking voltage V_s

The quantity V_s must have a frequency $\nu_e = 1/T_e$ much larger than the bandwidth of the proof-mass control loop, a period T_s so that $\nu_s = 1/T_s$ is smaller than the cut-off frequency of the filter in the scientific channel output, and must be added to $V_{c,k}$ for a number N_s of consecutive periods T_s , for an overall time $T = N_s \cdot T_s$.

The amplitude V_e of the sinusoidal voltage is chosen, so to induce on the proof mass a corresponding sinusoidal acceleration of amplitude A_e which repeats the profile of the V_s .

The relationship between V_e and A_e is:

$$A_e = G_{el} \cdot G_A \cdot V_e$$

where G_A is the nominal gain of the drive voltage amplifier (DVA) transfer function ($G_A = 3.98$ for the less sensitive axis; $G_A = 17.99$ for the ultra-sensitive axes) and the G_{el} is the nominal electrostatic gain of the accelerometer, whose expression (depending on the accelerometer axis considered) is

$$G_{el} = G_{el_X} = 8 \frac{\epsilon \bar{S}_X V_p}{m \bar{e}_X^2}, \text{ for the accelerometer less sensitive axis (denoted as X-axis in the Accelerometer Electrode}$$

System Reference Frame, AESRF);

$$G_{el} = G_{el_Y} = 4 \frac{\epsilon \bar{S}_Y V_p}{m \bar{e}_Y^2}, \text{ for the accelerometer ultra sensitive axis Y (in the AESRF);}$$

$$G_{el} = G_{el_Z} = 4 \frac{\epsilon \bar{S}_Z V_p}{m \bar{e}_Z^2}, \text{ for the accelerometer ultra sensitive axis Z (in the AESRF);}$$

with

- m = mass of the proof mass = 0.319 kg (nominal);
- \bar{e}_X = mean value of the gap between the proof mass and the electrodes X_i^+ , X_i^- ($i = 1,2,3,4$) = 32 μm (nominal);
- \bar{e}_Y = mean value of the gap between the proof mass and the electrodes Y_i^+ , Y_i^- ($i = 1,2$) = 299 μm (nominal);
- \bar{e}_Z = mean value of the gap between the proof mass and the electrodes Z_i^+ , Z_i^- ($i = 1,2$) = 299 μm (nominal);
- \bar{S}_X = mean value of the area of each electrode X_i^\pm ($i = 1,2,3,4$) = 2.62 cm^2 (nominal);
- \bar{S}_Z = mean value of the area of each electrode Y_i^\pm ($i = 1,2$) = 1.05 cm^2 (nominal);
- \bar{S}_Z = mean value of the area of each electrode Z_i^\pm ($i = 1,2$) = 1.05 cm^2 (nominal);
- ϵ = vacuum dielectric constant

For instance, an acceleration amplitude $A_e = 10^{-5} \text{ m/s}^2$ is achieved with a voltage $V_e = 18.97 \text{ mV}$.

The coupling of this input acceleration (successive trains of high-frequency sinusoids) on the proof mass with the accelerometer non linearity represented by the quadratic factor, produces in the acceleration ($a'_{i,k}$) measured by the accelerometer along the axis k a square wave signal with frequency $\nu_{sw} = \nu_s$ and amplitude:

$$A_{sw} = C(\nu_e, \nu_s) \frac{A_e^2}{2} K_{2,i,k} \quad (4.1.1)$$

where $C(\nu_e, \nu_s)$ is a correction factor that depends on the accelerometer output channel from which the measured acceleration ($a'_{i,k}$) is taken. When the measured acceleration is taken from the DFAC output channel of the accelerometer $C(\nu_e, \nu_s)$ has the following expression ([RD 10]):

$$C(\nu_e, \nu_s) = \left(\frac{H_A(\nu_s)}{G_A} \right)^{-1} \left(\frac{H_A(\nu_e)}{G_A} (1 - B_F(\nu_e)) \right)^2 \quad (4.1.2)$$

where $H_A(\nu)$ is the DVA transfer function, G_A is the gain of the DVA transfer function, $B_F(\nu)$ is the transfer function of the proof mass closed-loop control. Note that for ν_s inside the accelerometer MBW and ν_e much larger than the bandwidth of the proof-mass control loop

$$\frac{H_A(\nu_s)}{G_A} \cong 1 \quad \text{and} \quad (1 - B_F(\nu_e)) \cong 1.$$

The plot of the correction factor modulus and phase as function of the frequency ν_e , for $\nu_s = 50 \text{ mHz}$, is shown in Figure 4.1-2. The values of $|C(\nu_e, \nu_s)|$ for $\nu_s = 50 \text{ mHz}$ and $\nu_e = 100, 150, 200, 250, 300, 350 \text{ Hz}$ are 0.6489, 0.4312, 0.2779, 0.1795, 0.1180, 0.0792, respectively.

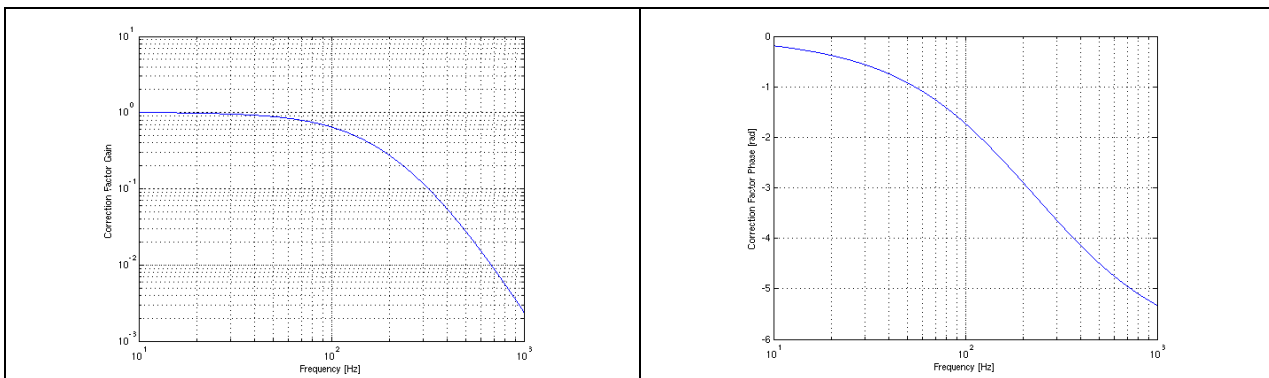


Figure 4.1-2: Modulus and phase of the correction factor $C(\nu_e, \nu_s)$ as function of ν_e , for $\nu_s = 50 \text{ mHz}$

Of course, this signal is not only contained in the acceleration ($a'_{i,k}$) measured by the “excited” accelerometer A_i (i.e. the accelerometer under calibration) along the excitation axis k , but also in any combination of $a'_{i,k}$ with the accelerations measured by the other accelerometers. The utilisation of the combination of measured accelerations for the determination of the quadratic factor is useful for removing most of the background noise affecting $a'_{i,k}$. In particular, the combinations of measured acceleration that shall be utilised are provided in Table 4.1-1. It is strictly limited to the quadratic factors that need to be necessarily measured and adjusted in flight in order to ensure the fulfilment of the gradiometric mission objectives (see section 3.3.1).

Any combination of measured accelerations (here denoted generically as a'_{mix}) must be processed in order to extract the amplitude (A_{sw}) of the square wave signal at frequency ν_s contained in it (i.e. in the measured acceleration $a'_{i,k}$ contained in a'_{mix}). This processing consists in a synchronous demodulation of a'_{mix} at the frequency ν_s . The synchronous demodulation must not only determine the amplitude of the square wave but also its sign, which is determined by the sign of the quadratic factor which multiplies the “excited” acceleration. The mathematical formulation of this synchronous demodulation is:

$$A_{\text{sw}} = \pi \sqrt{A_s^2 + A_c^2} \cdot \frac{A_s}{|A_s|} \quad (4.1.3)$$

$$\text{with } A_s = 2 \frac{1}{N} \sum_{i=1}^N a'_{\text{mix}}(T_i) \cdot \sin(2\pi\nu_s \cdot T_i), \quad A_c = 2 \frac{1}{N} \sum_{i=1}^N a'_{\text{mix}}(T_i) \cdot \cos(2\pi\nu_s \cdot T_i),$$

(the factor 2 “compensates” the factor 0.5 in the definition of a'_{mix})

where N is the number of points of the time series of a'_{mix} corresponding to the period ΔT in which the periodic acceleration signal has been applied to the accelerometer A_i (ΔT shall include an integer number of signal cycles, starting from a phase = 0 point, i.e. from the beginning of a cycle).

The term $\frac{A_s}{|A_s|}$ in the expression of A_{sw} allows to recovery also the sign information: the quadratic factor can be positive or negative, and so the sign of the resulting square wave in the measured acceleration. The equation (4.1.3) allows to recover the correct sign of $K2$, if the DVA and the proof mass closed-loop control transfer functions does not introduce phase shifts larger than 90° in the square wave resulting from the trains of high-frequency sinusoids.

From A_{sw} , the estimated value of $K2_{i,k}$ (quadratic factor of the accelerometer A_i along the axis k) is then obtained as:

$$\hat{K}2_{i,k} = CI(\nu_e, \nu_s) \frac{2}{A_e^2} A_{\text{sw}} \quad (4.1.4)$$

with $CI(\nu_e, \nu_s) = C(\nu_e, \nu_s)^{-1}$.

From the quadratic factor values so determined, the offset ($\Delta_{i,k}$) to be added in proof mass position control loop of the accelerometer A_i along the axis k ($k = X, Y, Z$), in order to nullify $K2_{i,k}$ is then obtained as follows:

$$\Delta_{i,k} = -G_{\text{dpos},i,k} \bar{e}_{i,k} V_p \bar{G}_{el,i,k} K2_{i,k} \quad (4.1.5)$$

where:

- V_p = nominal polarisation voltage applied to the accelerometer proof mass;
- $\bar{e}_{i,k}$ = mean value of the gap between the accelerometer A_i proof mass and the electrodes along the axis k ;
- $\bar{G}_{el,i,k}$ = mean value of the accelerometer A_i electrostatic gain for the axis k
- $G_{\text{dpos},i,k} = \langle G_{\text{det},i,k} \cdot G_{\text{pos},i,k} \rangle \cdot V_d$, where V_d is the detection voltage and $\langle \rangle$ denotes the mathematical average
- $G_{\text{det},i,k}$ = electronic gain of the detector (V/Farad/V);
- $G_{\text{pos},i,k}$ = geometric gain of the detector (Farad/m).

The quadratic factor measurements shall be performed in the same drag free control mode utilised for the scientific data acquisition. Table 4.1-2 reports the combinations of the accelerometer measurements that shall be utilised to feed the DFACS controllers during the measurement of the various quadratic factors. In order to avoid any possible interference between the

quadratic factor measurement and the drag-free control function, we consider now a scenario in which the DFACS is fed by the measurements of the two OAGs not containing the accelerometer under calibration, i.e. subject to shaking. This potential interference between the K2 measurement and the DFACS performance will be investigated by numerical simulations and, in case it will be found acceptable, no restriction in the use of the accelerometer measurements will be applied (the software which interfaces the gradiometer outputs with the DFACS is configured so that both solutions can be applied). The linear accelerations utilised by the DFACS controllers are synthesized using as far as possible ultra-sensitive axes. The table is filled taking into account that there is no longer drag free control along the Y and Z axes of the satellite, therefore it is no longer necessary to feed the DFACS controllers with the linear accelerations measured along these two axes. The three-axis angular acceleration measurement is instead still utilised by the DFACS, in spite of the “weakness” of the attitude control achievable by the magnetic torquers actuators (now replacing the micro-propulsion for the attitude control function).

In table 4.1-2, only the quadratic factors that need to be necessarily measured and adjusted in flight in order to ensure the fulfilment of the gradiometric mission objectives (see section 3.3.1) are considered.

Excited sensor, axis	Measured quadratic factor	Utilised combination of measured accelerations (a'_{mix}) ^(*)	Background noise main terms removed by a'_{mix}	Background noise main terms remaining in a'_{mix} (for a perfect gradiometer)
A ₁ X axis	K _{2,1,X}	$a'_{\text{mix}} = a'_{d,14,X} = \frac{1}{2} (a'_{1,X} - a'_{4,X})$	Common-mode accelerations	$-\frac{L_X}{2} (U_{XX} + \omega_Y^2 + \omega_Z^2) + n_{d,14,X}$
A ₄ X axis	K _{2,4,X}	$a'_{\text{mix}} = -a'_{d,14,X} = -\frac{1}{2} (a'_{1,X} - a'_{4,X})$	Common-mode accelerations	$\frac{L_X}{2} (U_{XX} + \omega_Y^2 + \omega_Z^2) - n_{d,14,X}$
A ₁ Z axis	K _{2,1,Z}	$a'_{\text{mix}} = a'_{d,14,Z} + \frac{L_X}{L_Z} a'_{d,36,X}$ $= \frac{1}{2} (a'_{1,Z} - a'_{4,Z}) + \frac{L_X}{L_Z} \frac{1}{2} (a'_{3,X} - a'_{6,X})$	Common-mode accelerations and $\dot{\omega}_Y$	$-L_X (U_{XZ} - \omega_X \omega_Z)$ $+ n_{d,14,Z} + \frac{L_X}{L_Z} n_{d,36,X}$ ^(**)
A ₄ Z axis	K _{2,4,Z}	$a'_{\text{mix}} = -a'_{d,14,Z} - \frac{L_X}{L_Z} a'_{d,36,X}$ $= -\frac{1}{2} (a'_{1,Z} - a'_{4,Z}) - \frac{L_X}{L_Z} \frac{1}{2} (a'_{3,X} - a'_{6,X})$	Common-mode accelerations and $\dot{\omega}_Y$	$L_X (U_{XZ} - \omega_X \omega_Z)$ $- n_{d,14,Z} - \frac{L_X}{L_Z} n_{d,36,X}$
A ₂ X axis	K _{2,2,X}	$a'_{\text{mix}} = a'_{d,25,X} + \frac{L_Y}{L_X} a'_{d,14,Y}$ $= \frac{1}{2} (a'_{2,X} - a'_{5,X}) + \frac{L_Y}{L_X} \frac{1}{2} (a'_{1,Y} - a'_{4,Y})$	Common-mode accelerations and $\dot{\omega}_Z$	$-L_Y (U_{XY} - \omega_X \omega_Y)$ $+ n_{d,25,X} + \frac{L_Y}{L_X} n_{d,14,Y}$
A ₅ X axis	K _{2,5,X}	$a'_{\text{mix}} = -a'_{d,25,X} - \frac{L_Y}{L_X} a'_{d,14,Y}$ $= -\frac{1}{2} (a'_{2,X} - a'_{5,X}) - \frac{L_Y}{L_X} \frac{1}{2} (a'_{1,Y} - a'_{4,Y})$	Common-mode accelerations and $\dot{\omega}_Z$	$L_Y (U_{XY} - \omega_X \omega_Y)$ $- n_{d,25,X} - \frac{L_Y}{L_X} n_{d,14,Y}$
A ₂ Y axis	K _{2,2,Y}	$a'_{\text{mix}} = a'_{d,25,Y} = \frac{1}{2} (a'_{2,Y} - a'_{5,Y})$	Common-mode accelerations	$-\frac{L_Y}{2} (U_{YY} + \omega_X^2 + \omega_Z^2) + n_{d,25,Y}$
A ₅ Y axis	K _{2,5,Y}	$a'_{\text{mix}} = -a'_{d,25,Y} = -\frac{1}{2} (a'_{2,Y} - a'_{5,Y})$	Common-mode accelerations	$\frac{L_Y}{2} (U_{YY} + \omega_X^2 + \omega_Z^2) - n_{d,25,Y}$

A_3 X axis	$K2_{3,X}$	$a'_{\text{mix}} = a'_{d,36,X} + \frac{L_Z}{L_X} a'_{d,14,Z}$ $= \frac{1}{2} (\underline{a'_{3,X}} - \underline{a'_{6,X}}) + \frac{L_Z}{L_X} \frac{1}{2} (a'_{1,Z} - \underline{a'_{4,Z}})$	Common-mode accelerations and $\dot{\omega}_Y$	$-L_Z (U_{XZ} - \omega_X \omega_Z)$ $+ n_{d,36,X} + \frac{L_Z}{L_X} n_{d,14,Z}$
A_6 X axis	$K2_{6,X}$	$a'_{\text{mix}} = -a'_{d,36,X} - \frac{L_Z}{L_X} a'_{d,14,Z}$ $= -\frac{1}{2} (\underline{a'_{3,X}} - \underline{a'_{6,X}}) - \frac{L_Z}{L_X} \frac{1}{2} (a'_{1,Z} - \underline{a'_{4,Z}})$	Common-mode accelerations and $\dot{\omega}_Y$	$L_Z (U_{XZ} - \omega_X \omega_Z)$ $- n_{d,36,X} - \frac{L_Z}{L_X} n_{d,14,Z}$
A_3 Z axis	$K2_{3,Z}$	$a'_{\text{mix}} = a'_{d,36,Z} = \frac{1}{2} (\underline{a'_{3,Z}} - \underline{a'_{6,Z}})$	Common-mode accelerations	$-\frac{L_Z}{2} (U_{ZZ} + \omega_X^2 + \omega_Y^2) + n_{d,36,Z}$
A_6 Z axis	$K2_{6,Z}$	$a'_{\text{mix}} = -a'_{d,36,Z} = -\frac{1}{2} (\underline{a'_{3,Z}} - \underline{a'_{6,Z}})$	Common-mode accelerations	$\frac{L_Z}{2} (U_{ZZ} + \omega_X^2 + \omega_Y^2) - n_{d,36,Z}$

(*) The underlined measured acceleration in the expression of a'_{mix} in the one containing the square wave signal.

(**) $n_{d,ij,k}$ denotes the differential acceleration measurement noise intrinsic of the accelerometer pair A_i, A_j along k

Table 4.1-1: Combinations of measured accelerations utilised to determine the various quadratic factors

Excited Sensor	Excited Axis	Measured quadratic factor	OAGs driving the DFACS	Synthesis of the linear (a_X) and angular ($\dot{\omega}_X, \dot{\omega}_Y, \dot{\omega}_Z$) accelerations utilised to feed the DFACS controllers
A_1	X	$K2_{1,X}$	OAG2, OAG3	$a_X = 0.5 \cdot (a_{c,25,X} + a_{c,36,X})$ $\dot{\omega}_X = -\frac{a_{d,36,Y}}{L_Z} + \frac{a_{d,25,Z}}{L_Y}, \dot{\omega}_Y = 2 \frac{a_{d,36,X}}{L_Z}, \dot{\omega}_Z = -2 \frac{a_{d,25,X}}{L_Y}$
A_4	X	$K2_{4,X}$		
A_1	Z	$K2_{1,Z}$		
A_4	Z	$K2_{4,Z}$		
A_2	X	$K2_{2,X}$	OAG1, OAG3	$a_X = 0.5 \cdot (a_{c,14,X} + a_{c,36,X})$ $\dot{\omega}_X = -2 \frac{a_{d,36,Y}}{L_Z}, \dot{\omega}_Y = -\frac{a_{d,14,Z}}{L_X} + \frac{a_{d,36,X}}{L_Z}, \dot{\omega}_Z = 2 \frac{a_{d,14,Y}}{L_X}$
A_5	X	$K2_{5,X}$		
A_2	Y	$K2_{2,Y}$		
A_5	Y	$K2_{5,Y}$		
A_3	X	$K2_{3,X}$	OAG1, OAG2	$a_X = 0.5 \cdot (a_{c,14,X} + a_{c,25,X})$ $\dot{\omega}_X = 2 \frac{a_{d,25,Z}}{L_Y}, \dot{\omega}_Y = -2 \frac{a_{d,14,Z}}{L_X}, \dot{\omega}_Z = -\frac{a_{d,25,X}}{L_Y} + \frac{a_{d,14,Y}}{L_X}$
A_6	X	$K2_{6,X}$		
A_3	Z	$K2_{3,Z}$		
A_6	Z	$K2_{6,Z}$		

Table 4.1-2: Combination of acceleration measurements feeding the DFACS (TBC) during the K2 measurement

4.2 METHOD ANALYSIS

4.2.1 Systematic Errors

Systematic errors in the determination of the quadratic factors with the method described before arise from:

1. The uncertainty in the knowledge of the actual amplitude (A_e) of the sinusoidal shaking which is applied to the proof mass.

The expression of this systematic error comes from the (4.1.4) and is: $\delta \hat{K} 2_{i,k} = -\frac{4}{A_e^3} A_{sw} \delta A_e = -2 \hat{K} 2_{i,k} \frac{\delta A_e}{A_e}$

2. The accuracy by which the product $(CI(v_e, v_s) \cdot A_{sw})$, between the amplitude of the square wave signal at frequency v_s contained in the measured accelerations and the correction factor of the accelerometer transfer function, can be determined.

The expression of this systematic error comes from the (4.1.4) and is: $\delta \hat{K} 2_{i,k} = \hat{K} 2_{i,k} \frac{\delta (CI(v_e, v_s) A_{sw})}{CI(v_e, v_s) A_{sw}}$

The values of these two types of systematic errors are summarised in Table 4.2-1. They have been computed from the following inputs:

- Values of the quadratic factors equal to their specified upper limits in-orbit, before their calibration (as per Table 3.1-3).
- Uncertainty in the knowledge of the actual amplitude of the sinusoidal shaking: $\frac{\delta A_e}{A_e} = 0.1\%$.
- Accuracy by which the the product $(CI(v_e, v_s) \cdot A_{sw})$, i.e. by which the amplitude A_{sw} of the square wave signal at frequency v_s is determined from the measured accelerations by the synchronous demodulation technique, and the correction factor $CI(v_e, v_s)$ is determined by the knowledge of the accelerometer transfer functions: $\frac{\delta (CI(v_e, v_s) A_{sw})}{CI(v_e, v_s) A_{sw}} = 0.1\%$.

Note that the systematic errors provided in Table 4.2-1 are larger than the specified measurement accuracy for the in-line quadratic factors (see Table 3.3-3). But the systematic errors are proportional to the value of the quadratic factor, and the computed error corresponds to a quadratic factor to be measured = 1206 s²/m (largest expected value). So after some measurement-correction iterations, the systematic errors will be reduced in parallel to K2. Therefore the systematic error is not a limiting factor for measuring and reducing the K2 below the specified target value. A similar iterative procedure is needed also to cope with the limitations on the quadratic factor adjustability (see section 3.3.1).

Quadratic factor	Quadratic factor value before calibration	Systematic error due to δA_e (1)	Systematic error due to $\delta(CI(v_e, v_s) \cdot A_{sw})$ (2)	Total systematic error (1) + (2)
$K2_{1,X}, K2_{4,X}$ ($K2_{c,14,X}, K2_{d,14,X}$)	1206 s ² /m	2.4 s ² /m	1.2 s ² /m	3.6 s ² /m
$K2_{1,Z}, K2_{4,Z}$ ($K2_{c,14,Z}, K2_{d,14,Z}$)	1206 s ² /m	2.4 s ² /m	1.2 s ² /m	3.6 s ² /m
$K2_{2,X}, K2_{5,X}$ ($K2_{c,25,X}, K2_{d,25,X}$)	1206 s ² /m	2.4 s ² /m	1.2 s ² /m	3.6 s ² /m
$K2_{2,Y}, K2_{5,Y}$ ($K2_{c,25,Y}, K2_{d,25,Y}$)	1206 s ² /m	2.4 s ² /m	1.2 s ² /m	3.6 s ² /m
$K2_{3,X}, K2_{6,X}$ ($K2_{c,36,X}, K2_{d,36,X}$)	1206 s ² /m	2.4 s ² /m	1.2 s ² /m	3.6 s ² /m
$K2_{3,Z}, K2_{6,Z}$ ($K2_{c,36,Z}, K2_{d,36,Z}$)	1206 s ² /m	2.4 s ² /m	1.2 s ² /m	3.6 s ² /m

Table 4.2-1: Systematic errors affecting the estimation of the quadratic factors

4.2.2 Random Errors

Random errors affecting the determination of the quadratic factors with the method described before arise from the background noise superimposed to the combination of measured accelerations (a'_{mix}) around the signal frequency (v_s). This noise comes from in turn from the environment (gravity gradient, residual linear/angular accelerations and angular rates under the action of the DFACS) and from the accelerometer intrinsic measurement error. Let's denote as \tilde{a}'_{mix} the spectral density of the background, random acceleration contained in a'_{mix} around the signal frequency v_s . Its standard deviation over the measurement duration T is

$$\sigma a'_{\text{mix}} = \frac{\tilde{a}'_{\text{mix}}}{\sqrt{T}}, \quad (4.1.6)$$

and represents the standard deviation of the random error on the amplitude ($\tilde{a}'_{\text{mix}}(v_s)$) of the harmonic component at the signal frequency (v_s) of a'_{mix} . This amplitude is related to A_{sw} and then to $K2_{i,k}$ as:

$$2 \tilde{a}'_{\text{mix}}(v_s) = 2 \frac{A_{sw}}{\pi} = C(v_e, v_s) \frac{A_e^2}{\pi} K2_{i,k} \quad (4.1.7)$$

The standard deviation of the random error on the corresponding $K2_{i,k}$ determined from a'_{mix} is

$$\sigma K2_{i,k} = \frac{\pi}{C(v_e, v_s) A_e^2} 2 \sigma a'_{\text{mix}} = \frac{\pi}{C(v_e, v_s) A_e^2} \frac{2 \tilde{a}'_{\text{mix}}}{\sqrt{T}} \quad (4.1.8)$$

By taking the 3σ random error on $K2_{i,k}$ ($\delta_r K2_{i,k} = 3\sigma K2_{i,k}$) and adding it quadratically to the total systematic error affecting the same element ($\delta_s K2_{i,k}$), the result shall not exceed the overall measurement accuracy specified for this element in Table 3.3-2 (the measurement accuracy required for the individual quadratic factors of two accelerometer belonging to a given pair, $\delta K2_{i,k}$, is equal to the measurement accuracy specified for the common/differential quadratic factors of that pair):

$$\sqrt{(\delta_r K2_{i,k})^2 + (\delta_s K2_{i,k})^2} \leq \delta K2_{i,k}, \quad \delta_r K2_{i,k} = 3 \frac{\pi}{C(v_e, v_s) A_e^2} \frac{2 \tilde{a}'_{\text{mix}}}{\sqrt{T}} \quad (4.1.9)$$

This relationship allows to establish the minimum duration T of the proof mass shaking necessary for reducing this random error below the established limit:

$$\delta_r K2_{i,k} = \sqrt{(\delta_s K2_{i,k})^2 - (\delta_s K2_{i,k})^2}, \quad T = \left(3 \frac{\pi}{C(v_e, v_s) A_e^2} \frac{2 \tilde{a}'_{\text{mix}}}{\delta_r K2_{i,k}} \right)^2. \quad (4.1.10)$$

The proof mass shaking duration has been computed considering the following random errors to be achieved in the K2 measurement processes:

- $\delta_r K2_{1,X} = \delta_r K2_{4,X} = 2 \text{ s}^2/\text{m}$, $\delta_r K2_{1,Z} = \delta_r K2_{4,Z} = 5 \text{ s}^2/\text{m}$
- $\delta_r K2_{2,X} = \delta_r K2_{5,X} = 5 \text{ s}^2/\text{m}$, $\delta_r K2_{2,Y} = \delta_r K2_{5,Y} = 2 \text{ s}^2/\text{m}$,
- $\delta_r K2_{3,X} = \delta_r K2_{6,X} = 5 \text{ s}^2/\text{m}$, $\delta_r K2_{3,Z} = \delta_r K2_{6,Z} = 2 \text{ s}^2/\text{m}$

This leaves for the systematic error a limit value of $\sim 1.8 \text{ s}^2/\text{m}$ for the in-line quadratic factors (achievable after one measurement-correction iterations, if initial $K2 = 1206 \text{ s}^2/\text{m}$), and of $\sim 6.5 \text{ s}^2/\text{m}$ for the transversal quadratic factors (achievable even at the first in-flight measurement of the K2).

For the other parameters involved in the computation of the proof mass shaking duration the following values have been used:

- Gradiometer baseline lengths: $L_X = 0.514 \text{ m}$, $L_Y = 0.49988 \text{ m}$, $L_Z = 0.500195 \text{ m}$ (measured values)
- Frequency of the square wave signal $v_s = 50 \text{ mHz}$ (frequency around which the spectral density of the background acceleration has been computed).
- Correction factor $C(v_e, v_s) = 0.6489$ (valid for $v_s = 50 \text{ mHz}$ and $v_e = 100 \text{ Hz}$). (this factor, computed for the DFACS output of the accelerometer is assumed here applicable to the scientific output too)
- Values of the elements of $d\mathbf{M}_{ij}$ equal to their upper limits all along the mission lifetime, as per Table 3.1-1 (this is equivalent to consider a non-calibrated Gradiometer, as it is before the first in-flight measurement of the quadratic factors). Spectral density of these elements $= 3 \cdot 10^{-7} \text{ Hz}^{-1/2}$ (common scale factors, specification for 50 mHz), $2.2 \cdot 10^{-7} \text{ Hz}^{-1/2}$ (differential scale factors, specification for 50 mHz), $= 10^{-8} \text{ Hz}^{-1/2}$ (common and differential misalignments + couplings, specification).
- Values of the quadratic factors equal to their upper limits in-orbit, as per Table 3.1-3 (this is the maximum values of the quadratic factors expected before their first in-flight measurement). Spectral density of these elements $= 0.01 \text{ s}^2/\text{m}/\text{Hz}^{1/2}$ (specification).
- Values of the GGT components in the GRF (maximum value and maximum spectral density level at v_s) as per APPENDIX A.
- Environmental conditions (residual linear accelerations, angular accelerations, angular rates) as nominally provided by the DFACS in science mode (see section 6.1.1).

Finally, two cases have been considered for the accelerometer output channel from which the acceleration a'_{mix} , utilized, for the determination of K2, is obtained:

Case a) a'_{mix} taken from the scientific output channel of the accelerometers

In this case the proof mass shaking duration has been computed considering:

- Accelerometer intrinsic noise $= 2 \cdot 10^{-12} \text{ m/s}^2/\text{Hz}^{1/2}$ (ultra sensitive axes), $= 3.5 \cdot 10^{-10} \text{ m/s}^2/\text{Hz}^{1/2}$ (less sensitive axes).
- Amplitude of the sinusoidal acceleration applied to the proof mass through the control electrodes:

$$A_e = 3 \cdot 10^{-6} \text{ m/s}^2, \text{ along all the shaken axes of the accelerometers } A_1, A_4, A_2, A_5, A_3, A_6$$

This amplitude corresponds to half of the full measurement range of the accelerometers in the scientific output channel ($\pm 6 \cdot 10^{-6} \text{ m/s}^2$).

Case b) a'_{mix} taken from the DFAC output channel of the accelerometers.

In this case the proof mass shaking duration has been computed considering:

- Accelerometer intrinsic noise = $1 \cdot 10^{-10} \text{ m/s}^2/\text{Hz}^{1/2}$ (ultra sensitive axes), = $1 \cdot 10^{-9} \text{ m/s}^2/\text{Hz}^{1/2}$ (less sensitive axes), taken from the budgets provided in [RD 11] with conservative margins.
- Amplitude of the sinusoidal acceleration applied to the proof mass through the control electrodes:

$$A_e = 1 \cdot 10^{-5} \text{ m/s}^2, \text{ along all the shaken axes of the accelerometers } A_1, A_4, A_2, A_5, A_3, A_6$$

This amplitude corresponds to half of the full measurement range of the accelerometers in the DFAC output channel ($\pm 2 \cdot 10^{-5} \text{ m/s}^2$).

The results for the two cases are provided in Table 4.2-2 and 4.2-3 respectively. From them, the advantage of using the DFAC output channel for the measurement of K2 is apparent (5 hours against ~19.8 days of total shaking time). In fact, the larger intrinsic noise of the accelerometer the DFAC channel is by far outweighed by the larger proof mass shaking acceleration applicable in this case. This is explained by equation (4.1.9), where T depends on the square of the acceleration measurement noise spectral density, but on the inverse of the fourth power of the amplitude of the shaking acceleration.

Another negative aspect of the utilisation of the science output channel is that the dominant error terms in this case are not the intrinsic accelerometer noise but the residual linear accelerations, angular accelerations and angular rates, which can change significantly (apart for the residual linear acceleration in the along track direction) as function of the orbital environment of the satellite.

The quadratic factors along the less sensitive axes of the accelerometers don't need to be necessarily measured and adjusted in flight because their by-construction value is already small and, in addition, they have a weaker impact on the gradiometric performance than the quadratic factors of the ultra-sensitive axes. An estimation of the proof mass shaking time required to measure the LS-axis K2 with a random error of $5 \text{ s}^2/\text{m}$ is however provided in Table 4.2-4. The shaking time is computed using the case b) inputs, i.e. assuming to use the DFAC measurements.

Quadratic factor	Required measurement accuracy	Random error limit	Proof mass shaking amplitude (A_e)	Noise spectral density of a'_{mix} around v_s ($\text{m/s}^2/\text{Hz}^{1/2}$)	Proof mass shaking duration T (s)
$K2_{1,X}$	$2.7 \text{ s}^2/\text{m}$	$2 \text{ s}^2/\text{m}$	$3 \cdot 10^{-6} \text{ m/s}^2$	$\tilde{a}'_{\text{mix}} = 4.87 \cdot 10^{-10}$	618300
$K2_{4,X}$	$2.7 \text{ s}^2/\text{m}$	$2 \text{ s}^2/\text{m}$	$3 \cdot 10^{-6} \text{ m/s}^2$		618300
$K2_{1,Z}$	$8.2 \text{ s}^2/\text{m}$	$5 \text{ s}^2/\text{m}$	$3 \cdot 10^{-6} \text{ m/s}^2$	$\tilde{a}'_{\text{mix}} = 4.90 \cdot 10^{-10}$	100000
$K2_{4,Z}$	$8.2 \text{ s}^2/\text{m}$	$5 \text{ s}^2/\text{m}$	$3 \cdot 10^{-6} \text{ m/s}^2$		100000
$K2_{2,X}$	$8.2 \text{ s}^2/\text{m}$	$5 \text{ s}^2/\text{m}$	$3 \cdot 10^{-6} \text{ m/s}^2$	$\tilde{a}'_{\text{mix}} = 2.52 \cdot 10^{-10}$	26400
$K2_{5,X}$	$8.2 \text{ s}^2/\text{m}$	$5 \text{ s}^2/\text{m}$	$3 \cdot 10^{-6} \text{ m/s}^2$		26400
$K2_{2,Y}$	$2.7 \text{ s}^2/\text{m}$	$2 \text{ s}^2/\text{m}$	$3 \cdot 10^{-6} \text{ m/s}^2$	$\tilde{a}'_{\text{mix}} = 5.17 \cdot 10^{-11}$	7000
$K2_{5,Y}$	$2.7 \text{ s}^2/\text{m}$	$2 \text{ s}^2/\text{m}$	$3 \cdot 10^{-6} \text{ m/s}^2$		7000
$K2_{3,X}$	$8.2 \text{ s}^2/\text{m}$	$5 \text{ s}^2/\text{m}$	$3 \cdot 10^{-6} \text{ m/s}^2$	$\tilde{a}'_{\text{mix}} = 4.77 \cdot 10^{-10}$	94700
$K2_{6,X}$	$8.2 \text{ s}^2/\text{m}$	$5 \text{ s}^2/\text{m}$	$3 \cdot 10^{-6} \text{ m/s}^2$		94700
$K2_{3,Z}$	$2.7 \text{ s}^2/\text{m}$	$2 \text{ s}^2/\text{m}$	$3 \cdot 10^{-6} \text{ m/s}^2$	$\tilde{a}'_{\text{mix}} = 5.90 \cdot 10^{-11}$	9100
$K2_{6,Z}$	$2.7 \text{ s}^2/\text{m}$	$2 \text{ s}^2/\text{m}$	$3 \cdot 10^{-6} \text{ m/s}^2$		9100
Total proof mass shaking time required for all K2 measurements					$1.711 \cdot 10^6 \text{ s}$

Table 4.2-2: Random errors affecting the estimation of K2, and proof mass shaking duration for case a)

Quadratic factor	Required measurement accuracy	Random error limit	Proof mass shaking amplitude (A _e)	Noise spectral density of a' _{mix} around v _s (m/s ² /Hz ^{1/2})	Proof mass shaking duration T (s)
K2 _{1,X}	2.7 s ² /m	2 s ² /m	1·10 ⁻⁵ m/s ²	$\tilde{a}'_{\text{mix}} = 4.92 \cdot 10^{-10}$	5200
K2 _{4,X}	2.7 s ² /m	2 s ² /m	1·10 ⁻⁵ m/s ²		5200
K2 _{1,Z}	8.2 s ² /m	5 s ² /m	1·10 ⁻⁵ m/s ²	$\tilde{a}'_{\text{mix}} = 5.00 \cdot 10^{-10}$	900
K2 _{4,Z}	8.2 s ² /m	5 s ² /m	1·10 ⁻⁵ m/s ²		900
K2 _{2,X}	8.2 s ² /m	5 s ² /m	1·10 ⁻⁵ m/s ²	$\tilde{a}'_{\text{mix}} = 6.95 \cdot 10^{-10}$	1700
K2 _{5,X}	8.2 s ² /m	5 s ² /m	1·10 ⁻⁵ m/s ²		1700
K2 _{2,Y}	2.7 s ² /m	2 s ² /m	1·10 ⁻⁵ m/s ²	$\tilde{a}'_{\text{mix}} = 8.76 \cdot 10^{-11}$	200
K2 _{5,Y}	2.7 s ² /m	2 s ² /m	1·10 ⁻⁵ m/s ²		200
K2 _{3,X}	8.2 s ² /m	5 s ² /m	1·10 ⁻⁵ m/s ²	$\tilde{a}'_{\text{mix}} = 4.87 \cdot 10^{-10}$	800
K2 _{6,X}	8.2 s ² /m	5 s ² /m	1·10 ⁻⁵ m/s ²		800
K2 _{3,Z}	2.7 s ² /m	2 s ² /m	1·10 ⁻⁵ m/s ²	$\tilde{a}'_{\text{mix}} = 9.21 \cdot 10^{-11}$	200
K2 _{6,Z}	2.7 s ² /m	2 s ² /m	1·10 ⁻⁵ m/s ²		200
Total proof mass shaking time required for all K2 measurements					18000 s

Table 4.2-3: Random errors affecting the estimation of K2, and proof mass shaking duration for case b)

Quadratic factor	Random error limit	Proof mass shaking amplitude (A_e)	Noise spectral density of a'_{mix} around v_s ($\text{m/s}^2/\text{Hz}^{1/2}$)	Proof mass shaking duration T (s)
$K2_{1,Y}$	$5 \text{ s}^2/\text{m}$	$1 \cdot 10^{-5} \text{ m/s}^2$	$\tilde{a}'_{\text{mix}} = 7.15 \cdot 10^{-10}$	1800
$K2_{4,Y}$	$5 \text{ s}^2/\text{m}$	$1 \cdot 10^{-5} \text{ m/s}^2$		1800
$K2_{2,Z}$	$5 \text{ s}^2/\text{m}$	$1 \cdot 10^{-5} \text{ m/s}^2$	$\tilde{a}'_{\text{mix}} = 1.00 \cdot 10^{-9}$	3400
$K2_{5,Z}$	$5 \text{ s}^2/\text{m}$	$1 \cdot 10^{-5} \text{ m/s}^2$		3400
$K2_{3,Y}$	$5 \text{ s}^2/\text{m}$	$1 \cdot 10^{-5} \text{ m/s}^2$	$\tilde{a}'_{\text{mix}} = 1.00 \cdot 10^{-9}$	3400
$K2_{6,Y}$	$5 \text{ s}^2/\text{m}$	$1 \cdot 10^{-5} \text{ m/s}^2$		3400
Total proof mass shaking time required for all K2 measurements				17200 s

Table 4.2-4: Proof mass shaking duration for K2 measurement along LS axis (using the DFAC channel)

5. DETERMINATION OF THE ELEMENTS OF THE INVERSE CALIBRATION MATRICES

Once the quadratic factors have been measured and physically reduced below the specified limits, the only errors that still affect the measurement of the common-mode and differential-mode accelerations are those due to the coupling of these accelerations with the differential and common scale factors, misalignments and couplings of the accelerometer pairs, i.e. with the elements of the Calibration Matrix. These elements cannot be physically adjusted. Therefore the knowledge of their value obtained during the on-orbit calibration of the Gradiometer is utilised in the Level 1a to Level 1b data processing, to remove numerically the corresponding errors from the measured accelerations.

The method described here for the determination of the elements of the IMCs involved in the GGT determination process is based on the satellite shaking and on the hypothesis that each individual component of the GGT (namely U_{XX} , U_{YY} , U_{ZZ} , U_{XY} , U_{XZ} , U_{YZ}) is very small in the upper part of the Gradiometer MBW, i.e. from 50 mHz to 100 mHz, so that it can be considered as a measurement noise. This hypothesis is corroborated by the simulations performed using the Earth gravity field model EGM96 complete up to degree and order 360. Therefore, if the Gradiometer was perfect (unitary scale factors, no inter-axes misalignments, couplings), the GGT components reconstructed from its measurements and from the star sensor measurements should be nearly zero between 50 mHz to 100 mHz in presence of any external disturbance of linear and angular accelerations. If the resulting GGT components are not zero, this is due to Gradiometer imperfections (deviations from the unitary scale factors, inter-axes misalignments, couplings). The values of the elements of the inverse Calibration Matrices (which are related to these Gradiometer imperfections) can be thus obtained as those values what best fit a null value of the GGT components from 50 mHz to 100 mHz, determined from a series of measurements. To highlight the effect of the Gradiometer imperfections in the resulting GGT components, and thus to reduce the time period in which the measurements for calibration must be collected, the satellite must be subject on purpose to external disturbances of linear and angular accelerations with a relatively large level in the spectral bandwidth from 50 mHz to 100 mHz. These disturbances must be as much as possible de-correlated among the various axes, so to excite evenly and independently any of the Gradiometer imperfections. The satellite shaking is accomplished by means of the ion thruster and the on-off cold-gas thrusters of the Gradiometer Calibration Device (GCD).

5.1 METHOD DESCRIPTION

5.1.1 Fundamental Equations Set up and Process Outline

The equations utilised for the determination of the $[MI]_{d,ij}$, $[MI]_{c,ij}$ elements ($ij = 14, 25, 36$) are obtained from the relationships between the differential accelerations at the accelerometer locations in the three OAGRFs, the GGT components and the satellite angular dynamics (angular accelerations and centrifugal accelerations). The derivation of the following equations is described in [RD 1]:

for the accelerometer pair (A_1, A_4)

$$\begin{aligned}
 -2 \frac{a_{d,14,X}}{L_X} &= U_{XX} + \omega_Y^2 + \omega_Z^2 \\
 -2 \frac{a_{d,14,Y}}{L_X} &= U_{XY} - \omega_X \omega_Y - \dot{\omega}_Z \\
 -2 \frac{a_{d,14,Z}}{L_X} &= U_{XZ} - \omega_X \omega_Z + \dot{\omega}_Y
 \end{aligned} \tag{5.1.1}$$

for the accelerometer pair (A_2, A_5)

$$\begin{aligned}
 -2 \frac{a_{d,25,X}}{L_Y} &= U_{XY} - \omega_X \omega_Y + \dot{\omega}_Z \\
 -2 \frac{a_{d,25,Y}}{L_Y} &= U_{YY} + \omega_X^2 + \omega_Z^2
 \end{aligned}$$

$$-2 \frac{a_{d,25,Z}}{L_Y} = U_{YZ} - \omega_Y \omega_Z - \dot{\omega}_X$$

for the accelerometer pair (A_3, A_6)

$$-2 \frac{a_{d,36,X}}{L_Z} = U_{XZ} - \omega_X \omega_Z - \dot{\omega}_Y$$

$$-2 \frac{a_{d,36,Y}}{L_Z} = U_{YZ} - \omega_Y \omega_Z + \dot{\omega}_X$$

$$-2 \frac{a_{d,36,Z}}{L_Z} = U_{ZZ} + \omega_X^2 + \omega_Y^2$$

$$-2 \frac{a_{d,14,X}}{L_X} = U_{XX} + \omega_Y^2 + \omega_Z^2 \quad -2 \frac{a_{d,14,Y}}{L_X} = U_{XY} - \omega_X \omega_Y - \dot{\omega}_Z \quad -2 \frac{a_{d,14,Z}}{L_X} = U_{XZ} - \omega_X \omega_Z + \dot{\omega}_Y$$

$$-2 \frac{a_{d,25,X}}{L_Y} = U_{XY} - \omega_X \omega_Y + \dot{\omega}_Z \quad -2 \frac{a_{d,25,Y}}{L_Y} = U_{YY} + \omega_X^2 + \omega_Z^2 \quad -2 \frac{a_{d,25,Z}}{L_Y} = U_{YZ} - \omega_Y \omega_Z - \dot{\omega}_X$$

$$-2 \frac{a_{d,36,X}}{L_Z} = U_{XZ} - \omega_X \omega_Z - \dot{\omega}_Y \quad -2 \frac{a_{d,36,Y}}{L_Z} = U_{YZ} - \omega_Y \omega_Z + \dot{\omega}_X \quad -2 \frac{a_{d,36,Z}}{L_Z} = U_{ZZ} + \omega_X^2 + \omega_Y^2$$

In the upper part of the MBW (in particular, from 50 mHz to 100 mHz) the gravity gradient signal is weak. For the the purpose of determining the elements of the ICM, we will consider the GGT components as an additional noise contribution to the measured accelerations. Based on this hypothesis and assuming to retain only the part of $a_{d,ij}$, angular and centrifugal accelerations with frequency contents between 50 and 100 mHz, we can set to zero U_{XX} , U_{YY} , U_{ZZ} , U_{XY} , U_{XZ} , U_{YZ} , in the previous equations. By expressing the angular accelerations as function of the differential accelerations, we get:

$$a_{d,14,X} = -\frac{L_X}{2} (\omega_Y^2 + \omega_Z^2)$$

$$a_{d,14,Y} = \frac{L_X}{2} (\omega_X \omega_Y + \dot{\omega}_Z) = \frac{L_X}{2} \left(2\omega_X \omega_Y - \frac{2}{L_Y} a_{d,25,X} \right) = L_X \omega_X \omega_Y - \frac{L_X}{L_Y} a_{d,25,X} \quad (5.1.2)$$

$$a_{d,14,Z} = \frac{L_X}{2} (\omega_X \omega_Z - \dot{\omega}_Y) = \frac{L_X}{2} \left(2\omega_X \omega_Z - \frac{2}{L_Z} a_{d,36,X} \right) = L_X \omega_X \omega_Z - \frac{L_X}{L_Z} a_{d,36,X}$$

$$a_{d,25,X} = \frac{L_Y}{2} (\omega_X \omega_Y - \dot{\omega}_Z) = \frac{L_Y}{2} \left(2\omega_X \omega_Y - \frac{2}{L_Y} a_{d,14,Y} \right) = L_Y \omega_X \omega_Y - \frac{L_Y}{L_X} a_{d,14,Y}$$

$$a_{d,25,Y} = -\frac{L_Y}{2} (\omega_X^2 + \omega_Z^2)$$

$$a_{d,25,Z} = \frac{L_Y}{2} (\omega_Y \omega_Z + \dot{\omega}_X) = \frac{L_Y}{2} \left(2\omega_Y \omega_Z - \frac{2}{L_Z} a_{d,36,Y} \right) = L_Y \omega_Y \omega_Z - \frac{L_Y}{L_Z} a_{d,36,Y}$$

$$a_{d,36,X} = \frac{L_Z}{2} (\omega_X \omega_Z + \dot{\omega}_Y) = \frac{L_Z}{2} \left(2\omega_X \omega_Z - \frac{2}{L_X} a_{d,14,Z} \right) = L_Z \omega_X \omega_Z - \frac{L_Z}{L_X} a_{d,14,Z}$$

$$a_{d,36,Y} = \frac{L_Z}{2} (\omega_Y \omega_Z - \dot{\omega}_X) = \frac{L_Z}{2} \left(2\omega_Y \omega_Z - \frac{2}{L_Y} a_{d,25,Z} \right) = L_Z \omega_Y \omega_Z - \frac{L_Z}{L_Y} a_{d,25,Z}$$

$$a_{d,36,Z} = -\frac{L_Z}{2} (\omega_X^2 + \omega_Y^2)$$

The elements of the ICM are included in the previous equations by expressing $\underline{a}_{d,ij}$ as function of the common mode and the differential mode accelerations measured by the three accelerometer pairs in their Accelerometer Reference Frames ($\underline{a}'_{c,ij}$, $\underline{a}'_{d,ij}$) using the (3.2):

(5.1.3)

$$\begin{aligned}
 MI_{14,41} a'_{c,14,X} + MI_{14,42} a'_{c,14,Y} + MI_{14,43} a'_{c,14,Z} + MI_{14,44} a'_{d,14,X} + MI_{14,45} a'_{d,14,Y} + MI_{14,46} a'_{d,14,Z} &= -\frac{L_X}{2} (\omega_Y^2 + \omega_Z^2) \\
 MI_{14,51} a'_{c,14,X} + MI_{14,52} a'_{c,14,Y} + MI_{14,53} a'_{c,14,Z} + MI_{14,54} a'_{d,14,X} + MI_{14,55} a'_{d,14,Y} + MI_{14,56} a'_{d,14,Z} &= L_X \omega_X \omega_Y - \frac{L_X}{L_Y} a_{d,25,X} \\
 MI_{14,61} a'_{c,14,X} + MI_{14,62} a'_{c,14,Y} + MI_{14,63} a'_{c,14,Z} + MI_{14,64} a'_{d,14,X} + MI_{14,65} a'_{d,14,Y} + MI_{14,66} a'_{d,14,Z} &= L_X \omega_X \omega_Z - \frac{L_X}{L_Z} a_{d,36,X} \\
 MI_{25,41} a'_{c,25,X} + MI_{25,42} a'_{c,25,Y} + MI_{25,43} a'_{c,25,Z} + MI_{25,44} a'_{d,25,X} + MI_{25,45} a'_{d,25,Y} + MI_{25,46} a'_{d,25,Z} &= L_Y \omega_X \omega_Y - \frac{L_Y}{L_X} a_{d,14,Y} \\
 MI_{25,51} a'_{c,25,X} + MI_{25,52} a'_{c,25,Y} + MI_{25,53} a'_{c,25,Z} + MI_{25,54} a'_{d,25,X} + MI_{25,55} a'_{d,25,Y} + MI_{25,56} a'_{d,25,Z} &= -\frac{L_Y}{2} (\omega_X^2 + \omega_Z^2) \\
 MI_{25,61} a'_{c,25,X} + MI_{25,62} a'_{c,25,Y} + MI_{25,63} a'_{c,25,Z} + MI_{25,64} a'_{d,25,X} + MI_{25,65} a'_{d,25,Y} + MI_{25,66} a'_{d,25,Z} &= L_Y \omega_Y \omega_Z - \frac{L_Y}{L_Z} a_{d,36,Y} \\
 MI_{36,41} a'_{c,36,X} + MI_{36,42} a'_{c,36,Y} + MI_{36,43} a'_{c,36,Z} + MI_{36,44} a'_{d,36,X} + MI_{36,45} a'_{d,36,Y} + MI_{36,46} a'_{d,36,Z} &= L_Z \omega_X \omega_Z - \frac{L_Z}{L_X} a_{d,14,Z} \\
 MI_{36,51} a'_{c,36,X} + MI_{36,52} a'_{c,36,Y} + MI_{36,53} a'_{c,36,Z} + MI_{36,54} a'_{d,36,X} + MI_{36,55} a'_{d,36,Y} + MI_{36,56} a'_{d,36,Z} &= L_Z \omega_Y \omega_Z - \frac{L_Z}{L_Y} a_{d,25,Z} \\
 MI_{36,61} a'_{c,36,X} + MI_{36,62} a'_{c,36,Y} + MI_{36,63} a'_{c,36,Z} + MI_{36,64} a'_{d,36,X} + MI_{36,65} a'_{d,36,Y} + MI_{36,66} a'_{d,36,Z} &= -\frac{L_Z}{2} (\omega_X^2 + \omega_Y^2)
 \end{aligned}$$

Finally, by setting

$$\begin{aligned}
 y_1 &= -\frac{L_X}{2} (\omega_Y^2 + \omega_Z^2), \quad y_2 = L_X \omega_X \omega_Y - \frac{L_X}{L_Y} a_{d,25,X}, \quad y_3 = L_X \omega_X \omega_Z - \frac{L_X}{L_Z} a_{d,36,X}, \\
 y_4 &= L_Y \omega_X \omega_Y - \frac{L_Y}{L_X} a_{d,14,Y}, \quad y_5 = -\frac{L_Y}{2} (\omega_X^2 + \omega_Z^2), \quad y_6 = L_Y \omega_Y \omega_Z - \frac{L_Y}{L_Z} a_{d,36,Y}, \\
 y_7 &= L_Z \omega_X \omega_Z - \frac{L_Z}{L_X} a_{d,14,Z}, \quad y_8 = L_Z \omega_Y \omega_Z - \frac{L_Z}{L_Y} a_{d,25,Z}, \quad y_9 = -\frac{L_Z}{2} (\omega_X^2 + \omega_Y^2),
 \end{aligned} \tag{5.1.4}$$

we can write the (5.1.3) in the following, more compact form:

$$\begin{aligned}
 MI_{14,41} a'_{c,14,X} + MI_{14,42} a'_{c,14,Y} + MI_{14,43} a'_{c,14,Z} + MI_{14,44} a'_{d,14,X} + MI_{14,45} a'_{d,14,Y} + MI_{14,46} a'_{d,14,Z} &= y_1 \\
 MI_{14,51} a'_{c,14,X} + MI_{14,52} a'_{c,14,Y} + MI_{14,53} a'_{c,14,Z} + MI_{14,54} a'_{d,14,X} + MI_{14,55} a'_{d,14,Y} + MI_{14,56} a'_{d,14,Z} &= y_2 \\
 MI_{14,61} a'_{c,14,X} + MI_{14,62} a'_{c,14,Y} + MI_{14,63} a'_{c,14,Z} + MI_{14,64} a'_{d,14,X} + MI_{14,65} a'_{d,14,Y} + MI_{14,66} a'_{d,14,Z} &= y_3 \\
 MI_{25,41} a'_{c,25,X} + MI_{25,42} a'_{c,25,Y} + MI_{25,43} a'_{c,25,Z} + MI_{25,44} a'_{d,25,X} + MI_{25,45} a'_{d,25,Y} + MI_{25,46} a'_{d,25,Z} &= y_4 \\
 MI_{25,51} a'_{c,25,X} + MI_{25,52} a'_{c,25,Y} + MI_{25,53} a'_{c,25,Z} + MI_{25,54} a'_{d,25,X} + MI_{25,55} a'_{d,25,Y} + MI_{25,56} a'_{d,25,Z} &= y_5
 \end{aligned} \tag{5.1.5}$$

$$MI_{25,61} a'_{c,25,X} + MI_{25,62} a'_{c,25,Y} + MI_{25,63} a'_{c,25,Z} + MI_{25,64} a'_{d,25,X} + MI_{25,65} a'_{d,25,Y} + MI_{25,66} a'_{d,25,Z} = y_6$$

$$MI_{36,41} a'_{c,36,X} + MI_{36,42} a'_{c,36,Y} + MI_{36,43} a'_{c,36,Z} + MI_{36,44} a'_{d,36,X} + MI_{36,45} a'_{d,36,Y} + MI_{36,46} a'_{d,36,Z} = y_7$$

$$MI_{36,51} a'_{c,36,X} + MI_{36,52} a'_{c,36,Y} + MI_{36,53} a'_{c,36,Z} + MI_{36,54} a'_{d,36,X} + MI_{36,55} a'_{d,36,Y} + MI_{36,56} a'_{d,36,Z} = y_8$$

$$MI_{36,61} a'_{c,36,X} + MI_{36,62} a'_{c,36,Y} + MI_{36,63} a'_{c,36,Z} + MI_{36,64} a'_{d,36,X} + MI_{36,65} a'_{d,36,Y} + MI_{36,66} a'_{d,36,Z} = y_9$$

The (5.1.5) are the fundamental equations utilised for the determination of the 54 elements of $[MI]_{d,ij}$, $[MI]_{c,ij}$ (among which, however, only 32 must be strictly measured in flight).

The number of equations (9) is not sufficient to solve for all the unknowns in a deterministic way. But we can transform each of the previous equations in a set of N equations by measuring the common and differential mode accelerations and the y_i quantities at N different times (t_1, t_2, \dots, t_N). So we get nine set of equations (labelled as (5.1.6)):

Equation set 1

$$MI_{14,41} a'_{c,14,X,1} + MI_{14,42} a'_{c,14,Y,1} + MI_{14,43} a'_{c,14,Z,1} + MI_{14,44} a'_{d,14,X,1} + MI_{14,45} a'_{d,14,Y,1} + MI_{14,46} a'_{d,14,Z,1} = y_{1,1} \text{ (for } t = t_1)$$

$$MI_{14,41} a'_{c,14,X,2} + MI_{14,42} a'_{c,14,Y,2} + MI_{14,43} a'_{c,14,Z,2} + MI_{14,44} a'_{d,14,X,2} + MI_{14,45} a'_{d,14,Y,2} + MI_{14,46} a'_{d,14,Z,2} = y_{1,1} \text{ (for } t = t_2)$$

.....

$$MI_{14,41} a'_{c,14,X,N} + MI_{14,42} a'_{c,14,Y,N} + MI_{14,43} a'_{c,14,Z,N} + MI_{14,44} a'_{d,14,X,N} + MI_{14,45} a'_{d,14,Y,N} + MI_{14,46} a'_{d,14,Z,N} = y_{1,N} \text{ (for } t = t_N)$$

or, in matrix notation:

$$\mathbf{A1} \cdot \mathbf{x1} = \mathbf{y1},$$

$$\mathbf{A1} = \begin{pmatrix} a'_{c,14,X,1} & a'_{c,14,Y,1} & a'_{c,14,Z,1} & a'_{d,14,X,1} & a'_{d,14,Y,1} & a'_{d,14,Z,1} \\ a'_{c,14,X,2} & a'_{c,14,Y,2} & a'_{c,14,Z,2} & a'_{d,14,X,2} & a'_{d,14,Y,2} & a'_{d,14,Z,2} \\ \vdots & \vdots & \vdots & \vdots & \vdots & \vdots \\ a'_{c,14,X,N} & a'_{c,14,Y,N} & a'_{c,14,Z,N} & a'_{d,14,X,N} & a'_{d,14,Y,N} & a'_{d,14,Z,N} \end{pmatrix}; \mathbf{y1} = \begin{pmatrix} y_{1,1} \\ y_{1,2} \\ \vdots \\ y_{1,N} \end{pmatrix}; \mathbf{x1} = \begin{pmatrix} MI_{14,41} \\ MI_{14,42} \\ MI_{14,43} \\ MI_{14,44} \\ MI_{14,45} \\ MI_{14,46} \end{pmatrix} \text{ (unknowns)}$$

Equation set 2

$$\mathbf{A2} \cdot \mathbf{x2} = \mathbf{y2},$$

$$\mathbf{A2} = \begin{pmatrix} a'_{c,14,X,1} & a'_{c,14,Y,1} & a'_{c,14,Z,1} & a'_{d,14,X,1} & a'_{d,14,Y,1} & a'_{d,14,Z,1} \\ a'_{c,14,X,2} & a'_{c,14,Y,2} & a'_{c,14,Z,2} & a'_{d,14,X,2} & a'_{d,14,Y,2} & a'_{d,14,Z,2} \\ \cdot & \cdot & \cdot & \cdot & \cdot & \cdot \\ a'_{c,14,X,N} & a'_{c,14,Y,N} & a'_{c,14,Z,N} & a'_{d,14,X,N} & a'_{d,14,Y,N} & a'_{d,14,Z,N} \end{pmatrix}; \mathbf{y2} = \begin{pmatrix} y_{2,1} \\ y_{2,2} \\ \cdot \\ y_{2,N} \end{pmatrix}; \mathbf{x2} = \begin{pmatrix} MI_{14,51} \\ MI_{14,52} \\ MI_{14,53} \\ MI_{14,54} \\ MI_{14,55} \\ MI_{14,56} \end{pmatrix} \text{ (unknowns)}$$

Equation set 3

$$\mathbf{A3} \cdot \mathbf{x3} = \mathbf{y3},$$

$$\mathbf{A3} = \begin{pmatrix} a'_{c,14,X,1} & a'_{c,14,Y,1} & a'_{c,14,Z,1} & a'_{d,14,X,1} & a'_{d,14,Y,1} & a'_{d,14,Z,1} \\ a'_{c,14,X,2} & a'_{c,14,Y,2} & a'_{c,14,Z,2} & a'_{d,14,X,2} & a'_{d,14,Y,2} & a'_{d,14,Z,2} \\ \cdot & \cdot & \cdot & \cdot & \cdot & \cdot \\ a'_{c,14,X,N} & a'_{c,14,Y,N} & a'_{c,14,Z,N} & a'_{d,14,X,N} & a'_{d,14,Y,N} & a'_{d,14,Z,N} \end{pmatrix}; \mathbf{y3} = \begin{pmatrix} y_{3,1} \\ y_{3,2} \\ \cdot \\ y_{3,N} \end{pmatrix}; \mathbf{x3} = \begin{pmatrix} MI_{14,61} \\ MI_{14,62} \\ MI_{14,63} \\ MI_{14,64} \\ MI_{14,65} \\ MI_{14,66} \end{pmatrix} \text{ (unknowns)}$$

Equation set 4

$$\mathbf{A4} \cdot \mathbf{x4} = \mathbf{y4},$$

$$\mathbf{A4} = \begin{pmatrix} a'_{c,25,X,1} & a'_{c,25,Y,1} & a'_{c,25,Z,1} & a'_{d,25,X,1} & a'_{d,25,Y,1} & a'_{d,25,Z,1} \\ a'_{c,25,X,2} & a'_{c,25,Y,2} & a'_{c,25,Z,2} & a'_{d,25,X,2} & a'_{d,25,Y,2} & a'_{d,25,Z,2} \\ \cdot & \cdot & \cdot & \cdot & \cdot & \cdot \\ a'_{c,25,X,N} & a'_{c,25,Y,N} & a'_{c,25,Z,N} & a'_{d,25,X,N} & a'_{d,25,Y,N} & a'_{d,25,Z,N} \end{pmatrix}; \mathbf{y4} = \begin{pmatrix} y_{4,1} \\ y_{4,2} \\ \cdot \\ y_{4,N} \end{pmatrix}; \mathbf{x4} = \begin{pmatrix} MI_{25,41} \\ MI_{25,42} \\ MI_{25,43} \\ MI_{25,44} \\ MI_{25,45} \\ MI_{25,46} \end{pmatrix} \text{ (unknowns)}$$

Equation set 5

$$\mathbf{A5} \cdot \mathbf{x5} = \mathbf{y5},$$

$$\mathbf{A5} = \begin{pmatrix} a'_{c,25,X,1} & a'_{c,25,Y,1} & a'_{c,25,Z,1} & a'_{d,25,X,1} & a'_{d,25,Y,1} & a'_{d,25,Z,1} \\ a'_{c,25,X,2} & a'_{c,25,Y,2} & a'_{c,25,Z,2} & a'_{d,25,X,2} & a'_{d,25,Y,2} & a'_{d,25,Z,2} \\ \cdot & \cdot & \cdot & \cdot & \cdot & \cdot \\ a'_{c,25,X,N} & a'_{c,25,Y,N} & a'_{c,25,Z,N} & a'_{d,25,X,N} & a'_{d,25,Y,N} & a'_{d,25,Z,N} \end{pmatrix}; \mathbf{y5} = \begin{pmatrix} y_{5,1} \\ y_{5,2} \\ \cdot \\ y_{5,N} \end{pmatrix}; \mathbf{x5} = \begin{pmatrix} MI_{25,51} \\ MI_{25,52} \\ MI_{25,53} \\ MI_{25,54} \\ MI_{25,55} \\ MI_{25,56} \end{pmatrix} \text{ (unknowns)}$$

Equation set 6

$$\mathbf{A6} \cdot \mathbf{x6} = \mathbf{y6},$$

$$\mathbf{A6} = \begin{pmatrix} a'_{c,25,X,1} & a'_{c,25,Y,1} & a'_{c,25,Z,1} & a'_{d,25,X,1} & a'_{d,25,Y,1} & a'_{d,25,Z,1} \\ a'_{c,25,X,2} & a'_{c,25,Y,2} & a'_{c,25,Z,2} & a'_{d,25,X,2} & a'_{d,25,Y,2} & a'_{d,25,Z,2} \\ \cdot & \cdot & \cdot & \cdot & \cdot & \cdot \\ a'_{c,25,X,N} & a'_{c,25,Y,N} & a'_{c,25,Z,N} & a'_{d,25,X,N} & a'_{d,25,Y,N} & a'_{d,25,Z,N} \end{pmatrix}; \mathbf{y6} = \begin{pmatrix} y_{6,1} \\ y_{6,2} \\ \cdot \\ y_{6,N} \end{pmatrix}; \mathbf{x6} = \begin{pmatrix} MI_{25,61} \\ MI_{25,62} \\ MI_{25,63} \\ MI_{25,64} \\ MI_{25,65} \\ MI_{25,66} \end{pmatrix} \text{ (unknowns)}$$

Equation set 7

$$\mathbf{A7} \cdot \mathbf{x7} = \mathbf{y7},$$

$$\mathbf{A7} = \begin{pmatrix} a'_{c,36,X,1} & a'_{c,36,Y,1} & a'_{c,36,Z,1} & a'_{d,36,X,1} & a'_{d,36,Y,1} & a'_{d,36,Z,1} \\ a'_{c,36,X,2} & a'_{c,36,Y,2} & a'_{c,36,Z,2} & a'_{d,36,X,2} & a'_{d,36,Y,2} & a'_{d,36,Z,2} \\ \cdot & \cdot & \cdot & \cdot & \cdot & \cdot \\ a'_{c,36,X,N} & a'_{c,36,Y,N} & a'_{c,36,Z,N} & a'_{d,36,X,N} & a'_{d,36,Y,N} & a'_{d,36,Z,N} \end{pmatrix}; \mathbf{y7} = \begin{pmatrix} y_{7,1} \\ y_{7,2} \\ \cdot \\ y_{7,N} \end{pmatrix}; \mathbf{x7} = \begin{pmatrix} MI_{36,41} \\ MI_{36,42} \\ MI_{36,43} \\ MI_{36,44} \\ MI_{36,45} \\ MI_{36,46} \end{pmatrix} \text{ (unknowns)}$$

Equation set 8

$$\mathbf{A8} \cdot \mathbf{x8} = \mathbf{y8},$$

$$\mathbf{A8} = \begin{pmatrix} a'_{c,36,X,1} & a'_{c,36,Y,1} & a'_{c,36,Z,1} & a'_{d,36,X,1} & a'_{d,36,Y,1} & a'_{d,36,Z,1} \\ a'_{c,36,X,2} & a'_{c,36,Y,2} & a'_{c,36,Z,2} & a'_{d,36,X,2} & a'_{d,36,Y,2} & a'_{d,36,Z,2} \\ \cdot & \cdot & \cdot & \cdot & \cdot & \cdot \\ a'_{c,36,X,N} & a'_{c,36,Y,N} & a'_{c,36,Z,N} & a'_{d,36,X,N} & a'_{d,36,Y,N} & a'_{d,36,Z,N} \end{pmatrix}; \mathbf{y8} = \begin{pmatrix} y_{8,1} \\ y_{8,2} \\ \cdot \\ y_{8,N} \end{pmatrix}; \mathbf{x8} = \begin{pmatrix} MI_{36,51} \\ MI_{36,52} \\ MI_{36,53} \\ MI_{36,54} \\ MI_{36,55} \\ MI_{36,56} \end{pmatrix} \text{ (unknowns)}$$

Equation set 9

$$\mathbf{A9} \cdot \mathbf{x9} = \mathbf{y9},$$

$$\mathbf{A9} = \begin{pmatrix} a'_{c,36,X,1} & a'_{c,36,Y,1} & a'_{c,36,Z,1} & a'_{d,36,X,1} & a'_{d,36,Y,1} & a'_{d,36,Z,1} \\ a'_{c,36,X,2} & a'_{c,36,Y,2} & a'_{c,36,Z,2} & a'_{d,36,X,2} & a'_{d,36,Y,2} & a'_{d,36,Z,2} \\ \cdot & \cdot & \cdot & \cdot & \cdot & \cdot \\ a'_{c,36,X,N} & a'_{c,36,Y,N} & a'_{c,36,Z,N} & a'_{d,36,X,N} & a'_{d,36,Y,N} & a'_{d,36,Z,N} \end{pmatrix}; \mathbf{y9} = \begin{pmatrix} y_{9,1} \\ y_{9,2} \\ \cdot \\ y_{9,N} \end{pmatrix}; \mathbf{x9} = \begin{pmatrix} MI_{36,61} \\ MI_{36,62} \\ MI_{36,63} \\ MI_{36,64} \\ MI_{36,65} \\ MI_{36,66} \end{pmatrix} \text{ (unknowns)}$$

Note that $\mathbf{A1} = \mathbf{A2} = \mathbf{A3}$, $\mathbf{A4} = \mathbf{A5} = \mathbf{A6}$, $\mathbf{A7} = \mathbf{A8} = \mathbf{A9}$.

At minimum the measurements must be performed at $N = 6$ different times, in order to solve for the 6 unknown parameters contained in each equation. Actually, being the measurements affected by errors, we must accumulate many measurements and to seek for the best solution in a “least-squares” sense.

If the measurement errors are independent and normally distributed, then the best possible solution of the set of linear equations $\mathbf{y} = \mathbf{A} \cdot \mathbf{x}$ is given by a vector \mathbf{x}_0 which minimises the quantity:

$$\|\mathbf{y} - \mathbf{A} \mathbf{x}_0\|^2 = (\mathbf{y} - \mathbf{A} \mathbf{x}_0)^T (\mathbf{y} - \mathbf{A} \mathbf{x}_0) = \sum_{i=1}^N (y_i - A_{i,1}x_{0,1} - A_{i,2}x_{0,2} - A_{i,3}x_{0,3} - A_{i,4}x_{0,4} - A_{i,5}x_{0,5} - A_{i,6}x_{0,6})^2, \quad (5.1.7)$$

in the sense that the “least-squares fitting” (5.1.5) is the maximum likelihood estimation of the fitted parameters.

The problem of finding the vector \mathbf{x} minimising the norm $\|\mathbf{y} - \mathbf{A} \mathbf{x}\|$ is named “linear least-squares problem”.

It can be proved [RD 6] that the linear least-squares problem has at least one solution \mathbf{x}_0 (minimum point), and that every minimum point is also a solution of the normal equation

$$\mathbf{x} = (\mathbf{A}^T \mathbf{A})^{-1} \mathbf{A}^T \mathbf{y}, \quad (5.1.8)$$

and conversely.

Therefore, using the (5.1.6) to compute a least-squares solution \mathbf{x}_0 does not guarantee that \mathbf{x}_0 is that minimum point of the least-squares problem which has the smallest norm $\|\mathbf{y} - \mathbf{A} \mathbf{x}\|$, in the event that the problem has not a unique minimum point. A solution which fulfils this property (to be the one with the smallest norm) can be instead computed as (see ref. [RD 6] for the demonstration):

$$\mathbf{x} = \mathbf{A}^+ \mathbf{y}, \quad (5.1.9)$$

where \mathbf{A}^+ denotes the pseudo-inverse of the matrix \mathbf{A} , obtained as:

$$\mathbf{A}^+ = \mathbf{V} \Sigma^{-1} \mathbf{U}^T, \quad (5.1.10)$$

where the matrices \mathbf{V} , Σ and \mathbf{U} are those defining the “singular-value decomposition” of \mathbf{A} ($\mathbf{A} = \mathbf{U} \Sigma \mathbf{V}^T$). Numerical method for computing the singular-value decomposition of a matrix can be found in [RD 6] and [RD 7]. However, if the inverse of $(\mathbf{A}^T \mathbf{A})$ exists, then: $\mathbf{A}^+ = (\mathbf{A}^T \mathbf{A})^{-1} \mathbf{A}^T$.

To complete the description of this method, we have to tell how to compute the quantities y_i ($i = 1, \dots, 9$). They are built with the differential accelerations along the transversal axes of the OAGRFs and with the angular rates of the Gradiometer. The rates are obtained by integrating the angular accelerations measured by the Gradiometer and by merging them with the rates derived from the star tracker measurements (attitude quaternions), in order to correct for drifts due to the accelerometer bias. But also to compute the precise angular accelerations of the Gradiometer we need the differential accelerations at the accelerometer locations in the three OAGRFs (along the transversal axes). These differential accelerations can be derived from the measured ones if the inverse Calibration Matrices are known!

A way out from this circular problem is to approach the solution through an iterative process, initialized by a first guess concerning $[\mathbf{M}\mathbf{I}]_{d,ij}$, $[\mathbf{M}\mathbf{I}]_{c,ij}$ elements ($ij = 14, 25, 36$), i.e. an a-priori solution of the problem. This guess is utilised to compute the differential accelerations from which the angular accelerations and the angular rates are computed. These are utilised to compute the y_i quantities and to set-up the 9 sets of linear equations for the elements of $[\mathbf{M}\mathbf{I}]_{d,ij}$, $[\mathbf{M}\mathbf{I}]_{c,ij}$. The solution of these equations provides an update (improvement) of the $[\mathbf{M}\mathbf{I}]_{d,ij}$, $[\mathbf{M}\mathbf{I}]_{c,ij}$ which is re-injected in the loop to compute the differential accelerations, and so on. Each time the equations (5.1.6) are solved the accuracy in the determination of the ICM elements should improve until the process converges.

Since the process starts from the assumption of an a-priori solution, it is advantageous to linearize the equations (5.1.6) around this solution, so to remove errors due to non-linearities and to reduce numerical (roundoff) errors in the computation of the a-posteriori solution. The (5.1.6) so become:

$$\begin{aligned} \mathbf{A1} \cdot \mathbf{x1} &= \mathbf{y1} \Rightarrow \mathbf{A1} \cdot (\mathbf{x1}_0 + \delta\mathbf{x1}) = \mathbf{y1} \Rightarrow \mathbf{A1} \cdot \delta\mathbf{x1} = \mathbf{y1} - \mathbf{A1} \cdot \mathbf{x1}_0 \\ \mathbf{A2} \cdot \delta\mathbf{x2} &= \mathbf{y2} - \mathbf{A2} \cdot \mathbf{x2}_0 \\ &\dots\dots\dots \\ \mathbf{A9} \cdot \delta\mathbf{x9} &= \mathbf{y9} - \mathbf{A9} \cdot \mathbf{x9}_0 \end{aligned} \quad (5.1.11)$$

where $\mathbf{x1}_0, \dots, \mathbf{x9}_0$ are the a-priori solutions, and $\delta\mathbf{x1}, \dots, \delta\mathbf{x9}$ are the deviations from these solutions (the unknowns to be determined). The a-posteriori solution for the ICMs elements ($\mathbf{x1}, \dots, \mathbf{x9}$) is then obtained by adding the $\delta\mathbf{x1}, \dots, \delta\mathbf{x9}$, obtained from the (5.1.8), to the a-priori solution:

$$\begin{aligned} \delta\mathbf{x1} &= (\mathbf{A1}^T \mathbf{A1})^{-1} \mathbf{A1}^T (\mathbf{y1} - \mathbf{A1} \cdot \mathbf{x1}_0) \Rightarrow \mathbf{x1} = \mathbf{x1}_0 + \delta\mathbf{x1} \\ &\dots\dots\dots \\ \delta\mathbf{x9} &= (\mathbf{A9}^T \mathbf{A9})^{-1} \mathbf{A9}^T (\mathbf{y9} - \mathbf{A9} \cdot \mathbf{x9}_0) \Rightarrow \mathbf{x9} = \mathbf{x9}_0 + \delta\mathbf{x9} \end{aligned} \quad (5.1.12)$$

The utilisation of the gradiometer measurements to build the y_i quantities, i.e. the right-hand-side of the equations (5.1.11), injects the gradiometer imperfections in the equations in a non linear way. The effect is that the least-squares solutions $\delta\mathbf{x1}$,

...., δx_9 are only approximately equal to the ICM element corrections sought for. This approximation was found to be good for all the ICM elements, but for the diagonal ones ($\delta MI_{14,44}$, $\delta MI_{14,55}$, $\delta MI_{14,66}$, $\delta MI_{25,44}$, $\delta MI_{25,55}$, $\delta MI_{25,66}$, $\delta MI_{36,44}$, $\delta MI_{36,55}$, $\delta MI_{36,66}$), linked to the common scale factors of the accelerometer pairs. In order to find the relationship between the corrections to the ICM diagonal elements found by the least-squares fit (hereafter denoted as $\delta MI'_{14,44}$, $\delta MI'_{14,55}$, $\delta MI'_{14,66}$, $\delta MI'_{25,44}$, $\delta MI'_{25,55}$, $\delta MI'_{25,66}$, $\delta MI'_{36,44}$, $\delta MI'_{36,55}$, $\delta MI'_{36,66}$) and the actual corrections (hereafter written without the apex “ ’ ”) we proceeded in a numerical way⁵, generating nine calibration test cases in which only a common scale factor at a time was applied to an ideal gradiometer and computing for each case the least-squares solutions (5.1.12). The results of this activity are the following relationships:

$$\begin{pmatrix} \delta MI'_{14,44} \\ \delta MI'_{14,55} \\ \delta MI'_{14,66} \\ \delta MI'_{25,44} \\ \delta MI'_{25,55} \\ \delta MI'_{25,66} \\ \delta MI'_{36,44} \\ \delta MI'_{36,55} \\ \delta MI'_{36,66} \end{pmatrix} = \begin{pmatrix} 1 & 0 & -\frac{1}{2} & 0 & 0 & 0 & -\frac{1}{2} & 0 & 0 \\ 0 & 1 & 0 & -1 & 0 & 0 & 0 & 0 & 0 \\ 0 & 0 & 1 & 0 & 0 & 0 & -1 & 0 & 0 \\ 0 & -1 & 0 & 1 & 0 & 0 & 0 & 0 & 0 \\ 0 & 0 & 0 & 0 & 1 & -\frac{1}{2} & 0 & -\frac{1}{2} & 0 \\ 0 & 0 & 0 & 0 & 0 & 1 & 0 & -1 & 0 \\ 0 & 0 & -1 & 0 & 0 & 0 & 1 & 0 & 0 \\ 0 & 0 & 0 & 0 & 0 & -1 & 0 & 1 & 0 \\ 0 & 0 & -\frac{3}{7} & 0 & 0 & -\frac{1}{14} & -\frac{3}{7} & -\frac{1}{14} & 1 \end{pmatrix} \cdot \begin{pmatrix} \delta MI_{14,44} \\ \delta MI_{14,55} \\ \delta MI_{14,66} \\ \delta MI_{25,44} \\ \delta MI_{25,55} \\ \delta MI_{25,66} \\ \delta MI_{36,44} \\ \delta MI_{36,55} \\ \delta MI_{36,66} \end{pmatrix} \equiv CI \cdot \begin{pmatrix} \delta MI_{14,44} \\ \delta MI_{14,55} \\ \delta MI_{14,66} \\ \delta MI_{25,44} \\ \delta MI_{25,55} \\ \delta MI_{25,66} \\ \delta MI_{36,44} \\ \delta MI_{36,55} \\ \delta MI_{36,66} \end{pmatrix} \quad (5.1.13)$$

In theory, the relationships (5.1.13) allow to pass from the least-squares solution ($\delta MI'_{14,44}$, $\delta MI'_{14,55}$, $\delta MI'_{14,66}$, $\delta MI'_{25,44}$, $\delta MI'_{25,55}$, $\delta MI'_{25,66}$, $\delta MI'_{36,44}$, $\delta MI'_{36,55}$, $\delta MI'_{36,66}$) to the actual correction to be applied to the ICM diagonal elements ($\delta MI_{14,44}$, $\delta MI_{14,55}$, $\delta MI_{14,66}$, $\delta MI_{25,44}$, $\delta MI_{25,55}$, $\delta MI_{25,66}$, $\delta MI_{36,44}$, $\delta MI_{36,55}$, $\delta MI_{36,66}$). But this is not possible because the matrix CI is singular⁶. In fact, only six of the nine linear equations (5.1.13) are independent. Thus three additional properties must be known about the ICM diagonal elements in order to invert the (5.1.13). Apparently there are no general properties applicable to these elements (by construction they can assume any value within the limits given in Table 3.1-2). Hence the only way we found so far to invert the (5.1.13) is to assume the knowledge of three elements among ($\delta MI_{14,44}$, $\delta MI_{14,55}$, $\delta MI_{14,66}$, $\delta MI_{25,44}$, $\delta MI_{25,55}$, $\delta MI_{25,66}$, $\delta MI_{36,44}$, $\delta MI_{36,55}$, $\delta MI_{36,66}$). In practice, this means that value of three common scale factors must be provided by another method. Assuming the knowledge of

- $\delta MI_{14,66}$ (correction to ICM element $MI_{14,66}$, involved in the measurement of $\dot{\omega}_Y$),
- $\delta MI_{25,44}$ (correction to ICM element $MI_{25,44}$, involved in the measurement of $\dot{\omega}_Z$),
- $\delta MI_{36,55}$ (correction to ICM element $MI_{36,55}$, involved in the measurement of $\dot{\omega}_X$),

we get the other corrections as (trying to use as far as possible measurements from the US axes only):

$$\delta MI_{14,44} = \delta MI_{14,66} - \frac{1}{4} \delta MI'_{14,66} + \frac{1}{4} \delta MI'_{36,44} + \delta MI'_{14,44}$$

$$\delta MI_{14,55} = \delta MI_{25,44} - \delta MI'_{25,44}$$

⁵ More insight would be achieved by attempting to retrieve these relationships analytically. Since this task appears quite complex and time consuming, it will be left to a future activity (some of them have been already determined analytically by ONERA [RD 8]). The “universality” of the relationships obtained numerically can be, and has been verified by applying it to general test cases in which all the gradiometer imperfections (scale factors, misalignments, couplings) are applied at the same time.

⁶ Probably this is due to the largest weight of the Gradiometer measurements w.r.t. the star tracker measurements in the construction of the right-hand-side of the equations (5.1.11), and is the mathematical translation of the fact that the common (absolute) scale factors of the Gradiometer cannot be obtained from measurements provided by the Gradiometer only.

$$\delta MI_{25,55} = \delta MI_{36,55} + \frac{1}{4} \delta MI'_{25,66} - \frac{1}{4} \delta MI'_{36,55} + \delta MI'_{25,55}$$

$$\delta MI_{25,66} = \delta MI_{36,55} + \frac{1}{2} \delta MI'_{25,66} - \frac{1}{2} \delta MI'_{36,55} \quad (5.1.14)$$

$$\delta MI_{36,44} = \delta MI_{14,66} - \frac{1}{2} \delta MI'_{14,66} + \frac{1}{2} \delta MI'_{36,44}$$

$$\delta MI_{36,66} = \frac{6}{7} \delta MI_{14,66} + \frac{1}{7} \delta MI_{36,55} + \frac{1}{28} \delta MI'_{25,66} - \frac{1}{28} \delta MI'_{36,55} - \frac{3}{14} \delta MI'_{14,66} + \frac{3}{14} \delta MI'_{36,44} + \delta MI'_{36,66}$$

The missing elements ($\delta MI_{14,66}$, $\delta MI_{25,44}$, $\delta MI_{36,55}$) to perform the inversion of the (5.1.13) can be determined by exploiting the angular acceleration measurements obtained by the star sensor only. Actually, in this way it is possible to determine the six elements of the ICM related to the common scale factors of the accelerometer pairs about the transversal axes of the OAGs: $MI_{14,55}$, $MI_{14,66}$, $MI_{25,44}$, $MI_{25,66}$, $MI_{36,44}$, $MI_{36,55}$. The method by which these elements are obtained is the following. Let's denote as $\hat{\omega}_{S,X}$, $\hat{\omega}_{S,Y}$, $\hat{\omega}_{S,Z}$ the angular accelerations estimated by the star sensor measurements. By comparing these angular accelerations with those obtained from the Gradiometer (i.e. from the difference of differential accelerations), we get the following equations:

$$\begin{aligned} \hat{\omega}_{S,X} = \dot{\omega}_X &= -\frac{a_{d,36,Y}}{L_Z} + \frac{a_{d,25,Z}}{L_Y} \\ \hat{\omega}_{S,Y} = \dot{\omega}_Y &= -\frac{a_{d,14,Z}}{L_X} + \frac{a_{d,36,X}}{L_Z} \\ \hat{\omega}_{S,Z} = \dot{\omega}_Z &= -\frac{a_{d,25,X}}{L_Y} + \frac{a_{d,14,Y}}{L_X} \end{aligned} \quad (5.1.15)$$

By expressing $a_{d,ij}$ as function of the common mode and the differential mode accelerations measured by the three accelerometer pairs ($a'_{c,ij}$, $a'_{d,ij}$), and exploiting the knowledge of the ICM elements determined with the previous method, we get:

$$\begin{aligned} a_{d,14,Y} &= MI_{14,51} a'_{c,14,X} + MI_{14,52} a'_{c,14,Y} + MI_{14,53} a'_{c,14,Z} + MI_{14,54} a'_{d,14,X} + MI_{14,55} a'_{d,14,Y} + MI_{14,56} a'_{d,14,Z} = MI_{14,55} a'_{d,14,Y} + \Delta a_{d,14,Y} \\ a_{d,14,Z} &= MI_{14,61} a'_{c,14,X} + MI_{14,62} a'_{c,14,Y} + MI_{14,63} a'_{c,14,Z} + MI_{14,64} a'_{d,14,X} + MI_{14,65} a'_{d,14,Y} + MI_{14,66} a'_{d,14,Z} = MI_{14,66} a'_{d,14,Z} + \Delta a_{d,14,Z} \\ a_{d,25,X} &= MI_{25,41} a'_{c,25,X} + MI_{25,42} a'_{c,25,Y} + MI_{25,43} a'_{c,25,Z} + MI_{25,44} a'_{d,25,X} + MI_{25,45} a'_{d,25,Y} + MI_{25,46} a'_{d,25,Z} = MI_{25,44} a'_{d,25,X} + \Delta a_{d,25,X} \\ a_{d,25,Z} &= MI_{25,61} a'_{c,25,X} + MI_{25,62} a'_{c,25,Y} + MI_{25,63} a'_{c,25,Z} + MI_{25,64} a'_{d,25,X} + MI_{25,65} a'_{d,25,Y} + MI_{25,66} a'_{d,25,Z} = MI_{25,66} a'_{d,25,Z} + \Delta a_{d,25,Z} \\ a_{d,36,X} &= MI_{36,41} a'_{c,36,X} + MI_{36,42} a'_{c,36,Y} + MI_{36,43} a'_{c,36,Z} + MI_{36,44} a'_{d,36,X} + MI_{36,45} a'_{d,36,Y} + MI_{36,46} a'_{d,36,Z} = MI_{36,44} a'_{d,36,X} + \Delta a_{d,36,X} \\ a_{d,36,Y} &= MI_{36,51} a'_{c,36,X} + MI_{36,52} a'_{c,36,Y} + MI_{36,53} a'_{c,36,Z} + MI_{36,54} a'_{d,36,X} + MI_{36,55} a'_{d,36,Y} + MI_{36,56} a'_{d,36,Z} = MI_{36,55} a'_{d,36,Y} + \Delta a_{d,36,Y} \end{aligned} \quad (5.1.16)$$

By plugging the above expressions in the (5.1.15), we get the following sets of equations:

$$MI_{36,55} \left(-\frac{1}{L_Z} a'_{d,36,Y} \right) + MI_{25,66} \left(\frac{1}{L_Y} a'_{d,25,Z} \right) = \dot{\omega}_X + \frac{1}{L_Z} \Delta a_{d,36,Y} - \frac{1}{L_Y} \Delta a_{d,25,Z} \Rightarrow \mathbf{A1}' \cdot \mathbf{x1}' = \mathbf{y1}',$$

$$\mathbf{A1}' = \begin{pmatrix} -\frac{1}{L_Z} a'_{d,36,Y,1} & \frac{1}{L_Y} a'_{d,25,Z,1} \\ -\frac{1}{L_Z} a'_{d,36,Y,2} & \frac{1}{L_Y} a'_{d,25,Z,2} \\ \vdots & \vdots \\ -\frac{1}{L_Z} a'_{d,36,Y,N} & \frac{1}{L_Y} a'_{d,25,Z,N} \end{pmatrix}, \mathbf{y1}' = \begin{pmatrix} \dot{\omega}_{X,1} + \frac{1}{L_Z} \Delta a_{d,36,Y,1} - \frac{1}{L_Y} \Delta a_{d,25,Z,1} \\ \dot{\omega}_{X,2} + \frac{1}{L_Z} \Delta a_{d,36,Y,2} - \frac{1}{L_Y} \Delta a_{d,25,Z,2} \\ \vdots \\ \dot{\omega}_{X,N} + \frac{1}{L_Z} \Delta a_{d,36,Y,N} - \frac{1}{L_Y} \Delta a_{d,25,Z,N} \end{pmatrix}; \mathbf{x1}' = \begin{pmatrix} MI_{36,55} \\ MI_{25,66} \end{pmatrix} \quad (5.1.17)$$

$$MI_{14,66} \left(-\frac{1}{L_X} a'_{d,14,Z} \right) + MI_{36,44} \left(\frac{1}{L_Z} a'_{d,36,X} \right) = \dot{\omega}_Y + \frac{1}{L_X} \Delta a_{d,14,Z} - \frac{1}{L_Z} \Delta a_{d,36,X} \Rightarrow \mathbf{A2}' \cdot \mathbf{x2}' = \mathbf{y2}',$$

$$\mathbf{A2}' = \begin{pmatrix} -\frac{1}{L_X} a'_{d,14,Z,1} & \frac{1}{L_Z} a'_{d,36,X,1} \\ -\frac{1}{L_X} a'_{d,14,Z,2} & \frac{1}{L_Z} a'_{d,36,X,2} \\ \vdots & \vdots \\ -\frac{1}{L_X} a'_{d,14,Z,N} & \frac{1}{L_Z} a'_{d,36,X,N} \end{pmatrix}, \mathbf{y2}' = \begin{pmatrix} \dot{\omega}_{Y,1} + \frac{1}{L_X} \Delta a_{d,14,Z,1} - \frac{1}{L_Z} \Delta a_{d,36,X,1} \\ \dot{\omega}_{Y,2} + \frac{1}{L_X} \Delta a_{d,14,Z,2} - \frac{1}{L_Z} \Delta a_{d,36,X,2} \\ \vdots \\ \dot{\omega}_{Y,N} + \frac{1}{L_X} \Delta a_{d,14,Z,N} - \frac{1}{L_Z} \Delta a_{d,36,X,N} \end{pmatrix}; \mathbf{x2}' = \begin{pmatrix} MI_{14,66} \\ MI_{36,44} \end{pmatrix}$$

$$MI_{25,44} \left(-\frac{1}{L_Y} a'_{d,25,X} \right) + MI_{14,55} \left(\frac{1}{L_X} a'_{d,14,Y} \right) = \dot{\omega}_Z + \frac{1}{L_Y} \Delta a_{d,25,X} - \frac{1}{L_X} \Delta a_{d,14,Y} \Rightarrow \mathbf{A3}' \cdot \mathbf{x3}' = \mathbf{y3}',$$

$$\mathbf{A3}' = \begin{pmatrix} -\frac{1}{L_Y} a'_{d,25,X,1} & \frac{1}{L_X} a'_{d,14,Y,1} \\ -\frac{1}{L_Y} a'_{d,25,X,2} & \frac{1}{L_X} a'_{d,14,Y,2} \\ \vdots & \vdots \\ -\frac{1}{L_Y} a'_{d,25,X,N} & \frac{1}{L_X} a'_{d,14,Y,N} \end{pmatrix}, \mathbf{y3}' = \begin{pmatrix} \dot{\omega}_{Z,1} + \frac{1}{L_Y} \Delta a_{d,25,X,1} - \frac{1}{L_X} \Delta a_{d,14,Y,1} \\ \dot{\omega}_{Z,2} + \frac{1}{L_Y} \Delta a_{d,25,X,2} - \frac{1}{L_X} \Delta a_{d,14,Y,2} \\ \vdots \\ \dot{\omega}_{Z,N} + \frac{1}{L_Y} \Delta a_{d,25,X,N} - \frac{1}{L_X} \Delta a_{d,14,Y,N} \end{pmatrix}; \mathbf{x3}' = \begin{pmatrix} MI_{25,44} \\ MI_{14,55} \end{pmatrix}$$

which again can be solved with the least-squares algorithms to get $MI_{14,55}, MI_{14,66}, MI_{25,44}, MI_{25,66}, MI_{36,44}, MI_{36,55}$.

In summary, all the 54 elements of the last three rows of the 6×6 ICMs elements can be determined in a three-step iterative process:

- Step 1) Determination of the ICM elements assuming a unitary value for the elements related to the common scale factors of the three accelerometer pairs (i.e. the nine elements $MI_{14,44}$, $MI_{14,55}$, $MI_{14,66}$, $MI_{25,44}$, $MI_{25,55}$, $MI_{25,66}$, $MI_{36,44}$, $MI_{36,55}$, $MI_{36,66}$). This first step determines therefore $54 - 9 = 45$ ICM elements.
- Step 2) Determination of the six ICM elements related to the “transversal” common scale factors of the three accelerometer pairs ($MI_{14,55}$, $MI_{14,66}$, $MI_{25,44}$, $MI_{25,66}$, $MI_{36,44}$, $MI_{36,55}$), using the partial ICMs determined at step 1.
- Step 3) Determination of all the 54 elements of the 4th, 5th, 6th rows of the ICMs using the partial ICMs determined at step 1 and the transversal common scale factors determined at step 2.

The steps 2) and 3) are iterated until the convergence is achieved: the new step 2) is fed by the ICMs determined at step 3); the new step 3) is fed by the new transversal common scale factors determined at step 2), and so on.

The functional block diagram of the procedure for the determination of all the 54 IMC elements is shown in Figure 5.1-1.

A similar iterative procedure is implemented in both steps 1) and 3). The differences are just in the inputs utilised to initialize the procedure and in the specific algorithms of one of the iterative steps, which is detailed in the following sections. This iterative procedure is described in the functional block diagram of Figure 5.1-2. The iteration steps are labelled with the letters (a), ..., (f) which are recalled in the algorithm description.

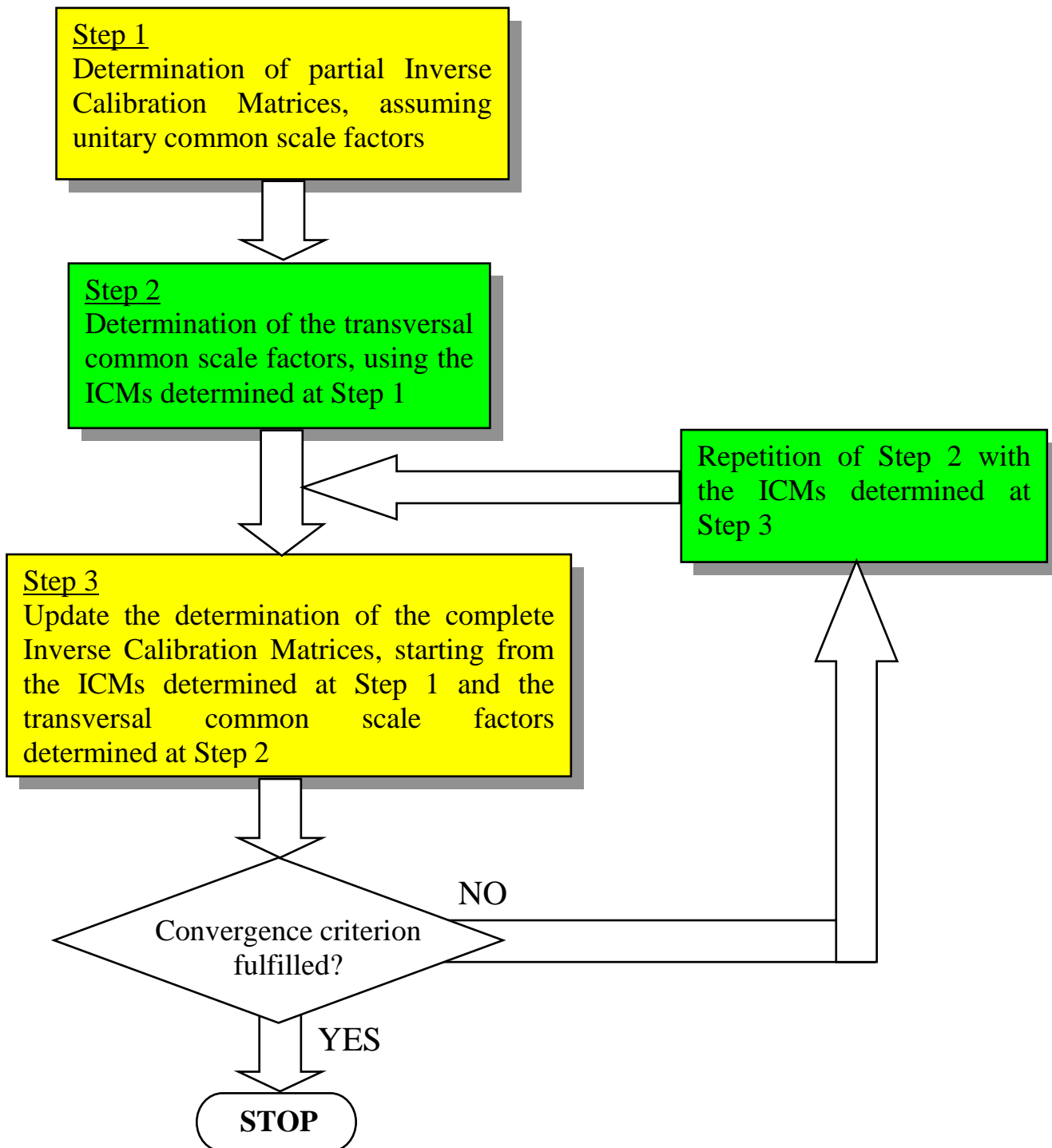


Figure 5.1-1: Functional block diagram of the overall procedure for the ICM elements determination

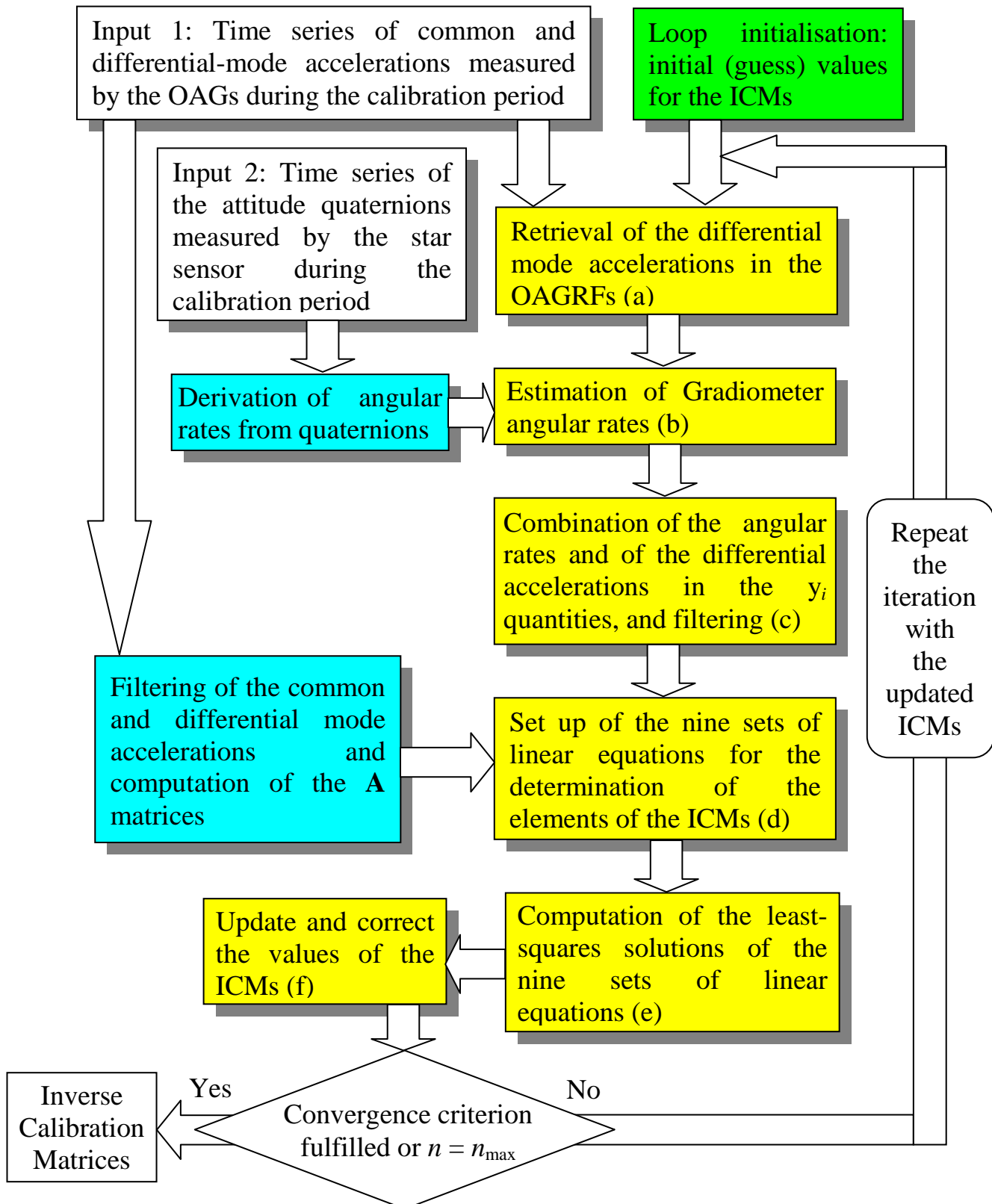


Figure 5.1-2: Functional block diagram of the Step 1) and Step 3) of the ICMs determination procedure

5.1.2 Step by Step Process

5.1.2.1 Iterative Process Inputs

Inputs to the iterative process for the determination of the ICMs are the time series of the common-mode and differential-mode accelerations ($\underline{a}'_{c,14}$, $\underline{a}'_{d,14}$, $\underline{a}'_{c,25}$, $\underline{a}'_{d,25}$, $\underline{a}'_{c,36}$, $\underline{a}'_{d,36}$) measured by the Gradiometer (at 1 Hz frequency) during the calibration period (of duration $\Delta T = T_{\text{start}} - T_{\text{end}}$), corrected for the gain and phase delay introduced by the accelerometer transfer function, and of the quaternions (q_1, q_2, q_3, q_4) defining the attitude of the SSRF in the IRF and computed on-board by the star sensor (at 2 Hz frequency) in the period ΔT .

During the calibration period, the satellite is subject to random, uncorrelated shaking about all the axes, in the bandwidth from 50 mHz to 100 mHz, by means of impulsive cold-gas thrusters of the GCD and of the ion thruster. This shaking is superimposed to the normal “drag free” control kept during the measurement phases by means of the magnetic torquers and the ITA.

5.1.2.2 Inputs Pre-processing

Before starting the iterative process:

- 1) Compute the rotation matrix from the SSRF to the IRF by means of the quaternions (q_1, q_2, q_3, q_4):

$$\mathbf{R}_{\text{IRF_SSRF}} = \begin{pmatrix} q_1^2 - q_2^2 - q_3^2 + q_4^2 & 2(q_{12} - q_{34}) & 2(q_{13} + q_{24}) \\ 2(q_{12} + q_{34}) & -q_1^2 + q_2^2 - q_3^2 + q_4^2 & 2(q_{23} - q_{14}) \\ 2(q_{13} - q_{24}) & 2(q_{23} + q_{14}) & -q_1^2 - q_2^2 + q_3^2 + q_4^2 \end{pmatrix}$$

$$q_{12} = q_1 q_2, q_{13} = q_1 q_3, q_{14} = q_1 q_4, q_{23} = q_2 q_3, q_{24} = q_2 q_4, q_{34} = q_3 q_4.$$

- 2) Compute the rotation matrix from the GRF to the IRF using the rotation matrices $\mathbf{R}_{\text{IRF_SSRF}}$ and $\mathbf{R}_{\text{SSRF_GRF}}$ (the latter defining the orientation of the SSRF in the GRF):

$$\mathbf{R}_{\text{IRF_GRF}} = \mathbf{R}_{\text{IRF_SSRF}} \cdot \mathbf{R}_{\text{SSRF_GRF}}$$

- 3) From the rotation matrix $\mathbf{R}_{\text{IRF_GRF}}$ compute the time series of the star sensor derived angular rates $\hat{\omega}_{S,k}(t_i)$ ($k = X, Y, Z$) of the GRF in the IRF, expressed in the GRF:

$$\begin{aligned} \hat{\omega}_{S,X}(t_i) &= \bar{\mathbf{R}}_{\text{IRF_GRF},13}(t_i) \frac{\tilde{\mathbf{R}}_{\text{IRF_GRF},12}(t_i)}{\Delta t} + \bar{\mathbf{R}}_{\text{IRF_GRF},23}(t_i) \frac{\tilde{\mathbf{R}}_{\text{IRF_GRF},22}(t_i)}{\Delta t} + \bar{\mathbf{R}}_{\text{IRF_GRF},33}(t_i) \frac{\tilde{\mathbf{R}}_{\text{IRF_GRF},32}(t_i)}{\Delta t} \\ \hat{\omega}_{S,Y}(t_i) &= \bar{\mathbf{R}}_{\text{IRF_GRF},21}(t_i) \frac{\tilde{\mathbf{R}}_{\text{IRF_GRF},23}(t_i)}{\Delta t} + \bar{\mathbf{R}}_{\text{IRF_GRF},31}(t_i) \frac{\tilde{\mathbf{R}}_{\text{IRF_GRF},33}(t_i)}{\Delta t} + \bar{\mathbf{R}}_{\text{IRF_GRF},11}(t_i) \frac{\tilde{\mathbf{R}}_{\text{IRF_GRF},13}(t_i)}{\Delta t}, \\ \hat{\omega}_{S,Z}(t_i) &= \bar{\mathbf{R}}_{\text{IRF_GRF},32}(t_i) \frac{\tilde{\mathbf{R}}_{\text{IRF_GRF},31}(t_i)}{\Delta t} + \bar{\mathbf{R}}_{\text{IRF_GRF},12}(t_i) \frac{\tilde{\mathbf{R}}_{\text{IRF_GRF},11}(t_i)}{\Delta t} + \bar{\mathbf{R}}_{\text{IRF_GRF},22}(t_i) \frac{\tilde{\mathbf{R}}_{\text{IRF_GRF},21}(t_i)}{\Delta t}, \quad i = 1, \dots, N. \end{aligned}$$

with

$$\bar{R}_{IRF_GRF}(t_i) = \begin{pmatrix} \bar{R}_{IRF_GRF,11} & \bar{R}_{IRF_GRF,12} & \bar{R}_{IRF_GRF,13} \\ \bar{R}_{IRF_GRF,21} & \bar{R}_{IRF_GRF,22} & \bar{R}_{IRF_GRF,23} \\ \bar{R}_{IRF_GRF,31} & \bar{R}_{IRF_GRF,32} & \bar{R}_{IRF_GRF,33} \end{pmatrix} = \frac{R_{IRF_GRF}(t_{i+1}) + R_{IRF_GRF}(t_{i-1})}{2},$$

$$\tilde{R}_{IRF_GRF}(t_i) = \begin{pmatrix} \tilde{R}_{IRF_GRF,11} & \tilde{R}_{IRF_GRF,12} & \tilde{R}_{IRF_GRF,13} \\ \tilde{R}_{IRF_GRF,21} & \tilde{R}_{IRF_GRF,22} & \tilde{R}_{IRF_GRF,23} \\ \tilde{R}_{IRF_GRF,31} & \tilde{R}_{IRF_GRF,32} & \tilde{R}_{IRF_GRF,33} \end{pmatrix} = R_{IRF_GRF}(t_{i+1}) - R_{IRF_GRF}(t_{i-1}), \Delta t = t_{i+1} - t_{i-1}.$$

The computed angular rate time series have a time step of 0.5 s.

- 4) Align the time histories of the so computed angular rates to the time history of the common-mode and differential-mode linear accelerations measured by the gradiometer as follows

- a) Compute the Fourier transform of each angular rate time history:

$$\hat{\omega}_k(t) \rightarrow \text{Fourier transform} \rightarrow [\text{Amplitude}_{\hat{\omega}_k}(\nu), \text{Phase}_{\hat{\omega}_k}(\nu)]$$

- b) Correct the phase with the time delay ΔT , computed as the difference between the first time ($t_{a,0}$) of the measured acceleration time history and the time ($t_{\omega,0}$) of the angular rate time history which is closest to $t_{a,0}$:

$$\Delta T = t_{a,0} - t_{\omega,0}, \text{Phase}_{\hat{\omega}_k}(\nu) \rightarrow \text{Phase}_{\hat{\omega}_k}'(\nu) = \text{Phase}_{\hat{\omega}_k}(\nu) + 2\pi \nu \Delta T$$

- c) Compute the time histories of the angular rates aligned to the time histories of the measured linear accelerations by inverse Fourier transform:

$$[\text{Amplitude}_{\hat{\omega}_k}(\nu), \text{Phase}_{\hat{\omega}_k}'(\nu)] \rightarrow \text{inverse Fourier transform} \rightarrow \hat{\omega}_k(t)_{\text{aligned}}$$

- 5) From the above star sensor derived angular rates, compute the time series of the star sensor derived angular accelerations $\hat{\omega}_{S,k}(t_i)$ ($k = X, Y, Z$) of the GRF in the IRF, expressed in the GRF, according to the procedure:

- Detrend the time series of the angular rate.
- Remove the high frequency component with apodization between 0.4 and 0.5 Hz going to work in the frequency domain and coming back to the time domain (the removal of energy content above 0.5 Hz is necessary before decimation at 1 Hz). The removal of the high frequency component is done in the frequency domain with a linear decay from 0.4 Hz to 0.5 Hz and setting to zero the frequency component from 0.5 to 1 Hz. Since the angular rate time series is sampled at 2 Hz, the apodization and energy removal is implemented according to:

$$\tilde{\omega}_k(\nu_j) = \frac{(0.5 - \nu_j)}{(0.5 - 0.4)} \omega_i(\nu_j) \text{ with } k = X, Y, Z, 0.4 \text{ Hz} \leq \nu_j \leq 0.5 \text{ Hz}; \tilde{\omega}_k(\nu_j) = 0 \text{ for } 0.5 \text{ Hz} < \nu_j \leq 1 \text{ Hz}.$$

- Retrend the time series.
- Compute the angular accelerations from the retrended time series of the angular rates: $\hat{\omega}_{S,k}(t) \rightarrow \text{Fourier transform} \rightarrow \hat{\omega}_{S,k}(\nu) \rightarrow \hat{\omega}_{S,k}'(\nu) = 2\pi\nu \tilde{\omega}_{S,k}(\nu) \rightarrow \text{inverse Fourier transform} \rightarrow \hat{\omega}_{S,k}(t)$.

Before computing the inverse Fourier transform, remove from the $\hat{\omega}_{S,k}(\nu)$ set the Fourier coefficients corresponding to frequencies $\nu \geq 0.01$ Hz.

On the time series of the star sensor derived angular rates $\hat{\omega}_{S,k}(t_i)$ (after the computation of the angular accelerations) and of the angular accelerations $\hat{\omega}_{S,k}(t_i)$ so obtained, perform the following two operations:

- a) Reduce the time series frequency from 2 to 1 Hz by picking one angular acceleration every two.
b) Skip the first and last N_p data points ($N_p = 500$ TBC), from time = T_{start} .
- 6) Pass the measured common-mode and differential-mode accelerations ($\underline{a}'_{c,14}, \underline{a}'_{d,14}, \underline{a}'_{c,25}, \underline{a}'_{d,25}, \underline{a}'_{c,36}, \underline{a}'_{d,36}$) first through a low-pass filter in the time domain for removing the frequency components above 200 mHz, and then through a band-pass filter in the time domain for removing the frequency components outside the $[50 \div 100 \text{ mHz}]$ bandwidth:

$$\underline{\hat{a}}''_{c,14,X}(t_n) = \sum_{k=+N_{bl}}^{-N_{bl}} bl_k \cdot \underline{a}'_{c,14,X}(t_{n-k}), \underline{\hat{a}}''_{c,14,Y}(t_n) = \sum_{k=+N_{bl}}^{-N_{bl}} bl_k \cdot \underline{a}'_{c,14,Y}(t_{n-k}), \dots, \underline{\hat{a}}''_{d,36,Z}(t_n) = \sum_{k=+N_{bl}}^{-N_{bl}} bl_k \cdot \underline{a}'_{d,36,Z}(t_{n-k})$$

$$\underline{\hat{a}}'_{c,14,X}(t_n) = \sum_{k=+N_b}^{-N_b} b_k \cdot \underline{\hat{a}}''_{c,14,X}(t_{n-k}), \underline{\hat{a}}'_{c,14,Y}(t_n) = \sum_{k=+N_b}^{-N_b} b_k \cdot \underline{\hat{a}}''_{c,14,Y}(t_{n-k}), \dots, \underline{\hat{a}}'_{d,36,Z}(t_n) = \sum_{k=+N_b}^{-N_b} b_k \cdot \underline{\hat{a}}''_{d,36,Z}(t_{n-k})$$

$$\underline{a}'_{c,14}, \underline{a}'_{d,14}, \underline{a}'_{c,25}, \underline{a}'_{d,25}, \underline{a}'_{c,36}, \underline{a}'_{d,36} \text{ (unfiltered)} \Rightarrow \underline{\hat{a}}''_{c,14}, \underline{\hat{a}}''_{d,14}, \underline{\hat{a}}''_{c,25}, \underline{\hat{a}}''_{d,25}, \underline{\hat{a}}''_{c,36}, \underline{\hat{a}}''_{d,36} \text{ (low-pass filtered)}$$

$$\Rightarrow \underline{\hat{a}}'_{c,14}, \underline{\hat{a}}'_{d,14}, \underline{\hat{a}}'_{c,25}, \underline{\hat{a}}'_{d,25}, \underline{\hat{a}}'_{c,36}, \underline{\hat{a}}'_{d,36} \text{ (band-pass filtered)}$$

where bl and b are vector of $2N_{bl}+1$ and $2N_b+1$ elements respectively containing the parameters of the band-pass filter.

In the common-mode and differential-mode accelerations time series so obtained, skip the first and last N_p data points ($N_p = 500$ TBC).

- 7) With the filtered accelerations, build the following $N \times 6$ **A** matrices:

$$\mathbf{A1} = \mathbf{A2} = \mathbf{A3} = \begin{pmatrix} \underline{\hat{a}}'_{c,14,X,1} & \underline{\hat{a}}'_{c,14,Y,1} & \underline{\hat{a}}'_{c,14,Z,1} & \underline{\hat{a}}'_{d,14,X,1} & \underline{\hat{a}}'_{d,14,Y,1} & \underline{\hat{a}}'_{d,14,Z,1} \\ \underline{\hat{a}}'_{c,14,X,2} & \underline{\hat{a}}'_{c,14,Y,2} & \underline{\hat{a}}'_{c,14,Z,2} & \underline{\hat{a}}'_{d,14,X,2} & \underline{\hat{a}}'_{d,14,Y,2} & \underline{\hat{a}}'_{d,14,Z,2} \\ \vdots & \vdots & \vdots & \vdots & \vdots & \vdots \\ \underline{\hat{a}}'_{c,14,X,N} & \underline{\hat{a}}'_{c,14,Y,N} & \underline{\hat{a}}'_{c,14,Z,N} & \underline{\hat{a}}'_{d,14,X,N} & \underline{\hat{a}}'_{d,14,Y,N} & \underline{\hat{a}}'_{d,14,Z,N} \end{pmatrix}$$

$$\mathbf{A4} = \mathbf{A5} = \mathbf{A6} = \begin{pmatrix} \underline{\hat{a}}'_{c,25,X,1} & \underline{\hat{a}}'_{c,25,Y,1} & \underline{\hat{a}}'_{c,25,Z,1} & \underline{\hat{a}}'_{d,25,X,1} & \underline{\hat{a}}'_{d,25,Y,1} & \underline{\hat{a}}'_{d,25,Z,1} \\ \underline{\hat{a}}'_{c,25,X,2} & \underline{\hat{a}}'_{c,25,Y,2} & \underline{\hat{a}}'_{c,25,Z,2} & \underline{\hat{a}}'_{d,25,X,2} & \underline{\hat{a}}'_{d,25,Y,2} & \underline{\hat{a}}'_{d,25,Z,2} \\ \vdots & \vdots & \vdots & \vdots & \vdots & \vdots \\ \underline{\hat{a}}'_{c,25,X,N} & \underline{\hat{a}}'_{c,25,Y,N} & \underline{\hat{a}}'_{c,25,Z,N} & \underline{\hat{a}}'_{d,25,X,N} & \underline{\hat{a}}'_{d,25,Y,N} & \underline{\hat{a}}'_{d,25,Z,N} \end{pmatrix}$$

$$\mathbf{A7} = \mathbf{A8} = \mathbf{A9} = \begin{pmatrix} \underline{\hat{a}}'_{c,36,X,1} & \underline{\hat{a}}'_{c,36,Y,1} & \underline{\hat{a}}'_{c,36,Z,1} & \underline{\hat{a}}'_{d,36,X,1} & \underline{\hat{a}}'_{d,36,Y,1} & \underline{\hat{a}}'_{d,36,Z,1} \\ \underline{\hat{a}}'_{c,36,X,2} & \underline{\hat{a}}'_{c,36,Y,2} & \underline{\hat{a}}'_{c,36,Z,2} & \underline{\hat{a}}'_{d,36,X,2} & \underline{\hat{a}}'_{d,36,Y,2} & \underline{\hat{a}}'_{d,36,Z,2} \\ \vdots & \vdots & \vdots & \vdots & \vdots & \vdots \\ \underline{\hat{a}}'_{c,36,X,N} & \underline{\hat{a}}'_{c,36,Y,N} & \underline{\hat{a}}'_{c,36,Z,N} & \underline{\hat{a}}'_{d,36,X,N} & \underline{\hat{a}}'_{d,36,Y,N} & \underline{\hat{a}}'_{d,36,Z,N} \end{pmatrix}$$

where $\underline{\hat{a}}'_{c,14,X,1} = \underline{\hat{a}}'_{c,14,X}$ measured at time $t = t_1, \dots, \underline{\hat{a}}'_{c,14,X,N} = \underline{\hat{a}}'_{c,14,X}$ measured at time $t = t_N$, etc...

- 8) Pass the star sensor derived angular accelerations $\hat{\omega}_{S,k}(t_i)$ through a band-pass filter in the time domain for removing the frequency components outside a $[v_{\min} \div v_{\max}]$ bandwidth:

$$\hat{\omega}_{S,X}(t_n) = \sum_{k=+N_h}^{-N_h} h_k^X \cdot \hat{\omega}_{S,X}(t_{n-k}), \hat{\omega}_{S,Y}(t_n) = \sum_{k=+N_h}^{-N_h} h_k^Y \cdot \hat{\omega}_{S,Y}(t_{n-k}), \hat{\omega}_{S,Z}(t_n) = \sum_{k=+N_h}^{-N_h} h_k^Z \cdot \hat{\omega}_{S,Z}(t_{n-k})$$

where h^X, h^Y, h^Z are vectors of $2N_h + 1$ elements containing the parameters of the band-pass filters.

5.1.2.3 Iterative Loop Initialisation

A set of initial values for the elements of the last three rows of the ICMs, i.e. an a-priori solution of the problem, must be assumed. A possibility (which does not rely on the measurements performed during the on-ground calibration of the Gradiometer) is to start assuming the accelerometer scale factors all equal to 1 and the misalignments, couplings all equal to 0:

$$\begin{aligned} \left(\begin{bmatrix} MI \end{bmatrix}_{d,14} \quad \begin{bmatrix} MI \end{bmatrix}_{c,14} \right)_{(1)} &= \begin{pmatrix} MI_{14,41} & MI_{14,42} & MI_{14,43} & MI_{14,44} & MI_{14,45} & MI_{14,46} \\ MI_{14,51} & MI_{14,52} & MI_{14,53} & MI_{14,54} & MI_{14,55} & MI_{14,56} \\ MI_{14,61} & MI_{14,62} & MI_{14,63} & MI_{14,64} & MI_{14,65} & MI_{14,66} \end{pmatrix}_{(1)} = \begin{pmatrix} 0 & 0 & 0 & 1 & 0 & 0 \\ 0 & 0 & 0 & 0 & 1 & 0 \\ 0 & 0 & 0 & 0 & 0 & 1 \end{pmatrix} \\ \left(\begin{bmatrix} MI \end{bmatrix}_{d,25} \quad \begin{bmatrix} MI \end{bmatrix}_{c,25} \right)_{(1)} &= \begin{pmatrix} MI_{25,41} & MI_{25,42} & MI_{25,43} & MI_{25,44} & MI_{25,45} & MI_{25,46} \\ MI_{25,51} & MI_{25,52} & MI_{25,53} & MI_{25,54} & MI_{25,55} & MI_{25,56} \\ MI_{25,61} & MI_{25,62} & MI_{25,63} & MI_{25,64} & MI_{25,65} & MI_{25,66} \end{pmatrix}_{(1)} = \begin{pmatrix} 0 & 0 & 0 & 1 & 0 & 0 \\ 0 & 0 & 0 & 0 & 1 & 0 \\ 0 & 0 & 0 & 0 & 0 & 1 \end{pmatrix} \\ \left(\begin{bmatrix} MI \end{bmatrix}_{d,36} \quad \begin{bmatrix} MI \end{bmatrix}_{c,36} \right)_{(1)} &= \begin{pmatrix} MI_{36,41} & MI_{36,42} & MI_{36,43} & MI_{36,44} & MI_{36,45} & MI_{36,46} \\ MI_{36,51} & MI_{36,52} & MI_{36,53} & MI_{36,54} & MI_{36,55} & MI_{36,56} \\ MI_{36,61} & MI_{36,62} & MI_{36,63} & MI_{36,64} & MI_{36,65} & MI_{36,66} \end{pmatrix}_{(1)} = \begin{pmatrix} 0 & 0 & 0 & 1 & 0 & 0 \\ 0 & 0 & 0 & 0 & 1 & 0 \\ 0 & 0 & 0 & 0 & 0 & 1 \end{pmatrix} \end{aligned}$$

5.1.2.4 Calibration Step 1

5.1.2.4.1 Iterative Loop Step (a): Retrieval of the Differential Mode Accelerations in the OAGRFs

Use the current estimation of the ICMs to compute the actual differential-mode accelerations at the accelerometer locations in the OAGRFs ($\hat{a}_{d,14}, \hat{a}_{d,25}, \hat{a}_{d,36}$) from the measured common-mode and differential-mode accelerations ($\underline{a}'_{c,14}, \underline{a}'_{d,14}, \underline{a}'_{c,25}, \underline{a}'_{d,25}, \underline{a}'_{c,36}, \underline{a}'_{d,36}$) measured over the calibration period (not filtered):

$$\begin{pmatrix} \hat{a}_{d,14,X} \\ \hat{a}_{d,14,Y} \\ \hat{a}_{d,14,Z} \end{pmatrix} = \left(\begin{bmatrix} MI \end{bmatrix}_{d,14} \quad \begin{bmatrix} MI \end{bmatrix}_{c,14} \right)_{(n)} \cdot \begin{pmatrix} a'_{c,14,X} \\ a'_{c,14,Y} \\ a'_{c,14,Z} \\ a'_{d,14,X} \\ a'_{d,14,Y} \\ a'_{d,14,Z} \end{pmatrix}$$

$$\begin{pmatrix} \hat{a}_{d,25,X} \\ \hat{a}_{d,25,Y} \\ \hat{a}_{d,25,Z} \end{pmatrix} = \begin{pmatrix} [MI]_{d,25} & [MI]_{c,25} \end{pmatrix}_{(n)} \cdot \begin{pmatrix} a'_{c,25,X} \\ a'_{c,25,Y} \\ a'_{c,25,Z} \\ a'_{d,25,X} \\ a'_{d,25,Y} \\ a'_{d,25,Z} \end{pmatrix}$$

$$\begin{pmatrix} \hat{a}_{d,36,X} \\ \hat{a}_{d,36,Y} \\ \hat{a}_{d,36,Z} \end{pmatrix} = \begin{pmatrix} [MI]_{d,36} & [MI]_{c,36} \end{pmatrix}_{(n)} \cdot \begin{pmatrix} a'_{c,36,X} \\ a'_{c,36,Y} \\ a'_{c,36,Z} \\ a'_{d,36,X} \\ a'_{d,36,Y} \\ a'_{d,36,Z} \end{pmatrix}$$

where $n = 1$ at the first iteration (in this case the initial “guess” for the ICM elements given shall be used – section 5.1.2.3).

5.1.2.4.2 Iterative Loop Step (b): Estimation of Gradiometer Angular Rates

Estimate the Gradiometer inertial angular rates $(\hat{\omega}_X, \hat{\omega}_Y, \hat{\omega}_Z)$ from the transversal differential accelerations $(\hat{a}_{d,14,Y}, \hat{a}_{d,14,Z}, \hat{a}_{d,25,X}, \hat{a}_{d,25,Z}, \hat{a}_{d,36,X}, \hat{a}_{d,36,Y})$ measured by the Gradiometer and from star sensor derived angular rates $\hat{\omega}_{S,k}(t)$, with the following procedure.

1) Computation angular accelerations from the gradiometer measurements:

- Skip the first and last N_p data points ($N_p = 500$ TBC) from time = T_{start} in the time series of the transversal differential accelerations.
- Filter the differential accelerations by convolution in the frequency range $[0 \div 200 \text{ mHz}]$ according to:

$$\hat{a}'_{d,14,Y}(t_n) = \sum_{k=-N_{b'}}^{-N_{b'}} b'_k \cdot \hat{a}_{d,14,Y}(t_{n-k}), \dots, \hat{a}'_{d,36,Y}(t_n) = \sum_{k=-N_{b'}}^{-N_{b'}} b'_k \cdot \hat{a}_{d,36,Y}(t_{n-k})$$

where b' is a vector of $2N_{b'} + 1$ elements containing the parameters of the bandpass filter.

- Build up the angular acceleration according to:

$$\hat{\omega}_X = -\frac{\hat{a}'_{d,36,Y}}{L_Z} + \frac{\hat{a}'_{d,25,Z}}{L_Y}, \quad \hat{\omega}_Y = -\frac{\hat{a}'_{d,14,Z}}{L_X} + \frac{\hat{a}'_{d,36,X}}{L_Z}, \quad \hat{\omega}_Z = -\frac{\hat{a}'_{d,25,X}}{L_Y} + \frac{\hat{a}'_{d,14,Y}}{L_X}.$$

2) Integration of $(\hat{\omega}_X, \hat{\omega}_Y, \hat{\omega}_Z)$ in the frequency domain to obtain Gradiometer-derived angular rates:

$$\hat{\omega}_k(t) \rightarrow \text{Fourier transform} \rightarrow \hat{\omega}_k(v) \rightarrow \hat{\omega}_k(v) = \frac{\hat{\omega}_k(v)}{2\pi v} \rightarrow \text{inverse Fourier transform} \rightarrow \hat{\omega}_{G,k}(t), \quad k = X, Y, Z$$

3) Evaluation and removal of the trends from the time series of $\hat{\omega}_{G,k}(t)$, $\hat{\omega}_{S,k}(t)$, to avoid spectral leakage:

- Perform a linear regression on these sets of points to evaluate the offset and slope (O_1, S_1) at the beginning of the time series and the offset and slope (O_N, S_N) at the end of the time series:

$$S_1 = \frac{\sum_{i=1}^p x_i y_i - \frac{1}{p} \sum_{i=1}^p x_i \sum_{i=1}^p y_i}{\sum_{i=1}^p x_i^2 - \frac{1}{p} \left(\sum_{i=1}^p x_i \right)^2}, \quad b_1 = \frac{1}{p} \left(\sum_{i=1}^p y_i - S_1 \sum_{i=1}^p x_i \right), \quad O_1 = S_1 + b_1$$

$$S_N = \frac{\sum_{i=1}^p x_i z_i - \frac{1}{p} \sum_{i=1}^p x_i \sum_{i=1}^p z_i}{\sum_{i=1}^p x_i^2 - \frac{1}{p} \left(\sum_{i=1}^p x_i \right)^2}, \quad b_N = \frac{1}{p} \left(\sum_{i=1}^p z_i - S_N \sum_{i=1}^p x_i \right), \quad O_N = S_N \cdot p + b_N$$

with $x_i = i$, $y_i = \hat{\omega}_{G,k}(t_i)$, $\hat{\omega}_{S,k}(t_i)$, $z_i = \hat{\omega}_{G,k}(t_{N-p+i})$, $\hat{\omega}_{S,k}(t_{N-p+i})$, $p = 250$.

- Compute the straight-line part of the trend $TL_i = O_1 + \frac{(O_N - O_1)(i-1)}{N-1}$ (this removes the step between the end and the beginning of the time series). Note: since the time series are noisy, the offsets (O_1, O_N) so computed are a better estimate of the difference from zero of $\hat{\omega}_{G,k}, \hat{\omega}_{S,k}$ at the initial/final time than the value of their first/last point. So the linear trend is computed between (O_1, O_N).

- Computed the damped-exponential parts of the trend $TE1_i = \frac{S_1 - \bar{S}}{2\pi f} e^{-(i-1)/\tau} \sin(2\pi f(i-1))$,

$$TEN_i = -\frac{S_N - \bar{S}}{2\pi f} e^{-(N-i+1)/\tau} \sin(2\pi f(N-i+1)), \text{ with } \tau = N/20, f = 2/N, \bar{S} = (S_1 + S_N)/2.$$

- Compute the total trend $TR_i = TL_i + TE1_i + TEN_i$ for $\hat{\omega}_{G,k}(t_i)$ and $\hat{\omega}_{S,k}(t_i)$ ($TR_{G,ik}, TR_{S,ik}$).
- Remove the trend: $\hat{\omega}'_{G,k}(t_i) = \hat{\omega}_{G,k}(t_i) - TR_{G,ik}$; $\hat{\omega}'_{S,k}(t_i) = \hat{\omega}_{S,k}(t_i) - TR_{S,ik}$ ($i = 1, \dots, N, k = X, Y, Z$).

4) Computation and concatenation of the Fourier transform of $\hat{\omega}'_{G,k}(t_i)$, $\hat{\omega}'_{S,k}(t_i)$:

$$\hat{\omega}'_{G,k}(t_i), \hat{\omega}'_{S,k}(t_i) \rightarrow \text{Fourier transform} \rightarrow \hat{\omega}'_{G,k}(v_i), \hat{\omega}'_{S,k}(v_i)$$

$$\hat{\omega}'_k(v_i) = \begin{cases} \hat{\omega}'_{S,k}(v_i) & \text{for } 1 \leq i < p_k \\ \hat{\omega}'_{G,k}(v_i) & \text{for } p_k \leq i \leq N \end{cases} \quad (i = 1, \dots, N, k = X, Y, Z).$$

with $p_k \equiv N \cdot \Delta t \cdot v_{c,k}$ (keeping an integer value), $\Delta t = (t_{i+1} - t_i)$, $v_{c,k}$ = cut-off frequencies

$$v_{c,X} = 1 \text{ mHz}, v_{c,Y} = 0.2 \text{ mHz}, v_{c,Z} = 0.5 \text{ mHz (TBC)}.$$

5) Computation of the angular rates ($\hat{\omega}_X, \hat{\omega}_Y, \hat{\omega}_Z$) by inverse Fourier transform and re-trending:

$$\hat{\omega}'_k(v_i) \rightarrow \text{inverse Fourier transform} \rightarrow \hat{\omega}'_k(t_i) \rightarrow \hat{\omega}_k(t_i) = \hat{\omega}'_k(t_i) + \text{TR}_{S,ik} \text{ (re-trending)}$$

5.1.2.4.3 Iterative Loop Step (c): Combination of Angular Rates and Differential Accelerations

From the transversal differential accelerations ($\hat{a}_{d,14,Y}, \hat{a}_{d,14,Z}, \hat{a}_{d,25,X}, \hat{a}_{d,25,Z}, \hat{a}_{d,36,X}, \hat{a}_{d,36,Y}$) and from the estimated angular rates ($\hat{\omega}_X, \hat{\omega}_Y, \hat{\omega}_Z$) build up the quantities

$$\begin{aligned} y_1 &= -\frac{L_X}{2}(\hat{\omega}_Y^2 + \hat{\omega}_Z^2), \quad y_2 = L_X \hat{\omega}_X \hat{\omega}_Y - \frac{L_X}{L_Y} \hat{a}_{d,25,X}, \quad y_3 = L_X \hat{\omega}_X \hat{\omega}_Z - \frac{L_X}{L_Z} \hat{a}_{d,36,X}, \\ y_4 &= L_Y \hat{\omega}_X \hat{\omega}_Y - \frac{L_Y}{L_X} \hat{a}_{d,14,Y}, \quad y_5 = -\frac{L_Y}{2}(\hat{\omega}_X^2 + \hat{\omega}_Z^2), \quad y_6 = L_Y \hat{\omega}_Y \hat{\omega}_Z - \frac{L_Y}{L_Z} \hat{a}_{d,36,Y}, \\ y_7 &= L_Z \hat{\omega}_X \hat{\omega}_Z - \frac{L_Z}{L_X} \hat{a}_{d,14,Z}, \quad y_8 = L_Z \hat{\omega}_Y \hat{\omega}_Z - \frac{L_Z}{L_Y} \hat{a}_{d,25,Z}, \quad y_9 = -\frac{L_Z}{2}(\hat{\omega}_X^2 + \hat{\omega}_Y^2), \end{aligned}$$

and pass through a band-pass filter in the frequency domain for removing the harmonic components outside the [50 ÷ 100 mHz] bandwidth:

$$\hat{y}_1(t_n) = \sum_{k=-N_b}^{-N_b} b_k \cdot y_1(t_{n-k}), \dots, \hat{y}_9(t_n) = \sum_{k=-N_b}^{-N_b} b_k \cdot y_9(t_{n-k})$$

$$y_1, y_2, y_3, y_4, y_5, y_6, y_7, y_8, y_9 \text{ (unfiltered)} \Rightarrow \hat{y}_1, \hat{y}_2, \hat{y}_3, \hat{y}_4, \hat{y}_5, \hat{y}_6, \hat{y}_7, \hat{y}_8, \hat{y}_9 \text{ (filtered)}$$

where b is a vector of $2N_b + 1$ elements containing the parameters of the band-pass filter.

5.1.2.4.4 Iterative Loop Step (d): Set up of the Nine Sets of Linear Equations

Use the \mathbf{A} matrices prepared in the pre-processing and the filtered y-quantities ($\hat{y}_1, \hat{y}_2, \hat{y}_3, \hat{y}_4, \hat{y}_5, \hat{y}_6$) to set up the nine sets of linear equations:

$$\begin{aligned} \mathbf{A1} \cdot \delta \mathbf{x1} &= \mathbf{y1} - \mathbf{A1} \cdot \mathbf{x1}_{(n)} \\ \mathbf{A2} \cdot \delta \mathbf{x2} &= \mathbf{y2} - \mathbf{A2} \cdot \mathbf{x2}_{(n)} \\ &\dots\dots\dots \\ \mathbf{A9} \cdot \delta \mathbf{x9} &= \mathbf{y9} - \mathbf{A9} \cdot \mathbf{x9}_{(n)} \end{aligned}$$

with

$$\mathbf{y1} = \begin{pmatrix} \hat{y}_{1,1} \\ \hat{y}_{1,2} \\ \vdots \\ \hat{y}_{1,N} \end{pmatrix}, \mathbf{y2} = \begin{pmatrix} \hat{y}_{2,1} \\ \hat{y}_{2,2} \\ \vdots \\ \hat{y}_{2,N} \end{pmatrix}, \dots, \mathbf{y9} = \begin{pmatrix} \hat{y}_{9,1} \\ \hat{y}_{9,2} \\ \vdots \\ \hat{y}_{9,N} \end{pmatrix} \quad (\hat{y}_{1,1} = \hat{y}_1 \text{ measured at } t = t_1 \text{ etc..})$$

$$\begin{aligned}
 \mathbf{x1}_{(n)} &= \begin{pmatrix} MI_{14,41,(n)} \\ MI_{14,42,(n)} \\ MI_{14,43,(n)} \\ MI_{14,44,(n)} \\ MI_{14,45,(n)} \\ MI_{14,46,(n)} \end{pmatrix}, \mathbf{x2}_{(n)} = \begin{pmatrix} MI_{14,51,(n)} \\ MI_{14,52,(n)} \\ MI_{14,53,(n)} \\ MI_{14,54,(n)} \\ MI_{14,55,(n)} \\ MI_{14,56,(n)} \end{pmatrix}, \mathbf{x3}_{(n)} = \begin{pmatrix} MI_{14,61,(n)} \\ MI_{14,62,(n)} \\ MI_{14,63,(n)} \\ MI_{14,64,(n)} \\ MI_{14,65,(n)} \\ MI_{14,66,(n)} \end{pmatrix}, \mathbf{x4}_{(n)} = \begin{pmatrix} MI_{25,41,(n)} \\ MI_{25,42,(n)} \\ MI_{25,43,(n)} \\ MI_{25,44,(n)} \\ MI_{25,45,(n)} \\ MI_{25,46,(n)} \end{pmatrix}, \mathbf{x5}_{(n)} = \begin{pmatrix} MI_{25,51,(n)} \\ MI_{25,52,(n)} \\ MI_{25,53,(n)} \\ MI_{25,54,(n)} \\ MI_{25,55,(n)} \\ MI_{25,56,(n)} \end{pmatrix}, \\
 \mathbf{x6}_{(n)} &= \begin{pmatrix} MI_{25,61,(n)} \\ MI_{25,62,(n)} \\ MI_{25,63,(n)} \\ MI_{25,64,(n)} \\ MI_{25,65,(n)} \\ MI_{25,66,(n)} \end{pmatrix}, \mathbf{x7}_{(n)} = \begin{pmatrix} MI_{36,41,(n)} \\ MI_{36,42,(n)} \\ MI_{36,43,(n)} \\ MI_{36,44,(n)} \\ MI_{36,45,(n)} \\ MI_{36,46,(n)} \end{pmatrix}, \mathbf{x8}_{(n)} = \begin{pmatrix} MI_{36,51,(n)} \\ MI_{36,52,(n)} \\ MI_{36,53,(n)} \\ MI_{36,54,(n)} \\ MI_{36,55,(n)} \\ MI_{36,56,(n)} \end{pmatrix}, \mathbf{x9}_{(n)} = \begin{pmatrix} MI_{36,61,(n)} \\ MI_{36,62,(n)} \\ MI_{36,63,(n)} \\ MI_{36,64,(n)} \\ MI_{36,65,(n)} \\ MI_{36,66,(n)} \end{pmatrix}
 \end{aligned}$$

(elements of the ICMs resulting from the previous iteration; for $n = 1$ use the the initial values of the ICM elements given in section 5.1.2.3).

$$\begin{aligned}
 \delta \mathbf{x1} &= \begin{pmatrix} \delta MI_{14,41} \\ \delta MI_{14,42} \\ \delta MI_{14,43} \\ \delta MI'_{14,44} \\ \delta MI_{14,45} \\ \delta MI_{14,46} \end{pmatrix}, \delta \mathbf{x2} = \begin{pmatrix} \delta MI_{14,51} \\ \delta MI_{14,52} \\ \delta MI_{14,53} \\ \delta MI_{14,54} \\ \delta MI'_{14,55} \\ \delta MI_{14,56} \end{pmatrix}, \delta \mathbf{x3} = \begin{pmatrix} \delta MI_{14,61} \\ \delta MI_{14,62} \\ \delta MI_{14,63} \\ \delta MI_{14,64} \\ \delta MI_{14,65} \\ \delta MI'_{14,66} \end{pmatrix}, \delta \mathbf{x4} = \begin{pmatrix} \delta MI_{25,41} \\ \delta MI_{25,42} \\ \delta MI_{25,43} \\ \delta MI'_{25,44} \\ \delta MI_{25,45} \\ \delta MI_{25,46} \end{pmatrix}, \delta \mathbf{x5} = \begin{pmatrix} \delta MI_{25,51} \\ \delta MI_{25,52} \\ \delta MI_{25,53} \\ \delta MI_{25,54} \\ \delta MI'_{25,55} \\ \delta MI_{25,56} \end{pmatrix}, \\
 \delta \mathbf{x6} &= \begin{pmatrix} \delta MI_{25,61} \\ \delta MI_{25,62} \\ \delta MI_{25,63} \\ \delta MI_{25,64} \\ \delta MI_{25,65} \\ \delta MI'_{25,66} \end{pmatrix}, \delta \mathbf{x7} = \begin{pmatrix} \delta MI_{36,41} \\ \delta MI_{36,42} \\ \delta MI_{36,43} \\ \delta MI'_{36,44} \\ \delta MI_{36,45} \\ \delta MI_{36,46} \end{pmatrix}, \delta \mathbf{x8} = \begin{pmatrix} \delta MI_{36,51} \\ \delta MI_{36,52} \\ \delta MI_{36,53} \\ \delta MI_{36,54} \\ \delta MI'_{36,55} \\ \delta MI_{36,56} \end{pmatrix}, \delta \mathbf{x9} = \begin{pmatrix} \delta MI_{36,61} \\ \delta MI_{36,62} \\ \delta MI_{36,63} \\ \delta MI_{36,64} \\ \delta MI_{36,65} \\ \delta MI'_{36,66} \end{pmatrix}
 \end{aligned}$$

(corrections to be applied to the elements of the ICMs resulting from the previous iteration).

5.1.2.4.5 Iterative Loop Step (e): Computation of the Least-Squares Solutions

Compute the least-squares solutions of the nine sets of linear equations, providing the corrections to be applied to the elements of the IMCs resulting from the previous iteration:

$$\delta \mathbf{x1} = \begin{pmatrix} \delta MI_{14,41} \\ \delta MI_{14,42} \\ \delta MI_{14,43} \\ \delta MI'_{14,44} \\ \delta MI_{14,45} \\ \delta MI_{14,46} \end{pmatrix} = \mathbf{A1}^+ \cdot (\mathbf{y1} - \mathbf{A1} \cdot \mathbf{x1}_{(n)}), \dots, \delta \mathbf{x9} = \begin{pmatrix} \delta MI_{36,61} \\ \delta MI_{36,62} \\ \delta MI_{36,63} \\ \delta MI_{36,64} \\ \delta MI_{36,65} \\ \delta MI'_{36,66} \end{pmatrix} = \mathbf{A9}^+ \cdot (\mathbf{y9} - \mathbf{A9} \cdot \mathbf{x9}_{(n)})$$

where $\mathbf{A1}^+$ denotes the pseudo-inverse of the matrix $\mathbf{A1}$, etc..

5.1.2.4.6 Iterative Loop Step (f): Update and Correct the Values of the ICMs

Use the least-squares solutions of the nine sets of linear equations to compute updated values for the elements of the last three rows of the inverse Calibration Matrices MI_{14} , MI_{25} , MI_{36} ($[MI]_{d,ij}$, $[MI]_{c,ij}$, $ij=14, 25, 36$).

Before proceeding with the update, all the corrections ($\delta MI'_{14,44}$, $\delta MI'_{14,55}$, $\delta MI'_{14,66}$, $\delta MI'_{25,44}$, $\delta MI'_{25,55}$, $\delta MI'_{25,66}$, $\delta MI'_{36,44}$, $\delta MI'_{36,55}$, $\delta MI'_{36,66}$) to the elements $MI_{14,44}$, $MI_{14,55}$, $MI_{14,66}$, $MI_{25,44}$, $MI_{25,55}$, $MI_{25,66}$, $MI_{36,44}$, $MI_{36,55}$, $MI_{36,66}$ computed by the least-squares fit shall be set to zero:

$$\delta \mathbf{x1} = \begin{pmatrix} \delta MI_{14,41} \\ \delta MI_{14,42} \\ \delta MI_{14,43} \\ \delta MI'_{14,44} \\ \delta MI_{14,45} \\ \delta MI_{14,46} \end{pmatrix} \rightarrow \begin{pmatrix} \delta MI_{14,41} \\ \delta MI_{14,42} \\ \delta MI_{14,43} \\ 0 \\ \delta MI_{14,45} \\ \delta MI_{14,46} \end{pmatrix}, \dots, \delta \mathbf{x9} = \begin{pmatrix} \delta MI_{36,61} \\ \delta MI_{36,62} \\ \delta MI_{36,63} \\ \delta MI_{36,64} \\ \delta MI_{36,65} \\ \delta MI'_{36,66} \end{pmatrix} \rightarrow \begin{pmatrix} \delta MI_{36,61} \\ \delta MI_{36,62} \\ \delta MI_{36,63} \\ \delta MI_{36,64} \\ \delta MI_{36,65} \\ 0 \end{pmatrix}$$

With the vectors $\delta \mathbf{x1}, \dots, \delta \mathbf{x9}$ so modified update the values of the ICM elements:

$$\mathbf{x1}_{(n+1)} = \begin{pmatrix} MI_{14,41,(n+1)} \\ MI_{14,42,(n+1)} \\ MI_{14,43,(n+1)} \\ MI_{14,44,(n+1)} \\ MI_{14,45,(n+1)} \\ MI_{14,46,(n+1)} \end{pmatrix} = \mathbf{x1}_{(n)} + CS1 \cdot \delta \mathbf{x1}, \dots, \mathbf{x9}_{(n+1)} = \begin{pmatrix} MI_{36,61,(n+1)} \\ MI_{36,62,(n+1)} \\ MI_{36,63,(n+1)} \\ MI_{36,64,(n+1)} \\ MI_{36,65,(n+1)} \\ MI_{36,66,(n+1)} \end{pmatrix} = \mathbf{x9}_{(n)} + CS2 \cdot \delta \mathbf{x9}, \text{ with}$$

$$CS1 = \begin{pmatrix} CS_{14,41} & 0 & 0 & 0 & 0 & 0 \\ 0 & CS_{14,42} & 0 & 0 & 0 & 0 \\ 0 & 0 & CS_{14,43} & 0 & 0 & 0 \\ 0 & 0 & 0 & CS_{14,44} & 0 & 0 \\ 0 & 0 & 0 & 0 & CS_{14,45} & 0 \\ 0 & 0 & 0 & 0 & 0 & CS_{14,46} \end{pmatrix}, \dots, CS9 = \begin{pmatrix} CS_{36,61} & 0 & 0 & 0 & 0 & 0 \\ 0 & CS_{36,62} & 0 & 0 & 0 & 0 \\ 0 & 0 & CS_{36,63} & 0 & 0 & 0 \\ 0 & 0 & 0 & CS_{36,64} & 0 & 0 \\ 0 & 0 & 0 & 0 & CS_{36,65} & 0 \\ 0 & 0 & 0 & 0 & 0 & CS_{36,66} \end{pmatrix}$$

The "convergence speed" factors $CS_{ij,hk}$ are numbers ≤ 1 defining the fraction of the corrections applied at each iteration to the IMC elements. This allows to tune the rate of change of the elements in successive iterations and so the speed of the convergence. Low values of the CS factors increase the number of steps in which the convergence is achieved, but ensures a smoother approach to the stable solution, thus reducing the risks of "oscillations" from one iteration to another one. Adequate values for the $CS_{ij,hk}$ are (TBC):

Factor	Value	Factor	Value	Factor	Value
CS _{14,41}	0.67	CS _{14,51}	0.67	CS _{14,61}	0.67
CS _{14,42}	0.67	CS _{14,52}	0.67	CS _{14,62}	0.67
CS _{14,43}	0.67	CS _{14,53}	0.67	CS _{14,63}	0.67
CS _{14,44}	0.67	CS _{14,54}	0.67	CS _{14,64}	0.67
CS _{14,45}	0.67	CS _{14,55}	0.67	CS _{14,65}	0.67
CS _{14,46}	0.67	CS _{14,56}	0.67	CS _{14,66}	0.67
CS _{25,41}	0.67	CS _{25,51}	0.67	CS _{25,61}	0.67
CS _{25,42}	0.67	CS _{25,52}	0.67	CS _{25,62}	0.67
CS _{25,43}	0.67	CS _{25,53}	0.67	CS _{25,63}	0.67
CS _{25,44}	0.67	CS _{25,54}	0.67	CS _{25,64}	0.67
CS _{25,45}	0.67	CS _{25,55}	0.67	CS _{25,65}	0.67
CS _{25,46}	0.67	CS _{25,56}	0.67	CS _{25,66}	0.67
CS _{36,41}	0.67	CS _{36,51}	0.67	CS _{36,61}	0.67
CS _{36,42}	0.67	CS _{36,52}	0.67	CS _{36,62}	0.67
CS _{36,43}	0.67	CS _{36,53}	0.67	CS _{36,63}	0.67
CS _{36,44}	0.67	CS _{36,54}	0.67	CS _{36,64}	0.67
CS _{36,45}	0.67	CS _{36,55}	0.67	CS _{36,65}	0.67
CS _{36,46}	0.67	CS _{36,56}	0.67	CS _{36,66}	0.67

Before inserting the elements so obtained in the ICMs, apply the following correction scheme:

if $|MI_{14,51,(n+1)} + MI_{14,42,(n+1)}| > 5.2 \cdot 10^{-5}$ then $MI_{14,51,(n+1)} = -MI_{14,42,(n+1)} + 5.2 \cdot 10^{-5} \cdot \text{sign}(MI_{14,51,(n+1)} + MI_{14,42,(n+1)})$
if $|MI_{14,61,(n+1)} + MI_{14,43,(n+1)}| > 2.4 \cdot 10^{-5}$ then $MI_{14,61,(n+1)} = -MI_{14,43,(n+1)} + 2.4 \cdot 10^{-5} \cdot \text{sign}(MI_{14,61,(n+1)} + MI_{14,43,(n+1)})$
if $|MI_{14,54,(n+1)} + MI_{14,45,(n+1)}| > 5.2 \cdot 10^{-5}$ then $MI_{14,54,(n+1)} = -MI_{14,45,(n+1)} + 5.2 \cdot 10^{-5} \cdot \text{sign}(MI_{14,54,(n+1)} + MI_{14,45,(n+1)})$
if $|MI_{14,64,(n+1)} + MI_{14,46,(n+1)}| > 2.4 \cdot 10^{-5}$ then $MI_{14,64,(n+1)} = -MI_{14,46,(n+1)} + 2.4 \cdot 10^{-5} \cdot \text{sign}(MI_{14,64,(n+1)} + MI_{14,46,(n+1)})$
if $|MI_{14,53,(n+1)} + MI_{14,62,(n+1)}| > 5.2 \cdot 10^{-5}$ then $MI_{14,53,(n+1)} = -MI_{14,62,(n+1)} + 5.2 \cdot 10^{-5} \cdot \text{sign}(MI_{14,53,(n+1)} + MI_{14,62,(n+1)})$
if $|MI_{14,56,(n+1)} + MI_{14,65,(n+1)}| > 5.2 \cdot 10^{-5}$ then $MI_{14,56,(n+1)} = -MI_{14,65,(n+1)} + 5.2 \cdot 10^{-5} \cdot \text{sign}(MI_{14,56,(n+1)} + MI_{14,65,(n+1)})$
if $|MI_{25,61,(n+1)} + MI_{25,43,(n+1)}| > 5.2 \cdot 10^{-5}$ then $MI_{25,61,(n+1)} = -MI_{25,43,(n+1)} + 5.2 \cdot 10^{-5} \cdot \text{sign}(MI_{25,61,(n+1)} + MI_{25,43,(n+1)})$
if $|MI_{25,64,(n+1)} + MI_{25,46,(n+1)}| > 5.2 \cdot 10^{-5}$ then $MI_{25,64,(n+1)} = -MI_{25,46,(n+1)} + 5.2 \cdot 10^{-5} \cdot \text{sign}(MI_{25,64,(n+1)} + MI_{25,46,(n+1)})$
if $|MI_{25,42,(n+1)} + MI_{25,51,(n+1)}| > 2.4 \cdot 10^{-5}$ then $MI_{25,42,(n+1)} = -MI_{25,51,(n+1)} + 2.4 \cdot 10^{-5} \cdot \text{sign}(MI_{25,42,(n+1)} + MI_{25,51,(n+1)})$
if $|MI_{25,62,(n+1)} + MI_{25,53,(n+1)}| > 5.2 \cdot 10^{-5}$ then $MI_{25,62,(n+1)} = -MI_{25,53,(n+1)} + 5.2 \cdot 10^{-5} \cdot \text{sign}(MI_{25,62,(n+1)} + MI_{25,53,(n+1)})$
if $|MI_{25,45,(n+1)} + MI_{25,54,(n+1)}| > 2.4 \cdot 10^{-5}$ then $MI_{25,45,(n+1)} = -MI_{25,54,(n+1)} + 2.4 \cdot 10^{-5} \cdot \text{sign}(MI_{25,45,(n+1)} + MI_{25,54,(n+1)})$
if $|MI_{25,65,(n+1)} + MI_{25,56,(n+1)}| > 5.2 \cdot 10^{-5}$ then $MI_{25,65,(n+1)} = -MI_{25,56,(n+1)} + 5.2 \cdot 10^{-5} \cdot \text{sign}(MI_{25,65,(n+1)} + MI_{25,56,(n+1)})$
if $|MI_{36,51,(n+1)} + MI_{36,42,(n+1)}| > 5.2 \cdot 10^{-5}$ then $MI_{36,51,(n+1)} = -MI_{36,42,(n+1)} + 5.2 \cdot 10^{-5} \cdot \text{sign}(MI_{36,51,(n+1)} + MI_{36,42,(n+1)})$
if $|MI_{36,54,(n+1)} + MI_{36,45,(n+1)}| > 5.2 \cdot 10^{-5}$ then $MI_{36,54,(n+1)} = -MI_{36,45,(n+1)} + 5.2 \cdot 10^{-5} \cdot \text{sign}(MI_{36,54,(n+1)} + MI_{36,45,(n+1)})$
if $|MI_{36,43,(n+1)} + MI_{36,61,(n+1)}| > 2.4 \cdot 10^{-5}$ then $MI_{36,43,(n+1)} = -MI_{36,61,(n+1)} + 2.4 \cdot 10^{-5} \cdot \text{sign}(MI_{36,43,(n+1)} + MI_{36,61,(n+1)})$
if $|MI_{36,53,(n+1)} + MI_{36,62,(n+1)}| > 5.2 \cdot 10^{-5}$ then $MI_{36,53,(n+1)} = -MI_{36,62,(n+1)} + 5.2 \cdot 10^{-5} \cdot \text{sign}(MI_{36,53,(n+1)} + MI_{36,62,(n+1)})$
if $|MI_{36,46,(n+1)} + MI_{36,64,(n+1)}| > 2.4 \cdot 10^{-5}$ then $MI_{36,46,(n+1)} = -MI_{36,64,(n+1)} + 2.4 \cdot 10^{-5} \cdot \text{sign}(MI_{36,46,(n+1)} + MI_{36,64,(n+1)})$
if $|MI_{36,56,(n+1)} + MI_{36,65,(n+1)}| > 5.2 \cdot 10^{-5}$ then $MI_{36,56,(n+1)} = -MI_{36,65,(n+1)} + 5.2 \cdot 10^{-5} \cdot \text{sign}(MI_{36,56,(n+1)} + MI_{36,65,(n+1)})$

After this check/correction, the updated ICMs are built:

$$([MI]_{d,14} \quad [MI]_{c,14})_{(n+1)} = \begin{pmatrix} MI_{14,41,(n+1)} & MI_{14,42,(n+1)} & MI_{14,43,(n+1)} & MI_{14,44,(n+1)} & MI_{14,45,(n+1)} & MI_{14,46,(n+1)} \\ MI_{14,51,(n+1)} & MI_{14,52,(n+1)} & MI_{14,53,(n+1)} & MI_{14,54,(n+1)} & MI_{14,55,(n+1)} & MI_{14,56,(n+1)} \\ MI_{14,61,(n+1)} & MI_{14,62,(n+1)} & MI_{14,63,(n+1)} & MI_{14,64,(n+1)} & MI_{14,65,(n+1)} & MI_{14,66,(n+1)} \end{pmatrix}$$

$$\begin{aligned}
 \left(\begin{bmatrix} MI \end{bmatrix}_{d,25} \quad \begin{bmatrix} MI \end{bmatrix}_{c,25} \right)_{(n+1)} &= \begin{pmatrix} MI_{25,41,(n+1)} & MI_{25,42,(n+1)} & MI_{25,43,(n+1)} & MI_{25,44,(n+1)} & MI_{25,45,(n+1)} & MI_{25,46,(n+1)} \\ MI_{25,51,(n+1)} & MI_{25,52,(n+1)} & MI_{25,53,(n+1)} & MI_{25,54,(n+1)} & MI_{25,55,(n+1)} & MI_{25,56,(n+1)} \\ MI_{25,61,(n+1)} & MI_{25,62,(n+1)} & MI_{25,63,(n+1)} & MI_{25,64,(n+1)} & MI_{25,65,(n+1)} & MI_{25,66,(n+1)} \end{pmatrix} \\
 \left(\begin{bmatrix} MI \end{bmatrix}_{d,36} \quad \begin{bmatrix} MI \end{bmatrix}_{c,36} \right)_{(n+1)} &= \begin{pmatrix} MI_{36,41,(n+1)} & MI_{36,42,(n+1)} & MI_{36,43,(n+1)} & MI_{36,44,(n+1)} & MI_{36,45,(n+1)} & MI_{36,46,(n+1)} \\ MI_{36,51,(n+1)} & MI_{36,52,(n+1)} & MI_{36,53,(n+1)} & MI_{36,54,(n+1)} & MI_{36,55,(n+1)} & MI_{36,56,(n+1)} \\ MI_{36,61,(n+1)} & MI_{36,62,(n+1)} & MI_{36,63,(n+1)} & MI_{36,64,(n+1)} & MI_{36,65,(n+1)} & MI_{36,66,(n+1)} \end{pmatrix}
 \end{aligned}$$

5.1.2.4.7 Step 1 Convergence Criterion

The elements of the new matrices so obtained are checked against the convergence criterion.

If the difference (in absolute value) between consecutive estimates of an ICM element is smaller than 5% of its specified measurement accuracy provided in Table 3.3-7:

$$|MI_{ij,hk(n+1)} - MI_{ij,hk(n)}| < 0.05 \cdot \delta MI_{ij,hk} \quad \text{for any } ij = 14, 25, 36 ; h = 4, 5, 6 ; k = 1, 2, 3, 4, 5, 6$$

then the value of this element is kept constant in all the successive iterations: $MI_{ij,hk(n+1)} = MI_{ij,hk(n)}$, for any n .

This check does not apply to the elements $MI_{14,44}$, $MI_{14,55}$, $MI_{14,66}$, $MI_{25,44}$, $MI_{25,55}$, $MI_{25,66}$, $MI_{36,44}$, $MI_{36,55}$, $MI_{36,66}$, which in fact are not change from their initial unitary value from one iteration to the other.

The iterative process is stopped when all the ICMs elements fulfil the above condition. At this point $\left(\begin{bmatrix} MI \end{bmatrix}_{d,14} \quad \begin{bmatrix} MI \end{bmatrix}_{c,14} \right)_{(n+1)}$, $\left(\begin{bmatrix} MI \end{bmatrix}_{d,25} \quad \begin{bmatrix} MI \end{bmatrix}_{c,25} \right)_{(n+1)}$, $\left(\begin{bmatrix} MI \end{bmatrix}_{d,36} \quad \begin{bmatrix} MI \end{bmatrix}_{c,36} \right)_{(n+1)}$ provides the ICMs sought for.

Otherwise the updated ICMs $\left(\begin{bmatrix} MI \end{bmatrix}_{d,14} \quad \begin{bmatrix} MI \end{bmatrix}_{c,14} \right)_{(n+1)}$, $\left(\begin{bmatrix} MI \end{bmatrix}_{d,25} \quad \begin{bmatrix} MI \end{bmatrix}_{c,25} \right)_{(n+1)}$, $\left(\begin{bmatrix} MI \end{bmatrix}_{d,36} \quad \begin{bmatrix} MI \end{bmatrix}_{c,36} \right)_{(n+1)}$, are re-introduced in the loop and the steps a) to f) are repeated until the process converges.

In case the convergence criteria is not fulfilled after $n = n_{\max}$ ($= 100$, TBC) iterations, the process shall be stopped anyway. The maximum number of iteration (100) is defined on the basis the tests of the method performed so far, in which the convergence occurred in much less iterations (around 10), and most of the calibration parameters are retrieved in the first few iterations. It is therefore concluded that if the method does not reach the convergence after 100 iterations, very likely it will not converge at all (for instance it could happen that the value of some parameter “oscillates” between two limits), and it is not worth to continue the process. On the other hands, if the method is stopped after 100 iterations without convergence it does not necessarily mean that the quality of the parameters determined at that point is poor.

The result of the Calibration Step 1 are the last three rows of the ICMs, but the elements related to the common scale factors ($MI_{14,44}$, $MI_{14,55}$, $MI_{14,66}$, $MI_{25,44}$, $MI_{25,55}$, $MI_{25,66}$, $MI_{36,44}$, $MI_{36,55}$, $MI_{36,66}$) which maintain their initial unitary value:

$$\left(\begin{bmatrix} MI \end{bmatrix}_{d,14} \quad \begin{bmatrix} MI \end{bmatrix}_{c,14} \right)_{\text{Step 1}} = \begin{pmatrix} MI_{14,41} & MI_{14,42} & MI_{14,43} & 1 & MI_{14,45} & MI_{14,46} \\ MI_{14,51} & MI_{14,52} & MI_{14,53} & MI_{14,54} & 1 & MI_{14,56} \\ MI_{14,61} & MI_{14,62} & MI_{14,63} & MI_{14,64} & MI_{14,65} & 1 \end{pmatrix}$$

$$\begin{aligned}
 ([MI]_{d,25} [MI]_{c,25})_{\text{Step 1}} &= \begin{pmatrix} MI_{25,41} & MI_{25,42} & MI_{25,43} & 1 & MI_{25,45} & MI_{25,46} \\ MI_{25,51} & MI_{25,52} & MI_{25,53} & MI_{25,54} & 1 & MI_{25,56} \\ MI_{25,61} & MI_{25,62} & MI_{25,63} & MI_{25,64} & MI_{25,65} & 1 \end{pmatrix} \\
 ([MI]_{d,36} [MI]_{c,36})_{\text{Step 1}} &= \begin{pmatrix} MI_{36,41} & MI_{36,42} & MI_{36,43} & 1 & MI_{36,45} & MI_{36,46} \\ MI_{36,51} & MI_{36,52} & MI_{36,53} & MI_{36,54} & 1 & MI_{36,56} \\ MI_{36,61} & MI_{36,62} & MI_{36,63} & MI_{36,64} & MI_{36,65} & 1 \end{pmatrix}
 \end{aligned}$$

5.1.2.5 Calibration Step 2

Skip the first and last N_p (= 500 TBC) data points from the common-mode and differential-mode accelerations ($\underline{a}'_{c,14}$, $\underline{a}'_{d,14}$, $\underline{a}'_{c,25}$, $\underline{a}'_{d,25}$, $\underline{a}'_{c,36}$, $\underline{a}'_{d,36}$) measured over the calibration period (not filtered).

From these accelerations, and from the inverse Calibration Matrices ($[MI]_{d,ij}$, $[MI]_{c,ij}$ $ij=14, 25, 36$) available as a result of the Step 1 (or of the Step 3), build up the following quantities:

$$\Delta a_{d,14,Y} = MI_{14,51} a'_{c,14,X} + MI_{14,52} a'_{c,14,Y} + MI_{14,53} a'_{c,14,Z} + MI_{14,54} a'_{d,14,X} + MI_{14,56} a'_{d,14,Z}$$

$$\Delta a_{d,14,Z} = MI_{14,61} a'_{c,14,X} + MI_{14,62} a'_{c,14,Y} + MI_{14,63} a'_{c,14,Z} + MI_{14,64} a'_{d,14,X} + MI_{14,65} a'_{d,14,Y}$$

$$\Delta a_{d,25,X} = MI_{25,41} a'_{c,25,X} + MI_{25,42} a'_{c,25,Y} + MI_{25,43} a'_{c,25,Z} + MI_{25,45} a'_{d,25,Y} + MI_{25,46} a'_{d,25,Z}$$

$$\Delta a_{d,25,Z} = MI_{25,61} a'_{c,25,X} + MI_{25,62} a'_{c,25,Y} + MI_{25,63} a'_{c,25,Z} + MI_{25,64} a'_{d,25,X} + MI_{25,65} a'_{d,25,Y}$$

$$\Delta a_{d,36,X} = MI_{36,41} a'_{c,36,X} + MI_{36,42} a'_{c,36,Y} + MI_{36,43} a'_{c,36,Z} + MI_{36,45} a'_{d,36,Y} + MI_{36,46} a'_{d,36,Z}$$

$$\Delta a_{d,36,Y} = MI_{36,51} a'_{c,36,X} + MI_{36,52} a'_{c,36,Y} + MI_{36,53} a'_{c,36,Z} + MI_{36,54} a'_{d,36,X} + MI_{36,56} a'_{d,36,Z}$$

Then pass these quantities and the measured differential-mode accelerations ($a'_{d,14,Y}$, $a'_{d,14,Z}$, $a'_{d,25,X}$, $a'_{d,25,Z}$, $a'_{d,36,X}$, $a'_{d,36,Y}$) through a band-pass filter in the time domain for removing the frequency components outside a $[v_{\min} \div v_{\max}]$ bandwidth:

$$\Delta \hat{a}_{d,36,Y}(t_n) = \sum_{k=+N_h}^{-N_h} h_k^X \cdot \Delta a_{d,36,Y}(t_{n-k}), \quad \Delta \hat{a}_{d,25,Z}(t_n) = \sum_{k=+N_h}^{-N_h} h_k^X \cdot \Delta a_{d,25,Z}(t_{n-k})$$

$$\hat{a}'_{d,36,Y}(t_n) = \sum_{k=+N_h}^{-N_h} h_k^X \cdot a'_{d,36,Y}(t_{n-k}), \quad \hat{a}'_{d,25,Z}(t_n) = \sum_{k=+N_h}^{-N_h} h_k^X \cdot a'_{d,25,Z}(t_{n-k}),$$

$$\Delta \hat{a}_{d,14,Z}(t_n) = \sum_{k=+N_h}^{-N_h} h_k^Y \cdot \Delta a_{d,14,Z}(t_{n-k}), \quad \Delta \hat{a}_{d,36,X}(t_n) = \sum_{k=+N_h}^{-N_h} h_k^Y \cdot \Delta a_{d,36,X}(t_{n-k})$$

$$\hat{a}'_{d,14,Z}(t_n) = \sum_{k=+N_h}^{-N_h} h_k^Y \cdot a'_{d,14,Z}(t_{n-k}), \quad \hat{a}'_{d,36,X}(t_n) = \sum_{k=+N_h}^{-N_h} h_k^Y \cdot a'_{d,36,X}(t_{n-k})$$

$$\Delta \hat{a}_{d,25,X}(t_n) = \sum_{k=+N_h}^{-N_h} h_k^Z \cdot \Delta a_{d,25,X}(t_{n-k}), \quad \Delta \hat{a}_{d,14,Y}(t_n) = \sum_{k=+N_h}^{-N_h} h_k^Z \cdot \Delta a_{d,14,Y}(t_{n-k})$$

$$\hat{a}'_{d,25,X}(t_n) = \sum_{k=+N_h}^{-N_h} h_k^Z \cdot a'_{d,25,X}(t_{n-k}), \quad \hat{a}'_{d,14,Y}(t_n) = \sum_{k=+N_h}^{-N_h} h_k^Z \cdot a'_{d,14,Y}(t_{n-k})$$

where h^X , h^Y , h^Z are vectors of $2N_h + 1$ elements containing the parameters of the band-pass filters.

Use the above filtered quantities and the star sensor derived angular accelerations (also filtered during the inputs pre-processing), to set up the three sets of linear equations:

$$\begin{aligned} \mathbf{A1}' \cdot \delta \mathbf{x1}' &= \mathbf{y1}' - \mathbf{A1}' \cdot \mathbf{x1}' \\ \mathbf{A2}' \cdot \delta \mathbf{x2}' &= \mathbf{y2}' - \mathbf{A2}' \cdot \mathbf{x2}' \\ \mathbf{A3}' \cdot \delta \mathbf{x3}' &= \mathbf{y3}' - \mathbf{A3}' \cdot \mathbf{x3}' \end{aligned}$$

with

$$\mathbf{A1}' = \begin{pmatrix} -\frac{1}{L_Z} \hat{a}'_{d,36,Y,1} & \frac{1}{L_Y} \hat{a}'_{d,25,Z,1} \\ -\frac{1}{L_Z} \hat{a}'_{d,36,Y,2} & \frac{1}{L_Y} \hat{a}'_{d,25,Z,2} \\ \vdots & \vdots \\ -\frac{1}{L_Z} \hat{a}'_{d,36,Y,N} & \frac{1}{L_Y} \hat{a}'_{d,25,Z,N} \end{pmatrix}, \mathbf{y1}' = \begin{pmatrix} \hat{\omega}_{S,X,1} + \frac{1}{L_Z} \Delta \hat{a}_{d,36,Y,1} - \frac{1}{L_Y} \Delta \hat{a}_{d,25,Z,1} \\ \hat{\omega}_{S,X,2} + \frac{1}{L_Z} \Delta \hat{a}_{d,36,Y,2} - \frac{1}{L_Y} \Delta \hat{a}_{d,25,Z,2} \\ \vdots \\ \hat{\omega}_{S,X,N} + \frac{1}{L_Z} \Delta \hat{a}_{d,36,Y,N} - \frac{1}{L_Y} \Delta \hat{a}_{d,25,Z,N} \end{pmatrix}, \delta \mathbf{x1}' = \begin{pmatrix} \delta MI_{36,55} \\ \delta MI_{25,66} \end{pmatrix}$$

$$\mathbf{A2}' = \begin{pmatrix} -\frac{1}{L_X} \hat{a}'_{d,14,Z,1} & \frac{1}{L_Z} \hat{a}'_{d,36,X,1} \\ -\frac{1}{L_X} \hat{a}'_{d,14,Z,2} & \frac{1}{L_Z} \hat{a}'_{d,36,X,2} \\ \vdots & \vdots \\ -\frac{1}{L_X} \hat{a}'_{d,14,Z,N} & \frac{1}{L_Z} \hat{a}'_{d,36,X,N} \end{pmatrix}, \mathbf{y2}' = \begin{pmatrix} \hat{\omega}_{S,Y,1} + \frac{1}{L_X} \Delta \hat{a}_{d,14,Z,1} - \frac{1}{L_Z} \Delta \hat{a}_{d,36,X,1} \\ \hat{\omega}_{S,Y,2} + \frac{1}{L_X} \Delta \hat{a}_{d,14,Z,2} - \frac{1}{L_Z} \Delta \hat{a}_{d,36,X,2} \\ \vdots \\ \hat{\omega}_{S,Y,N} + \frac{1}{L_X} \Delta \hat{a}_{d,14,Z,N} - \frac{1}{L_Z} \Delta \hat{a}_{d,36,X,N} \end{pmatrix}; \delta \mathbf{x2}' = \begin{pmatrix} \delta MI_{14,66} \\ \delta MI_{36,44} \end{pmatrix}$$

$$\mathbf{A3}' = \begin{pmatrix} -\frac{1}{L_Y} \hat{a}'_{d,25,X,1} & \frac{1}{L_X} \hat{a}'_{d,14,Y,1} \\ -\frac{1}{L_Y} \hat{a}'_{d,25,X,2} & \frac{1}{L_X} \hat{a}'_{d,14,Y,2} \\ \vdots & \vdots \\ -\frac{1}{L_Y} \hat{a}'_{d,25,X,N} & \frac{1}{L_X} \hat{a}'_{d,14,Y,N} \end{pmatrix}, \mathbf{y3}' = \begin{pmatrix} \hat{\omega}_{S,Z,1} + \frac{1}{L_Y} \Delta \hat{a}_{d,25,X,1} - \frac{1}{L_X} \Delta \hat{a}_{d,14,Y,1} \\ \hat{\omega}_{S,Z,2} + \frac{1}{L_Y} \Delta \hat{a}_{d,25,X,2} - \frac{1}{L_X} \Delta \hat{a}_{d,14,Y,2} \\ \vdots \\ \hat{\omega}_{S,Z,N} + \frac{1}{L_Y} \Delta \hat{a}_{d,25,X,N} - \frac{1}{L_X} \Delta \hat{a}_{d,14,Y,N} \end{pmatrix}; \delta \mathbf{x3}' = \begin{pmatrix} \delta MI_{25,44} \\ \delta MI_{14,55} \end{pmatrix}$$

$$\mathbf{x1}' = \mathbf{x2}' = \mathbf{x3}' = \begin{pmatrix} 1 \\ 1 \end{pmatrix}$$

($\Delta \hat{a}_{d,36,Y,1} = \Delta \hat{a}_{d,36,Y}$ measured at $t = t_1$ etc..).

Finally, compute the ICM elements related to the transversal common scale factors of the three accelerometer pairs ($MI_{14,55}$, $MI_{14,66}$, $MI_{25,44}$, $MI_{25,66}$, $MI_{36,44}$, $MI_{36,55}$) as the least-squares solutions of the three sets of linear equations:

$$\begin{aligned} \delta \mathbf{x1}' &= \begin{pmatrix} \delta MI_{36,55} \\ \delta MI_{25,66} \end{pmatrix} = \mathbf{A1}'^+ \cdot (\mathbf{y1}' - \mathbf{A1}' \cdot \mathbf{x1}') \Rightarrow \begin{pmatrix} MI_{36,55} \\ MI_{25,66} \end{pmatrix} = \begin{pmatrix} 1 + \delta MI_{36,55} \\ 1 + \delta MI_{25,66} \end{pmatrix} \\ \delta \mathbf{x2}' &= \begin{pmatrix} \delta MI_{14,66} \\ \delta MI_{36,44} \end{pmatrix} = \mathbf{A2}'^+ \cdot (\mathbf{y2}' - \mathbf{A2}' \cdot \mathbf{x2}') \Rightarrow \begin{pmatrix} MI_{14,66} \\ MI_{36,44} \end{pmatrix} = \begin{pmatrix} 1 + \delta MI_{14,66} \\ 1 + \delta MI_{36,44} \end{pmatrix} \end{aligned}$$

$$\delta \mathbf{x}_3' = \begin{pmatrix} \delta MI_{25,44} \\ \delta MI_{14,55} \end{pmatrix} = \mathbf{A}_3'^+ \cdot (\mathbf{y}_3' - \mathbf{A}_3' \cdot \mathbf{x}_3') \Rightarrow \begin{pmatrix} MI_{25,44} \\ MI_{14,55} \end{pmatrix} = \begin{pmatrix} 1 + \delta MI_{25,44} \\ 1 + \delta MI_{14,55} \end{pmatrix}$$

where $\mathbf{A}_1'^+$ denotes the pseudo-inverse of the matrix \mathbf{A}_1' , etc..

After the Calibration Step 1 and the first Calibration Step 2 the elements of the last three rows of the ICMs are determined, but those related to the in-line common scale factors ($MI_{14,44}$, $MI_{25,55}$, $MI_{36,66}$) which maintain their initial unitary value:

$$\begin{aligned} \left(\begin{bmatrix} MI \end{bmatrix}_{d,14} \begin{bmatrix} MI \end{bmatrix}_{c,14} \right)_{\text{Step 1, Step 2}} &= \begin{pmatrix} MI_{14,41} & MI_{14,42} & MI_{14,43} & 1 & MI_{14,45} & MI_{14,46} \\ MI_{14,51} & MI_{14,52} & MI_{14,53} & MI_{14,54} & MI_{14,55} & MI_{14,56} \\ MI_{14,61} & MI_{14,62} & MI_{14,63} & MI_{14,64} & MI_{14,65} & MI_{14,66} \end{pmatrix} \\ \left(\begin{bmatrix} MI \end{bmatrix}_{d,25} \begin{bmatrix} MI \end{bmatrix}_{c,25} \right)_{\text{Step 1, Step 2}} &= \begin{pmatrix} MI_{25,41} & MI_{25,42} & MI_{25,43} & MI_{25,44} & MI_{25,45} & MI_{25,46} \\ MI_{25,51} & MI_{25,52} & MI_{25,53} & MI_{25,54} & 1 & MI_{25,56} \\ MI_{25,61} & MI_{25,62} & MI_{25,63} & MI_{25,64} & MI_{25,65} & MI_{25,66} \end{pmatrix} \\ \left(\begin{bmatrix} MI \end{bmatrix}_{d,36} \begin{bmatrix} MI \end{bmatrix}_{c,36} \right)_{\text{Step 1, Step 2}} &= \begin{pmatrix} MI_{36,41} & MI_{36,42} & MI_{36,43} & MI_{36,44} & MI_{36,45} & MI_{36,46} \\ MI_{36,51} & MI_{36,52} & MI_{36,53} & MI_{36,54} & MI_{36,55} & MI_{36,56} \\ MI_{36,61} & MI_{36,62} & MI_{36,63} & MI_{36,64} & MI_{36,65} & 1 \end{pmatrix} \end{aligned}$$

5.1.2.6 Calibration Step 3

Iterative loop step (a)

Implemented in the same way of step (a) of the Calibration Step 1. At the first iteration ($n = 1$), the values of the ICM elements resulting from the previous Step 1 and Step 2 shall be used (i.e. the elements $MI_{14,44}$, $MI_{25,55}$, $MI_{36,66}$ are still equal to 1 at the beginning of the first iteration, but after the first Step 2 only).

Iterative loop step (b)

Implemented in the same way of step (b) of the Calibration Step 1.

Iterative loop step (c)

Implemented in the same way of step (c) of the Calibration Step 1.

Iterative loop step (d)

Implemented in the same way of step (d) of the Calibration Step 1. At the first iteration ($n = 1$), the values of the ICM elements resulting from the previous Step 1 and Step 2 shall be used.

Iterative loop step (e)

Implemented in the same way of step (e) of the Calibration Step 1.

Iterative loop step (f)

The implementation of this step is modified as follows.

Use the ICMs elements $MI_{14,66}$, $MI_{25,44}$, $MI_{36,55}$ determined from Step 2 and the elements $MI_{14,66,(n)}$, $MI_{25,44,(n)}$, $MI_{36,66,(n)}$, determined at the iteration n of the Step 3 to compute the quantities:

$$\begin{aligned}\delta MI_{14,66} &= MI_{14,66} - MI_{14,66,(n)} \\ \delta MI_{25,44} &= MI_{25,44} - MI_{25,44,(n)} \\ \delta MI_{36,55} &= MI_{36,55} - MI_{36,55,(n)}\end{aligned}$$

In practice at the first iteration $MI_{14,66,(1)} = MI_{25,44,(1)} = MI_{36,55,(1)} = 1$, and $\delta MI_{14,66}$, $\delta MI_{25,44}$, $\delta MI_{36,55}$ are zero.

Compute the corrections to the elements $MI_{14,44}$, $MI_{14,55}$, $MI_{25,55}$, $MI_{25,66}$, $MI_{36,44}$, $MI_{36,66}$ from the results ($\delta MI'_{14,44}$, $\delta MI'_{14,55}$, $\delta MI'_{14,66}$, $\delta MI'_{25,44}$, $\delta MI'_{25,55}$, $\delta MI'_{25,66}$, $\delta MI'_{36,44}$, $\delta MI'_{36,55}$, $\delta MI'_{36,66}$) of the least-squares solutions of the step (e) and from $\delta MI_{14,66}$, $\delta MI_{25,44}$, $\delta MI_{36,55}$ using the following relationships:

$$\begin{aligned}\delta MI_{14,44} &= \delta MI_{14,66} - \frac{1}{4} \delta MI'_{14,66} + \frac{1}{4} \delta MI'_{36,44} + \delta MI'_{14,44} \\ \delta MI_{14,55} &= \delta MI_{25,44} - \delta MI'_{25,44} \\ \delta MI_{25,55} &= \delta MI_{36,55} + \frac{1}{4} \delta MI'_{25,66} - \frac{1}{4} \delta MI'_{36,55} + \delta MI'_{25,55} \\ \delta MI_{25,66} &= \delta MI_{36,55} + \frac{1}{2} \delta MI'_{25,66} - \frac{1}{2} \delta MI'_{36,55} \\ \delta MI_{36,44} &= \delta MI_{14,66} - \frac{1}{2} \delta MI'_{14,66} + \frac{1}{2} \delta MI'_{36,44} \\ \delta MI_{36,66} &= \frac{6}{7} \delta MI_{14,66} + \frac{1}{7} \delta MI_{36,55} + \frac{1}{28} \delta MI'_{25,66} - \frac{1}{28} \delta MI'_{36,55} - \frac{3}{14} \delta MI'_{14,66} + \frac{3}{14} \delta MI'_{36,44} + \delta MI'_{36,66}\end{aligned}$$

Introduce these corrections in the least-squares solutions of the nine sets of linear equations computed at step (e):

$$\delta \mathbf{x1} = \begin{pmatrix} \delta MI_{14,41} \\ \delta MI_{14,42} \\ \delta MI_{14,43} \\ \delta MI'_{14,44} \\ \delta MI_{14,45} \\ \delta MI_{14,46} \end{pmatrix} \rightarrow \begin{pmatrix} \delta MI_{14,41} \\ \delta MI_{14,42} \\ \delta MI_{14,43} \\ \delta MI_{14,44} \\ \delta MI_{14,45} \\ \delta MI_{14,46} \end{pmatrix}, \delta \mathbf{x2} = \begin{pmatrix} \delta MI_{14,51} \\ \delta MI_{14,52} \\ \delta MI_{14,53} \\ \delta MI_{14,54} \\ \delta MI'_{14,55} \\ \delta MI_{14,56} \end{pmatrix} \rightarrow \begin{pmatrix} \delta MI_{14,51} \\ \delta MI_{14,52} \\ \delta MI_{14,53} \\ \delta MI_{14,54} \\ \delta MI_{14,55} \\ \delta MI_{14,56} \end{pmatrix}, \dots, \delta \mathbf{x9} = \begin{pmatrix} \delta MI_{36,61} \\ \delta MI_{36,62} \\ \delta MI_{36,63} \\ \delta MI_{36,64} \\ \delta MI_{36,65} \\ \delta MI'_{36,66} \end{pmatrix} \rightarrow \begin{pmatrix} \delta MI_{36,61} \\ \delta MI_{36,62} \\ \delta MI_{36,63} \\ \delta MI_{36,64} \\ \delta MI_{36,65} \\ \delta MI_{36,66} \end{pmatrix}$$

With the vectors $\delta \mathbf{x1}, \dots, \delta \mathbf{x9}$ so modified update the values of the ICM elements:

$$\mathbf{x1}_{(n+1)} = \begin{pmatrix} MI_{14,41,(n+1)} \\ MI_{14,42,(n+1)} \\ MI_{14,43,(n+1)} \\ MI_{14,44,(n+1)} \\ MI_{14,45,(n+1)} \\ MI_{14,46,(n+1)} \end{pmatrix} = \mathbf{x1}_{(n)} + \mathbf{CS1} \cdot \delta \mathbf{x1}, \dots, \mathbf{x9}_{(n+1)} = \begin{pmatrix} MI_{36,61,(n+1)} \\ MI_{36,62,(n+1)} \\ MI_{36,63,(n+1)} \\ MI_{36,64,(n+1)} \\ MI_{36,65,(n+1)} \\ MI_{36,66,(n+1)} \end{pmatrix} = \mathbf{x9}_{(n)} + \mathbf{CS2} \cdot \delta \mathbf{x9},$$

The remaining part of the step (f) is unchanged w.r.t that defined for the Calibration Step 1 (section 5.1.2.4.6), including the definition of the "convergence speed" factors $CS_{ij,hk}$.

Convergence criterion

The convergence criterion is implemented in the same way of the Calibration Step 1, with the only difference that now the check apply to all the elements of the ICM (including $MI_{14,44}$, $MI_{14,55}$, $MI_{14,66}$, $MI_{25,44}$, $MI_{25,55}$, $MI_{25,66}$, $MI_{36,44}$, $MI_{36,55}$, $MI_{36,66}$).

After the Calibration Step 1, Step 2 and Step 3 all the elements of the last three rows of the ICMs are determined:

$$\begin{aligned} \left(\begin{bmatrix} MI \end{bmatrix}_{d,14} \begin{bmatrix} MI \end{bmatrix}_{c,14} \right)_{\text{Step 1, Step 2, Step 3}} &= \begin{pmatrix} MI_{14,41} & MI_{14,42} & MI_{14,43} & MI_{14,44} & MI_{14,45} & MI_{14,46} \\ MI_{14,51} & MI_{14,52} & MI_{14,53} & MI_{14,54} & MI_{14,55} & MI_{14,56} \\ MI_{14,61} & MI_{14,62} & MI_{14,63} & MI_{14,64} & MI_{14,65} & MI_{14,66} \end{pmatrix} \\ \left(\begin{bmatrix} MI \end{bmatrix}_{d,25} \begin{bmatrix} MI \end{bmatrix}_{c,25} \right)_{\text{Step 1, Step 2, Step 3}} &= \begin{pmatrix} MI_{25,41} & MI_{25,42} & MI_{25,43} & MI_{25,44} & MI_{25,45} & MI_{25,46} \\ MI_{25,51} & MI_{25,52} & MI_{25,53} & MI_{25,54} & MI_{25,55} & MI_{25,56} \\ MI_{25,61} & MI_{25,62} & MI_{25,63} & MI_{25,64} & MI_{25,65} & MI_{25,66} \end{pmatrix} \\ \left(\begin{bmatrix} MI \end{bmatrix}_{d,36} \begin{bmatrix} MI \end{bmatrix}_{c,36} \right)_{\text{Step 1, Step 2, Step 3}} &= \begin{pmatrix} MI_{36,41} & MI_{36,42} & MI_{36,43} & MI_{36,44} & MI_{36,45} & MI_{36,46} \\ MI_{36,51} & MI_{36,52} & MI_{36,53} & MI_{36,54} & MI_{36,55} & MI_{36,56} \\ MI_{36,61} & MI_{36,62} & MI_{36,63} & MI_{36,64} & MI_{36,65} & MI_{36,66} \end{pmatrix} \end{aligned}$$

5.1.2.7 Step2 - Step 3 Loop Exit Condition

At the completion of the Calibration Step 3, the Step 2 is repeated (with the ICMs values determined at Step 3) to update the determination of the transverse common scale factors. The results are utilised to feed a new Step 3, and so on.

The value of the ICM's determined in two successive Steps 3 are compared. If the difference (in absolute value) between consecutive estimates of an ICM element is smaller than 5% of the values provided in Table 3.3-7:

$$|MI_{ij,hk}(\text{Step } 3 \text{ } n+1) - MI_{ij,hk}(\text{Step } 3 \text{ } n)| < 0.05 \cdot \delta MI_{ij,hk} \quad \text{for any } ij = 14, 25, 36 ; h = 4, 5, 6 ; k = 1, 2, 3, 4, 5, 6$$

then the value of this element is kept constant in all the successive Step 2- Step 3 iterations. The iterative process is stopped when all the ICMs elements fulfil the above condition.

At the exit of the Step 2 - Step 3 loop, the following final checks and corrections are performed on the ICM elements $MI_{14,26}$, $MI_{14,35}$, $MI_{25,16}$, $MI_{25,34}$, $MI_{36,15}$, $MI_{36,24}$:

$$\begin{aligned} \text{if } |MI_{14,56}| > MI_{LIM,14,26} &\text{ then } MI_{14,26} = 0 \\ \text{if } |MI_{14,65}| > MI_{LIM,14,35} &\text{ then } MI_{14,35} = 0 \\ \text{if } |MI_{25,46}| > MI_{LIM,25,16} &\text{ then } MI_{25,16} = 0 \\ \text{if } |MI_{25,64}| > MI_{LIM,25,34} &\text{ then } MI_{25,34} = 0 \\ \text{if } |MI_{36,45}| > MI_{LIM,36,15} &\text{ then } MI_{36,15} = 0 \\ \text{if } |MI_{36,54}| > MI_{LIM,36,24} &\text{ then } MI_{36,24} = 0 \end{aligned}$$

where

$$MI_{LIM,14,26} = MI_{LIM,14,35} = MI_{LIM,25,16} = MI_{LIM,25,34} = MI_{LIM,36,15} = MI_{LIM,36,24} = 1.9 \cdot 10^{-5}$$

5.2 METHOD ANALYSIS

5.2.1 Systematic Errors

Systematic errors in the determination of the ICM elements with the method described before arises from the limited knowledge of the gradiometer baseline lengths L_X , L_Y , L_Z , which appear in the right hand side of the equations (5.1.3). In fact, the baseline lengths are not among the parameters estimated by the calibration method, and their value must be assumed known from the on-ground characterisation of the Gradiometer.

The relative error induced on the elements of the ICM by δL_X , δL_Y , δL_Z is about

$$\begin{aligned}\delta MI_{14,hk} &\cong \frac{\delta L_X}{L_X} MI_{14,hk} \quad (h = 4,5,6; k = 1, \dots, 6) \\ \delta MI_{25,hk} &\cong \frac{\delta L_Y}{L_Y} MI_{25,hk} \quad (h = 4,5,6; k = 1, \dots, 6) \\ \delta MI_{36,hk} &\cong \frac{\delta L_Z}{L_Z} MI_{36,hk} \quad (h = 4,5,6; k = 1, \dots, 6)\end{aligned}\quad (5.2.1)$$

Since we have $L_i \cong 0.5$ m and $\delta L_i \leq 50 \cdot 10^{-6}$ m, the relative error on the gradiometer baseline lengths (and thus on the elements of the ICMs) is

$$\frac{\delta L_i}{L_i} \leq 10^{-4} \text{ (0.01\%)}$$

which is one order of magnitude smaller than the relative error limit specified for the measurement of the ICMs elements (see Table 3.3-7).

5.2.2 Random Errors

Random errors in the determination of the inverse Calibration Matrices elements arise from the errors affecting the measurement of the common and differential accelerations and the determination of the satellite angular rates.

Let's consider the equation for the determination of the 4th row of MI_{14} :

$$MI_{14,41} \hat{a}'_{c,14,X} + MI_{14,42} \hat{a}'_{c,14,Y} + MI_{14,43} \hat{a}'_{c,14,Z} + MI_{14,44} \hat{a}'_{d,14,X} + MI_{14,45} \hat{a}'_{d,14,Y} + MI_{14,46} \hat{a}'_{d,14,Z} = \hat{y}_1$$

The quantities $\hat{a}'_{c,14,X}, \dots, \hat{a}'_{d,14,Z}, \hat{y}_1$ are measured with a given error ($\delta \hat{a}'_{c,14,X}, \dots, \delta \hat{a}'_{d,14,Z}, \delta \hat{y}_1$).

The relationship between the variance $\sigma_{\hat{y}_1}^2$ of the error $\delta \hat{y}_1$ (computed over the N measurements of \hat{y}_1), the variances $\sigma_{\delta \hat{a}'_{c,14,X}}^2, \dots, \sigma_{\delta \hat{a}'_{d,14,Z}}^2$ of the errors $\delta \hat{a}'_{c,14,X}, \dots, \delta \hat{a}'_{d,14,Z}$ (computed over the N measurements of $\hat{a}'_{c,14,X}, \dots, \hat{a}'_{d,14,Z}$), and the resulting variances $\sigma_{MI_{14,41}}^2, \dots, \sigma_{MI_{14,46}}^2$ of the solutions $MI_{14,41}, \dots, MI_{14,46}$, of the least-squares problem $A\mathbf{1} \cdot \mathbf{x1} = \mathbf{y1}$ is (ref. [RD 9]):

$$\begin{pmatrix} \sigma_{MI_{14,41}}^2 & & & & & \\ & \sigma_{MI_{14,42}}^2 & & & & \\ & & \sigma_{MI_{14,43}}^2 & & & \\ & & & \sigma_{MI_{14,44}}^2 & & \\ & & & & \sigma_{MI_{14,45}}^2 & \\ & & & & & \sigma_{MI_{14,46}}^2 \end{pmatrix} = \quad (5.2.2)$$

$$\begin{pmatrix} \sigma_{\tilde{y}_1}^2 + (MI_{14,41} \ MI_{14,42} \ MI_{14,43} \ MI_{14,44} \ MI_{14,45} \ MI_{14,46}) \end{pmatrix} \begin{pmatrix} \sigma_{\tilde{a}'_{c,14,X}}^2 & & & & & \\ & \sigma_{\tilde{a}'_{c,14,Y}}^2 & & & & \\ & & \sigma_{\tilde{a}'_{c,14,Z}}^2 & & & \\ & & & \sigma_{\tilde{a}'_{d,14,X}}^2 & & \\ & & & & \sigma_{\tilde{a}'_{d,14,Y}}^2 & \\ & & & & & \sigma_{\tilde{a}'_{d,14,Z}}^2 \end{pmatrix} \begin{pmatrix} MI_{14,41} \\ MI_{14,42} \\ MI_{14,43} \\ MI_{14,44} \\ MI_{14,45} \\ MI_{14,46} \end{pmatrix} (\mathbf{A1}^T \mathbf{A1})^{-1}$$

$$= \left(\sigma_{\tilde{y}_1}^2 + MI_{14,41}^2 \sigma_{\tilde{a}'_{c,14,X}}^2 + MI_{14,42}^2 \sigma_{\tilde{a}'_{c,14,Y}}^2 + MI_{14,43}^2 \sigma_{\tilde{a}'_{c,14,Z}}^2 + MI_{14,44}^2 \sigma_{\tilde{a}'_{d,14,X}}^2 + MI_{14,45}^2 \sigma_{\tilde{a}'_{d,14,Y}}^2 + MI_{14,46}^2 \sigma_{\tilde{a}'_{d,14,Z}}^2 \right) (\mathbf{A1}^T \mathbf{A1})^{-1}$$

Since the measured accelerations which constitute the elements of the matrix $\mathbf{A1}$ have zero mean value (before building the equation set $\mathbf{A1} \cdot \mathbf{x1} = \mathbf{y1}$, they are passed through a band-pass filter removing the spectral components outside the 50÷100 mHz bandwidth), then the matrix $\mathbf{A1}^T \mathbf{A1}$ can be approximated as:

$$\mathbf{A1}^T \mathbf{A1} \cong N \begin{pmatrix} \sigma_{\tilde{a}'_{c,14,X}}^2 & & & & & \\ & \sigma_{\tilde{a}'_{c,14,Y}}^2 & & & & \\ & & \sigma_{\tilde{a}'_{c,14,Z}}^2 & & & \\ & & & \sigma_{\tilde{a}'_{d,14,X}}^2 & & \\ & & & & \sigma_{\tilde{a}'_{d,14,Y}}^2 & \\ & & & & & \sigma_{\tilde{a}'_{d,14,Z}}^2 \end{pmatrix}$$

$$\Rightarrow (\mathbf{A1}^T \mathbf{A1})^{-1} \cong \frac{1}{N} \begin{pmatrix} 1/\sigma_{\tilde{a}'_{c,14,X}}^2 & & & & & \\ & 1/\sigma_{\tilde{a}'_{c,14,Y}}^2 & & & & \\ & & 1/\sigma_{\tilde{a}'_{c,14,Z}}^2 & & & \\ & & & 1/\sigma_{\tilde{a}'_{d,14,X}}^2 & & \\ & & & & 1/\sigma_{\tilde{a}'_{d,14,Y}}^2 & \\ & & & & & 1/\sigma_{\tilde{a}'_{d,14,Z}}^2 \end{pmatrix} \quad (5.2.3)$$

where $\sigma_{\tilde{a}'_{c,14,X}}^2, \dots, \sigma_{\tilde{a}'_{d,14,Z}}^2$ are the variances of $\tilde{a}'_{c,14,X}, \dots, \tilde{a}'_{d,14,Z}$ computed over the N measurements of these quantities.

Thus, the following approximate relationships hold:

$$\sigma_{MI_{14,41}} \cong \frac{\sqrt{\sigma_{\tilde{y}_1}^2 + MI_{14,41}^2 \sigma_{\tilde{a}'_{c,14,X}}^2 + MI_{14,42}^2 \sigma_{\tilde{a}'_{c,14,Y}}^2 + MI_{14,43}^2 \sigma_{\tilde{a}'_{c,14,Z}}^2 + MI_{14,44}^2 \sigma_{\tilde{a}'_{d,14,X}}^2 + MI_{14,45}^2 \sigma_{\tilde{a}'_{d,14,Y}}^2 + MI_{14,46}^2 \sigma_{\tilde{a}'_{d,14,Z}}^2}}{\sqrt{N} \sigma_{\tilde{a}'_{c,14,X}}} \quad (5.2.4)$$

$$\sigma_{MI_{14,46}} \cong \frac{\sqrt{\sigma_{\tilde{y}_1}^2 + MI_{14,41}^2 \sigma_{\tilde{a}'_{c,14,X}}^2 + MI_{14,42}^2 \sigma_{\tilde{a}'_{c,14,Y}}^2 + MI_{14,43}^2 \sigma_{\tilde{a}'_{c,14,Z}}^2 + MI_{14,44}^2 \sigma_{\tilde{a}'_{d,14,X}}^2 + MI_{14,45}^2 \sigma_{\tilde{a}'_{d,14,Y}}^2 + MI_{14,46}^2 \sigma_{\tilde{a}'_{d,14,Z}}^2}}{\sqrt{N} \sigma_{\tilde{a}'_{d,14,Z}}}$$

where $\sigma_{MI_{14,41}}, \dots, \sigma_{MI_{14,46}}$ are the standard deviations of $MI_{14,41}, \dots, MI_{14,46}$.

The specified measurement accuracies for the ICM elements (Table 3.3-7), can be considered as the 3σ random error on these elements (the systematic errors in fact gives a very small contribution):

$$\delta MI_{14,41} = 3 \sigma_{MI_{14,41}}, \dots, \delta MI_{14,46} = 3 \sigma_{MI_{14,46}} \quad (5.2.5)$$

The variances of the errors ($\delta \tilde{a}'_{c,14,X}, \dots, \delta \tilde{a}'_{d,14,Z}, \delta \tilde{y}_1$) can be expressed as function of the spectral densities of these errors over the upper measurement bandwidth (UMBW = 50+100 mHz):

$$\sigma_{\tilde{a}'_{c,14,X}}^2 = (\delta \tilde{a}'_{c,14,X})^2 \Delta v_{UMBW}, \dots, \sigma_{\tilde{a}'_{d,14,Z}}^2 = (\delta \tilde{a}'_{d,14,Z})^2 \Delta v_{UMBW}, \sigma_{\tilde{y}_1}^2 = (\delta \tilde{y}_1)^2 \Delta v_{UMBW} \quad (5.2.6)$$

with $\Delta v_{UMBW} = 100 - 50 = 50$ mHz, and where $\delta \tilde{a}'_{c,14,X}$ is the value of the spectral density of the $\tilde{a}'_{c,14,X}$ in the UMBW, etc...

Analogously, the standard deviations of the measured accelerations $\tilde{a}'_{c,14,X}, \dots, \tilde{a}'_{d,14,Z}$, can be expressed as function of their spectral densities over the UMBW:

$$\sigma_{\tilde{a}'_{c,14,X}} = \tilde{a}'_{c,14,X} \sqrt{\Delta v_{UMBW}}, \dots, \sigma_{\tilde{a}'_{d,14,Z}} = \tilde{a}'_{d,14,Z} \sqrt{\Delta v_{UMBW}}, \quad (5.2.7)$$

where $\tilde{a}'_{c,14,X}$ is the value of the spectral density of the $\tilde{a}'_{c,14,X}$ in the UMBW, etc...

With the (5.2.5), (5.2.6), (5.2.7), the (5.2.4) become:

$$\delta MI_{14,41} \cong 3 \frac{\sqrt{(\delta \tilde{y}_1)^2 + MI_{14,41}^2 (\tilde{a}'_{c,14,X})^2 + MI_{14,42}^2 (\tilde{a}'_{c,14,Y})^2 + MI_{14,43}^2 (\tilde{a}'_{c,14,Z})^2 + MI_{14,44}^2 (\tilde{a}'_{d,14,X})^2 + MI_{14,45}^2 (\tilde{a}'_{d,14,Y})^2 + MI_{14,46}^2 (\tilde{a}'_{d,14,Z})^2}}{2\sqrt{N} \tilde{a}'_{c,14,X}} \quad (5.2.8)$$

$$\delta MI_{14,46} \cong 3 \frac{\sqrt{(\delta \tilde{y}_1)^2 + MI_{14,41}^2 (\tilde{a}'_{c,14,X})^2 + MI_{14,42}^2 (\tilde{a}'_{c,14,Y})^2 + MI_{14,43}^2 (\tilde{a}'_{c,14,Z})^2 + MI_{14,44}^2 (\tilde{a}'_{d,14,X})^2 + MI_{14,45}^2 (\tilde{a}'_{d,14,Y})^2 + MI_{14,46}^2 (\tilde{a}'_{d,14,Z})^2}}{2\sqrt{N} \tilde{a}'_{d,14,Z}}$$

For the accelerometer pair (A_1, A_4), $\delta \tilde{a}'_{c,14,X}, \delta \tilde{a}'_{c,14,Z}, \delta \tilde{a}'_{d,14,X}, \delta \tilde{a}'_{d,14,Z}$ are nearly equal to the spectral densities of the differential noise of the accelerometers along the ultra-sensitive axis (\tilde{n}_{US}^W), and $\delta \tilde{a}'_{c,14,Y}, \delta \tilde{a}'_{d,14,Y}$ are nearly

equal the spectral densities of the differential noise of the accelerometers along the less-sensitive axis (\tilde{n}_{LS}^W) (in both the common-mode and the differential-mode accelerations, the measurement noise is added quadratically). We can thus re-write the (5.2.8) as:

$$\delta MI_{14,41} \equiv 3 \frac{\sqrt{(\delta \tilde{y}_1^W)^2 + (\tilde{n}_{US}^W)^2 (MI_{14,41}^2 + MI_{14,43}^2 + MI_{14,44}^2 + MI_{14,46}^2) + (\tilde{n}_{LS}^W)^2 (MI_{14,42}^2 + MI_{14,45}^2)}}{\sqrt{N} \tilde{a}_{c,14,X}^W} \dots \dots \dots (5.2.9)$$

$$\delta MI_{14,46} \equiv 3 \frac{\sqrt{(\delta \tilde{y}_1^W)^2 + (\tilde{n}_{US}^W)^2 (MI_{14,41}^2 + MI_{14,43}^2 + MI_{14,44}^2 + MI_{14,46}^2) + (\tilde{n}_{LS}^W)^2 (MI_{14,42}^2 + MI_{14,45}^2)}}{\sqrt{N} \tilde{a}_{d,14,Z}^W}$$

From the above expression we can derive the number N of independed measurements of the common and differential mode accelerations needed to determine $MI_{14,41}, \dots, MI_{14,46}$ with an error $\delta MI_{14,41}, \dots, \delta MI_{14,46}$ (thus the number of equations in the set **A1 · x1 = y1**) and, with analogous procedure, for all the elements of the ICMs to be measured during the in-flight calibration (see Table 3.3-7).

$$\begin{aligned} N_{14,41} &\equiv 9 \frac{(\delta \tilde{y}_1^W)^2 + (\tilde{n}_{US}^W)^2 (MI_{14,41}^2 + MI_{14,43}^2 + MI_{14,44}^2 + MI_{14,46}^2) + (\tilde{n}_{LS}^W)^2 (MI_{14,42}^2 + MI_{14,45}^2)}{(\delta MI_{14,41} \tilde{a}_{c,14,X}^W)^2} \\ &\dots \dots \dots (5.2.10) \\ N_{14,46} &\equiv 9 \frac{(\delta \tilde{y}_1^W)^2 + (\tilde{n}_{US}^W)^2 (MI_{14,41}^2 + MI_{14,43}^2 + MI_{14,44}^2 + MI_{14,46}^2) + (\tilde{n}_{LS}^W)^2 (MI_{14,42}^2 + MI_{14,45}^2)}{(\delta MI_{14,41} \tilde{a}_{d,14,Z}^W)^2} \\ N_{14,52} &\equiv 9 \frac{(\delta \tilde{y}_2^W)^2 + (\tilde{n}_{US}^W)^2 (MI_{14,51}^2 + MI_{14,53}^2 + MI_{14,54}^2 + MI_{14,56}^2) + (\tilde{n}_{LS}^W)^2 (MI_{14,52}^2 + MI_{14,55}^2)}{(\delta MI_{14,52} \tilde{a}_{c,14,Y}^W)^2} \\ N_{14,55} &\equiv 9 \frac{(\delta \tilde{y}_2^W)^2 + (\tilde{n}_{US}^W)^2 (MI_{14,51}^2 + MI_{14,53}^2 + MI_{14,54}^2 + MI_{14,56}^2) + (\tilde{n}_{LS}^W)^2 (MI_{14,52}^2 + MI_{14,55}^2)}{(\delta MI_{14,55} \tilde{a}_{d,14,Y}^W)^2} \\ N_{14,62} &\equiv 9 \frac{(\delta \tilde{y}_3^W)^2 + (\tilde{n}_{US}^W)^2 (MI_{14,61}^2 + MI_{14,63}^2 + MI_{14,64}^2 + MI_{14,66}^2) + (\tilde{n}_{LS}^W)^2 (MI_{14,62}^2 + MI_{14,65}^2)}{(\delta MI_{14,62} \tilde{a}_{c,14,Y}^W)^2} \\ N_{14,63} &\equiv 9 \frac{(\delta \tilde{y}_3^W)^2 + (\tilde{n}_{US}^W)^2 (MI_{14,61}^2 + MI_{14,63}^2 + MI_{14,64}^2 + MI_{14,66}^2) + (\tilde{n}_{LS}^W)^2 (MI_{14,62}^2 + MI_{14,65}^2)}{(\delta MI_{14,63} \tilde{a}_{c,14,Z}^W)^2} \\ N_{14,66} &\equiv 9 \frac{(\delta \tilde{y}_3^W)^2 + (\tilde{n}_{US}^W)^2 (MI_{14,61}^2 + MI_{14,63}^2 + MI_{14,64}^2 + MI_{14,66}^2) + (\tilde{n}_{LS}^W)^2 (MI_{14,62}^2 + MI_{14,65}^2)}{(\delta MI_{14,66} \tilde{a}_{d,14,Z}^W)^2} \\ N_{25,41} &\equiv 9 \frac{(\delta \tilde{y}_4^W)^2 + (\tilde{n}_{US}^W)^2 (MI_{25,41}^2 + MI_{25,42}^2 + MI_{25,44}^2 + MI_{25,45}^2) + (\tilde{n}_{LS}^W)^2 (MI_{25,43}^2 + MI_{25,46}^2)}{(\delta MI_{25,41} \tilde{a}_{c,25,X}^W)^2} \\ N_{25,44} &\equiv 9 \frac{(\delta \tilde{y}_4^W)^2 + (\tilde{n}_{US}^W)^2 (MI_{25,41}^2 + MI_{25,42}^2 + MI_{25,44}^2 + MI_{25,45}^2) + (\tilde{n}_{LS}^W)^2 (MI_{25,43}^2 + MI_{25,46}^2)}{(\delta MI_{25,44} \tilde{a}_{d,25,X}^W)^2} \\ N_{25,51} &\equiv 9 \frac{(\delta \tilde{y}_5^W)^2 + (\tilde{n}_{US}^W)^2 (MI_{25,51}^2 + MI_{25,52}^2 + MI_{25,54}^2 + MI_{25,55}^2) + (\tilde{n}_{LS}^W)^2 (MI_{25,53}^2 + MI_{25,56}^2)}{(\delta MI_{25,51} \tilde{a}_{c,25,X}^W)^2} \\ &\dots \dots \dots \\ N_{25,56} &\equiv 9 \frac{(\delta \tilde{y}_5^W)^2 + (\tilde{n}_{US}^W)^2 (MI_{25,51}^2 + MI_{25,52}^2 + MI_{25,54}^2 + MI_{25,55}^2) + (\tilde{n}_{LS}^W)^2 (MI_{25,53}^2 + MI_{25,56}^2)}{(\delta MI_{25,56} \tilde{a}_{d,25,Z}^W)^2} \end{aligned}$$

$$\begin{aligned}
N_{25,63} &\equiv 9 \frac{(\delta \tilde{y}_6^W)^2 + (\tilde{n}_{US}^W)^2 (MI_{25,61}^2 + MI_{25,62}^2 + MI_{25,64}^2 + MI_{25,65}^2) + (\tilde{n}_{LS}^W)^2 (MI_{25,63}^2 + MI_{25,66}^2)}{(\delta MI_{25,63} \tilde{a}_{c,25,Z}^W)^2} \\
N_{25,66} &\equiv 9 \frac{(\delta \tilde{y}_6^W)^2 + (\tilde{n}_{US}^W)^2 (MI_{25,61}^2 + MI_{25,62}^2 + MI_{25,64}^2 + MI_{25,65}^2) + (\tilde{n}_{LS}^W)^2 (MI_{25,63}^2 + MI_{25,66}^2)}{(\delta MI_{25,66} \tilde{a}_{d,25,Z}^W)^2} \\
N_{36,41} &\equiv 9 \frac{(\delta \tilde{y}_7^W)^2 + (\tilde{n}_{US}^W)^2 (MI_{36,41}^2 + MI_{36,43}^2 + MI_{36,44}^2 + MI_{36,46}^2) + (\tilde{n}_{LS}^W)^2 (MI_{36,42}^2 + MI_{36,45}^2)}{(\delta MI_{36,41} \tilde{a}_{c,36,X}^W)^2} \\
N_{36,42} &\equiv 9 \frac{(\delta \tilde{y}_7^W)^2 + (\tilde{n}_{US}^W)^2 (MI_{36,41}^2 + MI_{36,43}^2 + MI_{36,44}^2 + MI_{36,46}^2) + (\tilde{n}_{LS}^W)^2 (MI_{36,42}^2 + MI_{36,45}^2)}{(\delta MI_{36,42} \tilde{a}_{c,36,Y}^W)^2} \\
N_{36,44} &\equiv 9 \frac{(\delta \tilde{y}_7^W)^2 + (\tilde{n}_{US}^W)^2 (MI_{36,41}^2 + MI_{36,43}^2 + MI_{36,44}^2 + MI_{36,46}^2) + (\tilde{n}_{LS}^W)^2 (MI_{36,42}^2 + MI_{36,45}^2)}{(\delta MI_{36,44} \tilde{a}_{d,36,X}^W)^2} \\
N_{36,52} &\equiv 9 \frac{(\delta \tilde{y}_8^W)^2 + (\tilde{n}_{US}^W)^2 (MI_{36,51}^2 + MI_{36,53}^2 + MI_{36,54}^2 + MI_{36,56}^2) + (\tilde{n}_{LS}^W)^2 (MI_{36,52}^2 + MI_{36,55}^2)}{(\delta MI_{36,52} \tilde{a}_{c,36,Y}^W)^2} \\
N_{36,55} &\equiv 9 \frac{(\delta \tilde{y}_8^W)^2 + (\tilde{n}_{US}^W)^2 (MI_{36,51}^2 + MI_{36,53}^2 + MI_{36,54}^2 + MI_{36,56}^2) + (\tilde{n}_{LS}^W)^2 (MI_{36,52}^2 + MI_{36,55}^2)}{(\delta MI_{36,55} \tilde{a}_{d,36,Y}^W)^2} \\
N_{36,61} &\equiv 9 \frac{(\delta \tilde{y}_9^W)^2 + (\tilde{n}_{US}^W)^2 (MI_{36,61}^2 + MI_{36,63}^2 + MI_{36,64}^2 + MI_{36,66}^2) + (\tilde{n}_{LS}^W)^2 (MI_{36,62}^2 + MI_{36,65}^2)}{(\delta MI_{36,61} \tilde{a}_{c,36,X}^W)^2} \\
&\dots\dots\dots \\
N_{36,66} &\equiv 9 \frac{(\delta \tilde{y}_9^W)^2 + (\tilde{n}_{US}^W)^2 (MI_{36,61}^2 + MI_{36,63}^2 + MI_{36,64}^2 + MI_{36,66}^2) + (\tilde{n}_{LS}^W)^2 (MI_{36,62}^2 + MI_{36,65}^2)}{(\delta MI_{36,66} \tilde{a}_{d,36,Z}^W)^2}
\end{aligned}$$

The minimum number of N independent measurements needed to determine the ICMs elements with the required accuracy are provided in Table 5.2-1. They are computed from the following inputs:

- Values of the elements of $MI_{ij,hk}$ equal to their upper limits all along the mission lifetime, as per Table 3.1-1. For $MI_{14,44}$, $MI_{14,55}$, $MI_{14,66}$, $MI_{25,44}$, $MI_{25,55}$, $MI_{25,66}$, $MI_{36,44}$, $MI_{36,55}$, $MI_{36,66}$ a unitary value has been considered.
- Values of the quadratic factors equal to their upper limits during the measurement phases, i.e. after the quadratic factor calibration (as per Table 3.3-1, with the common K2 set equal to the differential K2, which sets the most stringent limits). Spectral density of these elements = $0.01 \text{ s}^2/\text{m}/\text{Hz}^{1/2}$.
- Accelerometer intrinsic noise = $2 \cdot 10^{-12} \text{ m/s}^2/\text{Hz}^{1/2}$ (ultra sensitive axes), = $3.5 \cdot 10^{-10} \text{ m/s}^2/\text{Hz}^{1/2}$ (less sensitive axes) $\Rightarrow \tilde{n}_{US}^W = 2 \cdot 10^{-12}/\sqrt{2} \text{ m/s}^2/\text{Hz}^{1/2}$, $\tilde{n}_{LS}^W = 3.5 \cdot 10^{-10}/\sqrt{2} \text{ m/s}^2/\text{Hz}^{1/2}$.
- Spectral density of the GGT components in the UMBW as per APPENDIX A (this has been included in the measurement error $\delta \tilde{y}_i$).
- Measurement error of the angular rates: $\delta \hat{\omega}_X^0 = \delta \hat{\omega}_Y^0 = \delta \hat{\omega}_Z^0 = 5.0 \cdot 10^{-6} \text{ rad/s}$ below the MBW (10 times larger than the requirement for the science mode); $\delta \hat{\omega}_X^W = 8.5 \cdot 10^{-8}$, $\delta \hat{\omega}_Y^W = 4.1 \cdot 10^{-9}$, $\delta \hat{\omega}_Z^W = 3.2 \cdot 10^{-8} \text{ rad/s}/\text{Hz}^{1/2}$ in the UMBW (requirement for the science mode in the whole MBW).
- Spectral density of the common-and differential mode accelerations in the UMBW (resulting from the shaking action and from the “normal” DFACS activity): $\tilde{a}_{c,ij,k}^W = \tilde{a}_{d,ij,k}^W = 1.0 \cdot 10^{-7} \text{ m/s}^2/\text{Hz}^{1/2}$ (the same value has been considered here for all the shaking accelerations in order to highlight the effects of the measurement error in the computation of N ; actually the accelerations can be significantly different axis by axis).
- Folding inside the UMBW of the high-frequency noise of generated by the GCD thrusters (as specified in Table 6.2-1) through the accelerometer non linearities (quadratic factors).

The minimum number of measurements of Table 5.2-1 can be translated into the minimum duration of the measurement period of the second part of the calibration, by multiplying N by the minimum time interval separating two independent measurements. Being the measurements passed through a band-pass filter to remove the spectral components outside the MBW, the minimum interval between two independent measurements is $\delta t = 5$ s (to which corresponds the Nyquist frequency of 100 mHz). Therefore, considering the largest $N(N_{25,51})$, the minimum duration of the calibration is $15513 \cdot 5 \approx 78000$ s. This number, of course is strongly dependant on the assumption made about the shaking acceleration spectral density level.

MI_{ij} element	Required measurement accuracy	Noise spectral density of $\tilde{a}'_{c,ij,k}, \tilde{a}'_{d,ij,k}$, in the UMBW	Spectral density of $\delta\tilde{y}_i$ in the UMBW	Minimum number of independent measurements required
$MI_{14,41}$	$4.7 \cdot 10^{-6}$	$\tilde{a}'_{c,14,X} = 10^{-7} \text{ m/s}^2/\text{Hz}^{1/2}$	$\delta\tilde{y}_1^W = 4.9 \cdot 10^{-12} \text{ m/s}^2/\text{Hz}^{1/2}$	$N_{14,41} = 11487$
$MI_{14,42}$	$4.5 \cdot 10^{-6}$	$\tilde{a}'_{c,14,Y} = 10^{-7} \text{ m/s}^2/\text{Hz}^{1/2}$		$N_{14,42} = 12531$
$MI_{14,43}$	$4.5 \cdot 10^{-6}$	$\tilde{a}'_{c,14,Z} = 10^{-7} \text{ m/s}^2/\text{Hz}^{1/2}$		$N_{14,43} = 12531$
$MI_{14,44}$	$2.0 \cdot 10^{-3}$	$\tilde{a}'_{d,14,X} = 10^{-7} \text{ m/s}^2/\text{Hz}^{1/2}$		$N_{14,44} < 1$
$MI_{14,45}$	$5.0 \cdot 10^{-5}$	$\tilde{a}'_{d,14,Y} = 10^{-7} \text{ m/s}^2/\text{Hz}^{1/2}$		$N_{14,45} = 101$
$MI_{14,46}$	$5.0 \cdot 10^{-5}$	$\tilde{a}'_{d,14,Z} = 10^{-7} \text{ m/s}^2/\text{Hz}^{1/2}$		$N_{14,46} = 101$
$MI_{14,52}$	$5.0 \cdot 10^{-4}$	$\tilde{a}'_{c,14,Y} = 10^{-7} \text{ m/s}^2/\text{Hz}^{1/2}$	$\delta\tilde{y}_2^W = 5.3 \cdot 10^{-11} \text{ m/s}^2/\text{Hz}^{1/2}$	$N_{14,52} = 237$
$MI_{14,55}$	$1.0 \cdot 10^{-2}$	$\tilde{a}'_{d,14,Y} = 10^{-7} \text{ m/s}^2/\text{Hz}^{1/2}$		$N_{14,55} = 1$
$MI_{14,62}$	$4.5 \cdot 10^{-5}$	$\tilde{a}'_{c,14,Y} = 10^{-7} \text{ m/s}^2/\text{Hz}^{1/2}$	$\delta\tilde{y}_3^W = 1.1 \cdot 10^{-11} \text{ m/s}^2/\text{Hz}^{1/2}$	$N_{14,62} = 765$
$MI_{14,63}$	$4.87 \cdot 10^{-5}$	$\tilde{a}'_{c,14,Z} = 10^{-7} \text{ m/s}^2/\text{Hz}^{1/2}$		$N_{14,63} = 653$
$MI_{14,66}$	$2.0 \cdot 10^{-3}$	$\tilde{a}'_{d,14,Z} = 10^{-7} \text{ m/s}^2/\text{Hz}^{1/2}$		$N_{14,66} < 1$
$MI_{25,41}$	$1.0 \cdot 10^{-4}$	$\tilde{a}'_{c,25,X} = 10^{-7} \text{ m/s}^2/\text{Hz}^{1/2}$	$\delta\tilde{y}_4^W = 2.5 \cdot 10^{-10} \text{ m/s}^2/\text{Hz}^{1/2}$	$N_{25,41} = 5597$
$MI_{25,44}$	$2.0 \cdot 10^{-3}$	$\tilde{a}'_{d,25,X} = 10^{-7} \text{ m/s}^2/\text{Hz}^{1/2}$		$N_{25,44} = 14$
$MI_{25,51}$	$4.5 \cdot 10^{-6}$	$\tilde{a}'_{c,25,X} = 10^{-7} \text{ m/s}^2/\text{Hz}^{1/2}$	$\delta\tilde{y}_5^W = 9.5 \cdot 10^{-12} \text{ m/s}^2/\text{Hz}^{1/2}$	$N_{25,51} = 15513$
$MI_{25,52}$	$4.7 \cdot 10^{-6}$	$\tilde{a}'_{c,25,Y} = 10^{-7} \text{ m/s}^2/\text{Hz}^{1/2}$		$N_{25,52} = 14221$
$MI_{25,53}$	$4.5 \cdot 10^{-6}$	$\tilde{a}'_{c,25,Z} = 10^{-7} \text{ m/s}^2/\text{Hz}^{1/2}$		$N_{25,53} = 15513$
$MI_{25,54}$	$5.0 \cdot 10^{-5}$	$\tilde{a}'_{d,25,X} = 10^{-7} \text{ m/s}^2/\text{Hz}^{1/2}$		$N_{25,54} = 126$
$MI_{25,55}$	$2.0 \cdot 10^{-3}$	$\tilde{a}'_{d,25,Y} = 10^{-7} \text{ m/s}^2/\text{Hz}^{1/2}$		$N_{25,55} < 1$
$MI_{25,56}$	$5.0 \cdot 10^{-5}$	$\tilde{a}'_{d,25,Z} = 10^{-7} \text{ m/s}^2/\text{Hz}^{1/2}$		$N_{25,56} = 126$
$MI_{25,63}$	$5.0 \cdot 10^{-4}$	$\tilde{a}'_{c,25,Z} = 10^{-7} \text{ m/s}^2/\text{Hz}^{1/2}$	$\delta\tilde{y}_6^W = 2.5 \cdot 10^{-10} \text{ m/s}^2/\text{Hz}^{1/2}$	$N_{25,63} = 449$
$MI_{25,66}$	$1.0 \cdot 10^{-2}$	$\tilde{a}'_{d,25,Z} = 10^{-7} \text{ m/s}^2/\text{Hz}^{1/2}$		$N_{25,66} = 2$
$MI_{36,41}$	$4.87 \cdot 10^{-5}$	$\tilde{a}'_{c,36,X} = 10^{-7} \text{ m/s}^2/\text{Hz}^{1/2}$	$\delta\tilde{y}_7^W = 1.1 \cdot 10^{-11} \text{ m/s}^2/\text{Hz}^{1/2}$	$N_{36,41} = 650$
$MI_{36,42}$	$4.5 \cdot 10^{-5}$	$\tilde{a}'_{c,36,Y} = 10^{-7} \text{ m/s}^2/\text{Hz}^{1/2}$		$N_{36,42} = 762$
$MI_{36,44}$	$2.0 \cdot 10^{-3}$	$\tilde{a}'_{d,36,X} = 10^{-7} \text{ m/s}^2/\text{Hz}^{1/2}$		$N_{36,44} < 1$
$MI_{36,52}$	$5.0 \cdot 10^{-4}$	$\tilde{a}'_{c,36,Y} = 10^{-7} \text{ m/s}^2/\text{Hz}^{1/2}$		$N_{36,52} = 449$

$MI_{36,55}$	$1.0 \cdot 10^{-2}$	$\tilde{a}_{d,36,Y}^W = 10^{-7} \text{ m/s}^2/\text{Hz}^{1/2}$	$\delta \tilde{y}_8^W = 2.5 \cdot 10^{-10} \text{ m/s}^2/\text{Hz}^{1/2}$	$N_{36,55} = 2$
$MI_{36,61}$	$4.5 \cdot 10^{-6}$	$\tilde{a}_{c,36,X}^W = 10^{-7} \text{ m/s}^2/\text{Hz}^{1/2}$	$\delta \tilde{y}_9^W = 9.3 \cdot 10^{-12} \text{ m/s}^2/\text{Hz}^{1/2}$	$N_{36,61} = 15327$
$MI_{36,62}$	$4.5 \cdot 10^{-6}$	$\tilde{a}_{c,36,Y}^W = 10^{-7} \text{ m/s}^2/\text{Hz}^{1/2}$		$N_{36,62} = 15327$
$MI_{36,63}$	$4.7 \cdot 10^{-6}$	$\tilde{a}_{c,36,Z}^W = 10^{-7} \text{ m/s}^2/\text{Hz}^{1/2}$		$N_{36,63} = 14050$
$MI_{36,64}$	$5.0 \cdot 10^{-5}$	$\tilde{a}_{d,36,X}^W = 10^{-7} \text{ m/s}^2/\text{Hz}^{1/2}$		$N_{36,64} = 124$
$MI_{36,65}$	$5.0 \cdot 10^{-5}$	$\tilde{a}_{d,36,Y}^W = 10^{-7} \text{ m/s}^2/\text{Hz}^{1/2}$		$N_{36,65} = 124$
$MI_{36,66}$	$2.0 \cdot 10^{-3}$	$\tilde{a}_{d,36,Z}^W = 10^{-7} \text{ m/s}^2/\text{Hz}^{1/2}$		$N_{36,66} < 1$

Table 5.2-1: Minimum number of independent measurements needed to determine the ICMs elements to be measured in flight with the required accuracy.

6. REQUIREMENTS FOR DFACS AND GCD ARISING FROM IN-FLIGHT CALIBRATION

6.1 REQUIREMENTS ON THE DFACS

6.1.1 DFACS Performance Requirements for the Quadratic Factor Measurement

During the in-flight calibration phase devoted to the measurement of the quadratic factors, the DFACS shall control the linear accelerations, angular accelerations, angular rates, attitude angles as in science mode. In particular the performances considered for the K2 calibration analysis are (in the GRF):

- Maximum value of linear acceleration below the MBW (specification):

$$a_X^0 = 1 \cdot 10^{-6} \text{ m/s}^2 \text{ (to be ensured by the in-track linear acceleration control)}$$

$$a_Y^0, a_Z^0 = 1 \cdot 10^{-6} \text{ m/s}^2 \text{ (determined by the perturbation environment, since there is no Y,Z-acceleration control)}$$

- Maximum value of linear acceleration spectral density from 50 to 100 mHz (specification):

$$\tilde{a}_X \leq 2.5 \cdot 10^{-8} \text{ m/s}^2/\text{Hz}^{1/2} \text{ (to be ensured by the in-track linear acceleration control)}$$

$$\tilde{a}_Y \leq 1.0 \cdot 10^{-8} \text{ m/s}^2/\text{Hz}^{1/2} \text{ (determined by the perturbation environment, since there is no Y-acceleration control)}$$

$$\tilde{a}_Z \leq 1.0 \cdot 10^{-8} \text{ m/s}^2/\text{Hz}^{1/2} \text{ (determined by the perturbation environment, since there is no Z-acceleration control)}$$

- Maximum value of angular acceleration below the MBW (specification):

$$\dot{\omega}_X^0 = 2 \cdot 10^{-6} \text{ rad/s}^2 \text{ (to be ensured by the attitude control based on the magnetic torquers)}$$

$$\dot{\omega}_Y^0 = \dot{\omega}_Z^0 = 10^{-6} \text{ rad/s}^2 \text{ (to be ensured by the attitude control based on the magnetic torquers)}$$

- Maximum value of angular acceleration spectral density from 50 to 100 mHz (specification):

$$\tilde{\dot{\omega}}_X = \tilde{\dot{\omega}}_Y = \tilde{\dot{\omega}}_Z = 2 \cdot 10^{-8} \text{ rad/s}^2/\text{Hz}^{1/2} \text{ (determined by the attitude control based on the magnetic torquers and by the perturbation environment, since the control action is very weak in the upper part of the MBW)}$$

- Maximum value of angular rates below the MBW (specification):

$$\omega_X^0 = 2 \cdot 10^{-4} \text{ rad/s (to be ensured by the attitude control based on the magnetic torquers)}$$

$$\omega_Y^0 = 1.2 \cdot 10^{-3} \text{ rad/s (dominated by the spin rate of the satellite)}$$

$$\omega_Z^0 = 2 \cdot 10^{-4} \text{ rad/s (to be ensured by the attitude control based on the magnetic torquers)}$$

- Maximum value of angular rate spectral density from 50 to 100 mHz (specification):

$$\tilde{\omega}_X = 6 \cdot 10^{-7} \text{ rad/s/Hz}^{1/2}, \tilde{\omega}_Y = \tilde{\omega}_Z = 6 \cdot 10^{-8} \text{ rad/s/Hz}^{1/2} \text{ (determined by the attitude control based on the magnetic torquers and by the perturbation environment, since the control action is very weak in the upper part of the MBW)}$$

The difference with respect to the science mode is that the above performances shall be achieved with the DFACS fed by a combination of measured accelerations which is function of the K2 under measurement, as per Table 4.1-2 (TBC).

6.1.2 DFACS Performance Requirements for the Determination of the Inverse Calibration Matrices

During the in-flight calibration phase devoted to the measurement of the ICMs, the DFACS can use the same control laws of the linear accelerations, angular accelerations, angular rates, attitude angles as in science mode. It can be also fed by the same combination of measured accelerations as in science mode. The control of the X linear acceleration with the ion thruster shall be performed against a non-zero reference (see Figure 6.1-1) constituted by a pre-computed acceleration (a_{ref}) with a random profile computed so to:

- have a power spectrum in the 50 to 100 mHz frequency region only;
- be as much as possible de-correlated from the random acceleration profiles applied to the other axes by means of the GCD;
- be compatible with the ITA performances in terms of thrust level and slew rate.

There are no particular performance requirements concerning the spectral density of the linear accelerations, angular accelerations and angular rates in the MBW for this calibration. The same science-mode requirements apply instead to the maximum value of the linear accelerations, angular accelerations and angular rates (all these are related in this case to the accelerometer saturation), and to the maximum value of the attitude angles (these are defined by illumination condition of solar panels and radiators and by the field of view of the star trackers and of the GPS antennas). These requirements must be fulfilled in presence of the linear and angular shaking applied to the satellite by the GCD.

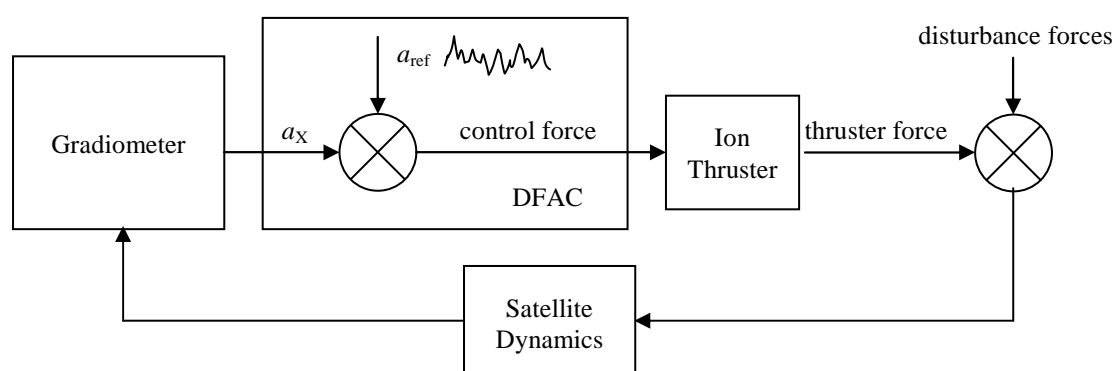


Figure 6.1-1: Control scheme of the X-linear acceleration during the in-flight calibration of the ICMs

6.2 REQUIREMENTS ON THE GRADIOMETER CALIBRATION DEVICE

The Gradiometer Calibration device is composed by 8 micro-thrusters fed by Nitrogen and endowed with on-off valves enabling a smooth transition from the closed condition to the open one. The thruster location and orientation is shown in Figure 6.2-1. The maximum linear accelerations along the Y and Z axes and the maximum angular accelerations about the X, Y, Z axes achievable for a given force F provided by each thruster are:

- $a_Y = \frac{4 \sin \alpha}{m} F$; $a_Z = \frac{4 \cos \alpha}{m} F$ ($\alpha = 55^\circ$, $m = \text{satellite mass} \approx 1000 \text{ kg}$)

- $\dot{\omega}_X = \frac{4R \sin \alpha}{I_X} F$; $\dot{\omega}_Y = \frac{4L \cos \alpha}{I_Y} F$, $\dot{\omega}_Z = \frac{4L \sin \alpha}{I_Z} F$ ($R = 0.44$ m, $L = 3.8$ m, $I_X =$ satellite inertia about X ≈ 130 kgm², $I_Y =$ satellite inertia about Y ≈ 2500 kgm², $I_Z =$ satellite inertia about Z ≈ 2500 kgm²).

During the in-flight calibration phase devoted to the measurement of the ICMs the calibration, the thrusters are operated according to a pre-computed on-off state sequence so to provide simultaneously linear accelerations along the Y and Z axes and angular accelerations along the X, Y, Z axes. These accelerations must:

- have a power spectrum as large as possible in the 50 to 100 mHz frequency region and as small as possible outside it;
- be as much as possible de-correlated from each other and from the random acceleration profiles applied to the X axis by means of the ITA.

The performance requirements applicable to the GCD are summarized in Table 6.2-1.

The most important requirement concerns the noise SD above 0.1 Hz, to avoid increasing the measurement noise in the UMBW by aliasing and non-linearity effects. The requirements on steady-state thrust stability, thrust response performance are not really mandatory (in the sense that a small deviation from the indicated value does not spoil the calibration process).

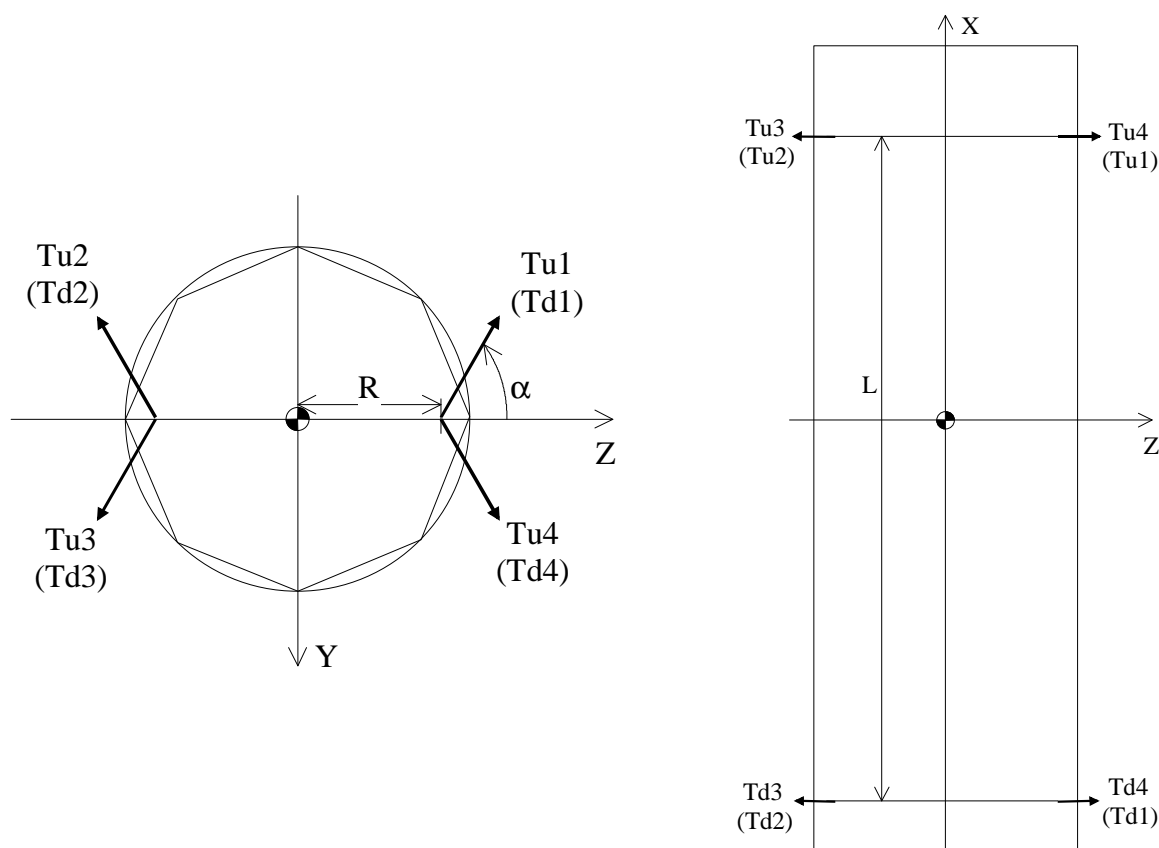


Figure 6.2-1: Sketch of the GCD micro-thruster layout on the GOCE satellite

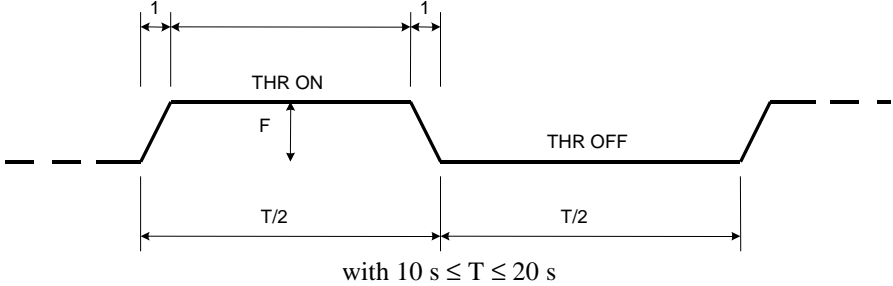
Requirement	Value
Effective thrust output per thruster	$F = 600 \mu\text{N}$ (nominal); $400 \mu\text{N} < F \leq 800 \mu\text{N}$ (acceptable)
Nominal activation profile of each thruster	 <p>with $10 \text{ s} \leq T \leq 20 \text{ s}$</p>
Steady-state thrust stability (during the $T/2$ period in which the thruster is on)	$\leq \pm 10\% F$
Activation of each thruster during a calibration period	50% duty cycle
Maximum number of thrusters activated simultaneously	6
Thrust response performance	<ul style="list-style-type: none"> - rise/ fall time $\leq 1 \text{ sec}$ - overshoot $\leq 10\% F$
Thrust vector stability	5° (3σ) overall (mounting, stability, lifetime)
Limit for the acceleration noise spectral density at the Gradiometer location produced by the overall cold-gas thruster system	$\tilde{a}(\nu) \leq 5 \cdot 10^{-7} \text{ m/s}^2/\text{Hz}^{1/2}$, for $0.1 \text{ Hz} < \nu < 100 \text{ Hz}$

Table 6.2-1: Performance requirements applicable to the GCD

7. ACRONYMS AND ABBREVIATIONS

ARF	Accelerometer Reference Frames
CM	Calibration Matrix
CDR	Critical Design Review
COM	Centre Of Mass
DFACS	Drag Free and Attitude Control
DFACS	Drag Free and Attitude Control Subsystem
DVA	Drive Voltage Amplifier
E	Eötvös (acceleration gradient measurement unit; $1 \text{ E} = 10^{-9} \text{ m/s}^2/\text{m}$)
GCD	Gradiometer Calibration Device
GGT	Gravity Gradient Tensor
GOCE	Gravity field and steady-state Ocean Circulation Explorer
K2	Quadratic factor
ICM	Inverse Calibration Matrix
ITA	Ion Thruster Assembly
LS	Less Sensitive (accelerometer axis)
LORF	Local Orbital Reference Frame
MBW	Measurement BandWidth (from 5 mHz to 100 mHz)
OAG	One Axis Gradiometer
OAGRF	One Axis Gradiometer Reference Frame
SD	Spectral Density
SNR	Signal to Noise Ratio
TBC	To Be Confirmed
TBD	To Be Defined
TBV	To Be Verified
UMBW	Upper Measurement BandWidth (from 50 mHz to 100 mHz)
US	Ultra Sensitive (accelerometer axis)
w.r.t.	with respect to

8. APPENDIX A: VALUES OF THE GGT CONSIDERED FOR THE CALIBRATION ANALYSES

The GGT components in the Local Orbital Reference Frame LORF (Table A1) have been obtained from the processing of the GGT time histories in the LORF generated along the GOCE orbit (250 km mean altitude) for a period of 6 months, using the gravity field model EGM96 complete up to degree and order 360.

The GGT components in the Gradiometer Reference Frame GRF (Table A2) have been obtained from the GGT components in the LORF, considering the following mispointing angles and angle stability of the GRF in the LORF:

$$\varphi_{\max} = 4^\circ \text{ (roll)}, \theta_{\max} = 1^\circ \text{ (roll)}, \psi_{\max} = 4^\circ \text{ (roll)}$$

$$\varphi^w = 1 \cdot 10^{-5} \text{ rad/Hz}^{1/2}, \theta^w = 1 \cdot 10^{-5} \text{ rad/Hz}^{1/2}, \psi^w = 1 \cdot 10^{-5} \text{ rad/Hz}^{1/2}.$$

In addition, a 30% margin has been applied to the maximum spectral density value in the MBW of the GGT components so obtained and a value of 10 mE/ $\sqrt{\text{Hz}}$ has been assumed (very conservatively) for the spectral density in the upper part of the MBW (above 50 mHz).

The values of the GGT in the GRF are those utilised for the calibration analyses.

	U_{XX}	U_{YY}	U_{ZZ}	U_{XY}	U_{XZ}	U_{YZ}
Mean value [E]	-1374.69	-1372.71	2747.40	$1.035 \cdot 10^{-5}$	$2.463 \cdot 10^{-4}$	$4.171 \cdot 10^{-3}$
U_{ij}^0 [E] ⁽¹⁾	1388.42	1384.52	2772.80	0.879	16.81	2.39
\tilde{U}_{ij}^w [mE/ $\sqrt{\text{Hz}}$] ⁽²⁾	1228.97	896.49	1858.76	673.57	1423.30	1129.02
\tilde{U}_{ij}^{HW} [mE/ $\sqrt{\text{Hz}}$] ⁽³⁾	< 1	< 1	< 1	< 1	< 1	< 1

⁽¹⁾ maximum value (in modulus) of U_{ij} in the low frequency region outside the measurement bandwidth (from DC to 5 mHz)

⁽²⁾ maximum value of the SD of U_{ij} in the MBW (5 to 100 mHz).

⁽³⁾ maximum value of the SD of U_{ij} in the upper part of the MBW (50 to 100 mHz).

Table A1: Reference GGT characteristics in the LORF

	U_{XX}	U_{YY}	U_{ZZ}	U_{XY}	U_{XZ}	U_{YZ}
U_{ij}^0 [E] ⁽¹⁾	1400	1400	2800	200	110	410
\tilde{U}_{ij}^w [mE/ $\sqrt{\text{Hz}}$] ⁽²⁾	1600	1200	2400	900	1900	1650
\tilde{U}_{ij}^{HW} [mE/ $\sqrt{\text{Hz}}$] ⁽³⁾	10	10	10	10	10	10

⁽¹⁾ maximum value (in modulus) of U_{ij} in the low frequency region outside the measurement bandwidth (from DC to 5 mHz)

⁽²⁾ maximum value of the SD of U_{ij} in the MBW (5 to 100 mHz) – a 30% margin w.r.t. the computed values has been applied here.

⁽³⁾ maximum value of the SD of U_{ij} in the upper part of the MBW (50 to 100 mHz) – a large margin w.r.t. to the computed values has been applied here.

Table A2: Reference GGT characteristics in the GRF (utilised for the calibration analyses)

9. APPENDIX B: NUMERICAL SIMULATIONS

9.1 NUMERICAL SIMULATIONS OF THE QUADRATIC FACTOR MEASUREMENT PROCEDURE

The 6-DoF Accelerometer model has been modified in order to support the simulation of the Lamarre test, i.e. the capability of estimating K2 using the strategy suggested by Daniel Lamarre with the DFAC output channel:

- the quadratic factor has been introduced at the level of the position sensor detector (see Figure 9.1-1) through a voltage offset $V_{i0} = K_{DETi} \cdot x_{i0}$, which mimics a unitary K2 for each electrode pair. The offset is multiplied by a gain $K2_i$, in order to have different K2 values for different axes, and by a global **K2 insertion gain**, which permits K2 switching on/off. The voltage offset for a unitary K2 is $G_{eli} \cdot V_p \cdot e_i \cdot K_{deti}$. The values adopted within the simulations are $K2_x = K2_z = 0$, $K2_y = 1$ and **K2 = 1** respectively.
- the Lamarre's signal (see Figure 9.1-2) has been added to the electrode voltages at the level of the DSP, after the PID network block, and after the digital processing of the DFAC. This train of pulses is obtained multiplying the output of a sinusoidal function generator (amplitude corresponding to 10^{-5} m/s^2 and frequency=100 Hz) by the output of a trapezoidal shaped pulse generator, with unitary amplitude, frequency=0.05 Hz, width=50% and trapezoid rising/falling time = 0 or 0.4 s. The train of pulses is then multiplied by the output of a signal inverter, which is a square wave generator with unitary amplitude and frequency=0.025 Hz

The position sensor detectors and DVAs are implemented as pure gains. The PID frequency adopted for the simulations is 1 kHz. The external loop frequency is 2 kHz, in order to implement the ADC1 delay of 1.5 ms. The DFAC channel is nominally implemented, with the 3rd order Butterworth filter ($f_c = 9.2 \text{ Hz}$), the FIR moving average filter, and the decimation @10 Hz for the US-axis.

A first set of two simulations spanning 600 s has been performed with the following boundary conditions:

- ✓ PID frequency = 1000 Hz
- ✓ External loop frequency = 2000 Hz
- ✓ ADC1 delay = 1.5 ms
- ✓ Accelerometer noise sources switched off
- ✓ No external accelerations
- ✓ Lamarre's signal insertion point after the DFAC output digital processing
- ✓ AC signal amplitude corresponding to 10^{-5} m/s^2 and $f_{AC} = 100 \text{ Hz}$
- ✓ $K2_y = 1$
- ✓ Trapezoidal Signal amplitude = 1, $f_{TS} = 0.05 \text{ Hz}$, pulse width = 50%

The two simulations differ for the rising/falling time of the trapezoidal wave generator:

- the first simulation implements a rectangular pulse shape (rising/falling time of the trapezoidal signal generator = 0 s), i.e. there is not the trapezoidal signal
- the second simulation implements a rising/falling time = 0.4s, i.e. a proper trapezoidal signal

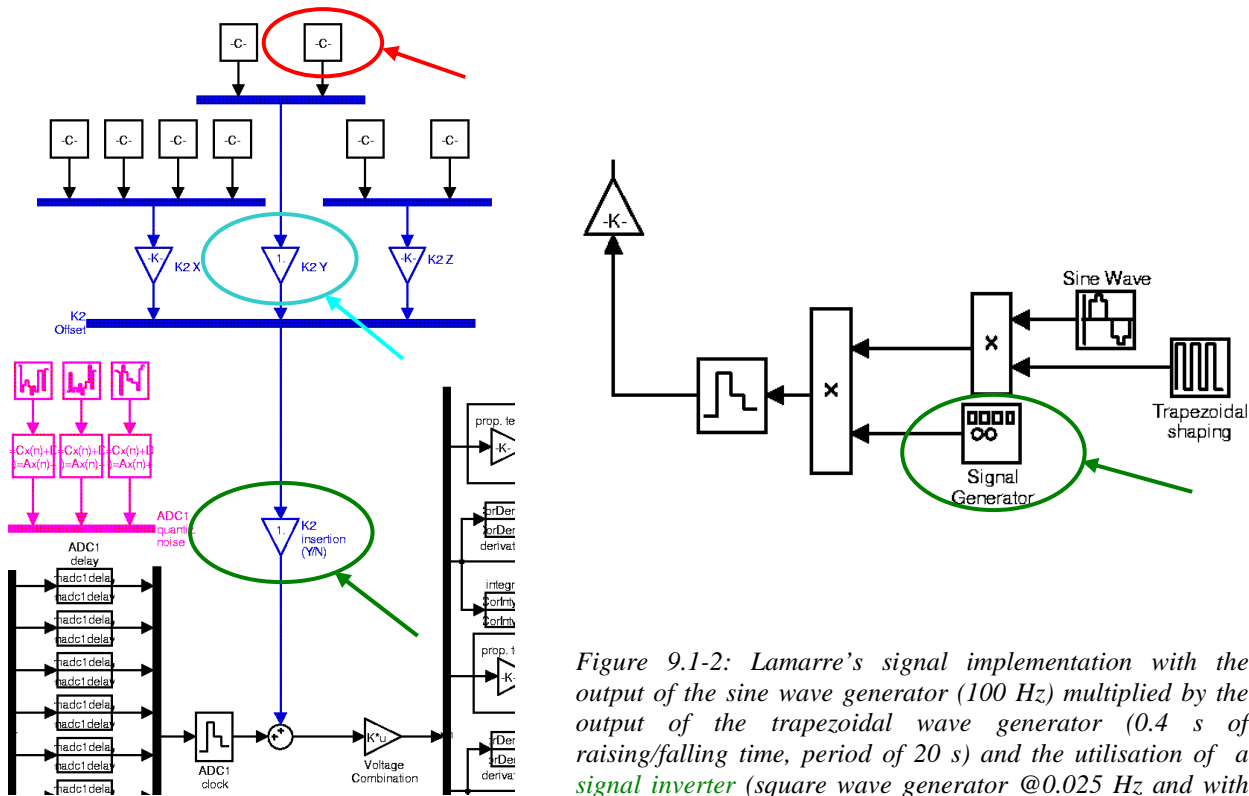


Figure 9.1-2: Lamarre's signal implementation with the output of the sine wave generator (100 Hz) multiplied by the output of the trapezoidal wave generator (0.4 s of raising/falling time, period of 20 s) and the utilisation of a **signal inverter** (square wave generator @0.025 Hz and with unitary amplitude)

Figure 9.1-1: Quadratic Term Implementation with unitary K2 offset voltages, K2 gains and K2 on/off switch

The signal that feeds the Butterworth filter of the DFAC channel has been saved as output of the accelerometer model. This signal, which is a 1 kHz voltage, demonstrates the effectiveness of the trapezoidal shape of the pulse with respect to the rectangular shape: it makes negligible the peaks at the pulse ending points (see Figure 9.1-3 and 9.1-4)

The difference in the DFAC output, @10 Hz, between the adoption of a pure rectangular shape or of a trapezoidal one for the 0.05 Hz pulse is shown in Figure 9.1-5 and 9.1-6. The trapezoidal shape reduces the amplitude of the spikes around the 0.05 Hz pulse edges by a factor close to 100.

The “cleaning” action due to the trapezoidal shape is also transparent when the amplitude spectrum of the DFAC y acceleration is computed for both the simulations, as shown in Figure 9.1-7 and 9.1-8. The K2 amplitude, @0.05 Hz, is a little peak among huge peaks in case of rectangular shape, and its measurement is feasible only due to the frequency separation produced from the sign inversion of the pulse signal. Instead, the K2 amplitude is the dominant peak below 0.1 Hz in case the trapezoidal shape is used for the pulse signal.

The amplitude @0.05 Hz of the y-acceleration is $A_{AC} = 3.1422 \cdot 10^{-11} \text{ m/s}^2$ in case of rectangular shape of the pulse and $A_{AC} = 3.1818 \cdot 10^{-11} \text{ m/s}^2$ in case of trapezoidal shape. The measured K2 is so:

- $K2 = 0.98715$, $\Delta K2 = 1.285 \cdot 10^{-2}$ in case of rectangular shape of the pulse
- $K2 = 0.99959$, $\Delta K2 = 4.1 \cdot 10^{-4}$ in case of trapezoidal shape of the pulse

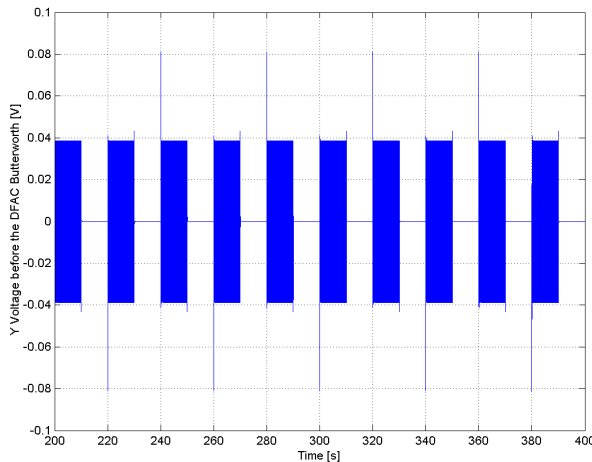


Figure 9.1-3: Y Voltage @1 kHz before DFAC Butterworth filtering with 0.05 Hz rectangular pulse: there is a peak at each pulse ending point

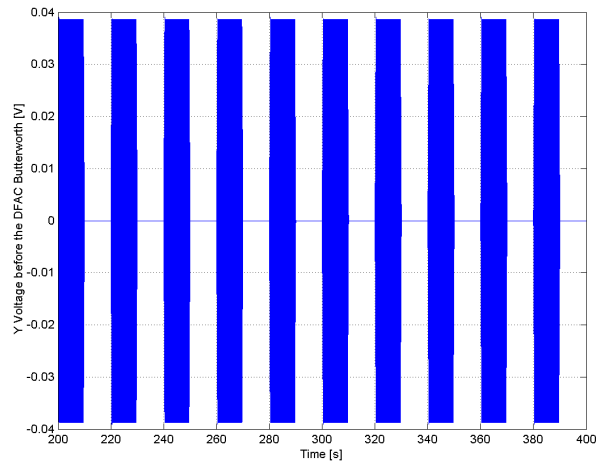


Figure 9.1-4: Y Voltage @1 kHz before DFAC Butterworth filtering with 0.05 Hz trapezoidal pulse: there are no peaks

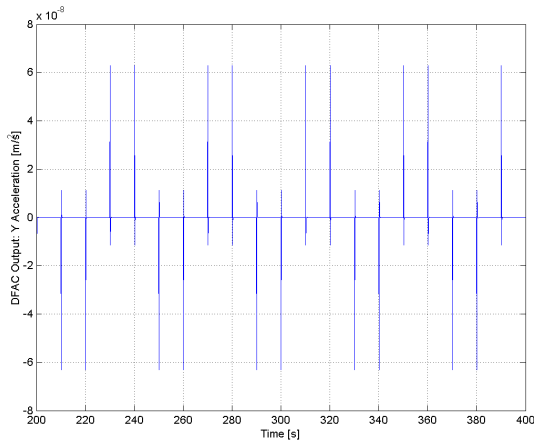


Figure 9.1-5: Y Acceleration of the DFAC Output Channel (rectangular shape of the pulse)

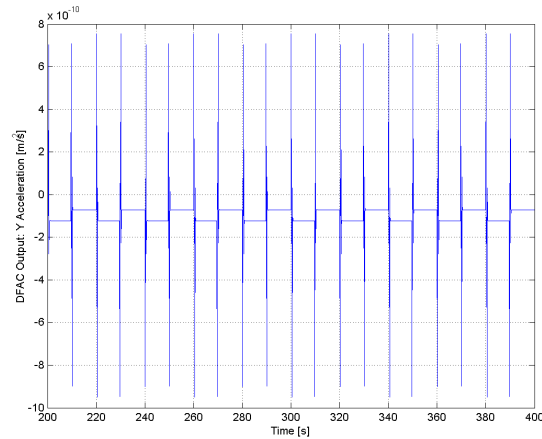


Figure 9.1-6: Y Acceleration of the DFAC Output Channel (trapezoidal shape of the pulse)

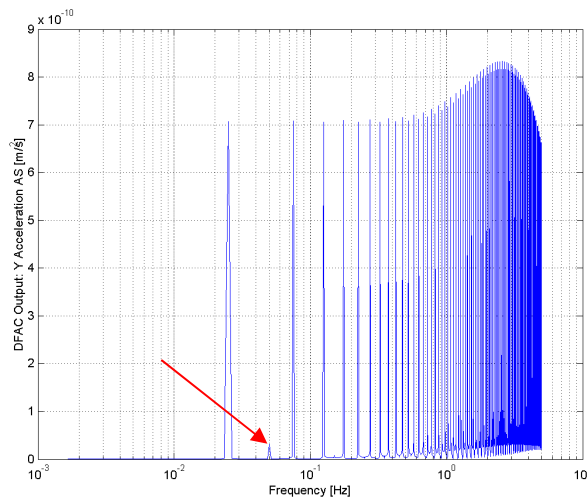


Figure 9.1-7: Amplitude Spectrum of the Y Acceleration of the DFAC Output Channel (rectangular shape of the pulse). K2 signal @0.05 Hz.

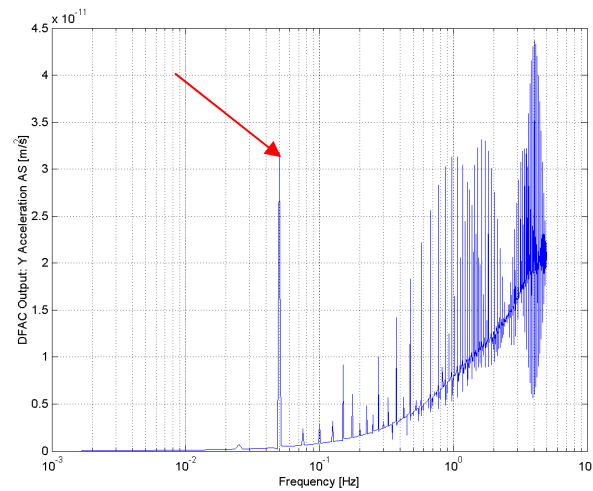


Figure 9.1-8: Amplitude Spectrum of the Y Acceleration of the DFAC Output Channel (trapezoidal shape of the pulse). K2 signal @0.05 Hz.

Note that the K2 retrieval without trapezoidal shape of the pulse is sensitive to the insertion point of the Lamarre's signal. If the insertion point is between the PID network and the DFAC digital processing, the amplitude @0.05 Hz is dominant below 0.1 Hz; if the signal is added after the DFAC digital processing, the amplitude @0.05 Hz is about 20 time smaller than the other components below 0.1 Hz.

The trapezoidal shape of the pulse makes the amplitude @0.05 Hz dominant below 1 Hz and mostly invariant with respect to the insertion point of the Lamarre's signal.

A simulation has been carried out with time spans of 8000 s, in order to check the accuracy of the K2 measurement. The boundary conditions are the same of the previous simulations, but with all the noise sources (parasitic noise, position sensor noise, ADC1, DAC, DVA, ADC2 and polarisation noise) switched on. As for the previous simulations the Lamarre's signal has been added after the DFAC digital processing. The trapezoidal shape of the pulse is applied. The amplitude A_{AC} @0.05 Hz and the retrieved K2 value is:

- Simulation spanning 8000 s with trapezoidale shape of the pulse and sign inversion. $A_{AC} = 3.2187 \cdot 10^{-11} \text{ m/s}^2$, $K2 = 1.01118$ and $\Delta K2 = 1.1 \cdot 10^{-2}$

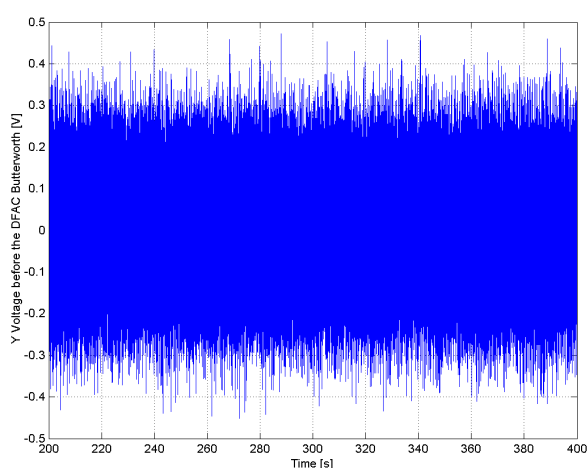


Figure 9.1-9: Y Voltage @1 kHz before DFAC Butterworth filtering with Lamarre's signal added after the DFAC branch

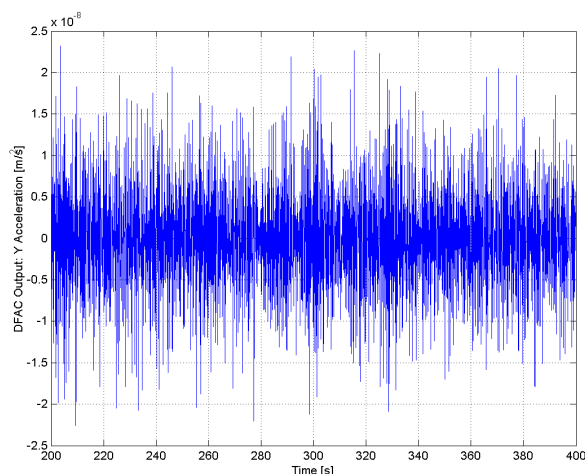


Figure 9.1-10: Y Acceleration @10 Hz of the DFAC Output Channel with Lamarre's signal added after the DFAC branch

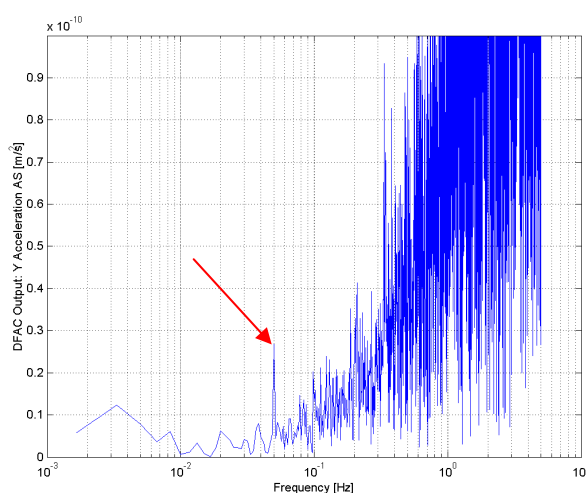


Figure 9.1-11: Amplitude Spectrum of the Y Acceleration of the DFAC Output Channel with Lamarre's signal added after the DFAC branch. K2 signal @0.05 Hz.

Figure 9.1-9 shows the time series of the Y voltage @1 kHz before the Butterworth filtering in the DFAC channel: it is the same of Figure 9.1-4, but with the noise.

Figure 9.1-10 represents the time series of the DFAC output for the Y US-axis (@10 Hz), and is the same of figure 9.1-6, but with noise.

Figure 9.1-11 shows the amplitude spectrum of the DFAC Y acceleration, and the red arrow points to the amplitude of the K2 signal, which is clearly identified and still dominant below 0.1 Hz also in presence of the noise.

The signal sign inversion and the trapezoidal shape of the pulse make the retrieval of the K2 value effective also in presence of all the inner noise sources. The capability of the DFAC channel for the K2 retrieval has been so demonstrated at the level of the accelerometer.

9.1.1 E2E Simulations of the Quadratic Factor Measurement Procedure

The procedure for the determination of the K2 has been tested by means of numerical simulations performed with the E2E GOCE System Simulator. The initial uncalibrated values for the K2 affecting the gradiometer are reported in the Table 9.1-1.

	GARF X		GARF Y		GARF Z	
	Initial K2 [s ² /m]	Axis type	Initial K2 [s ² /m]	Axis type	Initial K2 [s ² /m]	Axis type
ASH1	-1200.3	US	0.1	LS	120.9	US
ASH2	120.7	US	720.2	US	0.1	LS
ASH3	120.4	US	0.7	LS	-720.4	US
ASH4	-800.1	US	0.9	LS	120.6	US
ASH5	120.9	US	-1021.0	US	0.7	LS
ASH6	-120.4	US	0.1	LS	-1200.6	US

Table 9.1-1: Initial (uncalibrated) K2 values used to simulate the calibration procedure.

The duration of each proof mass shaking (along US-axes only) has been programmed according to the Table 9.1-2.

Excited sensor (K2_ASH)	Excited sensor axis		Measured Quadratic Factor (in ARF)	Utilised combination of measured DFACS accelerations (a_{mix})	Square-wave period (T_s) [s]	Shaking total duration (T) [s]	Number of square-wave cycles repetition (K2_NS)
	in AESRF (K2_DOE)	in ARF					
A ₁	Z _e axis	X ₁ axis	K _{2,1,X}	$a_{d,14,X}$	20	5200	260
A ₄	Z _e axis	X ₄ axis	K _{2,4,X}	$-a_{d,14,X}$	20	5200	260
A ₁	Y _e axis	Z ₁ axis	K _{2,1,Z}	$a_{d,14,Z} + \frac{L_X}{L_Z} a_{d,36,X}$	20	900	45
A ₄	Y _e axis	Z ₄ axis	K _{2,4,Z}	$-a_{d,14,Z} - \frac{L_X}{L_Z} a_{d,36,X}$	20	900	45
A ₂	Y _e axis	X ₂ axis	K _{2,2,X}	$a_{d,25,X} + \frac{L_Y}{L_X} a_{d,14,Y}$	20	1700	85
A ₅	Y _e axis	X ₅ axis	K _{2,5,X}	$-a_{d,25,X} - \frac{L_Y}{L_X} a_{d,14,Y}$	20	1700	85
A ₂	Z _e axis	Y ₂ axis	K _{2,2,Y}	$a_{d,25,Y}$	20	200	10
A ₅	Z _e axis	Y ₅ axis	K _{2,5,Y}	$-a_{d,25,Y}$	20	200	10
A ₃	Y _e axis	X ₃ axis	K _{2,3,X}	$a_{d,36,X} + \frac{L_Z}{L_X} a_{d,14,Z}$	20	800	40
A ₆	Y _e axis	X ₆ axis	K _{2,6,X}	$-a_{d,36,X} - \frac{L_Z}{L_X} a_{d,14,Z}$	20	800	40
A ₃	Z _e axis	Z ₃ axis	K _{2,3,Z}	$a_{d,36,Z}$	20	200	10
A ₆	Z _e axis	Z ₆ axis	K _{2,6,Z}	$-a_{d,36,Z}$	20	200	10
Total shaking duration for the calibration of all the quadratic factors						18000	

Table 9.1-2: Quadratic factors measurement: duration of shaking and number of square-wave periods used for each DoF shaking.

Two runs of K2 calibrations have been carried out in order to measure quadratic factors below the required value ($K2 < 3 \text{ s}^2/\text{m}$ for the in-line US-axes and $K2 < 9 \text{ s}^2/\text{m}$ for the transverse US-axes). The timetable of each shaking phase applied during the simulation is reported in Table 9.1-3. The proof mass shaking durations are those established in section 4.2.2 and listed in Table 4.2-3.

Excited ASH	AESRF axis	ARF axis	Measured K2	Shaking Initial time	Shaking final time
A ₁	Z _e axis	X ₁ axis	K _{2,1,X}	5000	10200
A ₁	Y _e axis	Z ₁ axis	K _{2,1,Z}	10220	11120
A ₂	Y _e axis	X ₂ axis	K _{2,2,X}	11140	12840
A ₂	Z _e axis	Y ₂ axis	K _{2,2,Y}	12860	13060
A ₃	Y _e axis	X ₃ axis	K _{2,3,X}	13080	13880
A ₃	Z _e axis	Z ₃ axis	K _{2,3,Z}	13900	14100
A ₄	Z _e axis	X ₄ axis	K _{2,4,X}	14120	19320
A ₄	Y _e axis	Z ₄ axis	K _{2,4,Z}	19340	20240
A ₅	Y _e axis	X ₅ axis	K _{2,5,X}	20260	21960
A ₅	Z _e axis	Y ₅ axis	K _{2,5,Y}	21980	22180
A ₆	Y _e axis	X ₆ axis	K _{2,6,X}	22200	23000
A ₆	Z _e axis	Z ₆ axis	K _{2,6,Z}	23020	23220

Table 9.1-3: E2E accelerometer shaking timetable used for the simulations: starting and final time for each calibrated US-axis.

The K2 measured values after the first and second measurement-correction iterations are reported in the tables below. Table 9.1-4 shows the results of the first K2 measurement. A second K2 measurement has been then carried out, after the application of the compensating voltage offset derived from the first run. Table 9.1-5 shows that all the new measured K2 are below the specified limits. In principle, a further correction/measurement iteration cannot be excluded in case of very large initial K2 values.

	ARF X		ARF Y		ARF Z	
	Measured K2 [s ² /m]	Compensating offset [V]	Measured K2 [s ² /m]	Compensating offset [V]	Measured K2 [s ² /m]	Compensating offset [V]
ASH1	-1163.6	4.41	Not measured	Not measured	116.9	-0.44
ASH2	111.8	-0.42	692.7	-2.63	Not measured	Not measured
ASH3	119.3	-0.45	Not measured	Not measured	-693.2	2.63
ASH4	-777.6	2.95	Not measured	Not measured	112.4	-0.43
ASH5	117.7	-0.45	-985.3	3.74	Not measured	Not measured
ASH6	-112.6	0.43	Not measured	Not measured	-1159.7	4.40

Table 9.1-4: Results of the first K2 in-flight measurement performed with the E2E simulator.

	ARF X		ARF Y		ARF Z	
	Measured K2 [s ² /m]	Compensating offset [V]	Measured K2 [s ² /m]	Compensating offset [V]	Measured K2 [s ² /m]	Compensating offset [V]
ASH1	-1.0	0.004	Not measured	Not measured	0.1	0.000
ASH2	-3.8	0.014	0.9	-0.003	Not measured	Not measured
ASH3	0.1	0.000	Not measured	Not measured	-0.9	0.003
ASH4	-0.7	0.002	Not measured	Not measured	0.2	0.000
ASH5	-0.7	0.002	-1.3	0.005	Not measured	Not measured
ASH6	-0.5	0.002	Not measured	Not measured	-1.4	0.005

Table 9.1-5: Results of the second K2 in-flight measurement performed with the E2E simulator.

9.2 NUMERICAL SIMULATIONS OF THE ICM MEASUREMENT PROCEDURE

The method for the determination of the ICM has been tested by means of numerical simulations performed with the E2E GOCE System Simulator.

The parameters which define the simulation cases are listed in the Table 9.2-1, together with the values or range of values assumed by these parameters in the simulations.

Twenty cases simulating a one-day calibration period have been run with the spacecraft controlled by the DFACS as in the science mode, with an additional random shaking applied about each axis by the GCD and by the ion thruster.

Each test case stems from a different choice of the simulation parameters listed in the Table 9.2-1, as indicated in Table 9.2-2. The time series of the atmospheric perturbations is different in each case. When the epoch, altitude and solar activity parameters are kept unchanged, the random fluctuations of the air density are generated using different seeds in the Hickey model of the short-scale fluctuations of the air density. The measurement noise of the star tracker and of the gradiometer, the actuation noise of the ion thruster and of the cold-gas thrusters are generated with different seeds from case to case. The imperfections applied to the gradiometer are different from case to case. Three different satellite shaking profiles by means of the GCD are used.

The spectral densities of the common-mode and differential-mode accelerations experienced by the accelerometer pairs in this condition are provided in Figure 9.2-1a, b and c.

A coupling factor between the angular and linear accelerations at accelerometer level has been introduced by using different values for the electrostatic gains of the various electrode pairs, corresponding to different values of the gaps. The effect of this coupling can be then (partially) recovered in the calibration data post processing by assuming a given knowledge of the electrostatic gains (corresponding to the knowledge of the differential value of the gaps), as expected from the ground measurements. The effectiveness of this partial recovering of the linear-angular coupling has been extensively analysed by applying the calibration post processing two times:

- first set of ICMs by adopting the nominal values of the electrostatic gains
- second set of ICMs by using the measured electrostatic gains

For each of the 20 test cases described in the Table 9.2-1 and Table 9.2-2 of any simulations set the quantity:

$$\Gamma_{ij_{kl}} = \frac{MI_{ij_{kl}}^{\text{Measured}} - MI_{ij_{kl}}^{\text{True}}}{\text{Accuracy } ij_{kl}}$$

expressing the ratio between the determination error of the elements of the ICMs and their required accuracy (Table 3.3-7) has been computed.

If $\Gamma_{ij_{kl}} \leq 1$, the element $ICM_{ij_{kl}}$ is retrieved with an accuracy \leq than the specification.

If $\Gamma_{ij_{kl}} > 1$, the element $ICM_{ij_{kl}}$ is retrieved with an accuracy exceeding the specification by a factor $\Gamma_{ij_{kl}}$.

For each of the three simulations sets of 20 calibration runs each, the following results are provided in the following sections:

- Mean value of $\Gamma_{ij_{kl}}$, computed over the 20 cases
- Standard deviation of $\Gamma_{ij_{kl}}$, computed over the 20 cases
- Maximum value of $\Gamma_{ij_{kl}}$, computed over the 20 cases

N.	Parameter description	Values/Range	Note
Mission parameters			
1	Epoch of the in-flight calibration (EPC)	15 October 2006, UTC 0:0:0 (EPC1) 15 October 2008, UTC 0:0:0 (EPC2)	EPC1: epoch inside POP1 for a launch in July 2006
2	Orbit mean spherical altitude (ALT)	240 km, 250 km, 260 km	Geodetic alt. \approx ALT +10 km
3	Solar activity parameter probability level (SAP)	SAP = 95%, = 50% (for F10.7, Ap)	Prediction probability level
4	Sun-synchronous orbit type (SSO)	Dusk-Dawn (DuDa) Dawn-Dusk (DaDu)	DuDa: Summer launch DaDu: Winter launch
5	Duration of the simulation mission (SIM)	1 to 5 days (1 day in calibration)	In order to use calibration

		mode + 4 days in science mode)	results in science data proc.
Satellite shaking actuators and attitude internal perturbations parameters			
6	Shaking profile with ion thruster (SHI)	Shaking acc. with $= 10^{-6} \text{ m/s}^2/\text{Hz}^{1/2}$ rectangular SD in 50÷100 mHz band	Shaking profiles pre-computed with 1 s time step
7	Shaking profile with cold-gas thruster (SHC)	Three different random shaking with $F_{\max} = 400 \text{ } \mu\text{N}$ (SHC1), $600 \text{ } \mu\text{N}$ (SHC2), $800 \text{ } \mu\text{N}$ (SHC3)	Shaking profiles pre-computed with 1 s time step
8	Ion thruster force noise (ITN)	Noise SD $= 5 \text{ mN/Hz}^{1/2}$ flat below 2 mHz, 1/f up to 0.3 Hz, flat above	Upper limit of the specified force noise SD
9	Ion thruster misalignment (ITM)	Rotations about Y, Z: $\alpha_Y = \alpha_Z = 0.4^\circ$	Rotations applied together
10	Cold-gas thruster noise (CTN)	Force noise $= 60 \text{ } \mu\text{N}$ 1σ (gaussian)	10% of mid range force.
11	Residual magnetic dipole (RMD)	1 Am^2 about each axis	After compensation
Star trackers parameters			
12	Star tracker utilised (STR)	STR1, STR2, STR3	STR3 is the skewed STR
13	Star tracker measurement errors (STE)	Boresight axis: bias $= 1.65''$, noise $= 20''$ 1σ Transversal axes: bias $= 1.65''$, noise $= 2''$ 1σ	Currently predicted values. White gaussian noise model. Bias corresponding to internal misalignments.
14	Star tracker misalignments in the GRF (STM)	$ \phi , \theta , \psi \leq 4 \cdot 10^{-4} \text{ rad}$	Align. knowledge accuracy
Gradiometer/accelerometer parameters			
15	Accelerometer noise (ACN)	Acceleration noise SD $\leq 2 \cdot 10^{-12} \text{ m/s}^2/\text{Hz}^{1/2}$ (US axis), $\leq 3 \cdot 10^{-10} \text{ m/s}^2/\text{Hz}^{1/2}$ (LS axis) in the MBW	Noise generated according the predicted SD profile from the current budget
16	Accelerometer bias (ACB)	Acceleration bias $= 1.3 \cdot 10^{-7} \text{ m/s}^2$ (US axis), $= 1.7 \cdot 10^{-5} \text{ m/s}^2$ (LS axis)	Values specified for US axis, predicted for LS axis
17	Accelerometer scale factor (ASF)	Scale factor: $K = 1 + \delta K$, $ \delta K \leq 4.05 \cdot 10^{-3}$ (US axis), $ \delta K \leq 5.18 \cdot 10^{-2}$ (LS axis)	Generated for the 6 sensors as random numbers with uniform distribution
18	ARF misalignment in the OAGRF (AFM)	Misalignment angles: $ \phi \leq 1.3 \cdot 10^{-4} \text{ rad}$, $ \theta \leq 1.3 \cdot 10^{-4} \text{ rad}$, $ \psi \leq 1.3 \cdot 10^{-4} \text{ rad}$	Generated for the 6 sensors as random numbers with uniform distribution
19	Coupling among accelerometer axes (ACA)	Coupling factors: $ \zeta \leq 1.0 \cdot 10^{-5} \text{ rad}$, $ \eta \leq 1.0 \cdot 10^{-5} \text{ rad}$, $ \epsilon \leq 1.0 \cdot 10^{-5} \text{ rad}$	Generated for the 6 sensors as random numbers with uniform distribution
20	Accelerometer quadratic factor (AK2)	$K2 \leq 7 \text{ s}^2/\text{m}$ (in-line US axis) $K2 \leq 20 \text{ s}^2/\text{m}$ (transversal US axis) $K2 \leq 3 \text{ s}^2/\text{m}$ (LS axis)	After in-flight adjustment. K2 values generated as random numbers (uniform).
21	ARF position offset in the OAGRF (AFO)	Position offset of each accelerometer along the baseline: $ \Delta_B \leq 25 \text{ } \mu\text{N}$	Corresponding to the max. error on baseline knowledge
22	OAGRFs centres offset in the GRF (OCO)	OAGRFs centres offset from GRF origin: $ \Delta_i \leq 30 \text{ } \mu\text{N}$ ($i = X, Y, Z$)	Corresponding to the max. error on OAGs centering
23	OAGRFs misalignments in the GRF (OGM)	Misalignment angles: $ \phi \leq 2.23 \cdot 10^{-4} \text{ rad}$, $ \theta \leq 2.23 \cdot 10^{-4}$, $ \psi \leq 2.23 \cdot 10^{-4} \text{ rad}$	Maximum misalignment
24	GRF offset from the satellite COM (GOC)	$ \Delta_X \leq 15 \text{ cm}$, $ \Delta_Y \leq \Delta_Z \leq 5 \text{ cm}$	Specified maximum offset
25	Angular/linear acceleration coupling (ALC)	Introduced with $ \Delta_{\text{gap}} \leq 2 \text{ } \mu\text{m}$	Recovered in ground proc.
26	Control of the accelerometer proof mass (PMC)	PMC1: 50%-50% control PMC2: 100% US transversal electro. PMC3: 100% US in-line electrodes	ω_X control distribution among the 4 US electrodes
27	Differential error on gap knowledge (DGK)	$\delta\epsilon_X \leq 0.04 \text{ } \mu\text{m}$ LS, $\delta\epsilon_{YZ} \leq 0.4 \text{ } \mu\text{m}$ US	Utilised in ground process.

Table 9.2-1: Simulation parameters

Simulation Parameters		Test case N.									
		1	2	3	4	5	6	7	8	9	10
1	EPC	EPC1	EPC1	EPC1	EPC1	EPC1	EPC1	EPC2	EPC2	EPC2	EPC2
2	ALT	240 km	240 km	250 km	250 km	250 km	250 km	250 km	250 km	260 km	260 km
3	SAP	95%	95%	95%	95%	95%	50%	95%	95%	95%	50%
4	SSO	DuDa	DuDa	DuDa	DuDa	DuDa	DuDa	DuDa	DuDa	DuDa	DuDa
5	SIM	1 day	1 day	1 day	1 day	1 day	1 day	1 day	1 day	1 day	1 day
7	SHC	SHC2	SHC2	SHC2	SHC1	SHC3	SHC1	SHC2	SHC3	SHC2	SHC1
12	STR	STR1	STR3	STR3	STR3	STR3	STR3	STR3	STR3	STR3	STR3
26	PMC	1a:PMC1 1b:PMC2 1c:PMC3	2a:PMC1 2b:PMC2 2c:PMC3	3a:PMC1 3b:PMC2 3c:PMC3	4a:PMC1 4b:PMC2 4c:PMC3	5a:PMC1 5b:PMC2 5c:PMC3	6a:PMC1 6b:PMC2 6c:PMC3	7a:PMC1 7b:PMC2 7c:PMC3	8a:PMC1 8b:PMC2 8c:PMC3	9a:PMC1 9b:PMC2 9c:PMC3	10a:PMC1 10b:PMC2 10c:PMC3

Simulation Parameters		Test case N.									
		11	12	13	14	15	16	17	18	19	20
1	EPC	EPC1	EPC1	EPC1	EPC1	EPC1	EPC1	EPC2	EPC2	EPC2	EPC2
2	ALT	240 km	240 km	250 km	250 km	240 km	260 km	250 km	250 km	260 km	260 km
3	SAP	95%	95%	95%	95%	95%	50%	95%	95%	95%	50%
4	SSO	DuDa	DuDa	DuDa	DuDa	DuDa	DuDa	DaDu	DaDu	DaDu	DaDu
5	SIM	1 day	1 day	1 day	1 day	1 day	1 day	1 day	1 day	1 day	1 day
7	SHC	SHC2	SHC2	SHC2	SHC1	SHC3	SHC1	SHC2	SHC3	SHC2	SHC1
12	STR	STR2	STR2	STR2	STR1	STR1	STR1	STR1	STR3	STR3	STR3
26	PMC	11a:PMC1 11b:PMC2 11c:PMC3	12a:PMC1 12b:PMC2 12c:PMC3	13a:PMC1 13b:PMC2 13c:PMC3	14a:PMC1 14b:PMC2 14c:PMC3	15a:PMC1 15b:PMC2 15c:PMC3	16a:PMC1 16b:PMC2 16c:PMC3	17a:PMC1 17b:PMC2 17c:PMC3	18a:PMC1 18b:PMC2 18c:PMC3	19a:PMC1 19b:PMC2 19c:PMC3	20a:PMC1 20b:PMC2 20c:PMC3

Table 9.2-2: Combination of the simulation parameters in the twenty test cases

The value of the other parameters not listed in Table 9.2.2 is randomly generated between the limits provided in Table 9.9-1 for all the 20 cases. The quantities ITM and RMD are kept constant for each case.

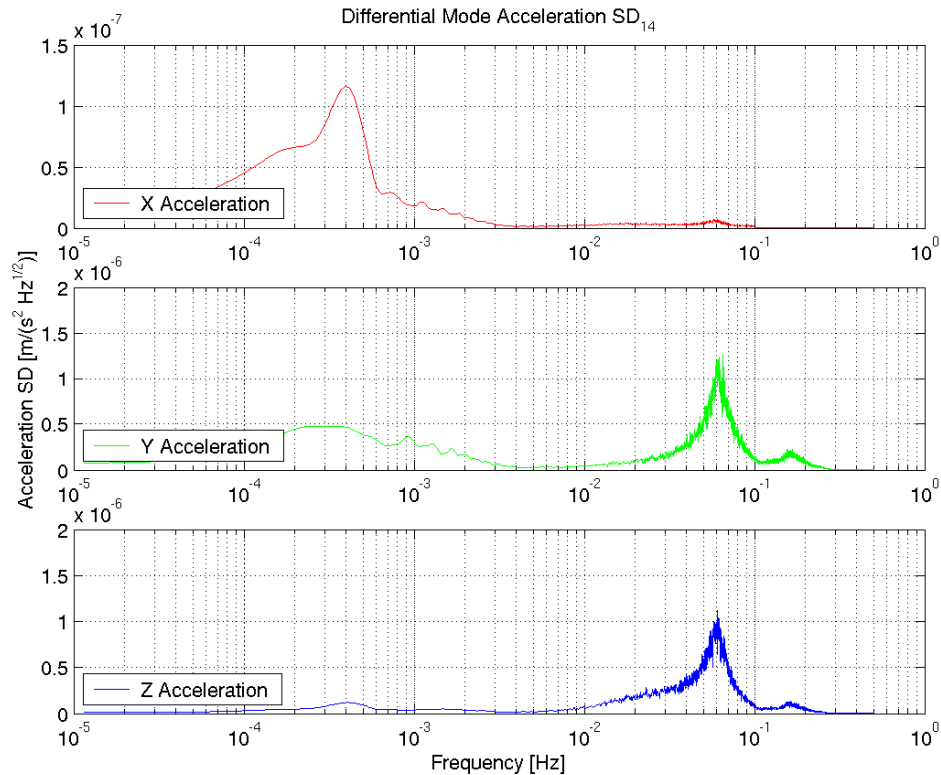
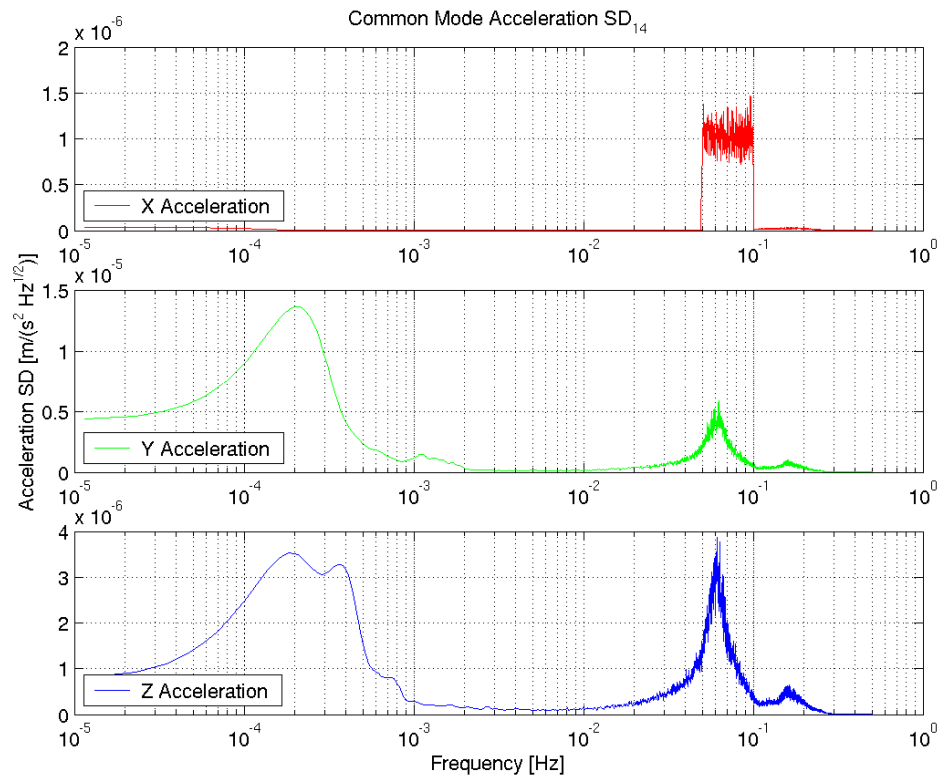


Figure 9.2-1a: Spectral densities of the common-mode and differential-mode accelerations of A_1 , A_4

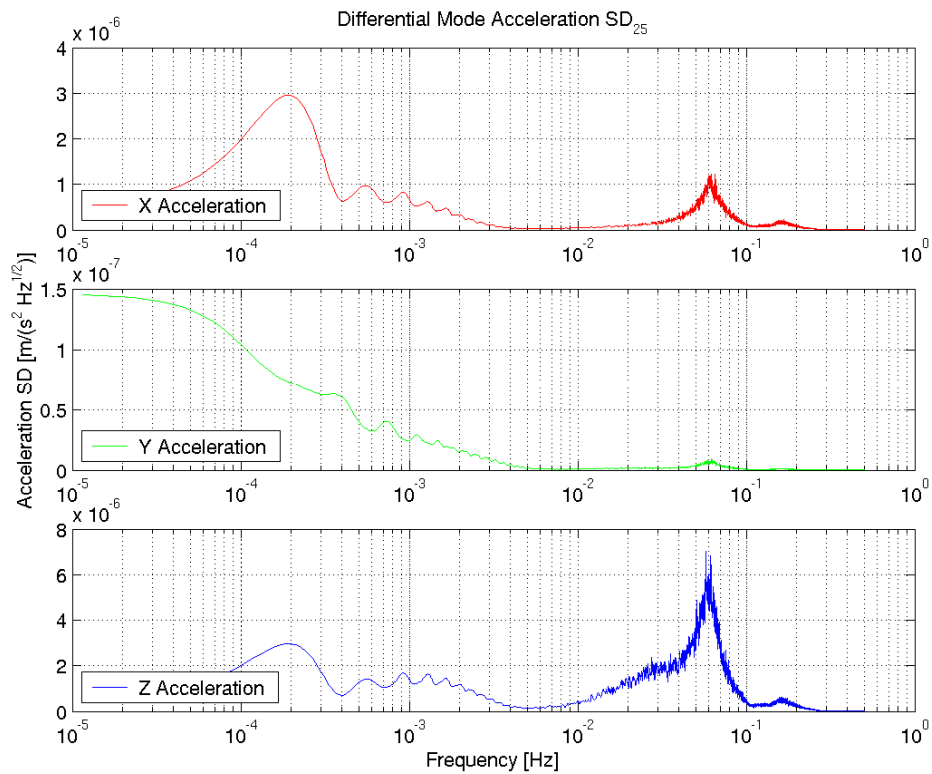
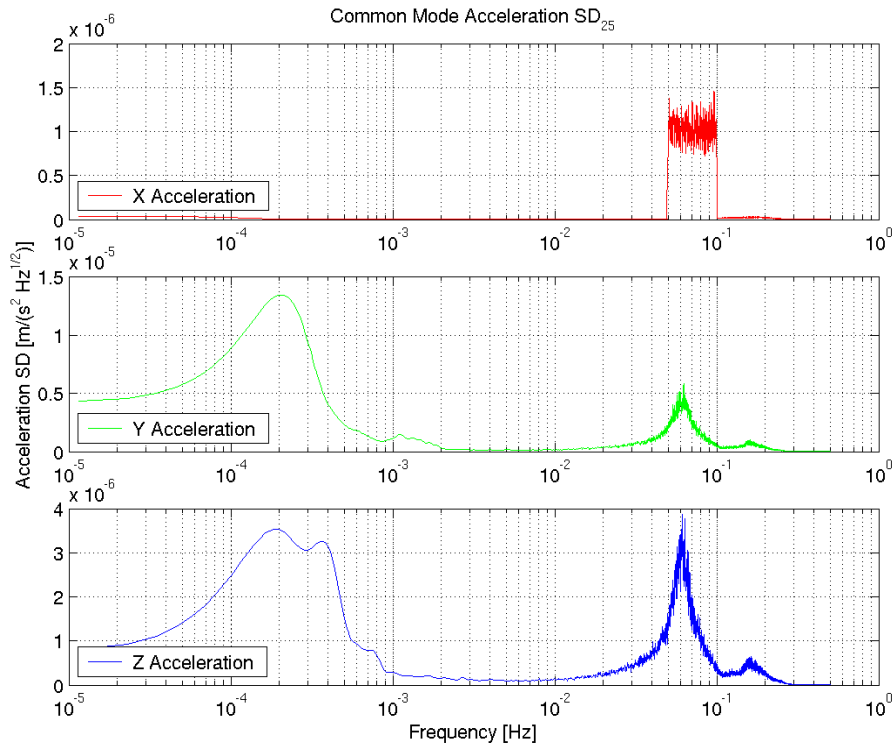


Figure 9.2-1b: Spectral densities of the common-mode and differential-mode accelerations of A_2 , A_5

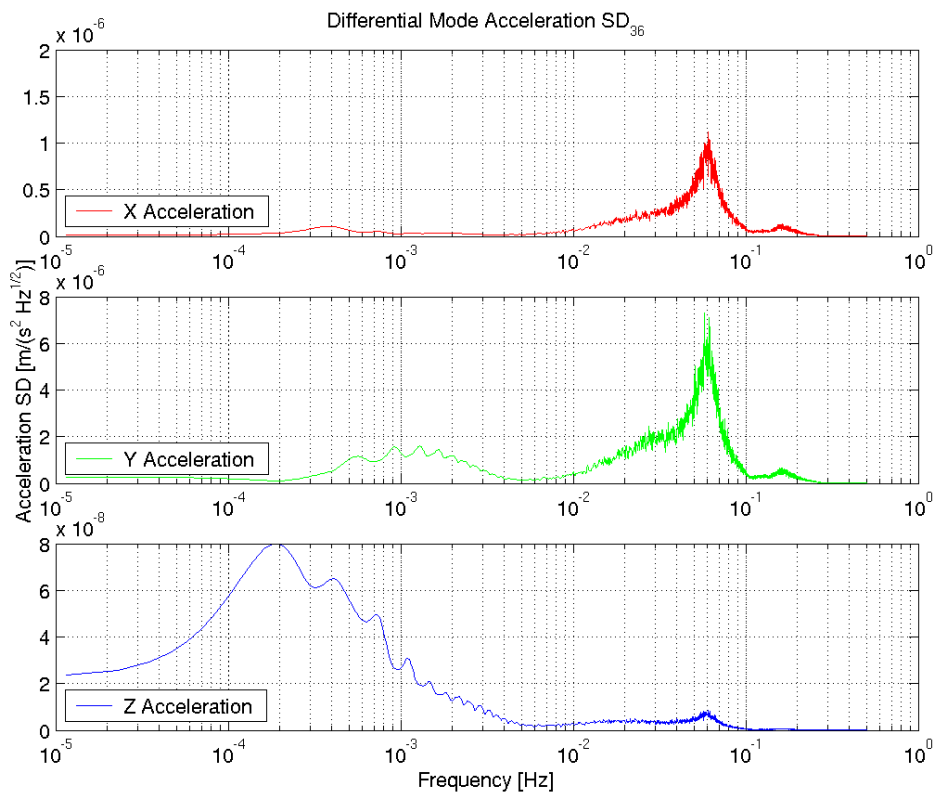
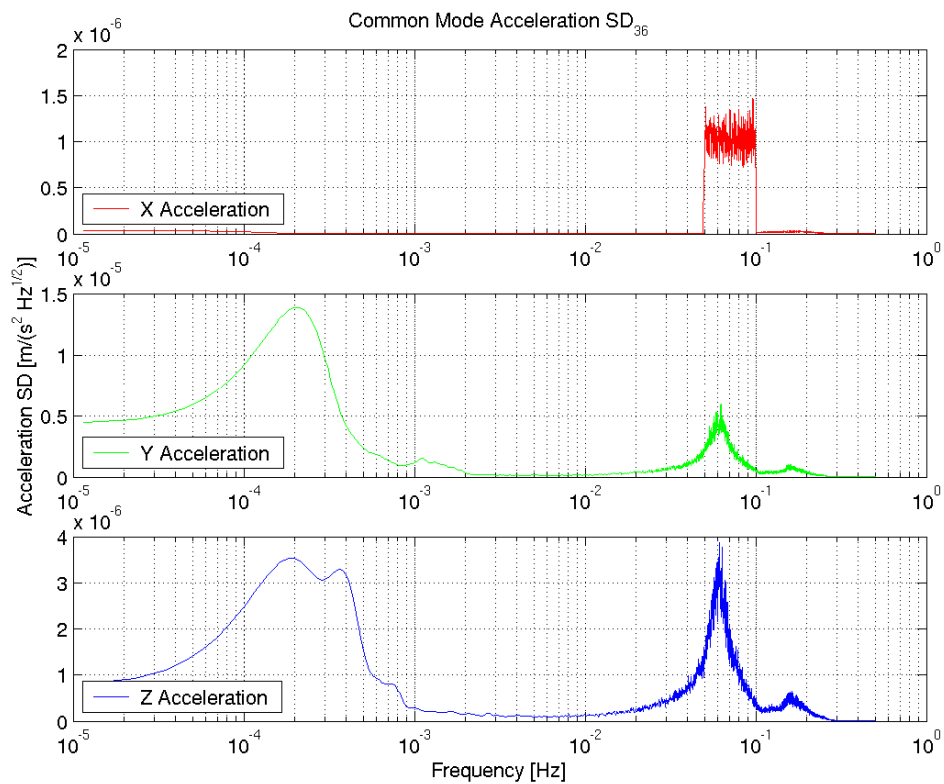


Figure 9.2-1c: Spectral densities of the common-mode and differential-mode accelerations of A_3 , A_6

9.2.1 Calibration Set 1 Results: retrieved ICMs using nominal electrostatic gains

The Set 1 of calibration results consisted in determining the ICM elements using the nominal values of the electrostatic gains in the post processing, i.e. the values that they are expected to have if all the accelerometer parameters were exactly as designed. The results of this processing are provided in Table 9.2.1-1 and shows, as expected, the effect of the linear-angular coupling in the Std and

Abs(Mean($\Gamma_{14_{kl}}$)) with nominal G_{el} gains					
0.156	0.032	0.153	0.304	0.001	0.056
0.045	0.513	0.032	0.055	0.077	0.033
0.063	0.157	0.117	0.060	0.021	0.316

Std($\Gamma_{14_{kl}}$) with nominal G_{el} gains					
1.017	0.081	0.868	0.580	0.052	2.328
0.117	0.808	0.430	0.231	0.239	0.098
0.273	1.047	0.336	1.310	0.101	0.597

Abs(Mean($\Gamma_{25_{kl}}$)) with nominal G_{el} gains					
0.058	0.062	0.042	0.084	0.548	0.001
0.156	0.089	0.003	0.551	0.553	0.016
0.007	0.023	0.286	0.006	0.085	0.060

Std($\Gamma_{25_{kl}}$) with nominal G_{el} gains					
0.145	0.088	0.502	1.162	3.893	0.093
1.049	1.468	0.055	3.834	1.006	0.049
0.494	0.129	1.086	0.084	0.206	0.181

Abs(Mean($\Gamma_{36_{kl}}$)) with nominal G_{el} gains					
0.039	0.153	0.073	0.352	0.027	0.496
0.052	0.274	0.007	0.023	0.051	0.017
0.139	0.023	0.050	0.449	0.030	0.306

Std($\Gamma_{36_{kl}}$) with nominal G_{el} gains					
0.279	1.062	0.275	0.620	0.088	2.642
0.462	1.336	0.162	0.071	0.194	0.302
0.844	0.058	1.847	2.728	0.053	0.535

Max(Abs($\Gamma_{14_{kl}}$)) with nominal G_{el} gains					
2.851	0.187	2.760	1.873	0.075	3.517
0.250	1.766	1.072	0.475	0.526	0.240
0.597	2.417	0.779	3.847	0.197	1.857

Max(Abs($\Gamma_{25_{kl}}$)) with nominal G_{el} gains					
0.296	0.181	1.153	1.919	7.342	0.153
2.750	2.951	0.091	6.841	2.773	0.075
1.053	0.256	2.513	0.151	0.459	0.303

Max(Abs($\Gamma_{36_{kl}}$)) with nominal G_{el} gains					
0.638	2.292	0.673	1.945	0.159	3.954
1.015	3.355	0.269	0.140	0.418	0.488
2.403	0.126	3.138	4.302	0.089	1.889

Table 9.2.1-1: Results of the calibration processing Set 1: nominal electrostatic gains applied and angular-linear coupling fully affecting the retrieved ICMs

9.2.2 Calibration Set 2 Results: retrieved ICMs using measured electrostatic gains

The Set 2 of calibration results consisted in determining the ICM elements using the “measured” values of the electrostatic gains in the post processing, i.e. exploits the knowledge of these elements provided by the on-ground characterisation of the accelerometers. The results of this processing are provided in Table 9.2.2-1 and shows, as expected, an improvement with respect to the previous case (the worst standard deviation value is now 1.53 vs 3.89 in case of nominal electrostatic gains adopted in the processing), which utilises nominal electrostatic gains, i.e. neglects any knowledge of these elements provided by the on-ground characterisation of the accelerometers.

Abs(Mean($\Gamma_{14_{kl}}$)) with measured G_{el} gains					
0.079	0.033	0.062	0.255	0.000	0.004
0.029	0.358	0.031	0.039	0.027	0.032
0.082	0.157	0.051	0.001	0.021	0.292

Std($\Gamma_{14_{kl}}$) with measured G_{el} gains					
0.451	0.071	0.347	0.528	0.051	0.941
0.130	0.627	0.443	0.257	0.139	0.097
0.278	1.047	0.327	0.929	0.101	0.541

Abs(Mean($\Gamma_{25_{kl}}$)) with measured G_{el} gains					
0.068	0.061	0.052	0.062	0.155	0.002
0.012	0.024	0.012	0.211	0.624	0.016
0.021	0.020	0.358	0.006	0.150	0.005

Std($\Gamma_{25_{kl}}$) with measured G_{el} gains					
0.154	0.090	0.433	0.726	1.498	0.094
0.422	1.182	0.059	1.530	0.897	0.049
0.450	0.136	0.628	0.084	0.166	0.103

Abs(Mean($\Gamma_{36_{kl}}$)) with measured G_{el} gains					
0.096	0.154	0.047	0.286	0.027	0.062
0.057	0.417	0.016	0.023	0.019	0.113
0.062	0.019	0.065	0.139	0.030	0.259

Std($\Gamma_{36_{kl}}$) with measured G_{el} gains					
0.267	1.063	0.302	0.513	0.088	1.027
0.438	0.684	0.161	0.071	0.139	0.234
0.354	0.051	1.390	1.081	0.053	0.478

Max(Abs($\Gamma_{14_{kl}}$)) with measured G_{el} gains					
1.499	0.172	1.140	1.677	0.073	1.535
0.249	1.522	1.072	0.474	0.362	0.237
0.567	2.417	0.713	2.046	0.197	1.747

Max(Abs($\Gamma_{25_{kl}}$)) with measured G_{el} gains					
0.360	0.272	1.082	1.741	2.811	0.153
0.156	1.350	0.114	2.761	2.000	0.076
0.982	0.256	1.567	0.151	0.460	0.204

Max(Abs($\Gamma_{36_{kl}}$)) with measured G_{el} gains					
0.474	2.292	0.627	1.707	0.159	1.775
0.991	1.672	0.268	0.140	0.262	0.448
0.986	0.101	3.525	1.649	0.092	1.679

Table 9.2.2-1: Results of the calibration processing Set 2; angular-linear coupling partially recovered using the measured electrostatic gains

9.2.3 Impact of ASH1 misalignment on Calibration and Science Performance

Some simulations have been carried out in order to study the impact of the misalignment of the accelerometer that is going to replace the EGG ASH1 on the science performance, due to the degradation of the ICM retrieval. Three 6-days long different simulations have been carried out taking into account:

- “nominal” unknown accelerometer misalignment (about 0.15 mrad)
- “intermediate” unknown accelerometer misalignment (about 0.5 mrad)
- “worst case” unknown accelerometer misalignment (1 mrad)

The first day of each simulation has been devoted to perform the EGG calibration, by shaking the satellite, in order to retrieve the ICM for each different ASH1 misalignment scenario. The remaining 5 days of science of each simulation (together with the corresponding retrieved ICMs) have then been used to verify the science performance, by computing the Spectral Density of the GGT trace.

9.2.3.1 Performance with the Nominal ASH1 Misalignment

Table 9.2.3-1 shows the results of the calibration, with the processing based on the partial knowledge of the electrostatic gains (measured ones). The so retrieved ICMs have been used to compute the calibrated EGG acceleration, which feed the reconstruction of the GGT trace.

Abs($\Gamma_{14_{kl}}$) with measured G_{el} gains					
0.505	0.035	0.085	0.441	0.036	1.387
0.049	1.396	0.612	0.067	0.151	0.101
0.007	1.598	0.132	1.481	0.101	0.537

Abs($\Gamma_{25_{kl}}$) with measured G_{el} gains					
0.163	0.124	0.538	0.149	2.018	0.079
0.492	0.006	0.028	1.576	0.636	0.049
0.654	0.117	1.395	0.070	0.249	0.086

Abs($\Gamma_{36_{kl}}$) with measured G_{el} gains					
0.018	1.731	0.011	0.537	0.064	1.015
0.793	1.639	0.227	0.057	0.138	0.348
0.047	0.107	1.373	1.262	0.032	0.448

Table 9.2.3-1: Results of the calibration for the test with “nominal” misalignment of the ASH1 accelerometer and angular-linear coupling partially recovered using the measured electrostatic gains

Figure 9.2.3-1 shows the Spectral Density of the GGT trace, i.e. the final science performance achieved with the 5 days of science mission. The conversion of the raw data into GGT components is here based on the EGG calibrated measured accelerations through the ICM retrieved in the previous step. The crucial step of calibration is highlighted from the comparison between the SD of the GGT trace obtained with and without the application of the ICMs provided by the previously described in-flight calibration. A misalignment of the ASH1 within the nominal range permits the achievement of the required science performance.

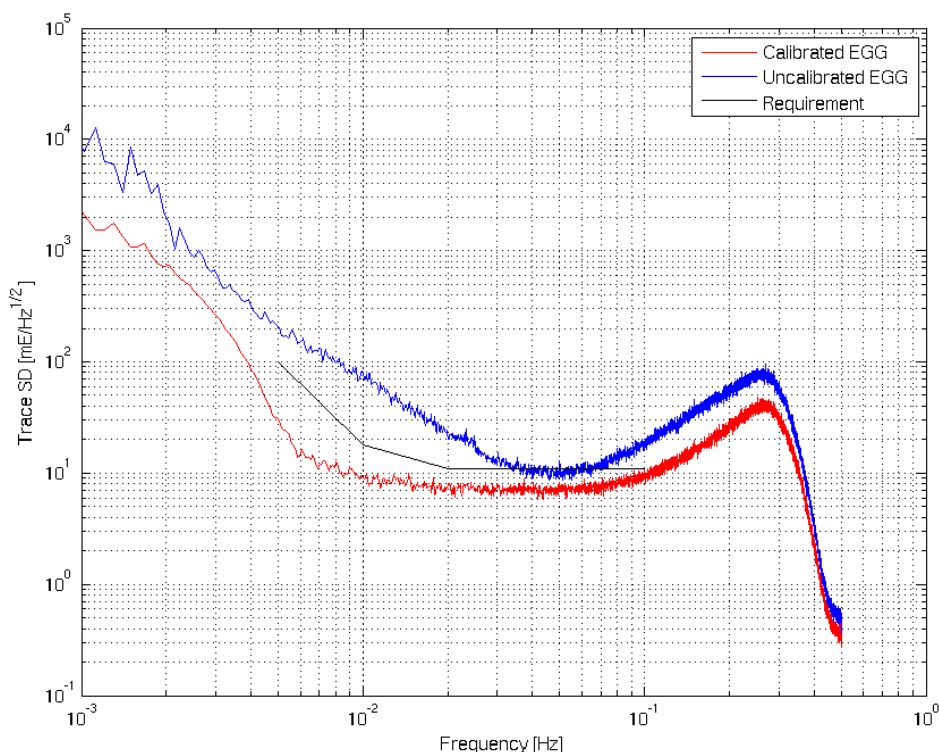


Figure 9.2.3-1: Spectral Density of the GGT trace in case of uncalibrated and calibrated (measured electrostatic gains) EGG measured accelerations. The calibration is mandatory for the achievement of the required science performance.

9.2.3.2 Performance with the Intermediate ASH1 Misalignment

Table 9.2.3-2 shows the results of the calibration for the “intermediate” test, with the processing based on the partial knowledge of the electrostatic gains (measured ones). The tables show also how the misalignment of one accelerometer affects not only the ICM of its EGG pair, but also some coefficients of the other pairs, which are retrieved by using also the ASH1 measurements. By the way, the larger effect is not on the differential scale factors, which directly affect the GGT measurements. The so retrieved ICMs have then been used to compute the calibrated EGG acceleration, which feed the reconstruction of the GGT trace.

Abs($\Gamma_{14_{kl}}$) with measured G_{el} gains					
0.863	0.235	0.125	2.288	0.096	1.417
0.137	1.531	3.267	0.034	0.146	0.439
0.424	7.179	0.299	1.327	0.334	2.384

Abs($\Gamma_{25_{kl}}$) with measured G_{el} gains					
0.226	0.110	3.435	0.217	1.836	0.096
0.331	0.187	0.071	1.603	1.122	0.044
3.336	0.154	1.102	0.105	0.007	0.084

Abs($\Gamma_{36_{kl}}$) with measured G_{el} gains					
0.494	7.130	0.294	2.913	0.063	1.185
3.226	1.427	0.222	0.034	0.144	0.167
0.020	0.080	1.179	1.265	0.080	2.433

Table 9.2.3-2: Results of the calibration for the test with “intermediate” misalignment of the ASH1 accelerometer and angular-linear coupling partially recovered using the measured electrostatic gains

Figure 9.2.3-2 shows the Spectral Density of the GGT trace, i.e. the final science performance achieved with the 5 days of science mission. The conversion of the raw data into GGT components is here based on the EGG calibrated measured accelerations through the ICM retrieved in the previous step. The crucial step of calibration is highlighted from the comparison between the SD of the GGT trace obtained with and without the application of the ICMs provided by the previously described in-flight calibration. A misalignment of the ASH1 within the midway range still permits the achievement of the required science performance. The effect of the worse misalignment is apparent only in the SD of the uncalibrated GGT trace (compare blu line of Figure 9.2.3-2 with blu line of Figure 9.2.3-1).

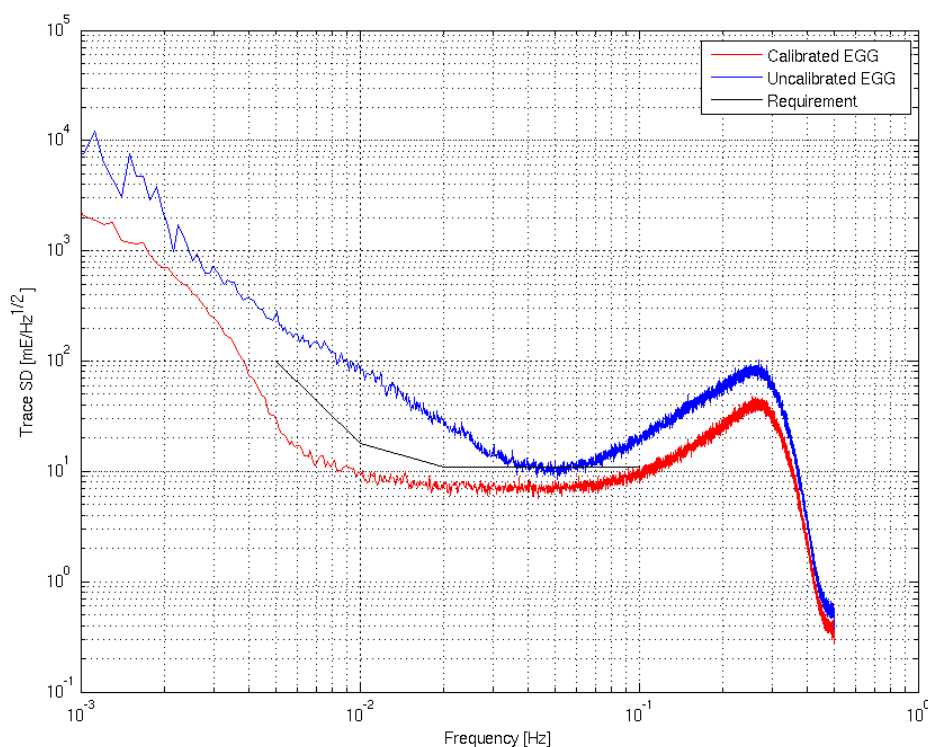


Figure 9.2.3-2: Spectral Density of the GGT trace in case of uncalibrated and calibrated (measured electrostatic gains) EGG measured accelerations. The calibration is mandatory for the achievement of the required science performance, which is almost the same of the case of “nominal” misalignment.

9.2.3.3 Performance with the Worst Case ASH1 misalignment

Table 9.2.3-3 shows the results of the calibration, with the processing based on the partial knowledge of the electrostatic gains (measured ones). The so retrieved ICMs have been used to compute the calibrated EGG acceleration, which feed the reconstruction of the GGT trace.

Abs($\Gamma_{14_{kl}}$) with measured G_{el} gains					
1.227	0.399	0.747	2.897	0.090	1.433
0.046	1.623	5.095	0.008	0.214	0.763
0.436	11.372	0.117	1.547	0.784	2.950

Abs($\Gamma_{25_{kl}}$) with measured G_{el} gains					
0.183	0.046	5.135	0.327	1.574	0.079
0.493	0.100	0.020	1.576	0.309	0.049
5.249	0.117	1.368	0.070	0.249	0.103

Abs($\Gamma_{36_{kl}}$) with measured G_{el} gains					
0.722	11.756	0.012	3.392	0.064	1.022
5.285	1.690	0.226	0.057	0.200	0.349
0.037	0.097	1.386	1.270	0.034	2.891

Table 9.2.3-3: Results of the calibration for the test with the “worst case” of misalignment of the ASH1 accelerometer and angular-linear coupling partially recovered using the measured electrostatic gains

Figure 9.2.3-3 shows the Spectral Density of the GGT trace, i.e. the final science performance achieved with the 5 days of science mission. The conversion of the raw data into GGT components is here based on the EGG calibrated measured accelerations through the ICM retrieved in the previous step. The calibration is still effective (compare the SD of the GGT trace obtained with and without the application of the ICMs provided by the previously described in-flight calibration), but the requirements are slightly violated.

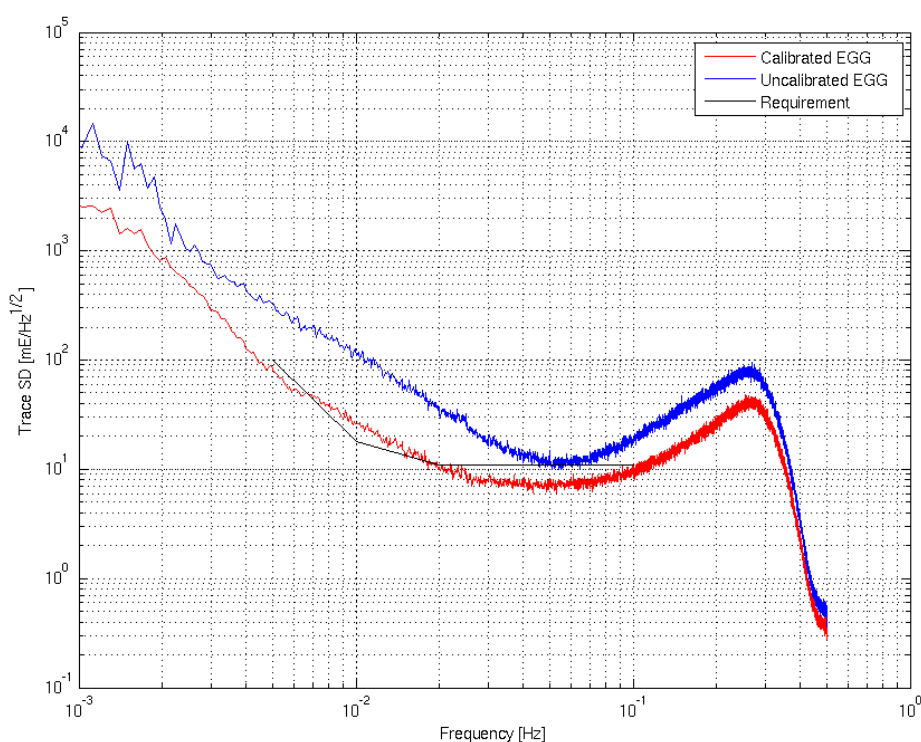


Figure 9.2.3-3: Spectral Density of the GGT trace in case of uncalibrated and calibrated (measured electrostatic gains) EGG measured accelerations. The calibration is still mandatory, but the misalignment is such that the requirements for the science performance are slightly violated.

END OF DOCUMENT